Vegetation and Environmental Changes Across the Cretaceous-Paleogene (K-Pg) Boundary in Northeastern Montana

Paige K. Wilson Deibel

A dissertation

submitted in partial fulfillment of the

requirements for the degree of

Doctor of Philosophy

University of Washington

2022

Reading Committee:

Caroline A.E. Strömberg, co-chair

Gregory P. Wilson Mantilla, co-chair

Thomas Tobin

Katherine Huntington

Program Authorized to Offer Degree:

Earth and Space Sciences

University of Washington

Abstract

Vegetation and Environmental Changes Across the Cretaceous-Paleogene (K-Pg) Boundary in Northeastern Montana

Paige K. Wilson Deibel

Chair of the Supervisory Committee:

Dr. Caroline A.E. Strömberg, co-chair

Dr. Gregory P. Wilson Mantilla, co-chair

Department of Biology

The Cretaceous-Paleogene (K/Pg) mass extinction was a pivotal event in Earth history; not only did this include the global extinction of non-avian dinosaurs but also the local disappearance of as much as 75% of vertebrate and invertebrate species. Our understanding of plants across the K/Pg is comparatively sparse, despite the central role of plants in shaping terrestrial ecosystems and as a food source. This gap in our understanding of plants across this significant time period motivates my study of plants from a ca. 2.3 Myr time interval around the K/Pg in northeastern Montana. Eleven megafloral localities are discussed here in terms of taxonomic affinities and diversity, morphologic diversity, climate implications, and ecological interpretation. This floral assemblage is also compared with contemporaneous fossil assemblages from around the globe.

The earliest fossil assemblage in this study, Seafood Salad, is a particularly diverse, angiosperm-dominated flora, interpreted as a "pre-disaster" community from the Late Cretaceous. The taxa at Seafood Salad are commonly unique (15 of 34 taxa are unique to this study), but the flora broadly shows an affinity with floral assemblages from similar stratigraphic intervals in the region, indicating shared regional taxonomy. The K-Pg event in northeastern Montana culminated in the disappearance of 63% of latest Cretaceous taxa and a ~28% drop in richness. Despite the dramatic turnover at the K-Pg boundary, however, the recovery was relatively rapid; early Paleocene floras regained pre-mass extinction levels of richness within 80 to 900 kyr after the boundary. Some aspects of plant ecological diversity (the diversity of ecological strategies) remained restricted, however, and fast-return taxa continued to dominate the floras. Overall, the plant communities in northeastern Montana experienced a significant restructuring (diminishment of dominant functional groups) even though there was no significant loss of ecomorphological richness and taxonomic diversity rebounded relatively quickly. These results point to a pattern of plant community response during biotic crises: ecological changes and diversity loss, short-term taxonomic decline, but few to no major (family-level) taxonomic extinctions. Moreover, this work indicates global and regional heterogeneity in the extinction magnitude and timing of both extinction and recovery across the K-Pg boundary.

Table of Contents

List of Figures

List of Tables

Acknowledgments

The work in this dissertation would not be possible without the aid and assistance of many people and organizations. First, I would like to thank my colleagues and friends in the Wilson Mantilla lab (Dave DeMar, Stephanie Smith, Dave Grossnickle, Luke Weaver, Alex Brannick, Brody Hovatter, Jordan Claytor, Henry Fulghum, Eddie Armstrong, Kirsten Meltesen, and many others) as well as colleagues and friends in the Strömberg lab (Alice Novello, Tim Gallaher, Camilla Crifò, Will Brightly, Alex Lowe, Elena Stiles, and many others). Thanks also go to a long list of field assistants (Paul Kester, Susan Kester, Mara Page, Matt Butrim, Tran Do, Sarah Reza, Aida Rusman, Anton Resing, Gregg Wilson, Moon Draper, Robert Spencer, Ben LeFebvre, and Mary Alice Benson), prep assistants (Gregg Wilson, Valerie Paquin, Guy Paquin, Wendell Ricketts, and Melanie Milnes), and research assistants (Teresa Di Leonardo, Emily Gallagher, Sherman Chen, Alison Phillips, Ellen Ng, Morgan Stewart, Anna Finch, Reverie Pope, Cassandra Taylor, and Xiaohan Yao) who contributed to this body of work. I would like to also thank the Burke Museum community (Ron Eng, Katie Anderson, Meredith Rivin, Liz Nesbitt, Kelsie Abrams, and so many others) for their support and help over the years. Finally, thank you to my home community in Earth and Space Sciences, from the incredible staff who made my graduate path possible to the faculty who have mentored me along the way to the incredible folks whose friendship I will always cherish. A special shout-out to the large Supergroup community for taking me under their wing as an orphan in the department!

I would especially like to thank my entire PhD committee for their tireless support and encouragement. Dr. Kate Huntington, Dr. Tom Tobin, and Dr. Brittany Johnson who all gave phenomenal advice along the way, as well as Dr. Alexis Licht who served in the first years of my PhD. And of course, thanks particularly to my exceptional advisors Dr. Caroline A. E. Strömberg and Dr. Greg Wilson Mantilla. You have balanced mentoring me through both labs, across two

departments, along with the many other commitments which deserve your attention. I am incredibly grateful for your time and efforts.

Funding for the fieldwork which provides the backbone of this work came the Colorado Scientific Society, Quaternary Research Center, American Philosophical Society's Lewis and Clark Grant, University of Washington's Earth and Space Sciences (ESS) Department (Jody Bourgeois Graduate Student Support Fund), the Paleontological Society and Bearded Lady Project, and the Geological Society of America. This research was also supported by the Hell Creek Project from the Myhrvold and Havranek Charitable Family Fund. The Burke Museum provided collections space and curational support to inventory and deposit this collection. The ESS Department (Dr. Jody Bourgeois Endowed Fellowship in Sedimentary Geology, Dr. Howard A. Coombs Scholarship Fund, Marie Ferrell Endowment Fund, Robert G. and Nadine E. Bassett Endowed Fund, David A. Johnston Fellowship, and George Edward Goodspeed Award) also provided funding during the curation, lab work, and writing of this project.

Permitting and land access was provided by the Charles M. Russell Wildlife Refuge (administered by the U.S. Army Corps of Engineers and the U.S. Fish and Wildlife Service), Montana State Department of Natural Resources and Conservation, Bureau of Land Management, as well as several private landowners (Dale and Jane Tharp, Cindy and Bill Stroh, Bob and Jane Engdahl, Les and Jerry Thomas, as well as Judd, Eva, Jay, and Gayle Twitchell).

I acknowledge that the fossils in this dissertation were collected on lands that are the traditional territory of the Fort Belknap Assiniboine & Gros Ventre Tribes and Fort Peck Assiniboine & Sioux Tribes. The Burke Museum of Natural History and Culture as well as the University of Washington are on the lands of the Coast Salish Peoples, whose ancestors resided

in this place since time immemorial; many Indigenous peoples thrive in this place, alive and strong. My sincere thanks to all the land stewards in this area, both past and present.

Dedication

This dissertation is dedicated to my family for their support, enduring love of science, and consistent cheerleading. Most especially, I dedicate this work to my husband who fed me, supported me, and kept me supplied in sweets and cocktails through this whole grad school rollercoaster!

Chapter 1: Introduction

The Cretaceous-Paleogene boundary (KPB) marks one of the most devastating biotic turnover events in Earth history (Raup and Sepkoski 1982). Globally, nearly 75% of species and 40% of genera are thought to have gone extinct (Sepkoski 1996, McGhee et al. 2013) including a massive turnover in many terrestrial vertebrate groups such as mammals (Wilson 2005, Wilson 2014, Longrich et al. 2016), dinosaurs (Sheehan et al. 1991, Fastovsky and Sheehan 2005, Brusatte 2015), birds (Longrich et al. 2011), and squamates (Longrich et al. 2012). Suggested ultimate drivers for the Cretaceous-Paleogene (K-Pg) mass extinction are Deccan volcanism and asteroid impact (Alvarez et al. 1980, Keller et al. 2010, Schulte et al. 2010, Renne et al. 2013, Bond and Grasby 2017). Studies of the KPB around the globe have indicated that environmental fluctuations across this boundary (Li and Keller 1998, Kennedy 2003, Tobin et al. 2014, Vellekoop et al. 2014, Petersen et al. 2016) resulted in ecosystem change on a global scale (Macleod et al. 1997, Norris 2001). Evidence for environmental change across the KPB comes from both local (Tobin et al. 2014) and regional (Wilf et al. 2003) records which indicate a period of warming during the Late Cretaceous followed by a ca. 5–8 °C drop in temperature at the KPB. Paleobotanical studies across the KPB record a major crisis in plant communities around the globe, including an estimated 15–30% turnover of palynoflora (pollen and spores), a prominent fern spike just after the KPB in most regions, and subsequently a gradual recovery period lasting millions of years before pre-extinction diversity levels were regained (McElwain and Punyasena 2007, Nichols and Johnson 2008, Vajda and Bercovici 2014,).

Despite the significant interest among researchers on this topic, there are relatively few stratigraphically constrained studies of megaflora spanning the full extinction and recovery intervals. Existing studies of terrestrial plants across the K-Pg are focused on palynology more

often than megafloras (see Nichols and Johnson 2008, Spicer and Collinson 2014, or Vajda and Bercovici 2014 for comprehensive review). What megafloral studies of the K-Pg mass extinction do exist often represent temporally discrete megafloras giving a small snapshot into KPB ecosystems (e.g., studies by Wing et al. 1995, Dunn 2003, Johnson and Ellis 2002, Peppe 2010, and Flynn and Peppe 2019). The megafloral records that do span the entire KPB interval are often not linked with robust vertebrate records (e.g., Johnson 2002 and Wilf and Johnson 2004), inhibiting our ability to draw broader inferences on terrestrial communities. Furthermore, megafloral records from the Denver Basin (Lyson et al. 2019) have indicated that the magnitude of extinction and timing of recovery may have varied locally due to differences in, e.g., climate and vegetation structure. Recent work in South America has expanded our understanding of megaflora across the KPB in Colombia (Carvalho et al. 2021) and Patagonian Argentina (Stiles et al. 2020), although these studies correlate meagafloras across a wide geographic area and are therefore difficult to directly compare with records from North America. Moreover, results from South America suggest highly variable plant responses to the mass extinction around the globe, such that a full understanding of vegetation change across the KPB necessitates collecting additional local records across the KPB. The currently narrow window into the dynamics of the K-Pg mass extinction have hindered scientists' abilities to connect major faunal and floral trends, extrapolate regional studies to understand global patterns, and reconstruct environmental trends at a basin scale.

This study aims to address these gaps in our current understanding of the K-Pg mass extinction. This work (1) provides a record of megaflora linked to robust existing vertebrate fossil records to analyze floral-faunal dynamics through time, (2) documents megafloral change over ca. 2.3 Myr across the KPB to capture the full extinction and recovery signal, and (3)

examines leaf physiognomy to analyze environmental and ecological changes potentially correlated with the biotic crisis.

This dissertation is founded on a collection of megafloras from northeastern (NE) Montana, which are particularly in need of study for a number of reasons. First, the Hell Creek area in Montana preserve some of the most significant vertebrate fossil records of the K-Pg mass extinction (Clemens and Hartman 2014; Wilson et al. 2014). By investigating the impact of this mass extinction on plants in Montana, this study links floral and faunal turnover to better understand the ecological implications of the mass extinction. Second, the exposures of KPB aged strata in Montana are precisely dated and well constrained, due to recent efforts applying high-precision $^{40}Ar/^{39}Ar$ geochronology, magnetostratigraphy, and lithostratigraphy (e.g., Swisher et al. 1993; LeCain et al. 2014; Moore et al. 2014; Sprain et al. 2015, 2018). Third, expanding research to Montana widens our understanding of regional and global extinction dynamics. Local changes in floral composition could be the result of local or global environmental drivers, and local taxonomic changes may be the result of migration, turnover, or extinction. Comparing local, regional, and global trends in plant community change across the KPB will enable a more nuanced understanding of plant response to mass extinction events.

This work aims to investigate how paleovegetation changed during the K-Pg mass extinction. This goal is associated with five core hypotheses (Fig. 1.1):

1. Global factors (e.g., climate change, bolide impact, volcanism) causing rapid environmental changes led to <u>significant turnover</u> of local Hell Creek area flora across the KPB.
2. <u>Regional floral associations</u> (e.g., those observed in North Dakota) will be reflected in the local KPB age flora of northeastern Montana.

3. The local and global faunal diversity crisis at the KPB was at least in part caused by changes in plant communities. Both were affected by abiotic changes in the environment. Thus, we would expect faunal changes in diversity to be temporally correlated with floral diversity and composition.
4. The observed diversity crisis at the KPB affected not only taxonomic diversity and composition but also plant ecological strategies (as expressed through functional traits) and vegetation structure.
5. Environmental fluctuation (demonstrated by prior studies on global isotope and floral records) also affected local climate and were a driving cause of the mass extinction. Therefore, environmental changes (as interpreted based on leaf physiognomy) will be highly correlated with floral turnover.

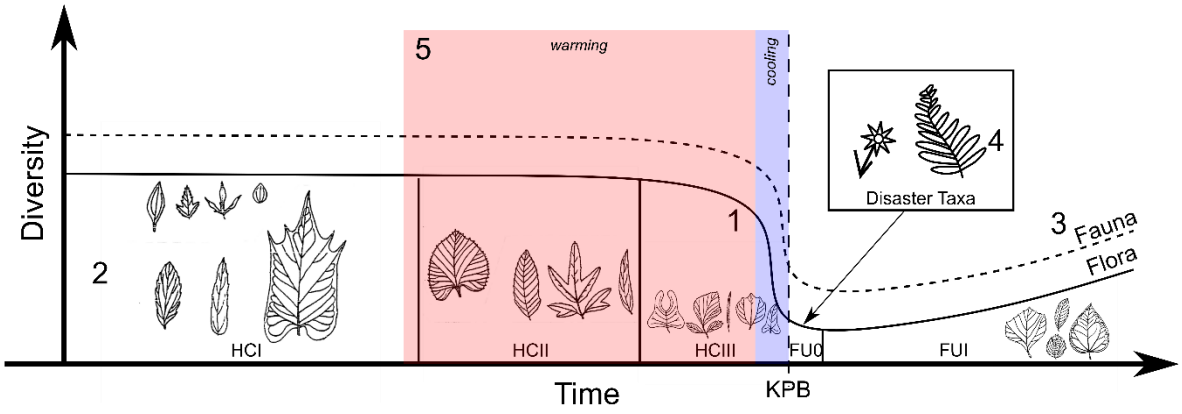

Figure 1.1: Predicted results of core hypotheses. Idealized timeline across the KPB (dashed line) showing changes in diversity through time; solid line represents floral diversity and dotted line represents faunal diversity. Note that these curves are meant to be idealized; various vertebrate groups (e.g., mammals; Wilson 2013) may show different patterns across the KPB. Illustrations of floras represent the succession of floral zones described from North Dakota (HCI, HCII, HCIII, FU0, and FUI; Johnson 1989, 2002). The FU0 interval is predicted to preserve "disaster" flora, with dramatic changes in plant ecology (i.e., weedy habit and fast-growing strategies). Red and blue shading indicates times of warming and cooling, respectively, as interpreted from leaf physiognomy in North Dakota (Wilf et al. 2003) and clumped isotope paleothermometry in Montana (Tobin et al. 2014). Numbers (1–5) indicate the corresponding hypotheses being depicted (see text).

Chapters 2 and 3 in this dissertation focus on the megafloral record in northeastern Montana and taxonomic diversity which can be investigated through these plant fossil assemblages. Chapter 2 entails a systematic description of a diverse Cretaceous florule (plant assemblage from a single locality) to describe the local taxa (defined by morphotypes) and methodology to distinguish morphotypes. Chapter 3 entails a detailed analysis of megaflora across a ca. 2.3 Myr time interval around the KPB: investigation of changes in taxonomic composition across the KPB, turnover (disappearances and appearances), changes in taxonomic diversity through time, and correlation of this megaflora with the robust Hell Creek area stratigraphic, temporal, and faunal records. These two chapters aim to address hypotheses 1, 2, and 3 above.

Chapter 4 in this dissertation addresses the broader environmental and ecological implications derived from these plant fossils. This chapter includes an assessment of plant ecomorphological diversity across the KPB as well as estimation of mean annual temperature and precipitation based on leaf physiognomy. In this way, chapter 4 aims to address hypotheses 4 and 5 above, utilizing the Hell Creek area megafloral record to infer local environmental and plant ecological conditions across the KPB.

Chapter 2: Seafood Salad: A Diverse Latest Cretaceous Flora from eastern Montana

The content of this chapter was published in

Cretaceous Research in 2021 with authors P. Wilson, G.P. Wilson Mantilla, and C.A.E. Strömberg

2.1 ABSTRACT

The Cretaceous-Paleogene (K/Pg) boundary marks a mass extinction resulting in global biotic turnover. Exposures of the Hell Creek Formation in northeastern Montana contain some of the most well-studied vertebrate localities recording this mass extinction; however, very little is known of the floral record in this area. As part of an effort to reconstruct floral changes across the K/Pg in northeastern Montana, this study presents a taxonomically diverse flora from the Seafood Salad locality, located ~ 65 m below the K/Pg boundary in the Hell Creek Formation, Garfield County, Montana. Leaves, stems, and reproductive structures (e.g., cones and seeds) are preserved as compression and impression fossils in massive, bedded siltstones and very fine sandstones. Seafood Salad is significant in that it is represents a "pre-disaster" community approximately 1.3 m.y. before the K/Pg mass extinction. We interpret the plants in these deposits as reflecting a local riparian community. The vegetation was taxonomically diverse and dominated by angiosperm trees; it also included abundant conifer specimens of a few taxa and relatively few ginkgoes and ferns. We describe 34 morphotypes and propose taxonomic affinities to modern groups and to fossil taxa from contemporaneous-age deposits in Montana and North Dakota. The Seafood Salad flora shares several taxa with other Late Cretaceous floras of the

Western Interior, but substantial differences in taxonomic composition and relative abundances among these assemblages indicate that regional plant communities in the latest Cretaceous were spatially heterogeneous, rapidly changing, or both.

2.2 INTRODUCTION

The Cretaceous-Paleogene boundary (KPB) marks one of the most pivotal events in Earth history (Raup and Sepkoski, 1982). Studies of both marine and terrestrial settings indicate that widespread environmental changes occurred leading up to and across the KPB (Li and Keller, 1998; Kennedy, 2003; Wilf and Johnson, 2004; Vellekoop et al., 2014; Petersen et al., 2016), resulting in ecosystem disruption and biotic turnover on a global scale, in both terrestrial and marine communities (Sepkoski, 1996, MacLeod et al., 1997; Norris, 2001; Schulte et al. 2010 and response Archibald et al. 2010).

Studies of the vegetation across the KPB are relatively rare, despite the central role of plants in shaping terrestrial ecosystems and as a source of food for animals. Most paleobotanical studies have focused on the palynofloral record across a wide geographic spread (e.g., western North America, New Zealand, the Netherlands, Japan [Vajda and Bercovici, 2014]). Palynofloral studies show an estimated 15–30% turnover of local palynoflora, a fern spike at or immediately after the KPB in many regions, followed by a gradual recovery of gymnosperm and angiosperm species richness over several million years (Nichols and Johnson, 2008). A limitation of palynofloral studies is that both the taxonomic and spatial resolution is often low (e.g., Nichols and Johnson, 2008; Vajda and Bercovici, 2014). In contrast, composite studies of megafloral records from New Mexico to Alberta show consistent extinction on the order of 50–75% of morphospecies across the KPB (Wolfe and Upchurch, 1986; Johnson et al., 2003; Barclay et al., 2003). However, these studies typically focus on individual megafloral localities (e.g., Wing et al., 1995; Johnson and Ellis, 2002; Dunn, 2003; Peppe, 2010) and are frequently biased towards Paleogene megafloras (e.g., Davies-Vollum, 1997; Dunn, 2003; Barclay and Johnson, 2004; Peppe, 2010; Flynn and Peppe, 2019). Therefore, they do not allow evaluation of the lead-up to

the mass extinction or the role of biogeography in shaping patterns of floral change (i.e., local extirpation versus extinction).

One of the few megafloral studies spanning the K/Pg mass extinction comes from fossil localities in the Williston Basin of North Dakota (Johnson, 1989, 2002; Wilf and Johnson, 2004; Nichols and Johnson, 2008). This record gives a high-resolution view of vegetational changes from a single basin (see Section 1.1 for detailed description). Their results indicate no signs of recovery among plant communities for several million years following the KPB (Wilf and Johnson, 2004). Nevertheless, recent analyses at other locations imply that the patterns from North Dakota might not be representative of the Western Interior as a whole; vegetational responses to the KPB event likely varied spatially and by habitat. For example, studies from the Denver Basin show that in at least some parts of the basin there was a relatively rapid post-KPB megafloral recovery (Lyson et al., 2019) and a high-diversity rainforest flora within 2.2 million years of the KPB (Johnson and Ellis, 2002; Kowalczyk et al., 2018).

The plant fossil record of eastern Montana presents an opportunity to further assess vegetational dynamics across the KPB as well as spatial variation in the northern Western Interior. The exposures of KPB-spanning rocks in eastern Montana preserve some of the best-sampled vertebrate records of the K/Pg mass extinction (see Clemens and Hartman, 2014; Wilson et al., 2014) and are precisely dated, due to recent efforts applying high-precision $^{40}Ar/^{39}Ar$ geochronology and magnetostratigraphy (Archibald et al., 1982; Swisher et al., 1993; Renne et al., 2013; LeCain et al., 2014; Sprain et al., 2015, 2018; Smith et al., 2018).

Several studies have reported on palynofloras from the Hell Creek Area (Tschudy et al., 1984; Tschudy and Tschudy, 1986; Hotton, 1988, 2002; Arens et al., 2014b), but mainly with the goal of understanding biostratigraphy immediately across the KPB. There have also been some

studies of the northeastern Montana megaflora (e.g., Shoemaker, 1966); however, these primarily focused on taxonomic collections. There is only one published detailed report on plant megafossils from the study area (Arens and Allen, 2014), focusing on a single plant locality (PDM) from the lowermost part of the Hell Creek Formation.

Here, we describe the Seafood Salad flora from the lower third of the Hell Creek Formation as another step towards building a detailed view of latest Cretaceous vegetation changes in northeastern Montana. The Seafood Salad locality represents one of the oldest and most well-preserved Maastrichtian megafloras reported to date from northeastern Montana, and can be directly tied to the local vertebrate faunal record (e.g., Wilson, 2005, 2014) and existing studies of palynoflora (e.g., Hotton, 2002). We describe the taxonomic composition and diversity of the flora and compare it with previously reported KPB megafloral records from the Western Interior (e.g., Dorf, 1942; Shoemaker, 1966; Hickey, 1977; Johnson, 1989, 1992, 1996, 2002; Johnson et al., 1989; Johnson and Hickey, 1990; Wilf and Johnson, 2004; Peppe et al., 2007; Arens and Allen, 2014). Our goal is to better understand the temporal and spatial variation in vegetation and paleofloral diversity in the northern Great Plains during the latest Cretaceous.

2.2.1. Plant records from the Williston Basin

The well-studied Williston Basin in North Dakota hosts numerous megafloral localities in exposures of the Late Cretaceous-age Hell Creek Formation (HCF) and Paleogene-age Fort Union Formation (FUF). This study region is roughly 270 km east of the Hell Creek Area in Montana. Based on over 10,000 plant megafossils from these localities, Kirk Johnson and others (Johnson, 1989; Johnson et al., 1989; Johnson and Hickey, 1990; Johnson, 2002; Wilf and Johnson, 2004) described a succession of floras that they divided into five biozones that span the KPB (Johnson and Hickey, 1990) (Figure 2.1). Three of these zones are from the latest

Cretaceous (HCI, HCII, and HCIII) and two are from the earliest Paleocene (FUI and FU0); the Cretaceous zones are further divided into subzones (Johnson and Hickey, 1990; Johnson, 2002). The megafloral zones represent levels of marked change in megafloral dominance and composition. This sequence records a transition from typical Cretaceous taxa characterized by highly dissected leaves and strongly impressed tertiary veins to a depauperate early Paleocene flora with only some Cretaceous plants persisting (e.g., palms and taxodiaceous conifers) and some archaic gymnosperms becoming extinct or extirpated (e.g., the cycad *Nilssonia* and *Ginkgo*) (Johnson, 2002). Some of these zones transition gradually (e.g., HCII to HCIII) and there are some gaps where no North Dakota floras have been recovered (i.e. between HCIII and FU0) (Figure 2.1). Each zone represents distinct local floras, likely representing vegetation changes through time; some are interpreted as responses to climate changes (e.g., HCIII contains numerous thermophilic taxa), while others may represent distinct facies associations and not time-constrained floral associations (e.g., HCIb) (Johnson, 2002).

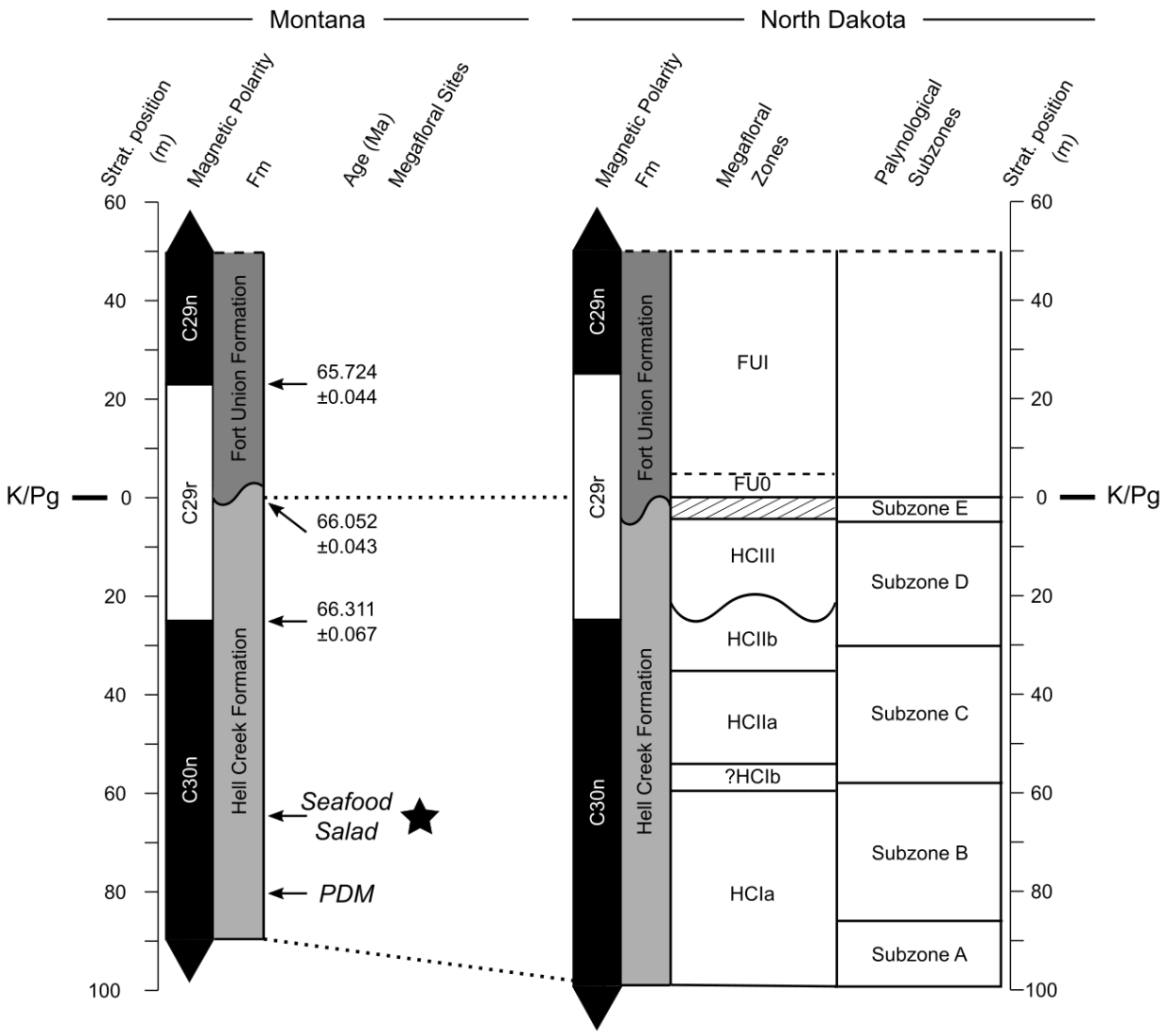

Figure 2.1 Floral biozone stratigraphy from North Dakota correlated with Montana stratigraphy. Megafloral zones based on the work of Johnson and others (Johnson and Hickey, 1990; Johnson, 2002) and palynological subzones based on the work of Nichols (2002). Montana stratigraphy and relative location of the Seafood Salad and PDM (Arens and Allen, 2014) floras shown, and correlation with stratigraphy in North Dakota interpreted. All contacts placed relative to the KPB. Magnetostratigraphy and lithostratigraphy based on the work of, and Hicks et al. (2002), Wilf and Johnson (2004), Moore et al. (2014), LeCain et al. (2014), and Sprain et al. (2015, 2018).

The lower half of the HCF in North Dakota preserves at least 24 localities and 1,482 specimens, classified in the HCI biozone (Figure 2.1) (Johnson, 2002). The HCIa subzone is typically found in the lower third of the HCF in North Dakota (between 55 and 105 m below the Hell Creek-Fort Union formational contact) and is characterized by abundant *"Dryophyllum"*

subfalcatum (HC49; 39%), *Leepierceia preartocarpoides* (HC86; 9%), *"Vitis" stantonii* (HC14; 9%), and *"Celastrus" taurenensis* (HC94; 7%) (Johnson and Hickey, 1990). *Leepierceia preartocarpoides* and *"Celastrus" taurenensis* become uncommon to rare shortly after the HCIa zone, and all of these numerically abundant taxa are extirpated before the KPB in North Dakota. The overlying HCIb subzone is also typical of the lower third of the HCF but is more stratigraphically restricted between 50 and 55 m below the Hell Creek-Fort Union formational contact. The HCIb subzone is dominated by a species in the Rosaceae family (HC81; 18%), an unnamed species in the Cannabaceae (HC80; 15%), and a species of unknown affinity (HC92; 13%) (Johnson and Hickey, 1990); however, Johnson (2002) proposed that the rarity of tree leaves and abundance of small shrub and herb leaves points to the HCIb subzone being a habitat association rather than a time-specific species association.

Plant megafossils have historically been regarded as poorly preserved and rare in the HCF and FUF of eastern Montana (Nichols and Johnson, 2008), even though early studies in the area reported numerous plant fossil localities (e.g., Berry, 1911, 1925, 1934; Brown, 1937, 1962; Dorf, 1940, 1942; Shoemaker, 1966). Recently, Arens and Allen (2014) described a florule from the PDM locality that was collected from the basal sandstone of the HCF in northeastern Montana, about 18 m stratigraphically below the Seafood Salad flora described herein (Figure 2.1). The basal sandstone is interpreted as a tidally influenced channel body, with leaf impressions preserved on some clay drapes representing a seasonal alluvial signal through the channel sandstone (Arens and Allen, 2014). From their census of 106 specimens, Arens and Allen (2014) described 17 morphotypes in the PDM flora. As predicted by the stratigraphic placement of the site, they found species associations typical of HCIa floras, but the high relative abundance of some taxa (e.g., "*Vitis stantoni"* and *Erlingdorfia montana*) also pointed to HCIIa

or HCIIb zones (Arens and Allen, 2014). Their study served as the first test of whether the North Dakota megafloral zones extend into the exposures of the HCF in eastern Montana, and it highlighted the need for a more comprehensive investigation of the megafloral record in Montana to document floristic turnover and vegetation change in this region.

2.3 GEOLOGIC SETTING AND LOCALITY

2.3.1 Regional Geology

The Seafood Salad locality is placed within the chronostratigraphic framework of the northeastern Montana study system, which is based on paleomagnetic data, radioisotopic age determination, and identification of the KPB impact layer (Archibald et al., 1982; Swisher et al., 1993; LeCain et al., 2014; Moore et al., 2014; Sprain et al., 2015, 2018). The locality is in the lower third of the approximately 90-m-thick HCF. Within central Garfield County, Montana, the HCF is latest Maastrichtian, Cretaceous in age (Sprain et al., 2018) and overlies the Fox Hills Formation with a generally conformable contact (Rigby and Rigby, 1990; Hartman et al., 2014). The Fox Hills-Hell Creek formational contact in Montana is typically placed at the base of a fine-grained sandstone unit (Hartman et al., 2014) overlying a thick concretionary sandstone ledge marking the uppermost Fox Hills Formation beds (Rigby and Rigby, 1990; Hartman et al., 2014). In our study area around the Seafood Salad locality, this basal sandstone unit of the HCF is visible, but the formational contact is approximated. Based on sedimentation rates, the age of this formational contact is approximately 67.8 Ma (Sprain et al., 2018). The upper contact of the HCF is typically placed at the base of the lower Z coal of the overlying Tullock Member of the FUF. At some localities, a thin claystone horizon lies just beneath the lower Z-coal and preserves an iridium anomaly and other signatures of the K/Pg impact event (Archibald et al., 1982; Rigby and Rigby, 1990; Hicks et al., 2002; Murphy et al., 2002; Moore et al., 2014). The lower Z coal associated with that iridium anomaly is referred to as the IrZ coal. Sanidines from a thin bentonite layer a few centimeters above the K/Pg impact layer in the IrZ coal were recently dated at 66.052 ± 0.008/0.043 Ma (Renne et al., 2013; Sprain et al., 2018). In central Garfield County, Montana the formational contact is approximately coincident with the K/Pg boundary (Archibald

et al., 1982; Fastovsky and Bercovici, 2016), although this contact is diachronous across the Williston Basin (see e.g., Lofgren 1995; Nichols and Johnson, 2002).

The HCF preserves channel, floodplain, mire, and pond deposits that are interpreted as the remains of a large paleo-river system that drained into the Western Interior Seaway (WIS) (Fastovsky, 1987; Scholz and Hartman, 2007; Fastovsky and Bercovici, 2016). The HCF is dominated by lenticular to massive sandstones and siltstones with rare lenticular lignites or carbonaceous shales and paleosols (Archibald et al., 1982; Rigby and Rigby, 1990; Murphy et al., 2002; Hartman et al., 2014). Work to refine the sequence stratigraphy within the HCF suggests that the lowest units (roughly the lowest tenth of the formation) were likely deposited in a more estuarine setting whereas the upper units were likely more fluvial as the shoreline of the WIS migrated further east (Flight, 2004).

2.3.2 Locality

The Seafood Salad locality (University of Washington Burke Museum [UWBM] locality P8078, P8077, B8198, P6909, P6910) is located west of Jasper Coulee near the Hell Creek drainage into the Fort Peck Reservoir in Garfield County, Montana (Figure 2.2). Specimens were collected under special use permits from the Charles M. Russell Wildlife Refuge (permit 15-2 in 2015) and United States Army Corps of Engineers (permits DACW45-3-16-6023 in 2016 and DACW45-3-18-6030 in 2018) to one of us (G.P.W.M.). Plant fossils were found at two discrete horizons and excavated at separate quarries (Seafood Salad I and II). The Seafood Salad I quarry (UWBM P8077, P6910, and P6909) is 21.1 m above and the Seafood Salad II quarry (UWBM P8078, B8198) is 22.4 m above the top of this basal HCF sandstone unit (Figure 2.3). Based on the average thickness of this basal sandstone unit (5.8 m thick at the Flag Butte lectostratoype section, roughly 4.25 km south of Seafood Salad [Hartman et al., 2014]), we estimate that the

locality is 28 m above the Fox Hills-Hell Creek formational contact. Based on a formational thickness of 85–90 m (Hartman et al., 2014), we estimate the site to be ~65 m below the KPB. Leaves were recovered from quarries near the top of a butte; outcrops along this butte expose a section of lowest HCF strata. The two distinct quarries (Seafood Salad I and II) are separated by ~0.75 m of strata and by 10 m along strike (Figure 2.3). Fossils are hosted in sandstone and siltstone beds that also yield abundant invertebrate fossils preserved as shell fragments (see Supplement for detailed lithologic information).

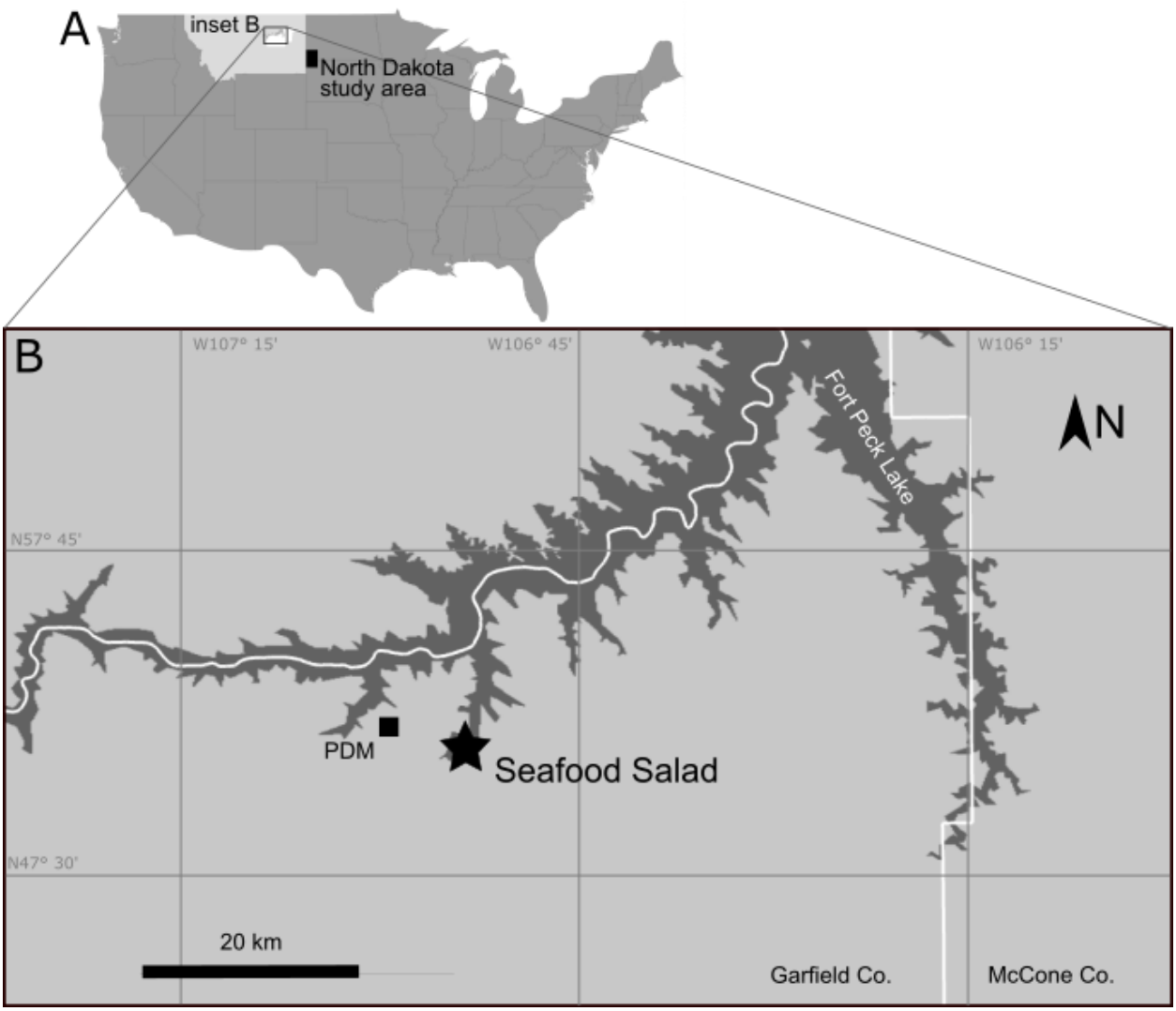

Figure 2.2 Map of study area. (A) Map of U.S.A. showing North Dakota study area (Johnson, 2002; Wilf and Johnson, 2004) and inset of Hell Creek Area. (B) Inset of Hell Creek Area in

northeastern Montana showing the Seafood Salad (this study) and the PDM localities (Arens and Allen, 2014).

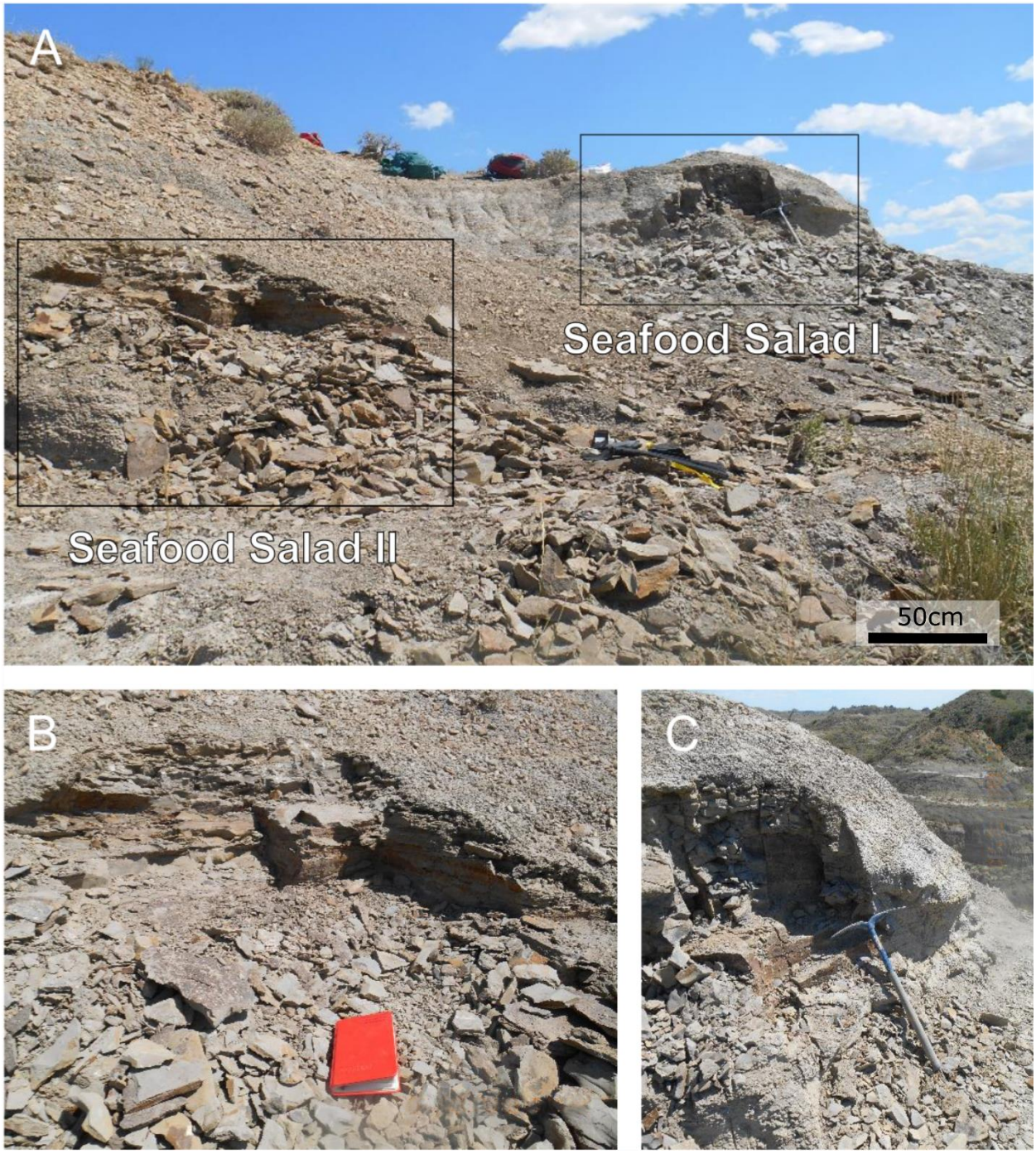

Figure 2.3 (A) Photo of locality taken in 2018 showing Seafood Salad I and II quarries (annotated). (B) Close-up photo of Seafood Salad I quarry in 2018. (C) Close up photo of Seafood Salad II quarry in 2018.

2.4 METHODS

2.4.1 Description of Stratigraphy

Using a Trimble GPS system with sub-meter vertical and horizontal accuracy, a Jacob's staff, and a hand level, we determined the stratigraphic and geographic positions of the locality relative to local marker beds and logged a section with detailed notes on sediment size, color, and structures. We described lithology and bed contacts on fresh surfaces to produce a stratigraphic section through both quarries (See Supplement and for detail).

2.4.2 Fossil Collection

We made census collections at the two Seafood Salad quarries over the summers in 2015, 2016, and 2018. We separated specimens by quarry and by collection year to account for any collector bias and to separately preserve the samples from the distinct horizons of the two quarries. Seafood Salad I and II contain distinct floras (see Section 5.1), but because they are separated by less than a meter of strata we consider them penecontemporaneous. Specimens are reposited at the University of Washington Burke Museum of Natural History and Culture (UWBM). All identifiable specimens were collected, and, in some cases, photographs and notes of exceptional specimens were taken in the field. In total, 590 fossil plant specimens have been recovered and identified from these collections along with 169 unidentifiable fossils.

2.4.3 Classification of the Flora

Our taxa are assigned to morphotypes based on organ type, gross morphology, and leaf architecture. Angiosperm leaves were grouped and described based on leaf architecture according to Ellis et al. (2009). Major venation patterns are generally stable within morphotypes, whereas size and shape may be variable (Ellis et al., 2009). Therefore, particular importance was

given to primary, secondary, and tertiary venation and secondarily to features such as laminar size and shape.

We assessed the affinity of each morphotype to taxa that have been described in the published literature of KPB-age floras from the northern Great Plains region (Table A.1). Thirteen of our 34 morphotypes are attributed to published species, and an additional three morphotypes are attributed to published or unpublished morphotypes from the Late Cretaceous (Dorf, 1942; Johnson, 1989, 1996, 2002; Peppe et al., 2007; Arens and Allen, 2014; K. Johnson, personal communication, June 23, 2018). Additionally, four of our morphotypes are similar to published taxa and are tentatively ascribed to or favorably compared with published species where appropriate. Fourteen of our morphotypes do not definitively match any known Late Cretaceous taxa from the Western Interior; in some instances, these are rare morphotypes in which poor preservation likely obscures identifying features; in other instances, the morphotypes might represent novel taxa.

2.4.4 Description of the Flora

Taxa are presented in taxonomic order, grouped by higher taxon (e.g., Gymnospermae, Angiospermae) and then within family and lower classification where known. Descriptions are given in a standardized format, outlined below. A summary of the species and material is given in Table A.1. Systematic paleobotany for all taxa is outlined in Table A.2. Morphotypes are grouped according to major architecture in Table A.3. A summary of material is given in Table 1.

Morphotype

Morphotypes are each assigned with an alphanumeric code; these codes were assigned in order of major architecture (see Table A.3). These specimens use MT as the prefix to distinguish

this study from work in North Dakota (which used FH, HC, and FU prefixes; Johnson, 1989; Peppe et al., 2007) and at other locations in Montana (which used FP prefix; Arens and Allen, 2014).

Synonymous Morphotypes

We list synonymous morphotypes from prior studies in Montana and North Dakota (Dorf, 1942; Johnson, 1989, 2002; Peppe et al., 2007; Arens and Allen, 2014; K. Johnson, personal communication, June 23, 2018) where appropriate.

Nomenclatural Summary

Whenever we could ascribe a morphotype to a genus and species, we list the first occurrence of that taxon in the published literature and any name changes for genus or species. However, as noted by previous workers (e.g., Brown, 1962; Arens and Allen, 2014) assignments of plant fossil taxa to Linnaean classifications are sometimes suspect. In cases where a consensus has emerged that fossil species do not belong in extant genera, we have applied quotations and stripped higher order classifications as necessary. Due to this uncertainty and problematic nomenclature, we have not erected new Linnaean species names for any of the morphotypes that, to the best of our knowledge, have not been described previously.

Material

We indicate the number of specimens assigned to a particular morphotype from the Seafood Salad locality and list exemplar specimens (see Table 1 for summary). These exemplars are the basis for the descriptions given and used to assess the Exemplar Quality Index of a given morphotype; they are more akin to 'holomorphotypes,' although here we choose not to use that terminology to emphasize that we are describing morphotypes rather than Linnean species. The exemplars are all specimens from the UWBM and are assigned paleobotany specimen numbers

preceded by PB. A numeric suffix is applied if the specimen is on a block with multiple plant fossils (e.g., PB 12340.2) to assign a unique identifier to each fossil on the block.

Morphotype Quality

We follow the procedure of previous workers (e.g., Hickey, 1977; Johnson, 1989; Arens and Allen, 2014) by including quality indices for each taxon. These indices give a general indication of how well-preserved and well-defined a given taxon is. Here we employ the standard Morphotype Quality Index (MQI; Johnson, 1989) as well as an Exemplar Quality Index (EQI), the latter being a modification of what is sometimes called holomorphotype quality index (Ash et al., 1999; Ellis et al., 2009).

The MQI scales 1–5, where 1 indicates more than ten well-preserved and whole specimens, 2 indicates two to ten well-preserved and/or whole specimens, 3 indicates one whole or partial well-preserved specimen, 4 indicates one whole or few to many partial to whole, but poorly preserved specimens, and 5 indicates one partial and poorly preserved specimen. A lower score indicates a morphotype that is abundant and well preserved.

The EQI scales 1–5 and is an assessment of the completeness of an exemplar specimen. We looked for detailed features on each exemplar. Morphotypes receive a point for each of the following features: base, apex, margin, third-order venation, and fourth-order venation. These characteristics are only applicable to net-veined angiosperm leaves, and thus we recorded NA (i.e., not applicable) for all other morphotypes. A higher score indicates reasonably complete exemplars, and our understanding and discriminatory power with that morphotype is greater; a score above 3 was considered well preserved when evaluating MQI.

Diagnosis

A brief summary description is given of the defining characters of each morphotype.

Description

Each morphotype is described based on the terminology outlined by Ellis et al. (2009), organized as follows: the margin and shape are described first, followed by teeth (if present), and then a description of venation from first order to the highest order visible.

Remarks

We discuss the circumscription, affinity, and other considerations of each morphotype.

2.4.5 Data Analyses

The diversity and composition of the Seafood Salad flora were quantitatively compared to similar-aged floras from North Dakota (data from Wilf and Johnson, 2004) and Montana (the PDM flora described by Arens and Allen, 2014) to assess regional and temporal patterns. The relative abundance of each morphotype and raw sample richness in Seafood Salad were compared to the North Dakota dataset and the PDM flora. We include only better-sampled localities from the North Dakota dataset (> 50 specimens; n=70) and separate out HCI zone localities for some analyses (n=14). We recognize that a larger sample size at each locality is ideal; however, the North Dakota dataset (Wilf and Johnson, 2004) contains only 30 localities with sample size greater than 250 (a common cutoff used in paleobotanical studies), only five of which are in the HCI biozone of interest. Therefore, we use a sample size cutoff at >50 specimens in order to incorporate a broader sampling of the North Dakota localities. Selecting localities that are relatively better-sampled, but maintaining a larger dataset should limit the bias of rare taxa. Using two different datasets allows us to test the hypothesis that floral composition at Seafood Salad is most similar to North Dakota localities of the HCI zone, and, more specifically, to which, if any, of the HCI subzones Seafood Salad is most similar. Furthermore, we investigated potential biases or trends within particular taxonomic groups by analyzing

various subsets of our morphotypes. Here we present results looking at either all taxa (including all morphotypes) or only vegetative morphotypes. The latter approach is a more conservative estimate of species richness, as using only vegetative morphotypes avoids potential double counting of species whose reproductive structures (i.e., seeds) and vegetative structures (i.e., leaves) were counted as separate morphotypes; this approach also avoids biases inherent in differential rates of production of different organs on a given plant.

Analytic rarefaction was used to standardize for sample size across floras, and we plotted rarefaction curves with 95% confidence intervals of the Seafood Salad, PDM, and North Dakota floras to compare richness and evenness. In addition, we calculated raw and rarefied richness as well as two other taxonomic diversity indices that incorporate richness and relative abundance data: Simpson's diversity index (1-D; Simpson, 1949) and Pielou's evenness (J'; Pielou, 1966). These indices are relatively easy to interpret, reflect differences in relative abundance of individuals within morphotypes in meaningful ways (McCune et al., 2002), and are standard for analysis of fossil floras (e.g., Smith et al., 2012; Wing et al., 2012).

Relative abundance data of morphotypes at Seafood Salad and the North Dakota localities were also plotted in ordination space using nonmetric multidimensional scaling (NMDS) (McCune et al., 2002) and detrended correspondence analysis (DCA) (Hill and Gauch, 1980). Ordination plots were visually similar regardless of method; NMDS plots are discussed and shown because this method is insensitive to data matrices with many zeros, such as ours, and it is the preferred method when the question asked does not relate to species distribution along environmental gradients (McCune et al., 2012; Clarke, 1993). For NMDS ordination, 95% confidence envelopes were also calculated. For each locality, relative abundance of morphotypes was calculated in order to standardize data and pairwise Bray-Curtis dissimilarities (Bray and

Curtis, 1957) were calculated between sites. We used Bray-Curtis distances as this metric is designed for use on species abundance data and is robust to small sample sizes and applicable to abundance data (McCune et al., 2002; Bray and Curtis, 1957). Analysis of similarity (ANOSIM), with 999 permutations based on Bray-Curtis dissimilarities, was used to test whether localities from a given floral biozone were more similar to one another than to localities from different zones. ANOSIM is a non-parametric test of similarity within groups; it operates as a distribution-free analog of one-way ANOVA tested by permutations of the rank similarity matrix (Clarke, 1993). ANOSIM was chosen because it is particularly complementary to NMDS; both work on ranked similarities between groups of samples (here floral zones) (Clarke, 1993).

Some rarefaction curves were calculated and plotted in PAST (Hammer et al., 2001). All diversity indices, richness, ANOSIM, and ordinations were conducted in R version 3.5.3 (R Core Team, 2019; http://www.r -project.org) using appropriate functions from the community ecology package vegan, version 2.5–4 (Okansen et al., 2019).

2.5 RESULTS

2.5.1 Systematic Paleobotany

Phylum PTERIDOPHYTA

Class FILICOPSIDA

Order HYDROPTERIDALES

Family HYDROPTERIDACEAE Rothwell and Stockey

Genus *HYDROPTERIS* Rothwell and Stockey, 1994

Hydropteris pinnata Rothwell and Stockey, 1994

Morphotype: MT033; Figure 2.4A.

Synonymous Morphotype: HC129 (Johnson, 1989, 2002).

Nomenclatural Summary:

1942 *Filicites knowltonii* Dorf pg. 127, pl. 4, figs. 7, 8, 10, 11

1994 *Hydropteris pinnata* Rothwell and Stockey p. 481, figs. 1–6.

Material: Morphotype MT033 is represented by one specimen, UWBM PB 103729.4.

Morphotype Quality: MQI is 3; EQI is NA.

Diagnosis: Small leaflets alternately arranged along major axis. Leaflets display 3–5 veins emerging at the base which form an anastomosing net distally. Margin entire.

Description: Leaflets sessile, arranged alternately and evenly spaced along central axis. Leaflets small, 5–10 mm long and 3–8 mm wide on average, oblong and entire-margined. Approximately five veins emerge from base of each pinnule and form an anastomosing net distally.

Remarks: We have identified this specimen as *Hydropteris pinnata* (Dorf, 1942; Johnson, 1989). It matches the description in Dorf (1942): small leaflets, oblong-elliptic in shape, with fine, anastomosing veins, arranged alternately along a central rachis. Another, unpublished taxon defined by Johnson (personal communication, January 18, 2018), HC397, is superficially similar but the leaflets on HC397 are more distantly spaced than on MT033.

Subclass uncertain

Morphotype Designation: MT031: Figure 2.4B.

Synonymous Morphotypes: HC115 (Johnson, 1989).

Material: Morphotype MT031 is represented by one specimen, UWBM PB 103633.2.

Morphotype Quality: MQI is 5; EQI is NA.

Diagnosis: Pinnate leaflets alternating along a central axis (rachis or rachillae). Attachment to central axis decurrent. Leaflets 4–7 mm long and decrease in size distally. Each leaflet is elliptic in shape with small (<1 mm) teeth.

Description: Pinnate leaflets arranged alternately along central axis (rachis or rachillae). Leaflets elliptic in shape; apex and base angles acute. Base attachment decurrent to central axis. Small serrate teeth on larger leaflets. Central midvein along each leaflet terminates at leaflet apex. No other venation visible.

Remarks: This morphotype is represented by a single specimen only 1.7 cm long and poorly preserved, making affinity difficult to ascertain. However, it appears to match an unnamed fern described by Johnson (1989) as HC115. HC115 and this specimen both have dissected leaflets

alternately attached and a thinning of the lamina to a constricted, decurrent attachment to the rachis.

Morphotype: MT032; Figure 2.4C.

Material: Morphotype MT032 is represented by four specimens, exemplars are UWBM PB 97845.2 and 97833.2.

Morphotype Quality: MQI is 4; EQI is NA.

Diagnosis: Anastomosing net venation supported by a central pinnate primary vein and secondaries attached decurrently to that midvein.

Description: Shape, attachment, and full size indeterminate. Central primary vein relatively wide (approximately 1–2 mm); secondaries attached decurrently to midvein. Venation between primary and secondary veins in evenly spaced anastomosing net.

Remarks: The overall impression of a net supported by these central axes is distinct and separates these specimens from any other morphotype recovered from this locality. Given how partial these specimens are, with no margin, shape, attachment, or organizational features to distinguish it, we are unable to ascribe this taxon to any known morphotypes or taxa from the region. However, the anastomosing venation lead us to interpret these specimens as likely representing fern pinnae, with the central midvein being the rachis.

Class uncertain

Morphotype: MT034; Figure 2.4D.

Material: Morphotype MT034 is represented by three specimens, exemplar is UWBM PB 97843.

Morphotype Quality: MQI is 4; EQI is NA.

Diagnosis: Small (approximately 2 cm) branching structures. At least three orders of branching axes which terminate in narrow (approximately 0.2 mm), nearly linear, lamina-like extensions.

Description: Small branching structures. Central axis, usually <0.5 mm wide supports finer gauge branchlets emerging alternately along its length. Smaller branchlets support further alternately arranged branchlets often only 1–2 mm long. Fine, lamina-like, nearly linear shaped structures arranged oppositely and closely spaced along each ultimate branchlet.

Remarks: These cryptic structures are compared to mosses based on their lack of megaphyll leaves, small stature, and dichotomizing structure. The many-ordered structure and fine, lamina-like termini are interpreted as small scale "leaves" arranged spirally or whorled around each ultimate branchlet. Three specimens of the morphotype have been recovered from this locality but none is larger than 3–4 cm. Based on this partial nature we cannot definitely ascribe this morphotype to any known taxon from the region. A taxon of fern defined by Johnson (personal communication, January 18, 2018), HC215, is somewhat reminiscent of this morphotype; however, HC215 shows a more regular structure than MT034 and lacks the distinctive terminal structures seen here. The only bryophyte described from K-Pg aged deposits in North Dakota (FU45; Johnson, 1989) bears significant resemblance to MT034: both morphotypes bear small lamina-like scale "leaves" arranged spirally around axis, with small axes (approximately 1 cm long). However, FU45 bears scale leaves closer to the central axis, the leaves are significantly smaller than in MT034, and this taxon is found only in the earliest Paleogene in North Dakota. Given these considerations, we consider MT034 possibly a bryophyte, potentially synonymous

or closely related to FU45 of North Dakota, but we are unable to definitively align MT034 with FU45 based on this small sample from Seafood Salad.

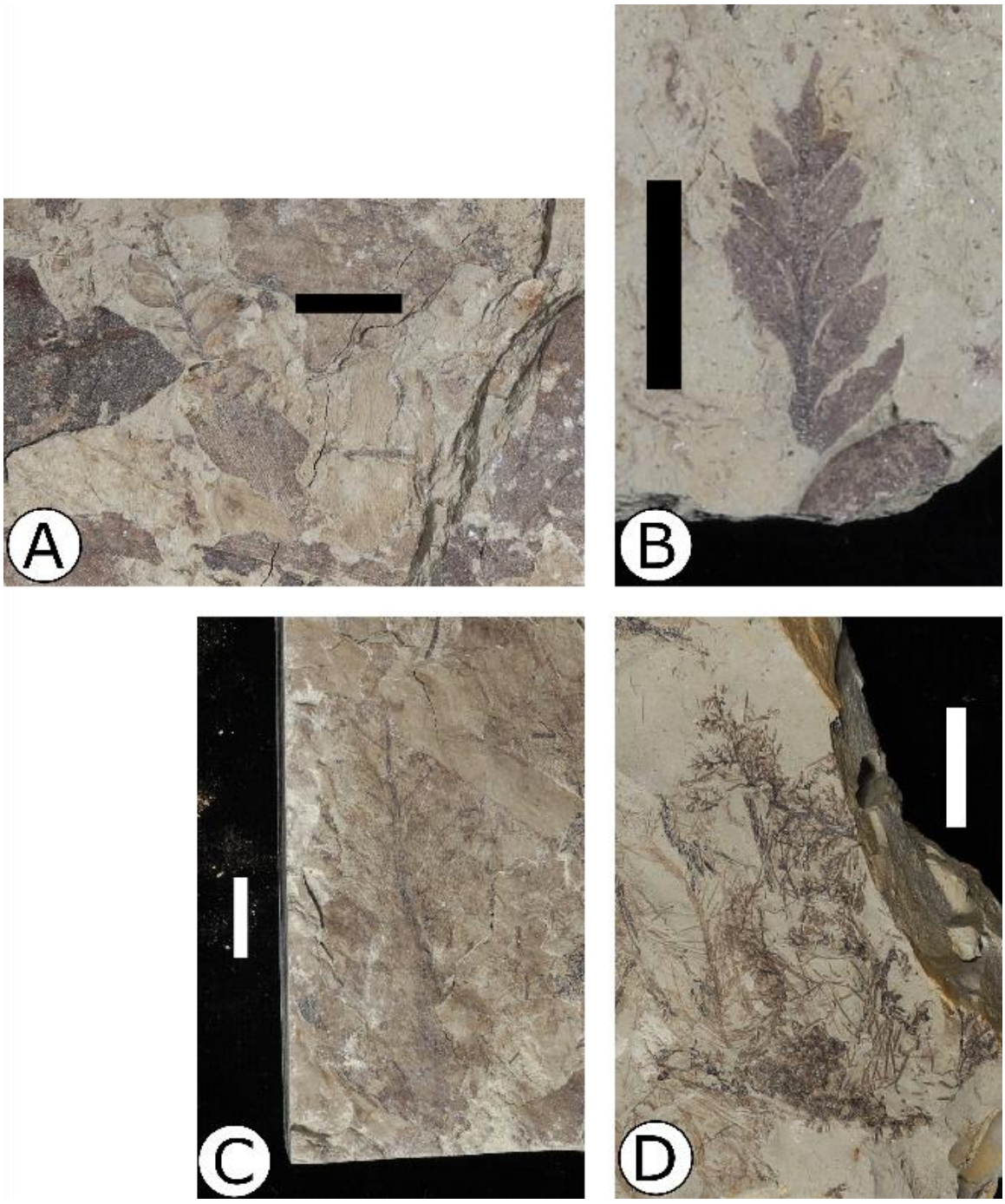

Figure 2.4 Fern and other morphotypes; (A) MT033 *Hydropteris pinnata*, UWBM PB 103729.4; (B) MT031 Filicales sp., UWBM PB 103633.2; (C) MT032 unidentified morphotype, UWBM PB 97833.2; (D) MT034 unidentified morphotype, UWBM PB 97843. Scale bar 1 cm.

Phylum GYMNOSPERMOPHYTA

Class CONIFEROPSIDA

Order CONIFERALES

Family CUPRESSACEAE (Richard) Bartling

Genus *DITAXOCLADUS* Guo and Sun (in Guo et al., 1984)

Ditaxocladus catenulatus (Bell) Guo et al. 2012

Morphotype: MT001; Figure 2.5A.

Synonymous Morphotypes: HC137 (Johnson, 1989, 2002).

Nomenclatural Summary:

1949 *Androvettia catenulata* Bell p. 46, pl. 15, figs. 1–5; pl. 16, fig. 4; pl. 27, figs. 7–8

1962 *Fokienia catenulata* (Bell) Brown p. 50, pl. 11, figs. 1–2

1989 *Androvettia catenulata* (Bell) Johnson p. 178, pl. 16, figs. 11, 12, 13

1990 *Fokieniopsis catenulata* (Bell) McIver and Basinger p. 1612.

2012 *Ditaxocladus catenulatus* (Bell) Guo, Kvaček, Manchester, Zhou p. 143

Material: Morphotype MT001 is represented by two specimens, exemplar is UWBM PB 96528.

Morphotype Quality: MQI is 3; EQI is NA.

Diagnosis: Axes oppositely branching and leaves arranged in whorls. Facial leaves appressed, lateral leaves decurrent. Leaves small, scale-like, with decurrent leaf bases and acuminate to rounded apex.

Description: Axes have three orders of branching, with second order axes oppositely arranged along the major branch axis, spacing smoothly decreasing distally. Axis diameter consistently 1–

2 mm. Leaves scale-like, opposite decussate, and four-ranked on highest order axes (branchlets). Facial leaves appressed, lateral leaves decurrent. Scale leaves consisting of extended, decurrent base, apex appressed by short free tips; leaf width 1–2 mm.

Remarks: MT001 most closely resembles HC137 of Johnson (1989, 2002), ascribed to *Ditaxocladus catenulatus* (then known as *Fokieniopsis catenulata*), which similarly has scale leaves oppositely arranged and on a series of oppositely attached, nested axes. These characteristics also resemble descriptions by McIver and Basinger (1990) who defined this taxon under a new genus *Fokieniopsis* based on the presence of Cupressaceae-like foliage but an absence of reproductive structures. This genus was later amended to *Ditaxocladus* (Guo and Sun) to return to the priority of this generic name.

The morphotype differs from *Cupressinocladus interruptus* (Johnson, 1989, 2002; Peppe et al., 2007) in that MT001 scale leaves are not arranged in decussate pairs and pairs of scale leaves are equally sized. MT001 does superficially resemble the *Cupressinocladus interruptus* described by Arens and Allen (2014) but based on the lack of decussate pairs of leaves we do not assign it there. This distinction is important as *Cupressinocladus interruptus* is considered more common than *Ditaxocladus catenulatus* from the Hell Creek and Fort Union Formations in North Dakota (Johnson, 1989, 2002; Peppe et al., 2007).

Genus *METASEQUOIA* Miki, 1941

Metasequoia occidentalis (Newberry) Chaney, 1951

Morphotype: MT002; Figures 2.6B, C.

Synonymous Morphotypes: FP002 (Arens and Allen, 2014); FU3 (Johnson, 1989); FH8 (Peppe et al., 2007).

Nomenclatural Summary:

1863 *Taxodium occidentale* Newberry p. 516

1951 *Metasequoia occidentalis* (Newberry) Chaney p. 225, pl. 1, fig. 3; pl. 2, figs. 1–3; pl. 4, figs. 1, 2, 9; pl. 5, figs. 1–3; pl. 6, fig. 2; pl. 7, figs. 1–6; pl. 8, figs. 1–3; pl. 9, figs. 3, 5, 6, 7; pl. 10, figs. 1a, 2a, 3–6; pl. 11, figs. 7, 8; pl. 12, figs. 1, 2, 5–8.

Material: Morphotype MT002 is represented by 274 specimens, exemplars are UWBM PB 96587, 99307.1, and 103535.2.

Morphotype Quality: MQI is 1; EQI is NA.

Diagnosis: Needle-like leaves oppositely arranged on flattened branchlets. Leaves oblong with blunt apices.

Description: Axes range from <1 cm to >20 cm in length and may preserve many orders of branching, with the highest order consisting of (typically) 1–3 cm long branchlets. Branchlets usually bear three to ten pairs of leaves each. Leaves decussately and distichously arranged, evenly spaced, form an angle between 31 and 77º with the axis, and are rotated to form a flattened plane. Average measurements for the type specimens listed above: leaves 6.2 by 1.4 mm and angled at 47.1º from the axis, branchlets 1.6 cm long on average and angled 46.0º to the main axis. Leaves are needle-like and oblong, approximately 6 by 1 mm with blunt apices and a single mid-vein. Leaf dimensions roughly consistent along length of axis but often smaller closer to the apex.

Remarks: This morphotype is by far the most common at this locality and is found ubiquitously through the area and region. Description as in Hickey (1977), taxonomy based on Johnson

(1989). Length to width ratios for specimens assigned to MT002 fall within the range described by Liu et al. (1999), towards the low end of their range; these authors conclude that fossil *Metasequoia* taxa represent a wide variation overlapping with extant *Metasequoia glyptostrobus*. Johnson (1989) recognized several *Metasequoia* sp. from the Hell Creek Formation in North Dakota; there may be some overlap between specimens assigned to MT002 and these related *Metasequoia* taxa. As described by Chaney (1951) considerable variation and diversity existed within *Sequoia* and *Metasequoia* during the Cretaceous in the Western Interior. *S. dakotensis* Brown and *S. nordenskiöldi* (Brongniart) Heer as identified by Dorf (1942) were largely placed under *Metasequoia cuneate* (Newberry) by Chaney (1951). Johnson (1989) recognized that *M. cuneate* may be synonymous with his HC35 (*Metasequoia sp.* #2). Based on the descriptions of Johnson (1989) and Hickey (1977), we acknowledge that there may be some overlap with our morphotype here and some of these varieties of *Metasequoia* and *Sequoia* but place them under *Metasequoia occidentalis* as the most correct nomenclature.

The extreme dominance of this taxon at Seafood Salad I is atypical for this study area. Likely this represents either an anomalous event (e.g., large storm) or distribution (e.g., a small community of *M. occidentalis* living near source). Given that almost all specimens were branchlets, shed annually in modern *Metasequoia*, these may represent needle fall from a relatively small number of individuals. Further, the relative abundance of *M. occidentalis* reproductive structures (n=5) is much lower than *M. occidentalis* branchlets (n=254), even accounting for their different rates of production on individual plants. This leads us to conclude that the abundance of *M. occidentalis* foliage (MT002) is likely taphonomic, due to high preservation rates which mask the true abundance of this taxon in the community.

Morphotype: MT003; Figure 2.5D.

Synonymous Morphotypes: FP002 (Arens and Allen, 2014); FU3 (Johnson, 1989, 2002); FH8 (Peppe et al., 2007).

Nomenclatural Summary:

1863 *Taxodium occidentale* Newberry p. 516

1951 *Metasequoia occidentalis* (Newberry) Chaney p. 225, pl. 1, fig. 3; pl. 2, figs. 1–3; pl. 4, figs. 1, 2, 9; pl. 5, figs. 1–3; pl. 6, fig. 2; pl. 7, figs. 1–6; pl. 8, figs. 1–3; pl. 9, figs. 3, 5, 6, 7; pl. 10, figs. 1a, 2a, 3–6; pl. 11, figs. 7, 8; pl. 12, figs. 1, 2, 5–8.

Material: Morphotype MT003 is represented by five specimens, exemplar is UWBM PB 96535.1.

Morphotype Quality: MQI is 2; EQI is NA.

Diagnosis: Small cone ellipsoidal or spheroidal in shape. Bracts spatulate. Distal end of bract in top-view widens to a triangular- or Y-shaped process.

Description: Cone ellipsoidal or spheroidal in shape. Type specimen 1.5 cm in diameter with over 10 bracts decussately attached around central axis. Bracts spatulate in shape in top-view and 5—10 mm long. Bracts less than 1 mm wide at proximal attachment but widen to 2–3 mm distally and flatten to form a triangular or Y-shaped apex (top-view).

Remarks: This morphotype is interpreted as female reproductive cones associated with MT002, *Metasequoia occidentalis*. Specimens are preserved as oblique, latitudinal, or longitudinal cross sections of carbonized woody material.

Reproductive cones from *Metasequoia occidentalis* have been described from the Cretaceous and Paleogene across the Western Interior (e.g., Chaney, 1951; Hickey, 1977; Johnson, 1989, 2002; Peppe et al., 2007; Arens and Allen, 2014). Specimens from this locality

strongly resemble the female cones described by Liu et al. (1999), with most being on the smaller end of cones of various *Metasequoia* species but falling clearly within the range of *M. occidentalis*. The descriptions by Chaney (1951) note that *Metasequoia* cones display decussate attachment of the scales and lack the spiral attachment seen in *Sequoia* cones. Based on this definition, our material aligns most closely with *Metasequoia* and furthermore matches descriptions of *Metasequioa occidentalis* cones by Hickey (1977).

Other authors (e.g., Johnson, 1989; Peppe et al., 2007; Arens and Allen, 2014) have chosen to assign reproductive and vegetative structures from *M. occidentalis* to a single morphotype. Here we separate the reproductive cones into their own morphotype to better capture the taphonomic signature of this site. See description of *M. occidentalis* branchlets (MT002) for discussion of potential taphonomic biases.

Genus *GLYPTOSTROBUS* Endlicher, 1847

Glyptostrobus europaeus (Brongiart) Heer Johnson, 1989

Morphotype: MT004; Figure 2.5E.

Synonymous Morphotypes: FP003 (Arens and Allen, 2014); FU4 (Johnson, 1989, 2002).

Nomenclatural Summary:

1833 *Taxodium europaeus* Brongniart p. 168, pl. 20 all figs.

1855 *Glyptostrobus europaeus* (Brongniart) Heer p. 51, pl. 19 all figs.; pl. 20, fig. 1

1936 *Glyptostrobus dakotensis* Brown p. 355, text figs. 2–4

1977 *Glyptostrobus europaeus* (Brongiart) Heer Hickey.

Material: Morphotype MT004 is represented by 34 specimens, exemplar is UWBM PB 96554.

Morphotype Quality: MQI is 1; EQI is NA.

Diagnosis: Needle leaves alternately arranged along long branches. Leaves short and narrow with an acute apex and decurrent attachment.

Description: Axes long and apparently infrequently branching. Needle leaves in seemingly alternate phyllotaxis and forming acute angle with axis (16.1° on average); attachment elongated and decurrent. Leaves relatively short and narrow; on type specimen 6.8 by 0.5 mm on average and acute-tipped.

Remarks: The needle leaf arrangement observed in this morphotype is distinctive: each leaf is held much closer to the branch than in MT002, MT005, or MT006 and the leaves are narrower than MT002 and shorter than MT005 or MT006. No axes with multiple branches of MT004 were recovered from this locality. The thin, linear leaves of this morphotype and acute angle of attachment to the axis match the descriptions of *Glyptostrobus europaeus* given by Hickey (1977), Johnson (1989), and Arens and Allen (2014). No fertile material that could be linked to MT004 was recovered from this locality. In accordance with Butala and Cridland (1978), in the absence of cones and given the similarity in vegetative material we assign all specimens of this morphotype to *G. europaeus*. Hickey (1977) notes that the separation of American Paleocene *Glyptostrobus* into multiple species by Brown (1936) and others was not based on valid differences and follow this author's recommendation to consider vegetative branches of this morphology as the species *G. europaeus.*

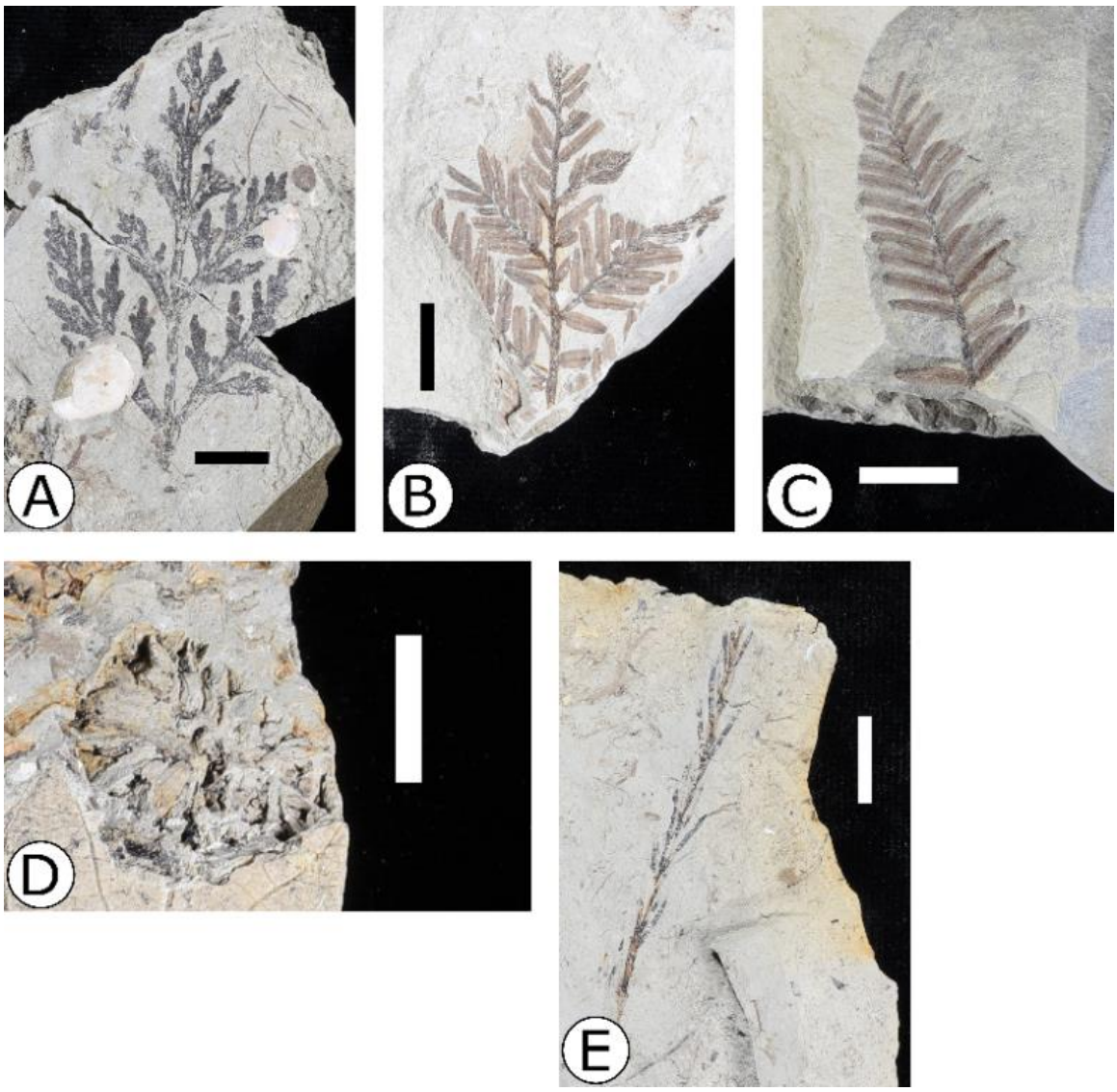

Figure 2.5 Gymnosperm morphotypes; (A) MT001 *Ditaxocladus catenulatus*, University of Washington Burke Museum (UWBM) specimen PB 96528; (B-C) MT002 *Metasequoia occidentalis*, B—UWBM PB 103535.2, C—UWBM PB 96587; (D) MT003 *Metasequoia occidentalis*, UWBM PB 96535.1; (E) MT004 *Glyptostrobus europaeus*, UWBM PB 96554. Scale bar 1 cm.

Family CUPRESSACEAE *sensu lato*

Genus *TAXODIUM* Richard, 1810

Taxodium olrikii (Heer) Brown, 1962

Morphotype: MT005; Figure 2.6A, B.

Synonymous Morphotypes: HC71 (Johnson, 1989, 2002); FH68 (Peppe et al., 2007)

Nomenclatural Summary:

1868 *Taxites olriki* Heer p. 95, pl. 1, figs. 21–24

1949 *Elatocladus (Taxodites?) tinajorum* (Heer) Bell p. 51, pl. 16, fig. 3

1962 *Taxodium olriki* (Heer) Brown p. 50, pl. 10, figs. 7, 11, 15; pl. 11, figs. 4–6.

Material: Morphotype MT005 is represented by 10 specimens, exemplars are UWBM PB 103629, 97830, and 96597.1.

Morphotype Quality: MQI is 2; EQI is NA.

Diagnosis: Axes thin and infrequently branching. Needle-like leaves alternately arranged along branch; leaves held at a moderate angle to axis. Leaves narrow and long.

Description: Axes thin and long, with apparently infrequent branching. Leaves arranged alternately and held at a moderate angle (22.5º on average) to the axis. Leaves widely spaced along the branch, with a few millimeters between each leaf attachment in most cases. Leaf attachment decurrent to abrupt. Leaves narrow and long; 8.5 by 0.8 mm on average from type specimen. Leaf shape linear with acute apex and single midvein.

Remarks: Several distinctive features distinguish specimens of this morphotype from other species described here. Leaves are held at a moderate angle to the branch (22.5º on average), intermediate between the average angles of MT002 and MT004. Leaves are narrow and long (8.5 by 0.8 mm on average from type specimen), whereas average leaf dimensions for MT002 are shorter (6.8 by 0.5 mm) and for MT004 are shorter and wider (6 by 1 mm). There is some variation in dimensions of these leaves; type specimen UWBM PB 96597.1 is an outlier in leaf

length (15.8 by 0.7 mm on average). However, given the small sample size and partial preservation, we accept this variability as reasonable phenotypic variation.

Branches of this morphotype most closely match the description of *Taxodium olriki* given by Brown (1962) and Johnson (1989). Brown (1962) particularly notes the alternate arrangement, pointed apex, and decurrent attachment of leaves in this species, which closely matches the material collected from this locality.

Family uncertain

Morphotype: MT006; Figure 2.6C.

Material: Morphotype MT006 is represented by one specimen, UWBM PB 96527.

Morphotype Quality: MQI is 4; EQI is NA.

Diagnosis: Thick axis with wide, long, needle-like leaves oppositely arranged. Leaves held at wide angle from axis, widely spaced along axis. Leaf shape oblong with rounded apex.

Description: Axis wide (approximately 1mm) with needle-like leaves oppositely arranged and widely spaced along branch. Spacing of leaves decreases distally, from roughly 5 to 2 mm. Base of lamina forms wide angle with axis (50.5º on average). However, leaves curve towards base along their length such that angle from apex of leaf to its point of attachment 36.1º on average. Leaves wide and long (15.7 by 2.1 mm on average). Leaf shape oblong but nearly linear; distal end tapered, and apex rounded to blunt.

Remarks: This single specimen shows unusually long and wide needle-like leaves. Although the length overlaps with that of *Metasequoia occidentalis*, *Metasequoia* sp., and *Taxodium olriki* described by Johnson (1989), the width of the leaves of MT006 exceeds that of any of the above

taxa. This does not appear to reasonably match any of the conifer taxa described from the Late Cretaceous of North America; however, the partial nature of this single specimen may be obscuring diagnostic features. Further study may indicate that this morphotype is more accurately a larger example of *Metasequoia occidentalis* (MT002).

Class GINKGOPSIDA

Order GINKGOALES

Family GINKGOACEAE Engler

Genus *GINKGO* Linnaeus, 1771

Ginkgo adiantoides (Unger) Seward, 1963

Morphotype: MT007; Figure 2.6D, E.

Synonymous Morphotypes: FP001 (Arens and Allen, 2014); HC114 (Johnson, 1989, 2002).

Nomenclatural Summary:

1850 *Salisburia adiantoides* Unger p. 163, pl. 1, fig. 1; pl. 6, fig. 18; pl. 7, fig. 2

1878 *Ginkgo adiantoides* (Unger) Heer p. 21, pl. 2, figs. 7–10

1963 *Ginkgoites obovate* (Nathorst) Seward p. 12

1963 *Ginkgo adiantoides* (Unger) Seward p. 29.

Material: Morphotype MT007 is represented by 14 specimens, exemplars are UWBM PB 97838.4 and 96540.

Morphotype Quality Index: MQI is 2; EQI is NA.

Diagnosis: Fan-shaped to orbiculate lamina with dichotomizing venation, size generally notophyll.

Description: Leaf lamina fan-shaped to orbiculate, size generally notophyll. Fan-shaped type often with erose margin at apex. Orbiculate shape known from a single specimen (UWBM PB 97838.4). Veins dichotomizing, or primary venation dichotomizing.

Remarks: *Ginkgo* taxa from the Western Interior during the Late Cretaceous and early Paleogene have been universally ascribed to *Ginkgo adiantoides*. Although most specimens here assigned to MT007 align with the shape and venation of *G. adiantoides* as described elsewhere in the Western Interior (e.g., Hickey, 1977; Johnson, 1989, 2002; Arens and Allen, 2014), one specimen (UWBM PB 97838.4) shows an unusual ovate shape rather than the typical fan shape. Based on the range of leaf shape seen in the extant *G. biloba* species, we believe this is a reasonable variation to find in fossil *G. adiantoides* specimens, although this appears to be a novel occurrence of the characteristic in this taxon. Many of the specimens assigned to MT007 are partial lamina for which shape, including petiole insertion and length, is unknown; thus, venation was used as a diagnostic feature when identifying specimens of this morphotype.

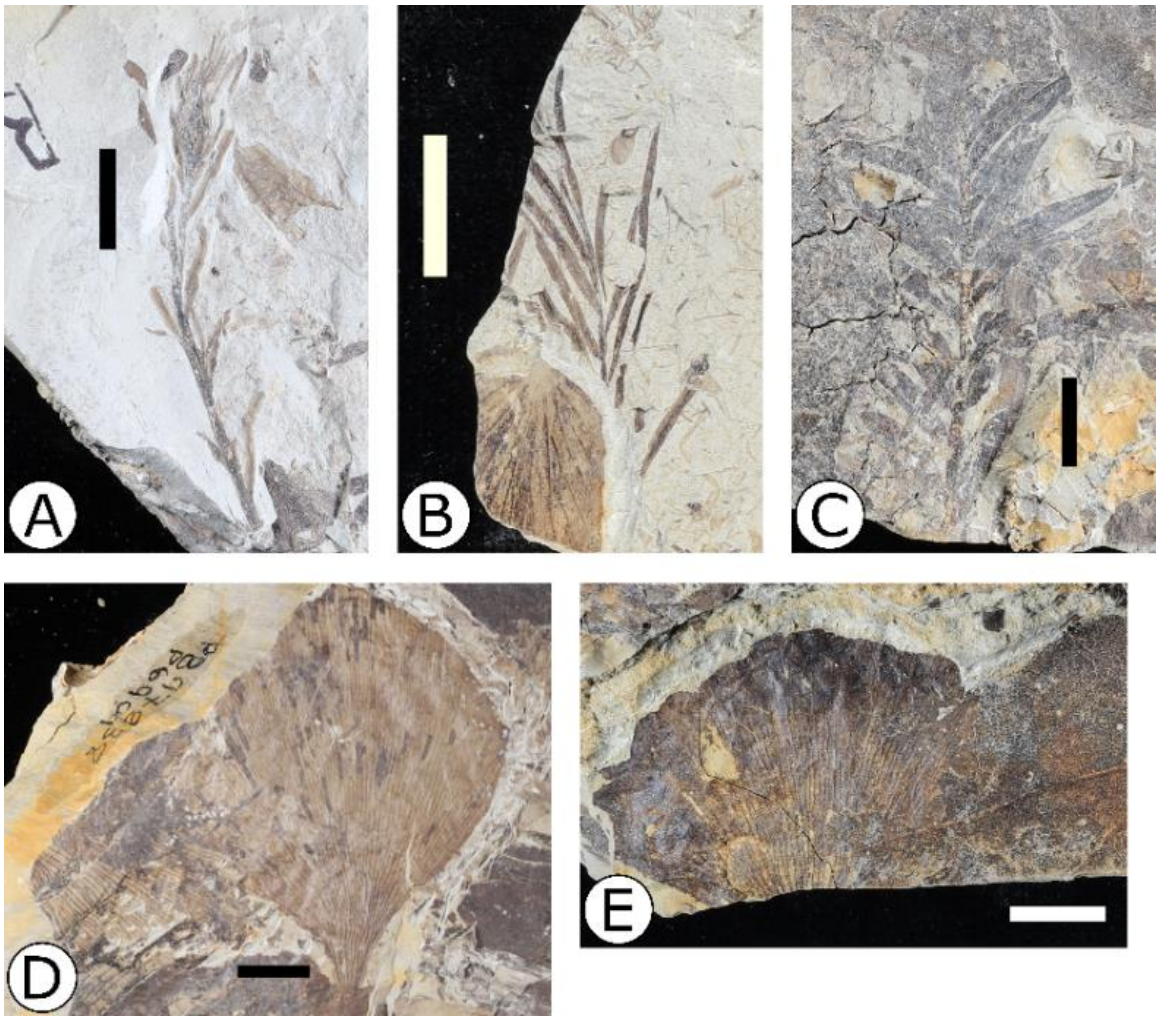

Figure 2.6 Gymnosperm morphotypes; (A-B) MT005 *Taxodium olriki*, A—University of Washington Burke Museum (UWBM) specimen PB 103621.2, B—UWBM PB 96597.1; (C) MT006 Coniferales sp., UWBM PB 96527; (D-E) MT007 *Ginkgo adiantoides*, D—UWBM PB 97838.4, E—UWBM PB 96540. Scale bar 1 cm.

Phylum ANTHOPHYTA

Class LILIOPSIDA

Subclass ARECIDAE

Order ALISMATALES

Family ARACEAE Jussieu, *nom. cons.*

Genus *COBBANIA* Stockey et al., 2007

Cobbania corrugata (Lesquereux) Stockey et al., 2007

Morphotype: MT008: Figure 2.7A.

Synonymous Morphotypes: HC077 (Johnson, 1989, 2002).

Nomenclatural Summary:

1876 *Pistia corrugata* Lesquereux p. 299.

2007 *Cobbania corrugata* (Lesquereux) Stockey et al. p. 611, figs. 1–13

Material: Morphotype MT008 is represented by one specimen, UWBM PB 103629.

Morphotype Quality: MQI is 5; EQI is 3.

Diagnosis: Lamina with distinctive orbiculate shape. Central region with flabellate palmate primary venation and composite epimedial tertiaries which form a "ladder-like" framework of secondary and tertiary gauge between primaries. Central region surrounded by distinctive laminar rim with anastomosing tertiary venation. Margin entire.

Description: Nearly orbicular (slightly elliptical) lamina of notophyll size. Margin entire and somewhat sinuous. Apex and base angles obtuse and shapes rounded. Four or more flabellate palmate basal primary veins diverge at relatively low angles from each other and anastomize and dichotomize distally. Veins of secondary gauge between, and parallel with, primaries are inter-secondaries, spaced approximately one per major intercostal region. Inter-secondaries lose gauge towards the margin and branch to join tertiary framework. Tertiary venation composite epimedial reticulate: veins of smaller gauge depart perpendicular to inter-secondaries and form a regular reticulate fabric. Overall appearance of this venation a "ladder-like" mesh between primaries composed of inter-secondary and tertiary veins. Exterior laminar ring approximately 8 mm wide. No primary veins extend to exterior ring; minor secondaries run approximately parallel to margin

along this exterior laminar ring, and exterior tertiaries extend from these minor secondaries and form closed loops towards the margin. Margin entire.

Remarks: This morphotype is represented by a single specimen but its unusual tertiary fabric and primary and inter-secondary framework distinguish this specimen from any other palmate, elliptic morphotype recovered from this locality and justify a new morphotype designation.

Johnson (1989) described *Pistia corrugata* with a thin rim displaying reticulate venation and a central orbicular region with flabellate venation. Although the specimen ascribed to MT008 here is partial, it matches closely with this description. Recent work has determined that this taxon constitutes a novel genus, *Cobbania,* of floating aquatic plants with rosettes of orbicular leaves and a marginal rim (Stockey et al., 2007). We apply this current species name, *C. corrugata*, to this taxon (Stockey et al., 2007). The exterior laminar ring present on this specimen matches the circular rim described by Stockey et al. (2007); lateral tertiary-gauge veins dichotomize along this rim While the one specimen of this morphotype is very partial, this circular, exterior ring is highly diagnostic and may indicate a difference in thickness, with a thicker, fleshier lamina in the mid-region. Based on the descriptions by Stockey et al. (2007), this specimen likely preserves the adaxial venation pattern.

Class MAGNOLIOPSIDA

Subclass SAXIFRAGALES or TROCHODENDRALES

Family uncertain

Morphotype: MT011; Figure 2.7B, C.

Material: Morphotype MT011 is represented by 37 specimens, exemplars are UWBM PB 103640.3 and 103745.2.

Morphotype Quality: MQI is 2; EQI is 4.

Diagnosis: Microphyll leaf with laminar shape typically elliptic, ranging from orbiculate to oblate. Apex shape variable (truncate, rounded, or acute convex) with small gland. Primary venation basal actinodromous palmate with three distinctive primaries and looping exterior tertiaries. Primary veins lose gauge by attenuation towards apex. Margin entire.

Description: Size generally microphyll. Lamina shape elliptic but highly variable; length to width ratio varies from 0.9:1 to 1.4:1, orbicular to oblate (3.4 cm long and 3.0 cm wide on average). Base angle obtuse and shape rounded or convex. Apex variable: usually angle obtuse and shape rounded to reflex, sometimes angle acute and shape convex. Apex presents indentation with small (~0.5 mm) cassidate gland. Primary venation is basal actinodromous with three distinctive basal primary veins and two lateral secondary veins emerging near the base. Lateral primaries looping; central primary reaches small gland at apex. Series of agrophic secondary veins forming series of loops. No secondaries emerge from the central primary in the proximal half of length. Intercostal tertiary veins regular to irregular reticulate; exterior tertiaries looping. Margin entire.

Remarks: This morphotype has a large variability in shape characteristics; further study may indicate that this group should be split into additional morphotypes. Venation typically consists of three primaries with loops of lesser gauge leading out distally from the base; this pattern could, alternatively, be interpreted in some specimens as a single midvein with two larger secondary veins leaving from the base and looping minor secondaries.

There is also some overlap in shape and venation with MT012 and MT010: all three morphotypes are elliptic in shape with three primary veins. However, margin type and detailed venation justify MT011 as a separate morphotype. For example, the entire margin of specimens within MT011 distinguish these specimens from MT012. The prominent teeth on the margin of MT012 are highly diagnostic, although poorly preserved specimens with obscured margins may make it difficult to distinguish between MT011 and MT012. MT011 specimens also display a prominent gland at the apex andminor secondaries forming loops along the margin; these features further separate MT011 from MT012. MT011 specimens also show a variability in base and apex shape: base can range from acute concavo-convex to rounded, while apex can be acute to obtuse rounded. MT010 overlaps these shape characteristics but is distinguished based on venation. Overall, we recognize that distinguishing between MT012 and MT011 can be difficult, and some specimens were unidentifiable to one specific morphotype and are not included in abundance counts.

In comparing these specimens with similar taxa from the study area we were unable to clearly assign this taxon to a known species or morphotype. There is significant overlap between characteristics of MT011 and several taxa described by Johnson (1989), however the unique apical gland and rounded base and apex set MT011 apart. The most compelling comparison is with morphotype HC43 of Johnson (1989); however, this taxon is described having large teeth bordering on lobes, which are absent in MT011 and Johnson makes no mention of the conspicuous gland noted above.

MT011, along with MT012 and MT010, has a strong resemblance to several of the "*Cercidiphyllum genetrix* complex" members as described by Hickey (1977). Based on the descriptions there given, we align this morphotype most closely with *Cercidiphyllum genetrix*,

however *C. genetrix* is most frequently toothed, rarely entire. Besides this major difference, however, the two taxa share a glandular margin, basal actinodromous primaries, huge variability in shape, looping secondaries marginal to the lateral primaries. This taxon is also similar to *Marmarthia pearsonii* (Johnson, 1996) in the elliptic shape, three primaries, and lateral brochidodromous secondaries nearly forming a knitted intramarginal vein. However, *M. pearsonii* does not appear to have the apicular gland prominent in most MT011 specimens, and the length to width ratio of *M. pearsonii* is characteristically greater than 2.5 (Johnson, 1996), much larger than specimens of MT011.

Given the similarities between MT011 and MT012 (see below), and the uncertainty around this morphotype's affinity, we tentatively place this in the Saxifragales (referred to by Johnson (1989) as Cercidiphyllales) or Trochodendrales.

cf. *Zizyphoides flabella* (Newberry) Crane, Manchester, and Dilcher, 1991

Morphotype Designation: MT012; Figure 2.7D.

Synonymous Morphotypes: cf. FU43 (Johnson, 1989, 2002).

Nomenclatural Summary:

1898 *Populus flabella* Newberry p. 44, pl. 20, fig. 4

1868 *Paliurus colombi* Heer p. 122, pl. 17, fig. 2D, pl. 19, figs. 2–4

1935 *Zizyphoides colombi* Seward and Conway p. 23, text fig. 8

1868 *Populus arctica* Heer p. 100, pl. 5, figs. 1a, 3, 8, 11

1898 *Populus rotundifolia* Newberry p. 51, pl. 29, figs. 1–4

1936 *Piper controvertabilis* Hollick [part] p. 59, pl. 114, fig. 5

1939 *Cercidiphyllum articum* (Heer) Brown [part] p. 492, pl. 53, figs. 3, 4

1966 *Cocculus flabella* (Newberry) Wolfe p. B9, pl. 1, fig. 1A

1977 "*Cocculus" flabella* Hickey p. 125, pl. 24, figs. 2–4, pl. 25, fig. 1

1977 *Menispermites parvareolatus* Hickey p. 126, 127, pl. 24, figs. 5, 6

1970 *Cocculus ezoensis* Tanai p. 479, pl. 11, figs. 1, 5, pl. 12, fig. 2

1974 *Cercidiphyllum cuneatum* (Newberry) Chandrasekharam p. 21, pl. 14, figs. 96–98, 100, 101, pls. 15–19

1974 *Trochodendroides kryshtofovichii* (Iljinskaja) Iljinskaja p. 121–122, pl. 47, figs. 1, 2, pl. 51, figs. 1–3, text fig. 76

1991 *Zizyphoides flabella* (Newberry) Crane et al. p. 1322, figs. 42–57.

Material: Morphotype MT012 is represented by six specimens, exemplars are UWBM PB 103691 and 103705.2.

Morphotype Quality: MQI is 2; **E**QI is 4.

Diagnosis: Size microphyll, leaf shape generally orbicular or elliptical. Primary venation basal actinodromous palmate; lateral secondaries form closed loops. Distinguished by teeth along the upper half of the leaf. Teeth small, approximately two per centimeter, with rounded sinuses and convex flanks.

Description: Leaves microphyll in size and orbicular or elliptical in shape. Length to width ratio between 1:1 and 1.3:1. Average lamina 2.8 cm long by 2.5 cm wide (based on subset of three mostly complete specimens). Base angle obtuse and shape convex or concavo-convex towards petiole. Apex angle obtuse and shape apparently round. Primary venation basal actinodromous palmate with three primary veins and two basal, lateral secondary veins. Primaries lose gauge towards apex. Secondary framework brochidodromous. Lateral secondaries form loops of lesser

gauge towards margin. Inter-marginal tertiary veins regular reticulate within these loops and exterior tertiaries looping towards margin. Small teeth along upper half of leaf. Teeth small, approximately two per centimeter. Sinuses between teeth rounded and flanks of each tooth concave; overall rounded appearance. Teeth vary between dentate and serrate orientation but most often crenate apices. No other obvious marginal features or glands.

Remarks: We interpret the venation of these leaves as palmate with three primaries and two lateral secondaries emerging from the base. However, these lateral secondaries approach the gauge of primaries; an alternative interpretation is that these veins are five primaries.

Similar to MT010 and MT011, this morphotype shows some variability in shape characteristics, although noticeably less variation is observed than in MT011. There is significant overlap among all of these morphotypes in leaf shape as well as apex and base shape. However, MT012 displays distinctive teeth which are used as the basis for this new morphotype.

In comparison with known taxa from the study area, we are unable to definitively assign this morphotype to a known taxon. Similar to MT011, there are several morphotypes described by Johnson (1989) which superficially resemble MT011, however the small serrate teeth set this morphotype apart in each of these comparisons.

MT012, along with MT011 and MT010, has a strong resemblance to several of the "*Cercidiphyllum genetrix* complex" members as described by Hickey (1977). Based on these designations, MT012 most closely resembles *Zizyphoides flabella* (Newberry) Crane, Manchester, and Dilcher (Crane et al., 1991) (described as *Menispermites parvareolatus* by Hickey, 1977). Johnson describes this taxon from North Dakota (*"Cocculus" flabella* FU43, formerly HC16) (Johnson, 1989, 2002). This comparison is the most compelling; MT012 conforms to the descriptions of *Z. flabella* in its orbicular to elliptical shape, microphyll size,

three basal primaries and lateral brochidodromous secondaries, and the dentate teeth on the upper half. However, MT012 apparently lacks the glands typical of *Z. flabella* and the tooth size is distinctly smaller than noted by Johnson (1989). According to Johnson, *Z. flabella* is typical of Paleocene deposits and only known as a Lazarus taxon (Jablonski, 1986) in the Cretaceous of North Dakota (Johnson, 1989). Based on these similarities, and recognizing the inexact match, we place this taxon as cf. *Z. flabella*.

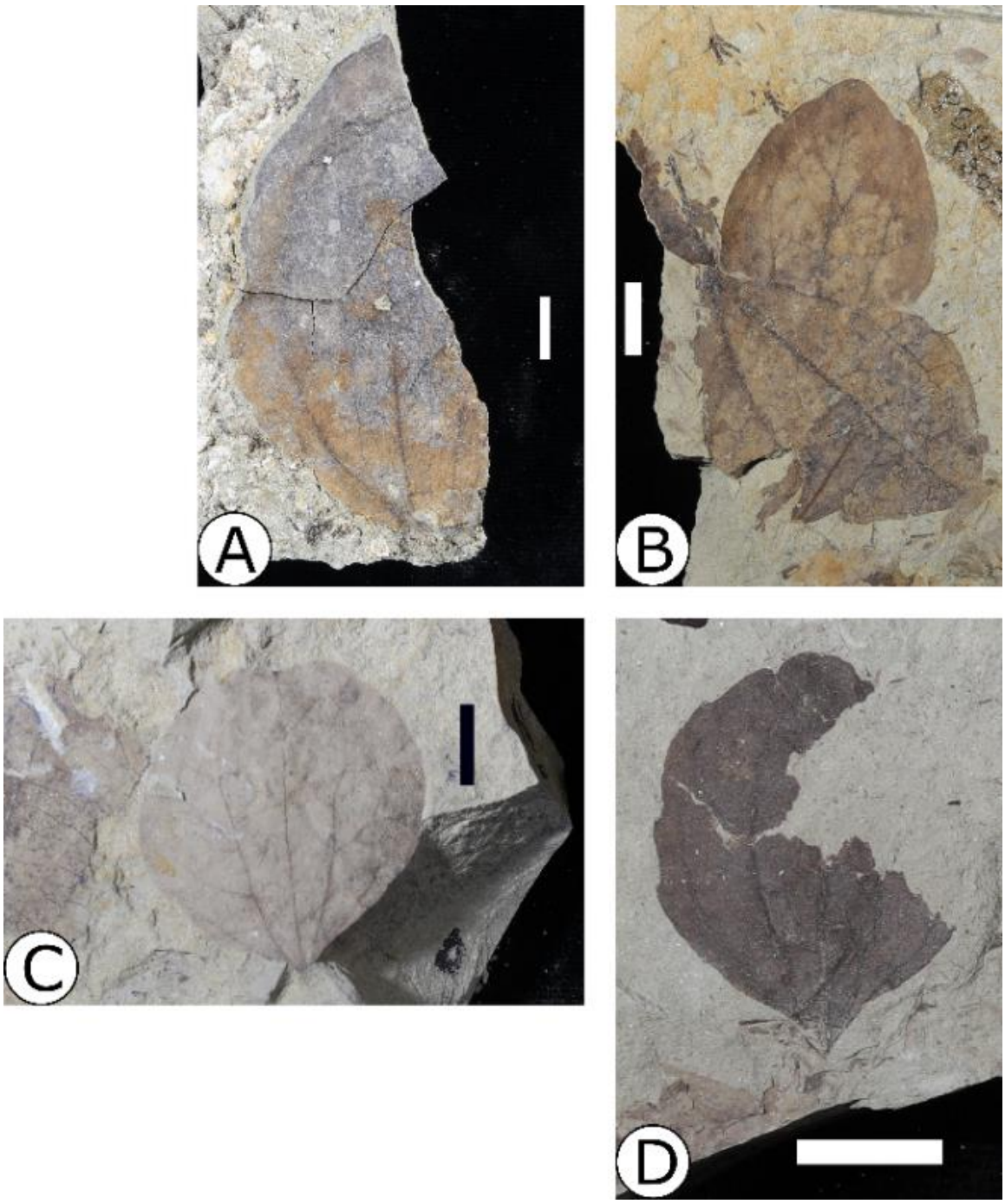

Figure 2.7 Angiosperm morphotypes; (A) MT008 *Cobbania corrugata*, UWBM PB 103629; (B-C) MT011 aff. Saxifrigales/Trochodendrales?, B—UWBM PB 103470.1, C—UWBM PB 103640.3; (D) MT012 cf. *Zizyphoides flabella*, UWBM PB 103691. Scale bar 1 cm.

Order PROTEALES Berchtold and J. Presl

Family PLATANACEAE T. Lestibudois, *nom. cons.*

Genus *ERLINGDORFIA* Johnson, 1996

Erlingdorfia montana (Brown) Johnson, 1996

Morphotype: MT009; Figure 2.8A.

Synonymous Morphotypes: HC57 (Johnson, 1989, 2002); FP005 (Arens and Allen, 2014).

Nomenclatural Summary:

1939 *Sassafras montana* Brown p. 250, pl. 52, fig. 4; pl. 55, fig. 4b

1942 *Platanophyllum montanum* (Brown) Dorf p. 136, pl. 9, figs. 1, 4

1996 *Erlingdorfia montana* (Brown) Johnson p. 7, figs. 60–77.

Material: Morphotype MT009 is represented by one specimen, UWBM PB 96537.

Morphotype Quality: MQI is 3; EQI is 4.

Diagnosis: Palmately lobed leaf. Lobes asymmetric, entire, and elliptic in shape. Indeterminate palmate primary framework and simple brochidodromous secondaries. Margin entire.

Description: Lamina size approximately mesophyll. Palmately lobed. Observed lateral lobe elliptic in shape and asymmetric around primary, with two-thirds of lamina on medial side. Lobe apex acute and rounded, and margin entire. Venation palmate with unknown number of primaries. Simple brochidodromous secondary veins spaced regularly and with decurrent attachment to primaries. Tertiary veins irregular reticulate with finer quaternary fabric also irregular reticulate. Margin entire.

Remarks: This morphotype is distinctive, despite being represented by only a single specimen. The asymmetry and shape of the margin where torn indicate that this specimen is part of a palmately lobed leaf, which is unique at this locality. The morphology of this specimen is closely aligned with a terminal leaflet of *Erlingdorfia montana* as described by Johnson (1989, 1996,

2002). *E. montana* is described as pinnately compound, with the terminal leaflet being three-lobed with deep, unequal sinuses and the lateral leaflet having two lobes and appearing "mitten" like (Johnson, 1996). Johnson specified HC57 as the terminal leaflet and HC64 as the lateral leaflet (1989). This specimen appears to represent the lateral lobe of one of these terminal leaflets. Dorf (1942) typified the taxon as having a dentate margin and noted this as a common feature among specimens of this taxon from the Western Interior. Johnson (1996) considers the margin either entire or toothed, and Arens and Allen (2014) describe an entire margin. Our specimen more closely resembles the description of Arens and Allen (2014) and Johnson (1996).

aff. PLATANACEAE T. Lestibudois, *nom. cons.*

Genus uncertain

Morphotype: MT021; Figure 2.8D.

Material: Morphotype MT021 is represented by two specimens, exemplar is UWBM PB 105324.

Nomenclatural Summary: aff. Platanaceae.

Morphotype Quality: MQI is 1; EQI is 3.

Diagnosis: Size approximately microphyll. Indeterminate shape. Primary venation pinnate, secondary venation semicraspedodromous, tertiary venation ramifying, and quaternary venation regular reticulate. Margin toothed; teeth dentate in shape, spaced approximately four per centimeter.

Description: Size approximately microphyll. Indeterminate shape. Apex angle obtuse and shape round; lamina roughly symmetric around midvein. Laminar dimensions 4.4 cm wide and at least

2.3 cm long (true length likely at least twice this measurement). Primary venation pinnate and secondary venation semicraspedodromous. Secondaries excurrent to midvein, oppositely arranged, evenly spaced, and at roughly equal angle along length of midvein. Major secondaries almost equal gauge to midvein proximally but lose gauge by attenuation towards margin and branch into two or more veins which ultimately terminate at apex of a small tooth. Sometimes major secondaries branch more than once and smaller gauge descendants reach margin at teeth. Tertiary veins transversely ramifying in most cases and oppositely arranged along secondaries. Exterior tertiaries (where present) terminate at teeth along margin, sometimes the same tooth that an adjacent secondary terminates at. Epimedial tertiary venation likely irregular reticulate where tertiaries eventually join into a net between adjacent secondaries. Fimbrial vein along margin. Quaternary fabric regular reticulate, forming anastomosing network. Margin toothed with dentate teeth protruding less than a millimeter from margin. Vein of secondary or tertiary gauge terminates at apex of each tooth. Apparent gland present at apex of each tooth. Teeth likely of multiple orders; variability in tooth size apparently correlates with gauge of vein reaching that tooth.

Remarks: This morphotype is known only from two very partial specimens at this locality but its distinctive dentate teeth, craspedodromous secondaries, and ramifying tertiaries set this specimen apart as a distinct new morphotype. In comparison with published taxa from this region, MT021 appears unique in the presence of dentate teeth and pinnate primary framework.

Comparison with local published floras does not yield any clear affinity. Teeth and marginal venation are similar to *"Vitis" stantoni* or *Platanites marginata* described by Johnson from North Dakota (Johnson, 1989, 1996, 2002) which are both common taxa in that study region. The venation, teeth, and sinuses seem to align with Platanaceae, so we place this taxon

with affinity to that family. However, given the partial nature of MT021 it is difficult to establish a more definitive affinity at this time.

Family uncertain

Leepierceia preartocarpoides (Brown) Johnson, 1996

Morphotype: MT016: Figure 2.8B, C.

Synonymous Morphotypes: HC86 (Johnson, 1989, 1996, 2002).

Nomenclatural Summary:

1883 *Ficus artocarpoides* Lesquereux Les p. 222, Plate 47, Figs. 1–5

1930 *Sterculia libbeyi* Knowlton p. 117, Plate 53, Fig. 2

1949 *Pterospermites dawsoni* (Knowlton) Bell p. 117, Plate 53, Figs. 1–2

1939 *Ficus preartocarpoides* Brown p. 249, pl. 53, figs. 3–5

1962 *Ficus artocarpoides* auct. non Lesquereux Brown [in part] p. 61–62, pl. 28, fig. 4

1989 "Ficus" artocarpoides (Brown) Johnson pl. 24, figs. 2, 4, pl. 25, figs. 2, 4, pl. 26, fig. 1, pl. 27, figs. 1, 2, text figs. 4–23

1996 *Leepierceia preartocarpoides* (Brown) Johnson p. 10–11, figs. 87–93.

Material: Morphotype MT016 is represented by 44 specimens, exemplars are UWBM PB 99303.1, 96606.2, and 96532.

Morphotype Quality: MQI is 1; EQI is 5.

Diagnosis: Leaf size notophyll to mesophyll. Leaf shape ovate. Apex angle acute and shape straight to acuminate; base angle obtuse to reflex and shape convex to cordate. Primary venation pinnate and secondaries simple brochidodromous, with minor secondaries forming a simple

agrophic network at base. Major secondaries evenly spaced and decurrent to midvein. Tertiary venation mixed percurrent, quaternary fabric reticulate, and quinternary venation reticulate to ramifying. Exterior tertiary veins looping. Marginal secondary often present. Margin entire.

Description: Leaves variable in size, ranging from notophyll to mesophyll; shape consistently ovate. Base usually with obtuse angle and convex shape but may be reflex angle and cordate shape. Rarely, asymmetric basal petiole insertion. Apex angle acute and shape either straight or rarely acuminate with possible drip tip at apex. Lamina symmetric around midvein at median and base. Primary venation pinnate and secondary veins simple brochidodromous. Major secondaries lose gauge towards margin and loop towards other major secondaries. Major secondaries roughly evenly spaced with consistent angle and decurrent attachment to midvein. Exterior tertiaries form loops of higher gauge leading out towards margin. Commonly, marginal secondary vein along leaf margin. Minor secondaries near base form a series of looped agrophic veins towards margin. Intercostal tertiary venation mixed percurrent and epimedial tertiaries perpendicular to midvein and then basiflexed. Quaternary fabric regular reticulate, and quinternary fabric either reticulate or ramified. Margin entire.

Remarks: Specimens of this morphotype show extremely consistent and distinctive venation: pinnate primary veins and simple brochidodromous secondary veins with minor secondaries forming agrophics. The shape is also consistently ovate with an acute tip and obtuse rounded or slightly cordate base. However, the size of specimens assigned to this morphotype can vary drastically. On average, specimens within this morphotype are 14.8 cm long and 6.4 cm wide with a length to width ratio of 2.3:1. However, standard deviation of these dimensions is +/- 7.9 cm length and +/- 2.9 cm width, showing a wide spread in values. Specimens within this morphotype tend to cluster into three size categories: smallest between 6.4 and 9.9 cm long,

medium between 12.2 and 14 cm long, and largest between 18.3 and 33 cm long (one-way ANOVA resulted in $p<0.001$). However, length to width ratio remains consistent across all three size classes and does not explain the variance between them (one-way ANOVA resulted in $p=0.5062$). This indicates that shape (as estimated by length to width ratio) is consistent across all specimens included in MT016 but that there may be discrete size categories which should be distinguished as separate morphotypes. We suggest further analysis of specimens from this study area to investigate.

The agrophic network, brochidodromous secondaries, and ovate shape distinguish this morphotype and separate it from most other taxa described from the study area. Several taxa described by Johnson (1989, 2002) are similar but lack the agrophics noted here (e.g., HC72, HC281). Other morphotypes described by Johnson (1989, 2002; personal communication, January 18, 2018) have wider spacing or angle of secondary attachment to midvein (e.g., HC250, HC346, HC120, FU 60).

Leepierceia preartocarpoides (Brown) Johnson (Johnson, 1989, 1996, 2002; Arens and Allen, 2014) is remarkably similar to MT016 in venation and shape characteristics and is one of the most common taxa in the HCIa biozone in North Dakota (Johnson, 2002). *L. preartocarpoides* has been described by Johnson (1989, 1996) as lobed or toothed and by Arens and Allen (2014) as toothed, with teeth resembling small lobes. However, according to Johnson (personal communication, June 23, 2019), entire margins are within the realm of variation exhibited by *L. preartocarpoides*. Interestingly, all specimens of this taxon recovered from Seafood Salad exhibit entire margins, although this could be due to taphonomy (i.e. partial preservation). Despite this confusion surrounding the margin of *L. preartocarpoides* we note the similarities in venation, shape, and size and therefore consider MT016 synonymous with this

taxon. Specimens of MT022 also closely resemble *L. preartocarpoides*, and possess the large teeth characteristic of this species, but marginal venation appears to separate MT022 specimens from MT016 specimens and descriptions of *L. preartocarpoides*. Further study may reveal that both morphotypes belong to *L. preartocarpoides*.

Order ROSALES

Family ULMACEAE Mirbel, *nom.cons.*

Genus *CARPITES* Schimper 1874

Carpites ulmiformis Dorf, 1942

Morphotype: MT027: Figure 2.8E, F.

Synonymous Morphotypes: HC54 (Johnson, 1989).

Nomenclatural Summary:

1897, 1930 *Ulmus* sp. Knowlton

1942 *Carpites ulmiformis* Dorf p. 157, pl. 17, figs. 17, 18.

Material: Morphotype MT027 is represented by 19 specimens, exemplar is UWBM PB 96578.2.

Morphotype Quality: MQI is 1; EQI is NA.

Diagnosis: Round, winged samaroid fruit with striations radiating out from central seed.

Description: Samaroid fruit measuring 1.5 to 1.7 cm wide and 1.8 to 2.1 cm long. Wing apex shape cordate or openly notched, base shape more or less elongate. Seed at center elliptic in shape, 0.9 to 1 cm wide by 1.7 to 2 cm long, with an acute, straight base and rounded, obtuse apex. Wing broad, approximately 2 to 4 mm wide around margin of seed, decreasing in width

towards base and apex. Striations along margin of wing radiate from seed to wing margin; striations angled roughly perpendicular to seed margin.

Remarks: Shape and wing characteristics of this morphotype are clearly aligned with *Carpites ulmiformis* as described by Johnson (1989) and Dorf (1942).

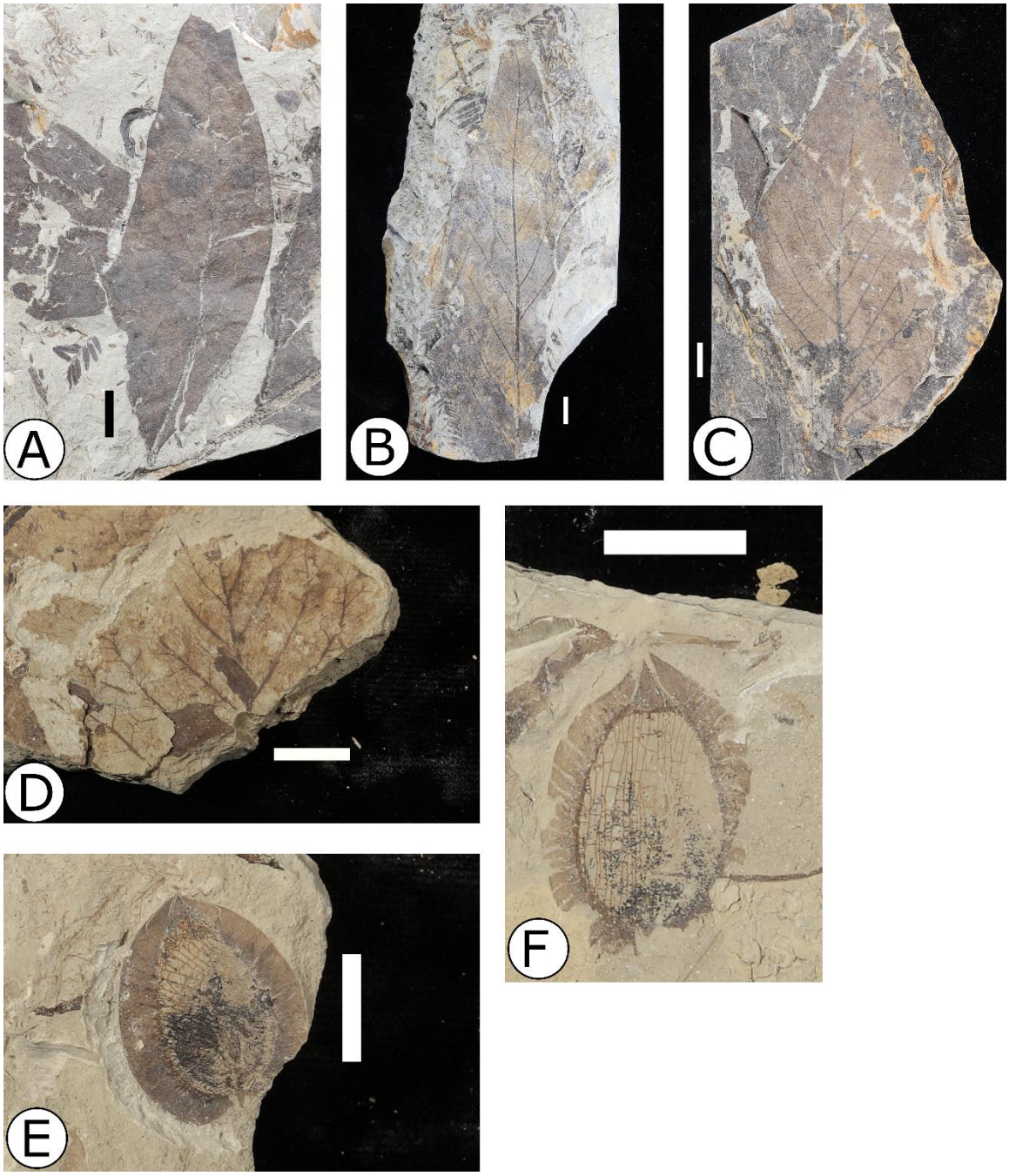

Figure 2.8 Angiosperm morphotypes; (A) MT009 *Erlingdorfia montana*, UWBM PB 96537; (B-C) MT016 *Leeperceia preartocarpoides*, B—UWBM PB 96606.2, C—UWBM PB 96532; (D) MT021 unidentified morphotype, UWBM PB 105324; (E-F) MT027 *Carpites ulmiformis*, E—UWBM PB 96578.2, F—UWBM PB 96570.1. Scale bar 1 cm.

Subclass ROSIDAE

Order SAPINDALES

Family uncertain

"Dryophyllum" subfalcatum (Lesqueruex) Johnson, 1989

Morphotype: MT023: Figure 2.9A, B.

Synonymous Morphotypes: FP008 (Arens and Allen, 2014); HC49 (Johnson, 1989, 2002).

Nomenclatural Summary:

1878 *Dryophyllum (Quercus) subfalcatum* Lesquereux p. 163, pl. LXIII, fig. 10; Dorf 1938 p. 51, pl. 5, figs. 1, 2, 6; 1942 p. 135, pl. 8, figs. 2, 4, 6, 7

1942 *Dryophyllum subfalcatum* (Lesquereux) Dorf p. 51–52, 135, pl. 5, figs. 1, 2, 6, pl. 8, figs. 2, 4, 6, 7

1942 *Salix lancensis* (Berry) Dorf p. 134, pl. 7, figs. 2, 5, 7, 8; pl. 8, fig. 3

1989 "*Dryophyllum" subfalcatum* (Lesqueruex) Johnson p. 248, pl. 22, figs. 5–10.

Material: Morphotype MT023 is represented by 32 specimens, exemplars are UWBM PB 96565, 103630, and 96530.

Morphotype Quality: MQI is 2; EQI is 4.

Diagnosis: Leaf elliptic or linear in shape with apex angle acute; base angle acute and shape straight, decurrent, or rounded. Primary venation pinnate with semicraspedodromous secondary framework. Secondary vein spacing gradually increases proximally and angle to midvein also gradually increases proximally. Tertiary veins opposite percurrent. Fimbrial vein at margin. Small teeth spaced evenly, roughly one per centimeter along the upper half of leaves.

Description: Leaf shape usually elliptic and size usually notophyll, but shape and size variable. Average length to width ratio 4.4:1. Laminar dimensions range from 3.7 to 19.4 cm long and from 0.9 to 4.5 cm wide, with an average of 9.4 cm long and 2 cm wide. Apex angle acute and

shape straight; base angle acute and shape straight or decurrent, rarely rounded. Primary venation pinnate and secondary framework semicraspedodromous. Major secondaries branch towards margin; proximal branch terminates at apex of a tooth, distal branch joins superjacent secondary. Spacing of major secondaries decreases distally and angle to midvein decreases distally. Major secondaries show excurrent attachment to midvein. Inter-secondaries simple brochidodromous and spaced roughly one per intercostal space. Tertiary venation alternate percurrent and tertiary veins usually perpendicular to the higher order veins. Epimedial tertiaries mixed percurrent, while exterior tertiaries looped towards margin. Fimbrial vein usually present, intersecting looped tertiaries. Quaternary fabric regular reticulate. Margin toothed; small serrate teeth along upper half of lamina. Teeth of a single order; each tooth millimeter scale and spaced no more than one per centimeter. Teeth serrate, with sinuses varying from round to angular. Tooth shape often pointed with straight proximal flank and concave distal flank.

Remarks: This morphotype is similar to other pinnate morphotypes described here but is between the length to width ratios of MT024 and MT020; the shape is generally elliptical but the length to width ratio of specimens in MT023 is 4.4:1 on average. This moderate length to width ratio helps to distinguish MT023 from MT020 and MT024. The teeth on specimens of morphotype MT023 are distinct from those of MT020; they exhibit more rounded sinuses and are often more evenly spaced and frequent. However, the partial nature of many of these specimens inhibits a more precise categorization. In fact, 28 specimens have been placed into an indeterminate group of affinity either with MT023 or MT020 and are therefore not included in specimen abundance counts. Without more complete specimens it is difficult to assess their size and tooth characteristics.

Small teeth along the upper half of the lamina are also reminiscent of MT024. In MT023, however, they are evenly spaced along the margins of the leaf and the apex comes to a fine tip, which distinguishes this morphotype from MT024. The presence of teeth along most of the margin distinguishes specimenns of MT023 from MT024.

The teeth, venation, and shape characteristics observed in MT023 place this morphotype within the species *"Dryophyllum" subfalcatum* described by Johnson (1989, 2002). As noted below, Johnson (1989) recognizes two common species with affinity to this genus from the study area. Our specimens assigned to MT023 more closely resemble *"Dryophyllum" subfalcatum* based on the larger width and semicraspedodromous secondaries. However, it should be noted that MT023 shows some variation in laminar shape and in tooth shape and spacing; some specimens display more dentate teeth or clusters of teeth along the apex rather than spread along the lateral edges as seen in *"Dryophyllum" subfalcatum.* This taxon is noted as a common species in the lower HC biozones in North Dakota (Johnson, 1989) and has been noted at several localities in our study area in the Hell Creek Formation of Montana (P. Wilson, unpublished data).

cf. *"Dryophyllum" tenneseensis* Johnson, 1989

Morphotype: MT020; Figure 2.9C, D.

Synonymous Morphotypes: cf. HC44 (Johnson, 1989, 2002).

Nomenclatural Summary:

1917 *Dryophyllum tenneseensis* Berry *auct. non* Knowlton p. 299, pl. 69, figs. 3–5

1989 *"Dryophyllum" tenneseensis* Johnson p. 247, pl. 22, figs. 2–4.

Material: Morphotype MT020 is represented by 5 specimens, exemplars are UWBM PB 103466.2 and 96553.2.

Morphotype Quality: MQI is 4; EQI is 5.

Diagnosis: Leaf shape linear, apex angle acute and shape straight. Leaves often four to six times as long as they are wide. Venation pinnate with simple brochidodromous secondaries. Small teeth on upper half of leaves.

Description: Linear shape and generally nanophyll to microphyll in size. Leaves over six times longer than wide, with laminar dimensions ranging from 4.2 to 9 cm long and 0.7 to 1.5 cm wide and average length to width ratio 6.4:1. Laminar width sometimes asymmetric at midpoint. Apex angle acute and shape straight. Primary venation pinnate and secondary venation simple brochidodromous to semicraspedodromous. Where margin is toothed, major secondaries branch with one vein looping towards superadjacent major secondary and an accessory vein terminating at tooth apex. Usually marginal secondary or fimbrial vein along margin. Infrequent simple brochidodromous inter-secondaries spaced between teeth; each inter-secondary branches to form a loop of secondary gauge but does not reach margin. Tertiary fabric apparently irregular reticulate. Small teeth along upper half of leaf, increasing in frequency towards apex and spaced approximately 3 per centimeter. Teeth serrate with angular sinuses. Apex of each tooth convex proximally and concave distally with small accessory vein terminating at apex of each tooth.

Remarks: This morphotype displays a distinctive shape which separates it from all other morphotypes identified at this locality. Two specimens of this morphotype show detailed venation down to third order; these specimens are the basis for this morphotype description. All specimens show characteristically large length to width ratio (6.4:1 on average) and consistent tooth morphology, primary framework, and secondary venation. Other morphotypes (e.g.,

MT023) exhibit similar elliptic shape and tooth morphology but are much wider compared to their lengths (see description of MT023 for more information).

Given the poor preservation of these specimens we are unable to definitively assign them to a published taxon. Johnson (1989) describes two taxa with affinity to the genus *"Dryophyllum"* which are similar to MT020. *"Dryophyllum" subfalcatum* is present from this locality (MT023) and *"Dryophyllum" tenneseensis* is extremely common at other localities in the Hell Creek Area of Montana based on our surveys (P. Wilson, unpublished data). However, both *"Dryophyllum"* taxa have distinctive serrate teeth evenly spaced along the margin which are absent or at least irregular in MT020. Given the partial nature of MT020 specimens we cannot definitively place it in either taxon but recognize that it is likely related to the *"Dryophyllum"* taxa described by Johnson (HC44, HC49, HC50, HC109, and HC125) and most closely resembles *"Dryophyllum" tenneseensis* given the large length to width ratio (Johnson, 1989, 2002). Therefore, we refer to it as cf. *"Dryophyllum" tenneseensis*.

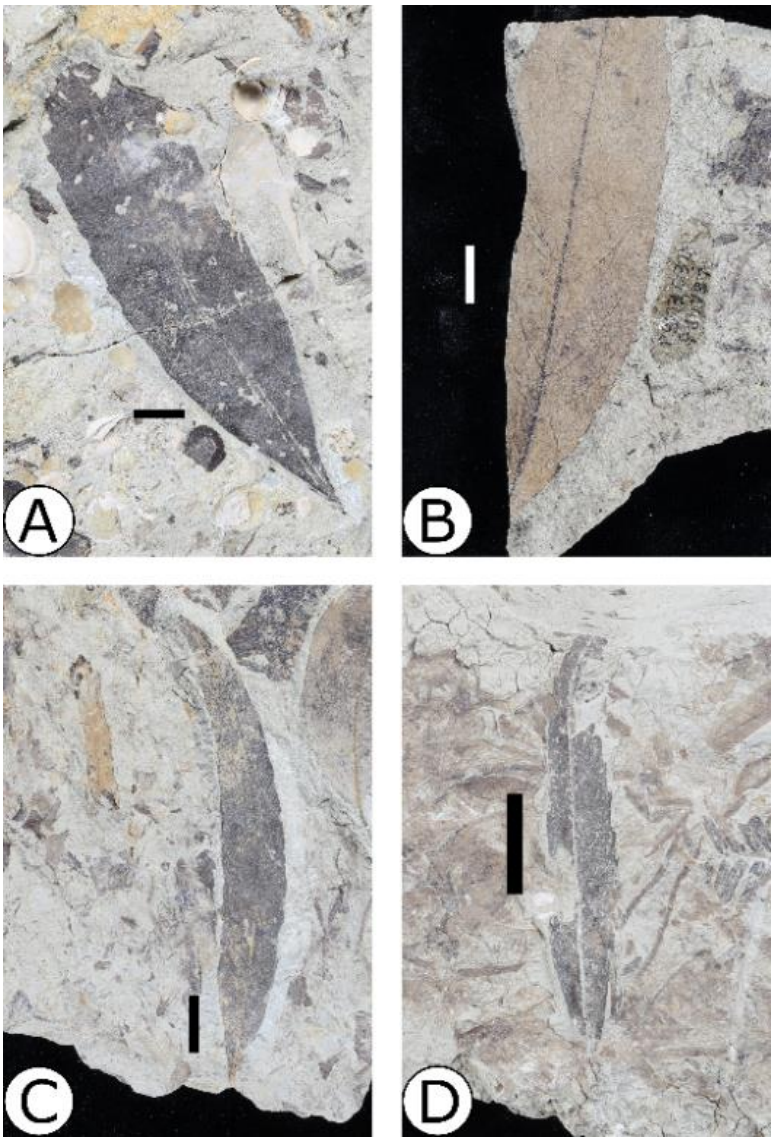

Figure 2.9 Angiosperm morphotypes; (A-B) MT023 *"Dryophyllum" subfalcatum*, A—UWBM PB 99312.3, B—UWBM PB 103630; (C-D) MT020 cf. *"Dryophyllum" tenneseensis*, C—UWBM PB 103466.2, D—UWBM PB 96553.2. Scale bar 1 cm.

Subclass uncertain

Morphotype: MT010; Figure 2.10A.

Material: Morphotype MT010 is represented by one specimen, UWBM PB 97847.1.

Morphotype Quality: MQI is 5; EQI is 3.

Diagnosis: Leaves notophyll and elliptic in shape. Primary venation basal actinodromous palmate with three basal primaries and strong agrophic minor secondaries on proximal half of lamina.

Description: Leaf notophyll in size. Shape roughly orbicular and length to width ratio likely close to or just under 1:1. Base shape rounded and petiole insertion wide and distinct. Primary venation basal actinodromous palmate; three prominent basal primary veins and lateral, basal secondary veins. Major secondary venation indeterminate. Minor secondaries form a series of at least four agrophic veins on each marginal side. Epimedial tertiary veins convex opposite percurrent and basiflexed, with relatively even spacing and angle of attachment to primaries. Exterior tertiaries between agrophic secondaries irregular looped. Quaternary fabric regular reticulate and quinternary fabric freely ramifying. Margin presumed entire.

Remarks: At this locality there is only a single specimen tentatively assigned to this morphotype designation. This specimen is partial but is clearly palmate with three basal actinodromous primaries and simple agrophic secondaries. The notophyll size and rounded base distinguish this specimen from MT011, the entire margin and shape distinguish it from MT012, and the simple agrophic veins are unique to this morphotype. Superficially, this specimen resembles a morphotype which is very common at other localities in this study area (P. Wilson, unpublished data), but further analysis is required to establish affinity.

In comparison with known taxa from the study area, this specimen superficially resembles several common taxa, notably *"Vitis" stantonii*, *"Ficus' planicostata*, and *Marmarthia trivialis* described by Johnson (1989, 1996). There are a suite of taxa described with affinity to *"Vitis" stantonii* and these taxa are common throughout the Late Cretaceous and earliest Paleogene in North Dakota and eastern Montana (e.g., Peppe et al., 2007; Arens and Allen,

2014). However, the rounded base and reticulate quaternary structure of MT010 set this specimen apart from these more common morphotypes. Additionally, the poor preservation of this specimen prevents us from evaluating apex or margin features, which may be obscuring the specimen's affinity.

MT010, along with MT011 and MT012, also has a strong resemblance to several of the "*Cercidiphyllum genetrix* complex" members as described by Hickey (1977). However, MT010 is distinguished by a strong tertiary network preserved as a series of highly arched percurrent tertiaries. These traits more closely align MT010 with Hickey's (1977) description of *Populus*, which is mentioned as being commonly confused with various *Cercidiphyllum*. Given the partial nature of this specimen, we are unable to place it more definitively into one of these taxa.

Genus *QUEREUXIA* Kryshtofovich, 1953

Quereuxia angulaga Kryshtofovich, 1988

Morphotype Designation: MT013; Figure 2.10B.

Synonymous Morphotypes: FU2 (Johnson, 1989, 2002).

Nomenclatural Summary:

1861 *Neuropteris? angulata* Newberry *in* Ives p. 131, pl. 3, fig 5

1878 *Trapa? microphylla* Lesquereux p. 295, pl. 61, figs. 16, 17a

1953 *Quereuxia angulata* Kryshtofovich p. 23, pl. 3, figs. 7–11, pl. 4, figs. 1–8

1959 *Trapa? microphylla* Lee and Li p. 33, p. 37, pl. 1, figs. 2–3, 5–8

1962 *Trapa angulata* (Newberry) Brown p. 83, pl. 58, figs. 1–12

1979 *Quereuxia angulata* (Lesquereux) Kryshtofovich *in* Krassilov 1979 p. 110, pl. 31, figs. 3–6

1983 *Thallites jiayinensis* Zhang p. 116, pl. 8, figs. 6, 7

1988 *Quereuxia angulata* Kryshtofovich Samylina p. 89, pl. 19, fig. 4a; pl. 34, pl. 25, figs. 15b–21

1997 *Trapago angulata* Stockey and Rothwell p. 84, figs. 2–21

2001 *Quereuxia angulata* Kryshtofovich Hickey p. 1119

Material: Morphotype MT013 is represented by 15 specimens, exemplars are UWBM PB 97833.3 and 103640.3.

Morphotype Quality: MQI is 1; EQI is 3.

Diagnosis: Leaves with serrate teeth along margin and basal actinodromous palmate primary veins which dichotomize distally. Secondary veins diverge at low angle forming dichotomizing network. Margin serrate.

Description: Small (microphyll) leaves, approximately 2–2.5 cm in diameter. Oblong-elliptic shape; often length is slightly less than width. Base angle obtuse and shape rounded to truncate; apex similar—angle obtuse and shape rounded to truncate. Primary venation of leaf is basal actinodromous, consisting of 5–10 basal primary veins which dichotomize distally. Major veins terminate at distal flank of each tooth. Secondary veins diverge at low angle and form dichotomizing network. Both orders of vein lose gauge towards margin. Margin toothed; small, serrate teeth spaced approximately four per centimeter. Sinus between teeth rounded and teeth apices straight proximally and concave distally. Teeth most prominent along sides of lamina, and small or non-existent at leaf apex.

Remarks: These specimens are preserved as individual leaves. Based on the strong venation patterns, obovate to elliptical shape, and small serrate teeth along the margin, we ascribe these leaves to the species *Quereuxia angulata*. *Q. angulata* has been found as rosettes of heteromorphic leaves and is interpreted as an aquatic taxon (Stockey and Rothwell, 1997). In some specimens of MT013 the small base preserves a darkened spot that likely marks the insertion point of a petiole. In all these features, the leaves strongly resemble the material described by Stockey and Rothwell (1997). According to Stockey and Rothwell (1997), similar leaves have been ascribed to *Neuropteris* Brongniart, *Trapa* Lesquereux, *Nymphaeites* Sternberg, *Quereuxia* Kryshtofovich, and *Trapago* McIver and Basinger. In North Dakota, Johnson has placed this taxon in *Quereuxia angulata,* following the description and nomenclature of workers in Russia (Johnson, 1989). Recently, workers have disputed whether this taxon belongs in a single genus (*Quereuxia*) or whether the genus *Trapago* is synonymous with North American occurrences of this taxon while *Quereuxia* describes a separate genus with distinct morphology and restricted to Russia (Stockey and Rothwell, 1997). Indeed, Stockey and Rothwell (1997) note at least eight different morphologies of *Trapago angulata* leaves depending on placement within the rosette, displaying a high degree of plasticity and potentially creating this confusion over the proper circumscription of the genus. We follow the more recent work of Hickey (2001) in reconciling these disparate names under the genus *Quereuxia.* Although we cannot speculate on the affinity of the various specimens from Russia to North America whose placement in this genus has been disputed, our material clearly matches the description of the species *Quereuxia angulata* by Johnson (1989, 2002).

Genus uncertain

Morphotype Designation: MT014; Figure 2.10C.

Material: Morphotype MT014 is represented by one specimen, UWBM PB 96536.2.

Morphotype Quality: MQI is 4; EQI is 4.

Diagnosis: Leaf mesophyll in size, pinnately lobed. Primary venation pinnate, each lobe supported by a single secondary vein. Minor secondaries form loops of much smaller gauge on at least one side of the major secondaries, with tertiary and quaternary fabric regular to irregular reticulate. Margin entire.

Description: Leaf mesophyll in size with thin, long pinnate lobes (approximately 1 cm wide and 7 cm long). Deeply cut sinuses between lobes reach almost to midvein, leaving only a millimeter-wide strip of lamina. Lobes arranged asymmetrically along midvein. Base angle obtuse and shape concave to decurrent. Primary venation pinnate; midvein distinct and wide (2–3 mm). Major secondary veins support lobes and are opposite or slightly offset along midvein. Along length of each lobe major secondaries are asymmetrically oriented on lobe lamina. Minor secondaries form series of closed loops which almost reach margin. Intramarginal secondary along entire leaf margin. Tertiary and quaternary fabrics reticulate, regular and irregular patterning in parts. Margin entire.

Remarks: This morphotype is represented by a single specimen from this locality but is distinct in being the only pinnately lobed lamina recovered from this site. The pinnate primary framework of MT014 is distinct from the only other lobed morphotype recovered from this site, *Erlingdorfia montana* (MT009), as described by Johnson (1996).

Morphotype Designation: MT015; Figure 2.10D.

Material: Morphotype MT015 is represented by one specimen, UWBM PB 96539.

Morphotype Quality: MQI is 4; EQI is 4.

Diagnosis: Leaf microphyll with ovate shape and strong pinnate venation. Tertiary and quaternary fabrics regular reticulate, and margin entire.

Description: Leaf microphyll in size with ovate shape. Base shape cordate. Primary venation pinnate with strong central midvein. Secondary venation apparently eucamptodromous or simple brochidodromous. Secondary veins irregularly spaced, and attachment to midvein excurrent. Intercostal tertiary venation regular reticulate. Distinctive epimedial tertiaries emerge perpendicular to midvein and are straight along their course. Quaternary fabric irregular reticulate. Margin entire.

Remarks: This morphotype is identified by a single specimen from this locality. Although this specimen is highly oxidized and some characteristics are difficult to distinguish, it displays a distinctive reticulate tertiary and quaternary venation and distinct perpendicular epimedial tertiaries which separate it from MT016. MT015 also does not display the asymmetric basal insertion or decurrent secondary attachment seen in MT017.

This specimen resembles several ovate, pinnate morphotypes described by Johnson (1989). However, none of these specimens exhibit the distinctive reticulate venation visible in MT015. The partial nature and poor preservation of this specimen also obscure features of venation, base, and margin which make affinity difficult to ascertain.

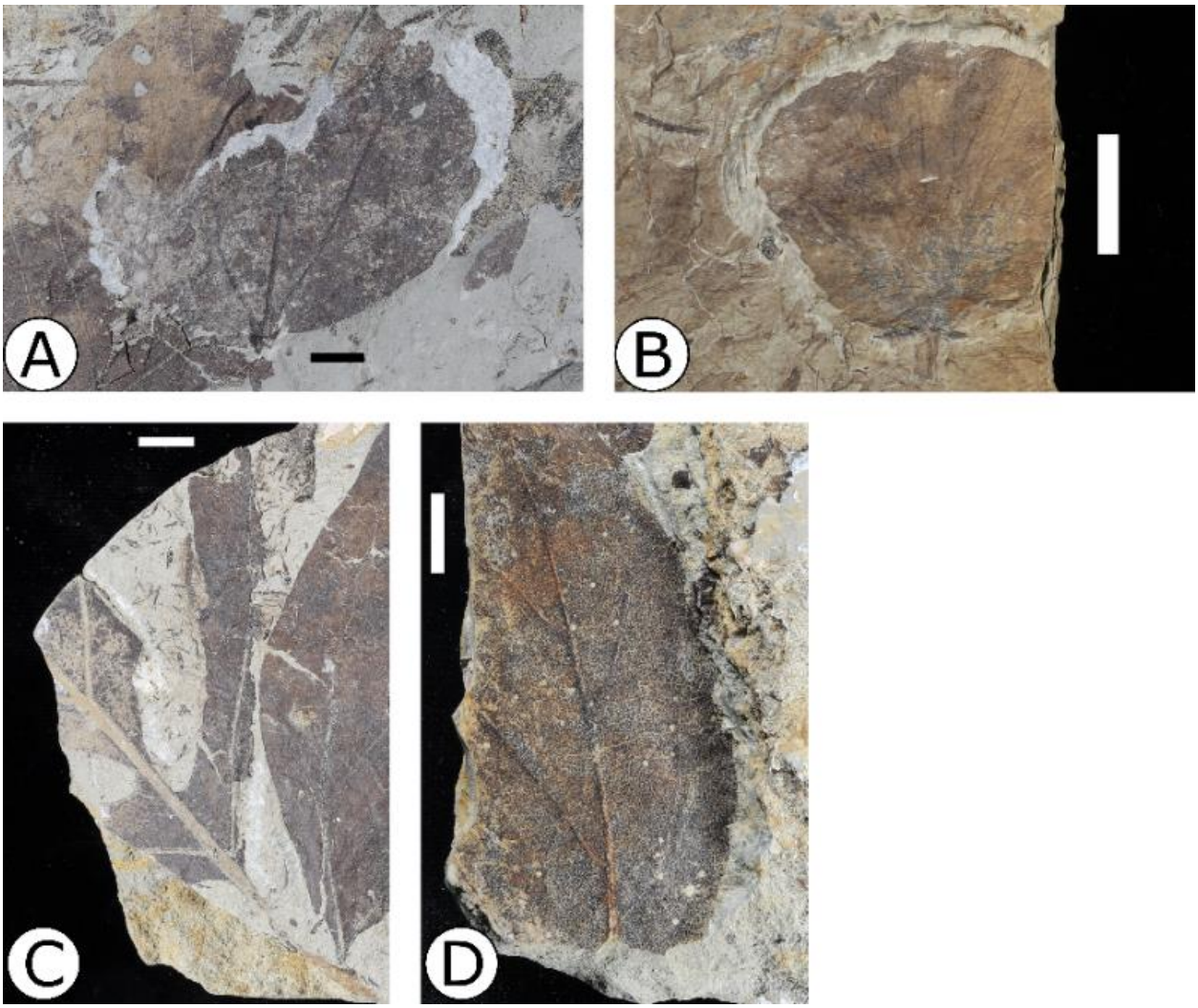

Figure 2.10 Angiosperm morphotypes; (A) MT010 unidentified morphotype, UWBM PB 97847.1; (B) MT013 *Quereuxia angulata*, UWBM PB 97833.3; (C) MT014 unidentified morphotype, UWBM PB 96536.2; (D) MT015 unidentified morphotype, UWBM PB 96539. Scale bar 1 cm.

Morphotype: MT017; Figure 2.11A.

Material: Morphotype MT017 is represented by one specimen, exemplar is UWBM PB 96557.

Morphotype Quality: MQI is 5; EQI is 2.

Diagnosis: Leaf notophyll and ovate in shape. Base angle obtuse and shape rounded with asymmetric basal insertion. Primary venation pinnate and secondaries eucamptodromous

becoming brochidodromous distally. Major secondary spacing increases distally and attachment to midvein decurrent. Marginal secondary vein. Margin entire.

Description: Leaf notophyll in size, measuring approximately 8 cm long (true length likely larger) and 5.5 cm wide. Shape ovate. Base angle obtuse and shape rounded; apex angle apparently acute. Base exhibits slightly asymmetric basal insertion. Primary venation pinnate and secondary veins strongly decurrent to midvein. Secondary framework apparently eucamptodromous becoming brochidodromous distally. Spacing of secondaries increases distally; proximal secondaries diverge only millimeters from base. Angle of secondary attachment decreases slightly distally. Marginal secondary vein around margin. Higher order venation indeterminate. Margin entire.

Remarks: Although this specimen is poorly preserved, the distinctive secondary venation and base differentiate it from other ovate morphotypes recovered from this locality (e.g., MT016). The lack of agrophics, asymmetric basal insertion, and apparent eucamptodromous proximal secondary venation are therefore used as distinguishing features of this morphotype.

Similar to MT016 and MT017 this specimen superficially resembles several known taxa from the study area. The most compelling is Johnson's HC21 morphotype (Johnson 1989, 2002) based on the eucamptodromous secondaries, constricted secondary spacing near the base, and entire margin. However, given how partial the single specimen of MT017 is, certain diagnostic features of HC21 (e.g., drip tip at apex) are missing and some features (e.g., asymmetry) are not present in MT017, making this assignment speculative. Several taxa described by Dorf (1942) in the genera *Magnolia, Juglans,* and *Ficus* resemble this morphotype; however the single specimen of MT017 cannot be definitively aligned with any of the species described by Dorf (1942).

Morphotype: MT018; Figure 2.11B.

Material: Morphotype MT018 is represented by three specimens, exemplar is UWBM PB 103660.2.

Morphotype Quality: MQI is 4; EQI is 3.

Diagnosis: Leaves notophyll with orbicular shape where length to width ratio is less than 1:1. Basal petiole insertion asymmetric. Apex shape truncate and nearly perpendicular to midvein; base angle obtuse and shape concavo-convex. Primary venation pinnate with thick midvein and secondary veins; secondary veins spaced irregularly along midvein. Margin entire.

Description: Leaves notophyll in size. Shape orbicular with length (approximately 6.7 cm although true length may be greater) less than width (11.6 cm). Apex shape extremely truncated, coming to nearly flat edge perpendicular to midvein. Base angle obtuse and shape concavo-convex; petiole asymmetrically inserted. Petiole long (> 6.5 cm) and relatively wide (0.3 cm). Primary venation pinnate with thick midvein (3–4 mm). Secondary veins spaced irregularly along midvein and also relatively thick (1–2 mm). Tertiary venation unclear, but possibly reticulate. Margin entire.

Remarks: The venation of this morphotype is poorly preserved but the distinctive shape is highly diagnostic and separates it from all other morphotypes recovered from this site. The orbicular shape, truncated apex, and asymmetric basal insertion of the petiole, in particular, are unique characters of this morphotype.

Johnson (personal communication, January 18, 2018) describes a morphotype from the Late Cretaceous of North Dakota (HC251) that is somewhat similar to MT018. Both taxa have

an asymmetric basal insertion and orbicular shape. However, the distinctive truncate apex and pinnate venation of MT018 is lacking in HC251.

Morphotype: MT019; Figure 2.11C.

Material: Morphotype MT019 is represented by 21 specimens, exemplar is UWBM PB 96525.

Morphotype Quality: MQI is 1; EQI is 3.

Diagnosis: Leaves notophyll and oblong with rounded base and apex. Primary venation pinnate with simple brochidodromous to eucamptodromous secondaries, mixed percurrent tertiaries, and fine reticulate quaternaries. Margin entire.

Description: Leaves usually notophyll in size, but vary from large (11 cm in length by 7 cm in width) to moderate (5.5 by 2.6 cm). Leaf shape ranges from oblong to orbicular, with length to width ratio 1.6:1 on average. Based on measurements of mostly complete specimens (n=10) average lamina 8.6 cm long and 6.2 cm wide. Apex and base shape usually rounded. Primary venation pinnate with wide (approximately 1–1.5 mm) midvein. Secondary venation simple brochidodromous to eucamptodromous, forming loops of higher gauge or losing gauge towards margin. Secondary spacing increases distally; secondary angle to midvein consistent. Agrophic secondaries may form series of simple loops. Perimarginal secondary vein present. Tertiary veins mixed percurrent, predominately alternate percurrent. Exterior tertiaries form loops which join perimarginal secondary vein at margin. Quaternary venation irregular reticulate with a finer gauge irregular reticulate quinternary fabric. Margin entire.

Remarks: The shape and venation characters of this morphotype are unique from this locality; specifically, the rounded apex and base and the simple brochidodromous secondaries separate the specimens of this morphotype from all others recovered from this locality. However, it

should be noted that the secondary venation is variable; in the pictured exemplar (UWBM PB 96525; Figure 2.11C) the distal secondaries are brochidodromous, although damage to the margin makes them appear almost craspedodromous, while the proximal secondaries are brochidodromous to eucamptodromous. In general, secondary venation in this taxon can be variable. Although 21 specimens have been placed in this morphotype, some additional specimens displayed similar shape characteristics and venation but were too partial to definitively place in it; these are therefore considered indeterminate and not included in abundance counts.

This taxon is relatively common at this locality and well preserved but does not appear to align with any published taxa. Several morphotypes described by Johnson (1989, 2002) are similar but differ in one or more characters. Most compelling is HC127 (Johnson, 1989, 2002); however, in HC127 the secondary veins form a wide angle with the primary, differentiating this taxon from MT019.

Morphotype: MT022; Figure 2.11D.

Material: Morphotype MT022 is represented by three specimens, UWBM PB 97846.2 and 99343.6.

Morphotype Quality: MQI is 4; EQI is 4.

Diagnosis: Leaves mesophyll and oblong. Primary venation pinnate with craspedodromous secondary veins. Tertiary venation opposite percurrent, quaternary fabric reticulate, and quinternary fabric freely ramifying. Margin toothed; teeth large and evenly spaced along margin. Teeth serrate and curved distally.

Description: Leaves mesophyll, oblong in shape with length to width ratio greater than 1.7:1. Primary venation pinnate and secondary venation craspedodromous. Major secondaries decurrent to midvein, departing at an even angle. Spacing of major secondaries decreases proximally. Inter-secondaries do not extend beyond 50% of adjacent major secondaries and occur roughly one per intercostal region. Inter-secondaries simple brochidodromous, forming loops of secondary gauge reaching approximately halfway to the margin. Minor secondaries form ladder of simple agrophic veins towards base. Marginal secondary vein present; major secondaries reach marginal vein at apex of each tooth. Tertiary venation mostly sinuous opposite percurrent and generally perpendicular to adjacent higher order veins. Epimedial tertiaries also opposite percurrent, departing perpendicular to midvein and then basiflexed along their length. Exterior tertiaries looped at margin and especially within each tooth. Quaternary fabric irregular reticulate, quinternary fabric is apparently freely ramifying. Margin serrate with large (>1 cm long) teeth evenly spaced roughly every 2 cm along margin. Each tooth with distal flank concave, proximal flank curving or concave, and acute apex.

Remarks: Only two specimens of the morphotype have been recovered from this locality. While the venation is well preserved the specimens are very partial, and particularly the apex and base are obscured in both. Tooth shape is a highly distinctive and diagnostic feature of this morphotype but it is difficult to say more about the leaf shape.

The large teeth of this specimen strongly resemble the teeth or lobes described by Johnson (1989, 1996) on specimens of *Leepierceia preartocarpoides*. The venation described along each tooth of *L. preartocarpoides* is identical to that of MT022. However, venation in MT022 is so poorly preserved on the remainder of the lamina that this affinity is still somewhat unclear. As mentioned above, MT016 strongly resembles *L. preartocarpoides* described by

Johnson (1989, 1996) but lacks the distinctive teeth and also differs from *L. preartocarpoides* as described by Arens and Allen (2014) who note large lobes on their specimen of this species. However, given the range of variation these authors describe for *L. preartocarpoides* we instead ascribe another morphotype, MT016 to this species (K. Johnson, personal communication, June 23, 2018) (see description of MT016 for more detail). It is possible that MT016 and MT022 represent an unlobed and lobed variety of this same species, but further study is needed to explore this hypothesis. Given the differences between MT016 and MT022 (i.e. large, curved teeth in MT022), we are unable to attribute MT022 to a particular species.

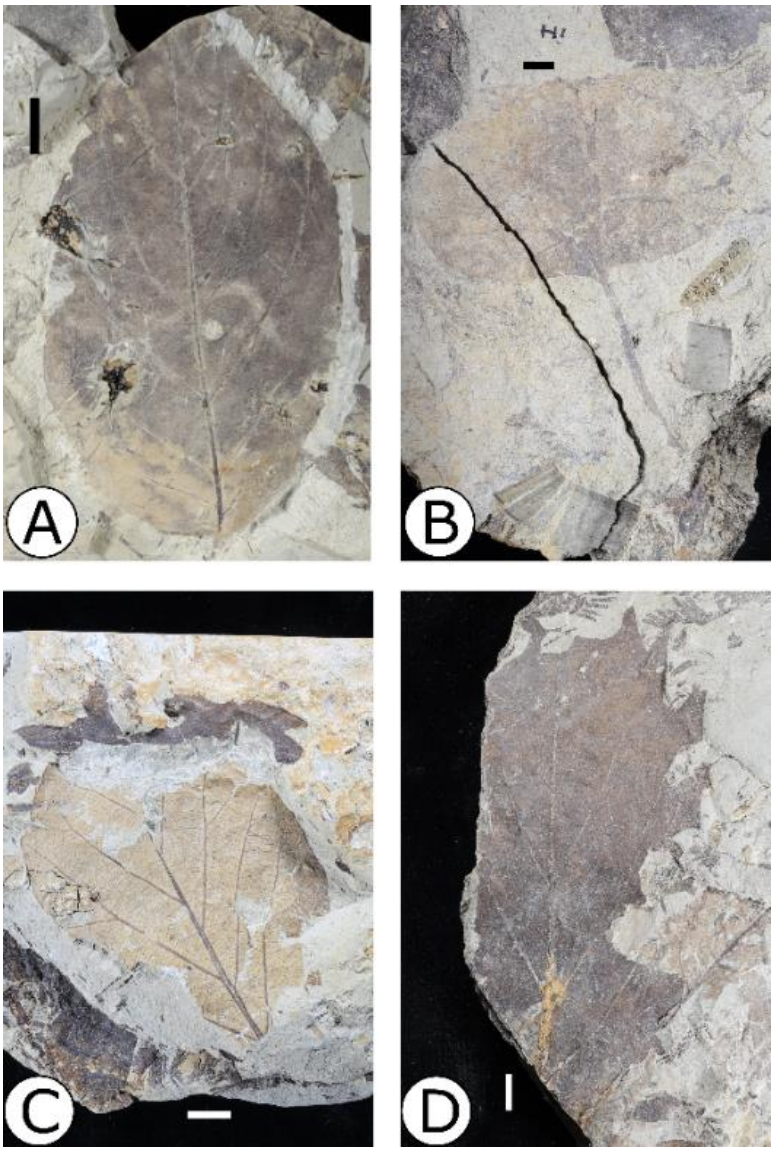

Figure 2.11 Angiosperm morphotypes; (A) MT017 unidentified morphotype, UWBM PB 96557; (B) MT018 unidentified morphotype, UWBM PB 103660.2; (C) MT019 unidentified morphotype, UWBM PB 96525; (D) MT022 unidentified morphotype, UWBM PB 99343.6. Scale bar 1 cm.

Morphotype: MT024: Figure 2.12A, B.

Material: Morphotype MT024 is represented by eight specimens, exemplar is UWBM PB 96541.

Morphotype Quality: MQI is 2; EQI is 4.

Diagnosis: Leaves microphyll and oblong. Primary venation pinnate and secondary venation brochidodromous. Base angle acute and shape straight or convex; apex shape truncate with small serrate and dentate teeth only at the apex.

Description: Leaves microphyll in size and oblong in shape. Length 5.7 cm and width 2 cm on average; length to width ratio 3.4:1 on average. Lamina symmetric at base but slightly asymmetric at middle. Base angle acute and shape straight or slightly convex; apex angle obtuse and shape truncate. Primary venation framework pinnate and secondary framework simple brochidodromous to semicraspedodromous near apex. Marginal secondary present. Major secondaries have excurrent attachment to midvein. Secondary spacing decreases distally and angle to midvein increases distally. Major secondaries form loops of higher gauge; towards leaf apex loops branch, with one of the branches reaching the margin at the apex of each tooth. Intercostal tertiary fabric mixed percurrent; epimedial tertiaries also mixed percurrent while exterior tertiaries loop. Higher order venation indeterminate. Small, serrate teeth spaced approximately three per centimeter only present at apex. Teeth regularly spaced with rounded sinuses. Tooth shape varies from proximally convex and distally convex to proximally straight and distally convex. Veins of secondary gauge terminate at distal flank of teeth and accessory veins loop.

Remarks: The unusual truncate apex and serrate teeth just bordering the apex set this morphotype apart from other morphotypes recovered from this locality (notably MT023). In certain specimens these teeth are difficult to distinguish, and their presence only at the apex sometimes makes this morphotype difficult to identify. It should also be noted that these distinctive teeth may be obscured or impacted by insect damage in our exemplar specimens; while these specimens do not clearly show signs of insect damage around the margin, it cannot

be entirely ruled out. A shorter length to width ratio also distinguish specimens identified as MT024 from those identified as MT023 (t-test resulted in $p<0.05$); this significance appears to stem primarily from length ($p<0.01$) while width is indistinguishable between the two morphotypes ($p=0.9$). These differences in shape, along with differences in the placement and size of teeth, justify these groups as separate morphotypes.

Although this morphotype is similar to MT023 (ascribed to *"Dryophyllum" subfalcatum*), the differences in apicular features and length to width ratio distinguish this morphotype from that taxon. We do not find any published taxa from contemporaneous floras which share this distinctive truncated apex with sparse teeth.

Morphotype: MT025: Figure 2.12C.

Material: Morphotype MT025 is represented by two specimens, UWBM PB 97845.2 and 103587.

Morphotype Quality: MQI is 2; EQI is 4.

Diagnosis: Highly variable size (notophyll to microphyll), shape ovate to oblong. Primary venation pinnate and secondary venation craspedodromous, with distinctive crenate margin. Teeth serrate with glands at tooth apices.

Description: Leaves notophyll to microphyll in size and ovate to oblong in shape. Apex angle apparently acute; base indeterminate. Primary venation framework pinnate with major secondaries evenly spaced, consistently angled, and attaching decurrently to midvein. Secondary venation craspedodromous with major secondaries ending at tooth apices. Minor secondaries visible in some intercostal regions running parallel to adjacent major secondary veins. Minor secondaries either lose gauge or become reticulate distally. Fimbrial or marginal secondary vein

sometimes present. Intercostal tertiary fabric mixed percurrent and attachment perpendicular to higher order veins. Epimedial tertiaries perpendicular to midvein and then basiflexed towards adjacent secondary. Exterior tertiaries looped towards the margin where they intersect marginal secondary veins. Quaternary fabric regular reticulate. Margin crenate, with teeth spaced approximately 1–3 per centimeter depending on leaf size. Teeth serrate or rounded in shape, with angular sinuses and convex proximal and distal flanks. One order of teeth, evenly spaced and of approximately equal size along margin. Apparent gland at apex of each tooth.

Remarks: Specimens of this morphotype share common shape, venation, and tooth patterns but also show substantial variability in size, ranging from 2.5 to 8 cm in length. Although the angle of secondary veins to the midvein is consistent along the length of the leaf, it appears to be narrower in the smaller specimen. Both of these differences could be ontogenetic or due to differences in growth conditions. Further investigation may result in subdivision of this morphotype.

MT025 shares characteristics with an unpublished morphotype of Johnson, HC395 (K. Johnson, personal communication, January 18, 2018). The teeth of Johnson's HC395 are particularly similar to those seen in MT025 which are distinctive of the morphotype. However, there is a detailed patterning indicating pubescent laminar texture in HC395 which is absent or at least not preserved in MT025. Another compelling comparison is with HC18, placed within Urticaceae (Johnson, 1989); the minor secondaries, arching tertiaries, basal actinodromous primary network, and large, convex-acuminate teeth are all similar. However, Johnson (1989) makes no mention of glands at the apices of each tooth, which are a prominent feature in MT025; additionally, given that the base of MT025 is not completely preserved, we are unable to definitively align this morphotype with HC18.

Morphotype: MT026; Figure 2.12D.

Material: Morphotype MT026 is represented by four specimens, exemplars are UWBM PB 97837 and 103569.

Morphotype Quality: MQI is 4; EQI is 4.

Diagnosis: Leaves notophyll, ovate in shape. Primary venation pinnate with major secondaries spaced evenly along midvein and at wide angle to midvein. Secondary venation craspedodromous; secondary and primary veins terminate at each tooth apex. Tertiary venation mixed percurrent and quaternary fabric irregular reticulate. Fimbrial vein present. Margin toothed with two to three orders of teeth. Tooth apices slightly notched.

Description: Leaves microphyll in size. Shape apparently ovate. Apex angle obtuse and shape rounded to straight; base indeterminate. Primary venation apparently pinnate, with major secondaries craspedodromous. Secondaries intersect midvein at wide angle and terminate at apex of first order teeth. Basal minor secondaries form simple agrophic framework and serve as principal vein on some first order teeth. Tertiary veins mixed percurrent. Exterior tertiaries looped within each tooth. Fimbrial vein sometimes present. Quaternary fabric regular to irregular reticulate. Quinternary fabric apparently ramifying. Margin serrately toothed with at least two orders of teeth on all sides. First order teeth spaced every 1.5 cm; second order teeth on proximal flank of most first order teeth. Sinuses between teeth rounded; distal and proximal flanks of each tooth convex, forming very rounded teeth. Small indentation at apex of each tooth where vein terminates.

Remarks: Specimens of this morphotype are partially preserved in most cases and their morphology is therefore poorly constrained. They resemble MT025 from this locality in that they

are pinnate with rounded, serrate teeth and craspedodromous secondaries ending at each tooth apex. MT026 is distinguished by a more ovate (as opposed to ovate to oblong) shape, the presence of two orders of teeth, and the lack of obvious glands on those teeth. In addition, the angle of secondaries intersecting the midvein is larger than seen in MT025, contributing to the wider, more ovate shape of MT026 specimens. Further study of these specimens may result in re-organization of these morphotypes.

In comparing this taxon with published taxa from the area, there is a strong resemblance to the toothed variety of *Marmarthia trivialis* (Lesquereux) Johnson (1996), referred to as HC105 (Johnson, 1989). *M. trivialis* has a basal actinodromous primary framework; MT026 is classified here as pinnate but may have palmate venation obscured by the poor preservation of specimens. *M. trivialis* is also characterized by basal lateral primaries that are decurrent to midvein and emerge close to the base, resulting in naked basal primaries; the lack of a clear base on any MT026 specimens prevents us from identifying these distinguishing features. Additionally, Johnson (1996) notes that *M. trivialis* may rarely have large obtuse simple teeth; by comparison, all four MT026 specimens are toothed, further calling this classification into doubt. Given these considerations, we are unable to definitively assign this morphotype to any published taxon.

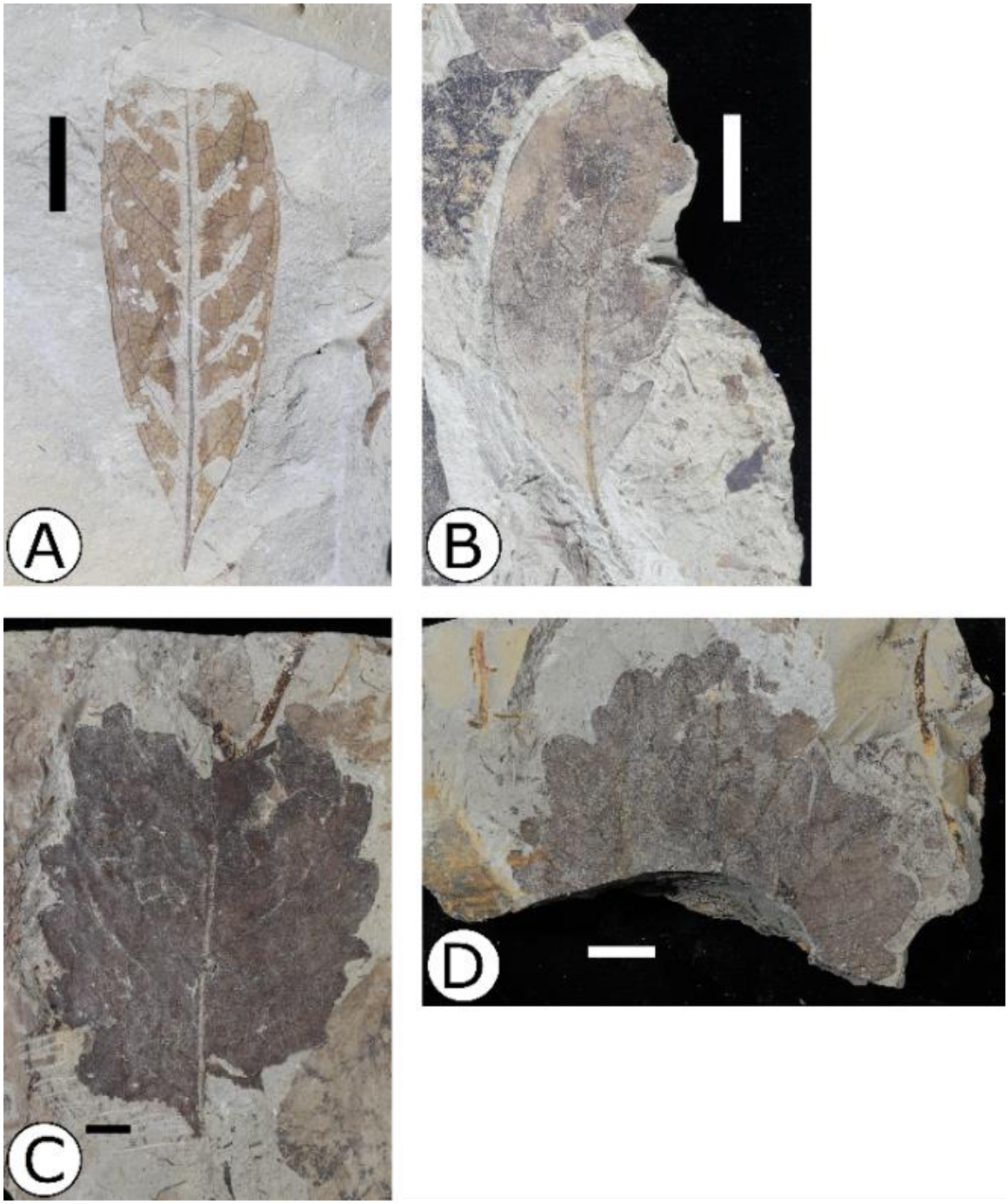

Figure 2.12 Angiosperm morphotypes; (A-B) MT024 unidentified morphotype, A—UWBM PB 96541, B—UWBM PB 103466.1; (C) MT025 unidentified morphotype, UWBM PB 97845.2; (D) MT026 unidentified morphotype, UWBM PB 97837. Scale bar 1 cm.

Uncertain seed

Morphotype: MT028; Figure 2.13A.

Material: Morphotype MT028 is represented by 25 specimens, exemplar is UWBM PB 103753.

Morphotype Quality: MQI is 4; EQI is NA.

Diagnosis: Round, small non-descript seed.

Description: Small seeds, usually 3–5 mm in diameter and almost perfectly round. Sometimes present, small rim less than 1 mm wide.

Remarks: MT028 encompasses a variety of seeds with non-descript morphology that are commonly found in the study area. They are often preserved in 'plant hash' containing multiple seeds and other poorly defined compression fossils. The rim present on some may represent a seed coat or other outer wall associated with the seed. No detailed descriptions of a similar morphotype or taxon have been published from Montana or North Dakota Upper Cretaceous deposits. We speculate that this absence might be due to the nondescript nature of this morphotype, and not a true absence of this taxon in other studies.

Morphotype: MT029; Figure 2.13B.

Material: Morphotype MT029 is represented by one specimen, UWBM PB 103588.2.

Morphotype Quality: MQI is 3; EQI is NA.

Diagnosis: Winged samara with "teardrop" shaped seed and asymmetric wing which tapers into a long tail extending out from the samara apex.

Description: Winged samara with central seed and long-tailed wing around margin. Overall samara dimensions 2.4 cm by 0.7 cm. Seed approximately 1.1 cm by 0.5 cm, tapering to an acute tip at apex, and rounded at base. Wing extends around seed asymmetrically; wing ranges from

<0.5 mm to 3 mm in width. Wing widens towards apex to form elongate samara apex approximately 1.2 cm long.

Remarks: This distinctive seed is reminiscent of seeds from *Acer* and other "dicot" angiosperm taxa. Johnson (1989; personal communication, January 18, 2018) described two winged seeds (HC384 and HC240) from North Dakota which are reminiscent of this morphotype. However, the wing of HC384 is attached asymmetrically to the seed and does not extend around the entire seed exterior. The wing of HC240 is much wider and shorter than seen in MT029. Therefore, we distinguish this morphotype as unique to this study area.

Morphotype: MT030: Figure 2.13C.

Material: Morphotype MT030 is represented by seven specimens, exemplars are UWBM PB 96535.1, 103638, and 103659.2.

Morphotype Quality: MQI is 2; EQI is NA.

Diagnosis: Large seed or nut with concavo-convex apex.

Description: Highly variable in shape and size. All over 1 cm in diameter (typically approximately 2–2.5 cm in diameter) and rounded. Seed wall relatively thick, 1–2 mm in some specimens. Apex shape concavo-convex, likely where seed attached to inflorescence.

Remarks: This morphotype encompasses specimens displaying variable morphology. All are rounded, large and interpreted as a seed or nut. These specimens are preserved as compression fossils and often show evidence of woody material partially carbonized in their preservation. This morphotype does not resemble any published taxa known from this study area. However, it appears to be consistent with an unpublished morphotype defined by Johnson, HC431 (K. Johnson, personal communication, January 18, 2018).

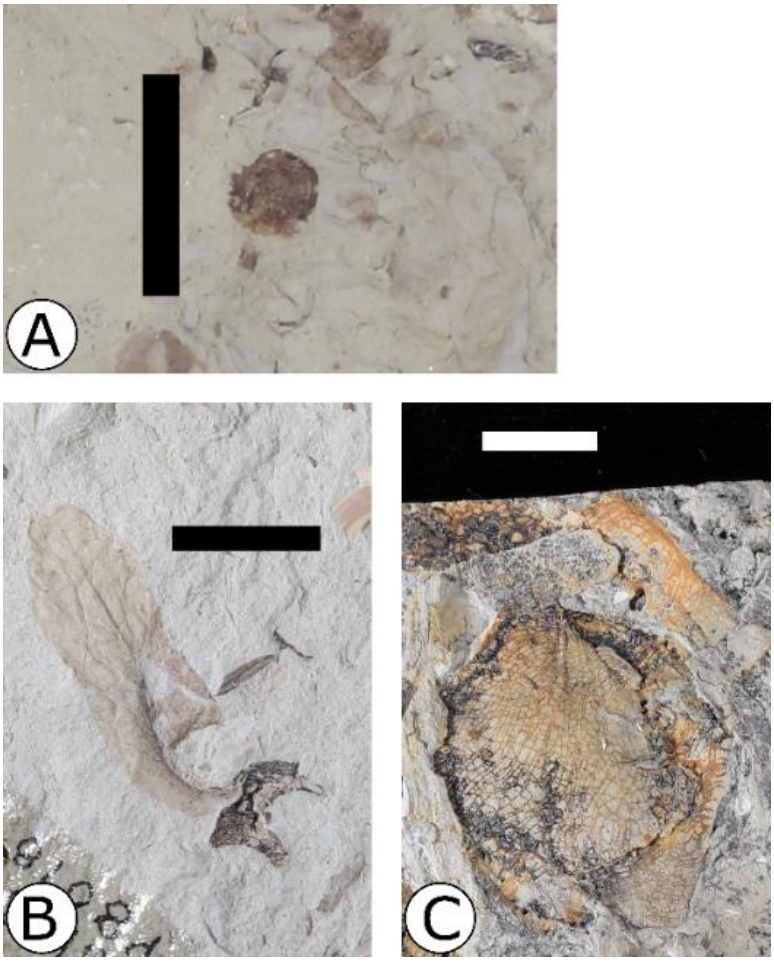

Figure 2.13 Other morphotypes; (A) MT028 unidentified morphotype, UWBM PB 103753; (B) MT029 unidentified morphotype, UWBM PB 103588.2; (C) MT030 unidentified morphotype, UWBM PB 96535.1. Scale bar 1 cm.

2.6 FLORAL DESCRIPTION AND COMPARISON

2.6.1 Summary Description of Seafood Salad Flora

The Seafood Salad I and Seafood Salad II quarries represent distinct facies. We interpret the Seafood Salad II deposit as a crevasse splay or levee deposit based on the thin bedding of sandstones and siltstones that are penetrated in some areas by root traces (cf. discussion in Johnson, 2002). We interpret the Seafood Salad I deposit as a pond according to the classifications of Johnson (2002) based on fine grain size and unoxidized sediments, the presence of which help exclude other facies. We acknowledge that lack of bedding or other sedimentary features (e.g., root traces or oxide deposits) leave this interpretation somewhat uncertain. See Supplement for detailed stratigraphic information.

The Seafood Salad I assemblage differs from the Seafood Salad II assemblage in that the plant fossils tend to be preserved with greater detail and as isolated specimens, and the assemblage is dominated by *Metasequoia occidentalis* (MT002) branchlets. This taxon makes up at least 53% of specimens recovered from Seafood Salad I, compared to 31% of specimens from Seafood Salad II. In contrast, the megafossils from Seafood Salad II include mostly angiosperm vegetative structures. Differences in production as well as landscape heterogeneity may have promoted higher abundance of *M. occidentalis* in the Seafood Salad I assemblage. Nevertheless, there is broad overlap in the taxa preserved at both quarries. Although the invertebrate assemblage from Seafood Salad awaits detailed study, it can be noted that the Seafood Salad I quarry tends to preserve isolated, more or less intact, gastropod shells, whereas the Seafood Salad II quarry tends to preserve fragmented shell material concentrated into thin horizons. Those compositional differences imply taphonomic differences between the quarries: the slower moving water, fine-grained sediments, and more anoxic conditions associated with the Seafood

Salad I depositional environment would have favored preservation of more complete specimens, smaller specimens, and more detailed leaf anatomy. Despite these compositional and taphonomic differences, we combined the relative abundance data from the two quarry assemblages for the analyses presented herein. We justify this on the grounds that the stratigraphic distance between these two quarries (0.75 m) likely represents less than 15 kyr according to the sediment-accumulation rates for the HCF from Sprain et al. (2018). Moreover, there are no obvious signs of depositional hiatus or environmental change between the two fossiliferous horizons.

The combined Seafood Salad flora is taxonomically rich, with many angiosperm taxa, few but abundant gymnosperm taxa, and relatively few fern or fern ally taxa. The few but abundant conifer taxa (six, not including reproductive cones of *Metasequoia occidentalis*) constitute 58% of the total number of specimens in the flora. Vegetative structures from *M. occidentalis* (MT002) make up as much as 46% of the assemblage in total.

Relative to gymnosperms, angiosperms have a much higher taxonomic richness of vegetative taxa (S=19), whereas their relative abundance of specimens is relatively low (32%). Among these angiosperms, the most common morphotypes are *Leepierceia preartocarpoides* (MT016; 23%), a "dicot" likely belonging to the families Saxifrigales (previously referred to as Cercidiphyllales or Trochodendrales) (MT011; 20%), *"Dryophyllum" subfalcatum* (MT023; 17%), another unidentified "dicot" (MT019; 11%), and *Quereuxia angulata* (MT013; 8%).

The four angiosperm reproductive structures recovered from Seafood Salad include *Carpites ulmiformis* (MT027) and an unnamed seed morphotype (MT030), both of which have been identified in North Dakota; the other two (MT028 and MT029) do not match any previously published taxa.

Among the three fern taxa in the Seafood Salad assemblage, two match descriptions of fern taxa from North Dakota: an unidentified fern (MT031) and *Hydropteris pinnata* (MT033). The other fern is too partial to clearly align with any previously published fern species. The putative bryophyte taxon (MT034) is poorly preserved and only tentatively compared to the bryophytes.

TABLE 2.1 ABSOLUTE ABUNDANCE AND AFFINITY OF MORPHOTYPES FROM THIS STUDY

Affinity*	Morphotype	Species Name (where known)	Abundance
GYM	MT001	*Ditaxocladus catenulatus*	2
GYM	MT002	*Metasequoia occidentalis*	274
GYM	MT003	*Metasequoia occidentalis*	5
GYM	MT004	*Glyptostrobus europaeus*	34
GYM	MT005	*Taxodium olriki*	11
GYM	MT006		1
GYM	MT007	*Ginkgo adiantoides*	14
MON	MT008	*Cobbania corrugata*	1
DIC	MT009	*Erlingdorfia montana*	1
DIC	MT010		1
DIC	MT011		37
DIC	MT012	cf. *Zizyphoides flabella*	6
DIC	MT013	*Quereuxia angulata*	15
DIC	MT014		1
DIC	MT015		1
DIC	MT016	*Leepierceia preartocarpoides*	44
DIC	MT017		1
DIC	MT018		3
DIC	MT019		21
DIC	MT020	cf. *"Dryophyllum" tenneseensis*	5
DIC	MT021		2
DIC	MT022		3
DIC	MT023	*"Dryophyllum" subfalcatum*	32
DIC	MT024		8
DIC	MT025		2
DIC	MT026		4
DIC	MT027	*Carpites ulmiformis*	19
DIC	MT028		25
DIC	MT029		1
DIC	MT030		7

PTE	MT031		1
PTE	MT032		4
PTE	MT033	*Hydropteris pinnata*	1
BRY?	MT034		3

* Taxonomic group; (GYM = gymnosperm, MON = monocot, DIC = non-monocot angiosperm, PTE = pteridophyte, BRY = bryophyte)

2.6.2 Comparison with North Dakota Late Cretaceous and early Paleogene Floras

On the basis of its stratigraphic position, we hypothesized that the Seafood Salad assemblage would be similar in morphotype composition to HCIa floral zone assemblages from the lower HCF of North Dakota (ND). Alternative hypotheses are that the Seafood Salad assemblage shows compositional affinity with assemblages based on lithofacies or that its morphotype composition is distinct from the ND assemblages due to spatial heterogeneity.

Among the five most common Seafood Salad angiosperm morphotypes only two occur in ND: *"Dryophyllum" subfalcatum* (MT023 in this assemblage, HC49 in North Dakota) and *Quereuxia angulata* (MT023 in this assemblage, FU2 in North Dakota). Whereas *"Dryophyllum" subfalcatum* is abundant throughout the HCI and HCII biozones in ND, *Quereuxia angulata* becomes a "dominant" taxon in only FUI megafloral assemblages (6% of specimens; Johnson, 1989). Note that *Quereuxia angulata* is an aquatic angiosperm with rosettes, each of which has many leaves (Stockey and Rothwell, 1997) and only individual leaves have been collected at Seafood Salad.

More broadly among the 19 angiosperm morphotypes from Seafood Salad, six can be referred to morphotypes from ND: *Cobbania corrugata* (MT008 in this assemblage; HC77 in North Dakota), *Erlingdorfia montana* (MT009 in this assemblage; HC64 in ND), *Quereuxia angulata* (MT013 in this assemblage; FU2 in ND), *Leepierceia preartocarpoides* (MT016 in this assemblage; HC86 in ND), and *"Dryophyllum" subfalcatum* (MT023 in this assemblage; HC49 in ND) (Johnson, 1989, 2002). We suggest that three other morphotypes described from Seafood

Salad are closely related to morphotypes from ND: MT020 to *"Dryophyllum" tenneseensis* (HC49 in ND), MT012 to *Zizyphoides flabella* (HC43 in ND), and MT022 to *Leepierceia preartocarpoides* (HC86 in ND). Several of the most common morphotypes from Seafood Salad (e.g., MT019) are not recognized among the published taxa from ND. Among those taxa found in both Montana and North Dakota, *"Dryophyllum" tenneseensis* is absent from the HCI zone in ND (Johnson, 1989, 2002); its presence in the Seafood Salad flora of Montana represents a stratigraphic and geographic range extension.

Among the five angiosperm reproductive morphotypes from Seafood Salad, only two can be linked to ND morphotypes: *Carpites lancensis* (MT027 in this assemblage; HC54, which is restricted to the HCIIa biozone in ND), and MT030 (the unpublished morphotype HC431 in ND; K. Johnson, personal communication, January 18, 2019).

Five of the six gymnosperm taxa found at Seafood Salad are also found in the HCI biozone in ND. These include *Ditaxocladus catenulatus* (MT001 in this assemblage; HC137 in ND), *Metasequoia occidentalis* (MT002 in this assemblage; FU3 in ND), *Glyptostrobus europaeus* (MT004 in this assemblage; FU4 in ND), *Taxodium olrikii* (MT005 in this assemblage; HC71 in ND), and *Ginkgo adiantoides* (MT007 in this assemblage; HC114 in ND). *M. occidentalis* and *G. europaeus* are found only in the HCI biozone of ND (i.e., in five of the 14 most well-sampled HCI localities; sample size >50); whereas the other three (*D. catenulatus*, *T. olrikii*, and *G. adiantoides*) span all HC and FU biozones. Only the Seafood Salad gymnosperm morphotype MT006 is absent in ND. Although the high relative abundance of gymnosperms in the Seafood Salad flora is distinctive, the taxonomic composition of gymnosperms is similar to those from the HCI biozone of ND.

Among the four fern or putative bryophyte taxa from Seafood Salad, two overlap with taxa described by Johnson (2002; personal communication, January 18, 2018): MT031 in this assemblage corresponds with HC115, and MT033 has been identified as *Hydropteris pinnata* (HC129). MT031 (HC115) is found only in the megafloral localities from Ekalaka, Montana (Johnson, 2002; personal communication, January 18, 2018) and is not represented in any HC or FU floral biozones from ND (Johnson, 1989). *Hydropteris pinnata* (MT033 in this assemblage; HC129 in ND) is found in the HCIIa biozone in ND. The last two morphotypes in this group (MT032 and MT034) are represented by very fragmentary specimens and not identifiable to any known taxa. The poor preservation of these two morphotypes may obscure features that would refer these morphotypes to known taxa from ND.

TABLE 2.2 DIVERSITY METRICS FOR SEAFOOD SALAD AND CONTEMPORANEOUS FLORAS

Dataset*	**Raw Richness**		**Rarefied Richness****		**Simpson's diversity**		**Pielou's evenness**	
	All Taxa †	*Vegetative Morpho-types Only*	*All Taxa*	*Vegetative Morpho-types Only*	*All Taxa*	*Vegetative Morpho-types Only*	*All Taxa*	*Vegetative Morpho-types Only*
Seafood Salad (this study)	34	29	12.16 ± 1.78	14.31 ± 1.9	0.71	0.75	0.58	0.62
Average of North Dakota K-Pg aged floras (with n >50)***	15.03 ± 12.53	13.87 ± 11.9615	7.99 ± 1.08	8.37 ± 4.17	0.63 ± 0.24	0.63 ± 0.24	0.61 ± 0.18	0.60 ± 0.18
Average of North Dakota HCI zone floras (with n >50)***	14.57 ± 10.49	13.14 ± 9.00	8.00 ± 1.08	8.41 ± 4.47	0.62 ± 0.27	0.63 ± 0.27	0.59 ± 0.23	0.59 ± 0.23
PDM			12.57 ± 1.43	12.57 ± 1.44	0.85	0.85	0.79	0.79

* Metrics calculated based on species abundance matrices of (1) the Seafood Salad locality, (2) North Dakota K/Pg aged floras with a sample size >50 (70 localities; data from Wilf and Johnson (2004)), (3) North Dakota K/Pg aged floras identifiable to the HCI zone with a sample >50 (14 localities; data from Wilf and Johnson (2004)), and (4) the PDM locality of Montana (data from Arens and Allen (2014)).

** Rarefied richness analytically calculated; richness rarefied to lowest sample size (n=50) and ± $1\sigma_{\bar{x}}$ given.

† All metrics calculated for abundance data of all morphotypes as well as abundance data of only vegetative morphotypes (i.e. leaves) so as to reduce potential redundancy of species (e.g. counting seeds and leaves of a single species as separate morphotypes).

*** Metrics calculated based on species abundance data at each locality and then averaged for that dataset; the mean value ± 1σ is given.

All calculations performed in R version 3.5.3 (R Core Team, 2019; http://www.r-project.org)

The Seafood Salad flora is taxonomically rich, preserving 34 morphotypes (22 at Seafood Salad II, 30 at Seafood Salad I). In comparison, the well-sampled HCF and FUF assemblages from ND have 14.57 morphotypes on average, but note that these values vary greatly across assemblages ($\sigma = 10.49$) (Table 2) (Wilf and Johnson, 2004). This pattern is consistent across all other measures of diversity that we examined (rarefied richness, Simpson's diversity, and Pielou's evenness): the Seafood Salad flora is among the most diverse KPB-aged floras in Montana and North Dakota (Table 2). The rarefaction curves graphically illustrate that pattern as well (Figure 2.14).

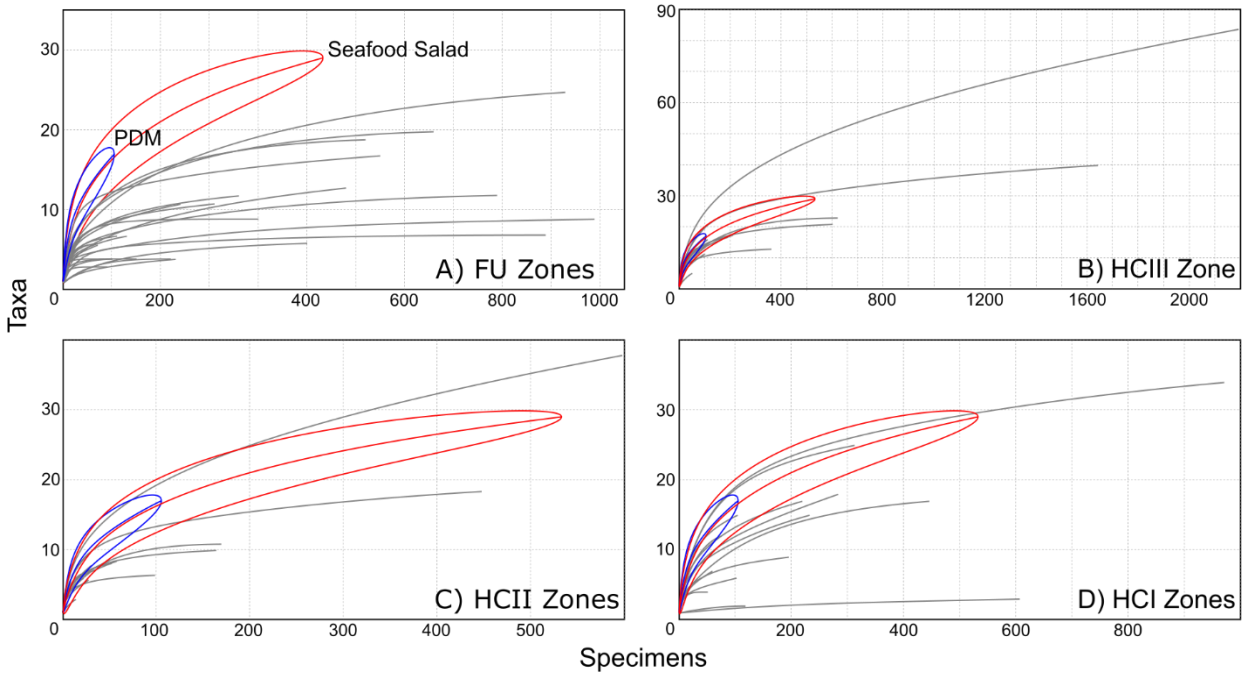

Figure 2.14 Rarefaction curves of Seafood Salad and PDM floras from the Hell Creek Area, Montana and the KPB floras from North Dakota showing that both Seafood Salad and PDM appear to be among the most diverse Late Cretaceous floras, and more diverse than early Paleogene floras in this dataset. All analyses are based on vegetative morphotypes (data from this study, Arens and Allen, 2014, and Wilf and Johnson, 2004, respectively). Each panel shows the Seafood Salad flora (red), PDM flora (blue), and North Dakota KPB floras (gray), of which the latter are arranged according to biozone. Seafood Salad and PDM are both shown with 95% confidence intervals.

The NMDS ordination and ANOSIM results (R=0.7104, p=0.001) show that ND floras cluster largely according to floral zones (Figure 2.15). The stress value, which is an estimate of how well the NMDS ordination summarizes the observed distances between groups, is low (0.0655), indicating that there is very little risk of drawing false inferences (Clarke, 1993). The strong separation between Cretaceous and Paleogene floras (ANOSIM of Cretaceous vs. Paleogene floras: R=06194, p=0.001) is largely driven by characteristic Cretaceous taxa that disappear at the KPB (e.g., HC49 *"Dryophyllum" subfalcatum*; Johnson, 1989) and by characteristic Paleogene taxa that only appear after the KPB (e.g. FU43 *Ziziphoides flabella*; Johnson, 1989).

The taxonomic composition of the Seafood Salad flora is most similar to those of the HCIa floras of Johnson (2002) (Figure 2.15). However, there is significant overlap among the Cretaceous-age HC zones, particularly the lower HCI and HCIIa zones. When 95% confidence ellipses (not shown) are considered, there is almost no distinction between the HCI and HCII biozones or between the two FU biozones. Despite this lack of resolution, NMDS and ANOSIM both indicate that the Seafood Salad locality is compositionally similar to the HC floras of North Dakota, and in particular to the HCIa subzone. This clustering supports our hypothesis that, based on its stratigraphic position, the Seafood Salad locality would show closest affinity with the HCIa biozone.

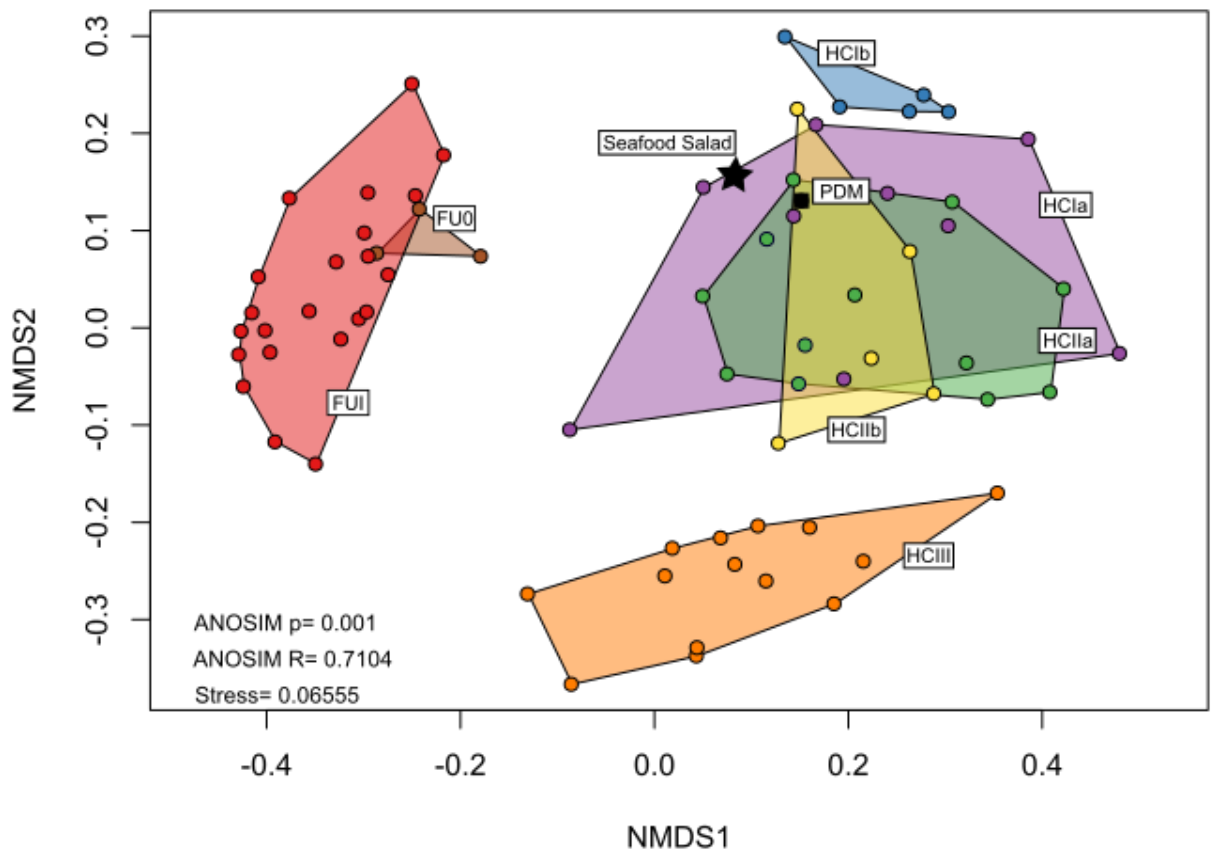

Figure 2.15 Nonmetric multidimensional scaling (NMDS) ordination plot of Seafood Salad, PDM, and North Dakota KPB floras showing that Seafood Salad falls within the HC1a zone, but that there is substantial overlap among biozones (abundance data for North Dakota localities from Wilf and Johnson, 2004 and for PDM locality from Arens and Allen, 2014). Analyses run on relative abundance data of vegetative morphotypes. Colors indicate floral biozone (red = FUI, brown = FU0, orange = HCIII, yellow = HCIIb, green = HCIIa, blue = HCIa, and purple = HCIa) and floras (black square = PDM, black star = Seafood Salad). NMDS stress value and analysis of similarity (ANOSIM) R and p-values are given for this analysis.

2.6.3 Comparison with PDM Flora

The previously published PDM megafloral locality is also from the Hell Creek study area (Arens and Allen, 2014); it is 15 m stratigraphically lower and 7 km NW of the Seafood Salad site. The PDM flora is hosted in a sandstone channel deposit, whereas the Seafood Salad flora is deposited in a backwater environment (i.e., pond or proximal floodplain). The much smaller sample size (n=106) of PDM compared to that of Seafood Salad (n=590) hampers comparison of

these two floras; nevertheless, there is relatively little taxonomic overlap between the two assemblages. Three of the four gymnosperm taxa from PDM also occur at Seafood Salad (*Metasequoia occidentalis*, *Glyptostrobus europaeus*, and *Ginkgo adiantoides*); whereas only three of the 13 angiosperm vegetative morphotypes from PDM occur at Seafood Salad (*Leepierceia preartocarpoides*, *"Dryophyllum" subfalcatam*, and *Erlingdorfia montana*). Despite its lower sample size, PDM has similar morphotype richness, and higher Simpson's diversity and Pielou's evenness values relative to both the Seafood Salad and ND floras (Table 2). Comparing rarefaction curves for PDM with Seafood Salad and the ND floras, PDM is of similar diversity (both estimated rarefied richness and evenness) to Seafood Salad (Figure 2.14). However, these rarefaction curves also illustrate that PDM is relatively under-sampled to date. In the NMDS ordination based on taxonomic composition, PDM clusters with the HCIa floras from ND, but also within the ordination space of HCIIb and HCIIa floras (Figure 2.15). Taken together, the differences in plant communities inferred from the PDM and Seafood Salad assemblages might reflect spatial heterogeneity in vegetation, the result of age differences between these floras reflecting environmental changes, relatively low sample size at PDM, or some combination thereof. We are currently studying additional megafloral assemblages from the Montana HCF section to allow us to distinguish among these alternatives (Wilson et al., 2020).

2.6.4 Comparison with Other K/Pg Aged Floras of the Western Interior

Our floral comparisons indicate that the gymnosperms are taxonomically similar across Late Cretaceous-age formations in the northern Great Plains, whereas the angiosperm taxa are more endemic. Three gymnosperms (MT002, MT003, and MT005), three angiosperms (MT013, MT017, and MT027), and one pteridophyte (MT033) described from Seafood Salad can be

attributed to taxa reported from elsewhere in the Williston Basin (Hickey, 1977; Peppe et al., 2007) and the Hanna Basin (Dorf, 1942; Dunn, 2003) (see Table A.1 for list of synonymous taxa). In contrast, the Denver Basin (Johnson et al., 2003; Lyson et al., 2019), Raton Basin (Wolfe and Upchurch, 1987), and San Juan Basin (Flynn and Peppe, 2019) only yield Paleocene-age megaflora and share few taxa in common with the Seafood Salad flora. Although most of the paleofloras from these Western Interior basins are taxonomically dominated by angiosperm taxa (as noted by others, e.g., Wing and Boucher, 1998), the taxa shared across these basins are most frequently gymnosperms (e.g., *Metasequoia*, *Glyptostrobus*, *Taxodium*, and *Ginkgo*). This pattern supports the hypothesis that angiosperms, although locally abundant and taxonomically rich, were also more endemic across Late Cretaceous landscapes. This may relate to a difference in habitat partitioning, preservation potential, or both. Wing et al. (1995, 2012) observed a similar pattern in an earlier Maastrichtian megaflora from Big Cedar Ridge, albeit on a much smaller spatial scale (<5 km). Whereas Seafood Salad shares some taxa with other, similarly aged fossil floras from the Western Interior, this assemblage represents an under-studied time interval in the region. Additional sampling of those other basins will help further elucidate potential regional heterogeneity and endemism.

2.7 SUMMARY AND PROSPECTUS

The Seafood Salad locality represents a diverse riparian community from the Late Cretaceous of Montana. The flora is preserved as compression and impression fossils in allochthonous deposits likely representing pond and proximal floodplain facies. Collection at this locality has yielded over 590 specimens representing 34 morphotypes: six gymnosperm taxa (and one gymnosperm reproductive structure), 19 angiosperm taxa (and four angiosperm reproductive structures), and four pteridophyte taxa (one of which may be a cryptic bryophyte). The flora is dominated by *Metasequoia occidentalis*, making up over 50% of the material collected, whereas angiosperms form the largest component in terms of taxonomic richness. The few abundant gymnosperms preserved in this flora are common across the Great Plains from similar Late Cretaceous-aged assemblages, indicating that these taxa were geographically widespread. The Seafood Salad site is in the lower third of the Hell Creek Formation, which would overlap with the HCI biozone of Johnson (1989, 2002) in North Dakota; we find that the Seafood Salad assemblage is broadly in accord with typical floras of this zone in terms of taxonomic representation and diversity. However, the distinct floral composition of Seafood Salad points to heterogeneity in plant communities among the Northern Great Plains during the Late Cretaceous. In addition, the taxa preserved at Seafood Salad differ from assemblages recovered from earlier or later deposits in the Hell Creek Area in northeastern Montana (Hickey, 1977; Peppe et al., 2007; Arens and Allen, 2014), suggesting turnover in dominant taxa through time as well as within regions.

The Seafood Salad locality constitutes one of the first findings of megaflora from northeastern Montana and emphasizes the need for a more in-depth paleobotanical investigation in the Hell Creek Area. Our results suggest that further work has the potential of yielding a more

nuanced picture of vegetation change leading up to and across the K/Pg boundary in the Western Interior.

Chapter 3: Plant taxonomic turnover and diversity across the Cretaceous-Paleogene boundary in northeastern Montana

The content of this chapter is intended for submission to

Paleobiology with authors P.K. Wilson Deibel, G.P. Wilson Mantilla, and C.A.E. Strömberg

3.1 ABSTRACT

The Cretaceous-Paleogene (K-Pg) mass extinction was a pivotal event in Earth history, the latest among five mass extinctions that devastated marine and terrestrial life. Whereas much research has focused on the global demise of dominant vertebrate groups, relatively little is known about local scale changes particularly among plant communities across the K-Pg boundary. This study investigates a suite of 11 floral assemblages spanning the K-Pg boundary in northeastern Montana constrained within a well-resolved chronostratigraphic framework. We evaluate the impact of the K-Pg mass extinction on local plant communities as well as the timing of recovery after the mass extinction. Our results indicate that taxonomic richness dropped by ~28% from the Late Cretaceous to Paleocene, a moderate decline compared with other records of plants across the K-Pg boundary. We also find that plant taxonomic composition changed; 63% of latest Cretaceous plant taxa disappeared across the K-Pg boundary, and while conifers were more likely to survive the K-Pg event they declined in abundance. Plant taxonomic richness returned to Late Cretaceous levels within 900 kyr after the K-Pg boundary. Overall, plant communities experienced major restructuring (changes in relative abundance) during the K-Pg mass extinction, even though no large (e.g., family-level) plant groups went extinct and local communities were quick to recover in terms of taxonomic diversity. These results have direct

bearing on our understanding of vegetation change during diversity crises, the differing responses of various plant taxonomic groups, and spatial variation in extinction and recovery timing.

3.2 INTRODUCTION

Mass extinctions are pivotal events in Earth history (Gould 1985) that vitally influenced the assembly of modern communities and that inform our current biodiversity crisis (e.g., Barnosky et al. 2011; Ceballos et al. 2020). The most recent of the 'Big Five' mass extinctions (Raup and Sepkoski 1982), the Cretaceous-Paleogene (K-Pg), constituted biotic turnover on a global scale which severely affected diverse aspects of both marine and terrestrial biotas (MacLeod et al. 1997; D'Hondt 2005). Proposed ultimate causes include the Chicxulub bolide impact (e.g., Alvarez et al. 1980; Schulte et al. 2010), Deccan volcanism (e.g., Keller et al. 2009), or some combination thereof (e.g., Arens and West 2008); proximal causes may have included short-term environmental change (e.g., temperature change, wildfire, acid rain) leading up to and across the K-Pg boundary (KPB), resulting in global ecosystem disruption (see e.g., MacLeod et al. 1997). Given its relative recency, the K-Pg mass extinction has particular relevance for modern times. It is documented by a greater quantity and quality of geological and paleontological data than are other mass extinction events, and it involved a greater proportion of taxa with living descendants or modern analogs whose ecology is well understood (Jablonski et al. 2003). Detailed studies of the K-Pg event in terrestrial settings have largely derived from study areas in the western interior of North America (WINA), with the Hell Creek study area of NE Montana among the most prominent (Clemens and Hartman 2014). The extensive and well-constrained geological and paleontological records of this study area have been used to document patterns of both the mass extinction and recovery of terrestrial vertebrate faunas (e.g., Wilson 2014); however, far less attention has been directed toward understanding the patterns among plants in NE Montana.

Data from the last four of the Big Five mass extinctions indicate that plants did not follow the turnover patterns of other marine or terrestrial biota (Wing 2004; McElwain and Punyasena

2007; Green et al. 2011). Plants did not undergo family-level extinctions; instead, selective extirpation of species at the local or regional level unseated dominant plant taxa and allowed so-called ‘disaster taxa’ to flourish until stable plant communities could once again reemerge (McElwain and Punyasena 2007; Vajda and Bercovici 2014). By comparison, terrestrial faunas experienced extinction of as much as 62% of families globally during past mass extinctions (Benton 1995). Potential drivers of this difference include the ability of plants to survive short-term disruption to their reproductive cycle (i.e., vegetative reproduction, seed dormancy), dietary differences (i.e., specialized diets in animals), and ecological differences (i.e., plant families with a variety of ecological or life strategies) (Wing 2004; McElwain and Punyasena 2007; Green et al. 2011). Given these fundamental differences between plants and animals, we that they would exhibit different responses to environmental crises (e.g., bolide impact). Evaluating whether such advantages for plant extinction and survival operated during the K-Pg mass extinction specifically requires additional, temporally well-resolved local records of floral dynamics.

The well-dated plant fossil record of northeastern (NE) Montana presents an excellent opportunity to document local floral dynamics across the KPB and to assess potentially important regional variation in turnover patterns. Our current understanding of plants across the K-Pg mass extinction is largely derived from studies in North Dakota, Colorado, and South America (see Background on Plants across the KPB); these studies document the regional and global variation in extinction magnitude and recovery timing. Previous work locally in NE Montana has investigated palynofloras (e.g., Hotton 2002; Arens et al. 2014b) and a few individual megafloras (e.g., Shoemaker 1966; Arens and Allen 2014; Wilson et al. 2021); however, these studies largely focus on biostratigraphy and taxonomy rather than diversity. Based on our current understanding of the event (see Background on Plants across the KPB), we

hypothesize that (H1) plant community composition was significantly altered by the K-Pg mass extinction event (and that this pattern was not driven by differences in depositional environments); and that (H2) plant species richness declined across the KPB, driven largely by elevated disappearances. Based on studies of Paleocene floras in North Dakota (Johnson 2002; Wilf and Johnson 2004), we also hypothesize that (H3) Paleocene floras in NE Montana remained taxonomically depauperate compared to Cretaceous floras for over 1 Myr after the KPB. Here, we test these hypotheses by documenting changes in taxonomic composition and richness in a composite stratigraphic sequence of 11 megafloral localities spanning ca. 2.3 Myr across the KPB (Fig. 3.1–2). We then compare our results from NE Montana with previous studies of plant response across the KPB in other areas to understand the spatial diversity of vegetational patterns during the mass extinction.

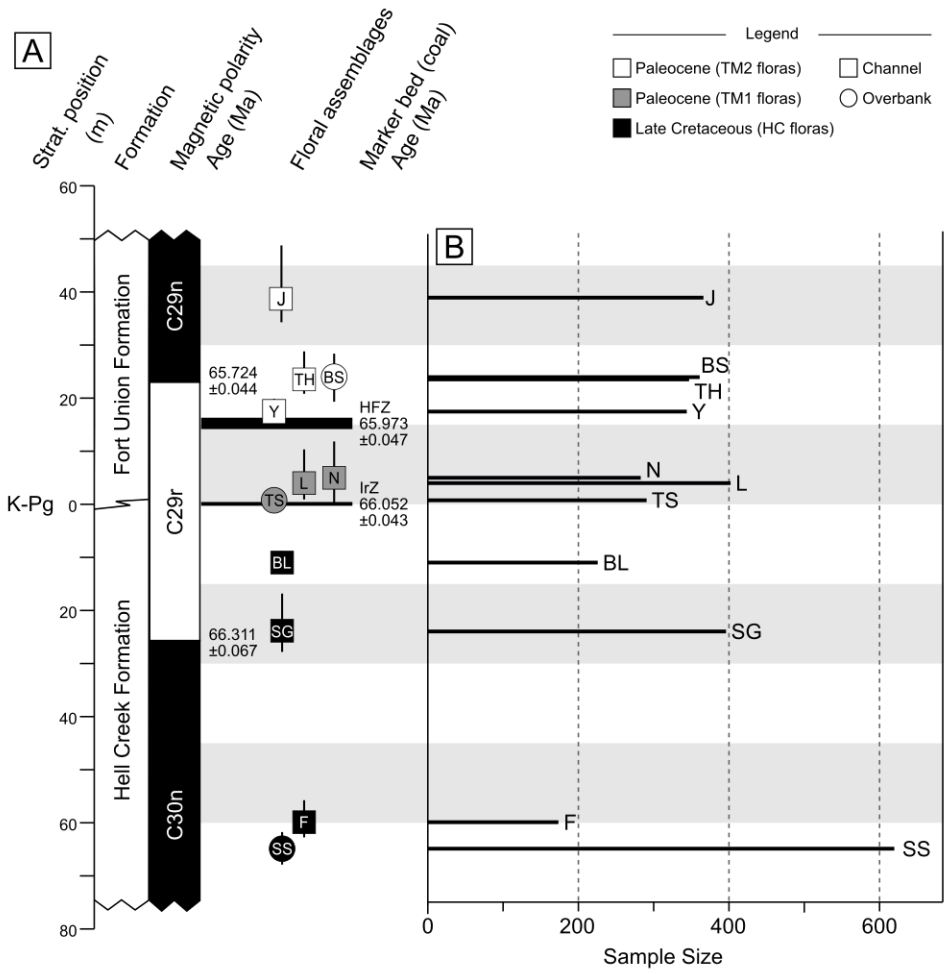

Figure 3.1: Chronostratagraphic framework and sampling of floral sites. A) Magnetostratigraphy, lithostratigraphy, and radioisotopic dating based on Moore et al. (2014), LeCain et al. (2014), and Sprain et al. (2015, 2018). Floras from this study are shown in stratigraphic position relative to observed marker beds. Floral assemblage abbreviations are as follows: SS = Seafood Salad, F = Fisk I, SG = Smurphy's Guess II, BL = Bruce Leaf, TS = The Swamp, L = Lerbekmo N, N = New York, Y = Yabba Dabba Do, TH = Tharp's Market, BS = Biscuit Springs, and J = Jane's. On the symbol of each floral assemblage, the vertical bar indicates stratigraphic position error (see text for method of estimation), the symbol color indicates the temporal interval, and the symbol shape indicates the sedimentary facies. Horizontal gray bars delineate 15-m stratigraphic intervals. B) The sample size of each assemblage is shown in the bar graph.

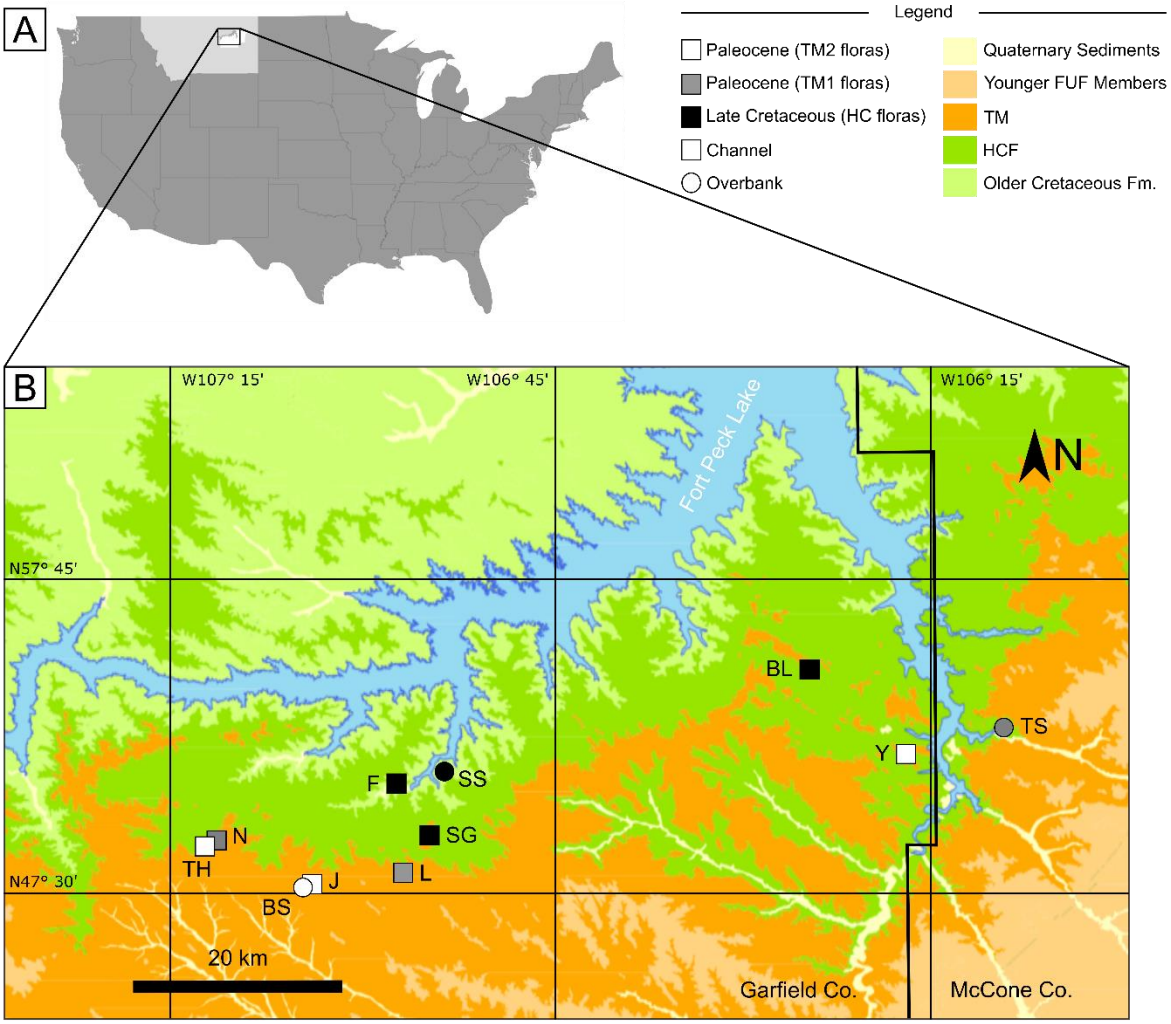

Figure 3.2: Map of Hell Creek study area. (A) Map of U.S.A. showing inset of Hell Creek area in Montana. (B) Inset of Hell Creek area in NE Montana showing the 11 localities in this study. Floral site symbols indicate the temporal interval (color) and sedimentary facies (shape). Floral assemblage abbreviations as in Fig. 3.1. Geologic formations mapped across the study area indicating approximate location of outcrops of the Hell Creek Formation (HCF) and Tullock Member (TM) of the Fort Union Formation (FUF) as well as other geologic units (based on Raines and Johnson 1995).

3.2.1 Background on Plants across the KPB

The pattern of plant turnover at the KPB varies globally, regionally, and with the type of plant fossil record analyzed (i.e., palynoflora versus megaflora). Palynofloral studies of the K-Pg mass extinction are more numerous and sample a larger geographic extent (both in terms of

global coverage and study area size) than megafloral studies do (see reviews by Spicer and Collinson [2014] and Vajda and Bercovici [2014]). Palynofloral studies generally document extirpation of 10–30% of the local palynotaxa (Vajda and Bercovici 2014). Comparatively, there are relatively few studies of megaflora capturing the lead-up, mass extinction, and recovery intervals. Recent study of Colombian pollen and leaf assemblages indicates that local taxonomic composition changed across the KPB, but extinction magnitude was not calculated (Carvalho et al. 2021). Megafloras from Argentinian Patagonia were greatly affected by the mass extinction, with loss of up to 90% of plant taxa (Stiles et al. 2020). Studies of megaflora from WINA show lower KPB extinction or extirpation, on the order of 50–75% of morphospecies (e.g., Wolfe and Upchurch 1986; Johnson 2002; Barclay et al. 2003; Wilf and Johnson 2004; Lyson et al. 2019).

Studies of the recovery after the K-Pg mass extinction show similar heterogeneity across the globe. Floras from the Williston Basin, North Dakota, remained depauperate throughout the Paleocene (ca. 10 Myr) (Johnson 2002; Wilf and Johnson 2004; Peppe 2010); incomplete records from the Bighorn and Hanna basins, Wyoming, similarly point to species-poor Paleocene floras (Hickey 1980; Wing et al. 1995; Dunn 2003). By contrast, plant communities in the Denver Basin, Colorado apparently recovered much more quickly (ca. 300 kyr post-KPB; Lyson et al. 2019). It has been postulated that diversity in the early Paleocene Denver Basin may have varied with topographic relief (Johnson and Ellis 2002; Johnson et al. 2003). Extinction selectivity may have differed in lowland versus upland environments or environmental heterogeneity in the uplands may have led to higher origination (Badgley et al. 2017; Antonelli et al. 2018). Farther south, Paleocene floras in the San Juan Basin exhibited higher species richness compared to the northern Great Plains, possibly the result of a latitudinal diversity gradient in plant communities linked to warmer and wetter climate conditions in southern WINA (Flynn and Peppe 2019).

Proximity to the causal mechanism or ecological stability associated with latitudinal diversity gradients may also have contributed to latitudinal selectivity during the mass extinction (Vilhena et al. 2012). The pattern of recovery is also variable in South America. Patagonian and Colombian Paleocene floras were relatively species-rich compared with WINA Paleocene floras, but Patagonian floras remained homogeneous through space and time during the Paleocene (Iglesias et al. 2007, 2021; Stiles et al. 2020) and Colombian floras did not regain pre-KPB species richness until the Eocene (Carvalho et al. 2021).

The highly variable patterns of K-Pg extinction and recovery among global plant communities may correlate with proximity to the causal mechanism, underlying ecosystem vulnerability, paleoclimate and topography, or biases inherent in the fossil record. Given this variability, high-resolution, local fossil records present the best opportunity to understand the effects of the K-Pg mass extinction and recovery. Furthermore, a nuanced understanding of such local records during mass extinctions is vital for better predicting patterns of ongoing and future biodiversity loss.

3.2.2 Geologic Setting of the Hell Creek study area

The Hell Creek Formation (HCF) and Tullock Member (TM) of the Fort Union Formation (FUF) are exposed in the northern Great Plains region and preserve rich fossil assemblages dated to the latest Cretaceous and earliest Paleogene. Researchers have developed a high-resolution chronostratigraphic framework for the HCF and TM based on biostratigraphy, lithostratigraphy, geochemistry, magnetostratigraphy, and geochronology. Sanidine-bearing tephras within discrete lignite beds (henceforth referred to as coals) have been dated using $^{40}Ar/^{39}Ar$ age determination (Sprain et al. 2015, 2018). The resulting ages for the coals have then been used to interpolate ages of the paleomagnetic reversals identified in local sections (Swisher

et al. 1993; LeCain et al. 2014; Sprain et al. 2015, 2018). We use the stratigraphic position of the plant fossil localities relative to marker beds to integrate our floras into this chronostratigraphic framework (summarized in Fig. 3.1; Archibald et al. 1982; Swisher et al. 1993; Renne et al. 2013; LeCain et al. 2014; Moore et al. 2014; Sprain et al. 2015, 2018).

The HCF is typically ~85–90 m thick (Hartman et al. 2014; Moore et al. 2014) and spans the magnetochron 30n/29r boundary (dated to 66.311 ± 0.067 Ma; Sprain et al. 2018). The upper contact of the HCF is typically placed at the base of the lowest, laterally continuous coal of the overlying FUF, referred to as the lower Z coal. In those exposures where a thin (~2 cm) claystone immediately below the lower Z coal preserves an iridium anomaly and other signatures of the K-Pg impact event (see review in Moore et al. 2014), the lower Z coal is referred to as the Iridium Z or IrZ coal (Archibald et al. 1982; Smit and Van Der Kaars 1984; Rigby and Rigby 1990; Murphy et al. 2002; Moore et al. 2014). A sanidine-bearing tuff recovered from the IrZ coal was recently dated to 66.052 ± 0.008/0.043 Ma (Sprain et al. 2018). In central Garfield County (where most of our fossil localities are), the HCF-FUF formational contact is often coincident with the KPB (identified by the presence of an impact claystone bed; Archibald et al. 1982; Moore et al. 2014). However, this formational contact is diachronous across the Williston Basin (see e.g., Nichols and Johnson 2002 and Clemens 2002 for discussion). In eastern Garfield and western McCone counties, the coal present at the base of the FUF is referred to as the McGuire Creek Z or MCZ. Prior studies indicate that the KPB (identified by chemostratigraphy and palynostratigraphy; Lofgren 1995; Arens et al. 2014a) is some few meters below the FUF-HCF contact in this area (Sprain et al. 2015; Smith et al. 2018). Recent work by Tobin et al. (2021) suggests that while the HCF-FUF contact and KPB are likely diachronous in this region, the stratigraphic placement of the KPB by Arens et al. (2014b) is suspect. We note this

diachroneity in our stratigraphic framework (Fig. 3.1) and account for this in our age determination of fossil localities. The TM spans the C29r/C29n reversal (dated to 65.724 ± 0.044 Ma; Sprain et al. 2018) and contains many dated marker beds. Here, we use the Hauso Flats or HFZ coal (dated to 65.973 ± 0.047 Ma; Sprain et al. 2015) as a marker bed to separate lower TM (TM1) localities from our middle TM (TM2) localities.

The HCF and FUF record terrestrial deposition in floodplain environments to the west of the receding Western Interior Seaway (Archibald 1982; Archibald et al. 1982; Fastovsky and McSweeney 1987; Swisher et al. 1993; Johnson et al. 2002; Murphy et al. 2002; Flight 2004; Hartman et al. 2014; Moore et al. 2014; Fastovsky and Bercovici 2016; Fowler 2020). Depositional environments in the HCF and FUF can largely be divided into channel and overbank settings. Channel deposits are typified by coarser grain size, often with inclined strata, and typically a higher degree of oxidation; overbank deposits (i.e., flood plain) are typified by finer grain size, horizontal massive or tabular strata, and lower oxidation (Fastovsky 1987; Johnson 2002). The rise in base level coincident with the deposition of the FUF is thought to be responsible for the increase in channel size and frequency and the widespread flood/pond horizons in the FUF (Fastovsky and McSweeney 1987; Retallack 1994). In this study, these characterizations are the basis for assignment of our localities to either channel or overbank facies and depositional environments (following the categorizations of Johnson [2002]).

3.3 METHODS

3.3.1 Fossil Collection

Here, we describe and analyze plant megafossils collected from 11 localities (3,809 identifiable specimens from 37 quarries) between 2015–2019 by a team of volunteers and researchers from the University of Washington. As voucher collections, all identifiable fossils were collected and accessioned into the University of Washington Burke Museum of Natural History and Culture (UWBM) with permissions from the Bureau of Land Management, the Charles M. Russell Wildlife Refuge administered by U.S. Fish and Wildlife and the Army Corps of Engineers, and private landowners (Table S3.1). The localities include relocated localities previously sampled by other researchers as well as localities discovered by our team. We excavated fossils using hand tools (i.e., pickaxe, chisel, and rock hammer). These collections primarily include compression and impression fossils of vegetative and reproductive plant structures.

A fossil assemblage may include collections from multiple quarries where plant fossils were distributed at multiple fossiliferous horizons or where a fossiliferous horizon cropped out at multiple points along a stretch of outcrop. We consider a plant fossil assemblage (or flora) as all fossils collected from quarries spanning no more than 40 m along strike and no more than 3 m of stratigraphic height at a given outcrop. Each quarry was given a unique UWBM locality number to distinguish them for future studies and collecting (Table S3.1). In this study, we aggregate collections from each locality into the 11 plant fossil assemblages described herein (Figs. 3.1–2).

3.3.2 Sedimentological Description and Stratigraphy

At each locality, we used a hand level and Jacob's Staff to measure stratigraphic thicknesses and distance to identified marker beds. We also recorded detailed lithological

descriptions of the fossiliferous horizon and surrounding 2–7 m of stratigraphy (Fig. S3.1). Each time we visited a locality, we verified the GPS coordinates of the quarry using a high-precision (< 1 m vertical and horizontal) Trimble R2 GNSS receiver. We also measured the stratigraphic distance of our locality to the nearest marker bed (i.e., dated coal bed, formational contact) using both a hand level with a Jacob's staff and the Trimble R2 GNSS receiver. For each stratigraphic distance measurement, we estimated uncertainty as some combination of instrument error (GPS accuracy, height of the fossiliferous horizon) and geologic context (height of channel body where appropriate). Because a channel body incises older strata, the floral assemblage within that channel body is younger than its stratigraphic height implies; therefore, the stratigraphic error bar may be vertically asymmetrical. These stratigraphic positional data were used to integrate each floral assemblage into the chronostratigraphic framework (Fig. 3.1).

Of the 11 localities in this study, four are Late Cretaceous (HC floras) and seven are early Paleocene (TM floras). The youngest Late Cretaceous flora (Bruce Leaf) is constrained to ca. 110 kyr before the KPB based on linear extrapolation of the stratigraphic positions and ages of the C30n/29r reversal and the IrZ coal nearby (data from Thomas Ranch compiled by Sprain et al. 2018). The oldest Paleocene flora (The Swamp) is 1.3 m below the MCZ coal; this stratigraphic position makes The Swamp most likely Paleocene in age, given the diachroneity between the HCF-FUF contact and the KPB in this region (see Geologic Setting). In addition, characteristic taxa (e.g., MT037 *Paranymphaea crassifolia*) indicate a Paleocene age for this flora. Three TM floras are from the TM1 temporal interval; their localities are stratigraphically above the KPB and below the HFZ coal and thereby constrained to within ca. 80 kyr after the KPB (between 66.052 ± 0.043 Ma and 65.973 ± 0.047 Ma; Sprain et al. 2015, 2018). The remaining four TM floras are from the TM2 temporal interval; their localities are

stratigraphically above the HFZ and below the W coal (65.118 ± 0.048 Ma; Sprain et al. 2015, 2018) constrained to ca. 80 to 900 kyr after the KPB (Fig. 3.1). These coals are not traceable at all our localities, but their stratigraphic positions are inferred through extrapolation; therefore, these age constraints should be considered approximate.

Using lithology to interpret depositional environment (summarized as channel versus overbank lithofacies, following Johnson [2002]), we classified eight of the localities as channel deposits (three Cretaceous and six Paleocene) and three as overbank deposits (one Cretaceous and two Paleocene) (Fig. 3.1).

3.3.3 Morphotype Identification and Taxon Assignment

We identified 3,809 specimens to morphotype based on organ type, gross morphology, and leaf architecture. The 11 floral assemblages in this study range from 173 to 618 identified specimens (Fig. 3.1). Angiosperm leaves were grouped and described based on leaf architecture following Ellis et al. (2009) (Table S3.2). Each morphotype was assigned a unique alphanumeric code (e.g., MT001; Table 3.1) to distinguish it from morphotypes in previous studies of leaf fossils from North Dakota (which used FH, HC, and FU prefixes; Johnson 1989; Peppe 2003; Peppe et al. 2007) and other locations in Montana (which used FP prefix; Arens and Allen 2014). Morphotypes that occur in the Seafood Salad flora were described in detail by Wilson et al. (2021).

We recognize 122 plant fossil morphotypes in this study: 95 are non-monocotyledonous angiosperms (“dicot”), nine are conifers, seven are pteridophytes, five are of indeterminate affinity, four are monocotyledonous angiosperms, one is a cycad, and one is a ginkgo. Of these, most are fossils of leaves or shoots with leaves (96), some are reproductive structures (e.g., fruits or cones; 20), and some are other vegetative structures (e.g., roots; 6) (Table 3.1). Each

individual specimen identified in our census count constitutes a single plant organ (e.g., leaf, root, fruit, or cone) for most morphotypes or a shoot with multiple leaves in the case of conifer vegetative morphotypes.

Morphotype Number	**Abundance**	**Species Name (where known)**	**Affinity**	**Structure**
MT090	681		DIC	Leaf
MT002	424	*Metasequoia occidentalis*	CON	Branchlet
MT004	321	*Glyptostrobus europaeus*	CON	Branchlet
MT012	318	cf. *Zizyphoides flabella*	DIC	Leaf
MT037	318	*Paranymphaea crassifolia*	DIC	Leaf
MT078	289		DIC	Leaflet
MT053	148		DIC	Leaf
MT023	112	*"Dryophyllum" subfalcatum*	DIC	Leaf
MT020	78	cf. *"Dryophyllum" tenneseensis*	DIC	Leaf
MT016	68	*Leepierceia preartocarpoides*	DIC	Leaf
MT096	68		DIC	Leaf
MT006	65		CON	Branchlet
MT039	61		DIC	Leaf
MT028	58		DIC	Seed
MT054	58		PTE	Leaflet
MT003	49	*Metasequoia occidentalis*	CON	Cone
MT050	48	*Nyssidium* sp.	DIC	Fruit
MT005	45	*Taxodium olrikii*	CON	Branchlet
MT013	43	*Quereuxia angulata*	DIC	Leaflet
MT091	39		DIC	Leaf
MT088	37		DIC	Leaf
MT106	31	*Limnobiophyllum scutatum*	MON	Leaf
MT108	27		MON	Vegetative
MT035	25		DIC	Leaf
MT009	24	*Erlingdorfia montana*	DIC	Leaf
MT007	22	*Ginkgo adiantoides*	GIN	Leaf
MT019	21		DIC	Leaf
MT079	21		DIC	Leaf
MT123	20		DIC	Leaf
MT027	19	*Carpites ulmiformis*	DIC	Fruit
MT047	19		DIC	Leaf
MT121	15		DIC	Leaf
MT030	14		DIC	Seed
MT095	13		DIC	Leaf
MT100	13		DIC	Leaf
MT127	13	*Equisetum* sp.	PTE	Stem

MT034	12	*Azolla* sp.	PTE	Branchlet
MT073	12		DIC	Leaf
MT087	12		DIC	Leaf
MT099	11		DIC	Leaf
MT110	11		DIC	Leaf
MT125	10		DIC	Leaf
MT045	9		DIC	Leaf
MT024	8		DIC	Leaf
MT092	8		DIC	Leaf
MT044	7		DIC	Leaf
MT077	7		DIC	Leaf
MT056	6		DIC	Fruit
MT101	6		DIC	Leaf
MT104	6		DIC	Leaf
MT112	6		DIC	Leaf
MT124	6		DIC	Leaf
MT010	5		DIC	Leaf
MT026	5		DIC	Leaf
MT032	5		PTE	Leaflet
MT040	5	*Mciveriella hydrocotyloidea*	DIC	Leaf
MT043	5		DIC	Leaf
MT069	5		DIC	Leaf
MT082	5		DIC	Leaf
MT083	5		DIC	Leaf
MT089	5		DIC	Leaf
MT068	4		DIC	Leaf
MT084	4		DIC	Leaf
MT018	3		DIC	Leaf
MT022	3		DIC	Leaf
MT025	3		DIC	Leaf
MT062	3		MON	Leaf
MT113	3		DIC	Root
MT001	2	*Fokieniopsis catenulata*	CON	Branchlet
MT021	2		DIC	Leaf
MT041	2		DIC	Leaf
MT049	2		DIC	Leaf
MT061	2		DIC	Leaf
MT063	2		CON	Branchlet
MT064	2		DIC	Fruit
MT070	2		DIC	Leaf
MT071	2		DIC	Seed
MT074	2		DIC	Leaf
MT081	2		DIC	Leaf

MT085	2		DIC	Seed
MT086	2		DIC	Leaf
MT094	2		DIC	Leaf
MT098	2		DIC	Leaf
MT103	2	*Nilssonia comtula*	CYC	Leaf
MT109	2		indet.	Stem
MT117	2		DIC	Leaf
MT118	2		DIC	Leaf
MT119	2		DIC	Leaf
MT120	2		CON	Cone
MT126	2		DIC	Leaf
MT008	1	*Cobbania corrugata*	MON	Leaf
MT014	1		DIC	Leaf
MT015	1		DIC	Leaf
MT017	1		DIC	Leaf
MT029	1		DIC	Fruit
MT031	1		PTE	Leaflet
MT033	1	*Hydropteris pinnata*	PTE	Leaflet
MT036	1	*Nelumbo* sp.	DIC	Leaf
MT038	1		DIC	Fruit
MT042	1		DIC	Leaf
MT046	1		DIC	Leaf
MT048	1		DIC	Leaf
MT051	1		indet.	Vegetative
MT052	1		indet.	Reproductive
MT057	1		DIC	Seed
MT058	1		DIC	Seed
MT059	1		DIC	Seed
MT065	1		DIC	Leaf
MT067	1		indet.	Reproductive
MT072	1		indet.	Reproductive
MT075	1		DIC	Leaf
MT076	1		DIC	Leaf
MT080	1		DIC	Fruit
MT093	1		PTE	Stem
MT097	1		DIC	Leaf
MT102	1		DIC	Fruit
MT105	1		DIC	Root
MT111	1		DIC	Leaf
MT114	1		DIC	Leaf
MT115	1		DIC	Leaf
MT116	1		DIC	Leaf
MT122	1		CON	Branchlet

Table 3.1: Abundance and affinity of morphotypes. Taxonomic affinities included when known. CON = conifer; CYC = cycad; DIC = dicot/non-monocotyledonous angiosperm; GIN = ginkgophyte; MON = monocotyledonous angiosperm; indet. = indeterminate; PTE = pteridophyte.

3.3.4 Data Analyses

Fossil datasets.

We used three permutations of the fossil census data in our analyses to account for potential biases (Table 3.2). The most inclusive dataset (Dataset 1; Table S3.3) includes the abundance of each morphotype by locality. Some studies recommend the removal of singletons from analyses to mitigate preservational or taphonomic biases (Foote 2000); Dataset 2 therefore excludes singletons (Table S3.4). Additionally, reproductive morphotypes may come from the same species as vegetative morphotypes and thereby inflate species richness estimates. To account for this, Dataset 3 includes leaf morphotypes only (Table S3.5) as a minimum estimate of taxonomic diversity (following Wilf and Johnson 2004).

For most analyses, we compare taxonomic abundance or presence/absence by floral assemblage (specimens from a single locality). We also pool specimens from each floral assemblage into HC, TM1, and TM2 temporal intervals to examine floral changes across and after the KPB.

Dataset	Description	Number of Morphotypes
Dataset 1	All plant groups, all organs.	122
Dataset 2	All plant groups, all organs, excluding singleton taxa.	43
Dataset 3	All plant groups, only leaf morphotypes.	95

Table 3.2: Summary of datasets used in analyses in this study. All datasets use abundances of morphotypes by locality.

Taxonomic Composition

We first analyzed changes in community composition across this interval using an ordination and ANOSIM of relative abundance data to test our first hypothesis (H1). Ordination

analyses are commonly used in community ecology to plot communities in low-dimensional space based on their taxonomic similarity (see Reyment 1963; Kovach 1989). Here we used an unconstrained nonmetric multidimensional scaling (NMDS) ordination because this method is appropriate for species abundance data, avoids assumption of linearity among variables, and is relatively robust to the arch effect (Minchin 1987; Clarke 1993). Although there are drawbacks to NMDS (e.g., see discussion in Donohue et al. 2013), careful selection of ordination parameters (number of dimensions and distance metric) and vetting of stress for significance can alleviate these concerns.

We conducted our NMDS ordination based on relative abundance using the Bray-Curtis distance metric (designed for species abundance data; Bray and Curtis 1957), reducing to $k = 2$ dimensions, and running the analysis 100 times to find the minimum stress solution. We calculated both taxon and flora scores in this ordination. To evaluate the fit of the NMDS, we ran a Monte Carlo simulation (see Supplement for code; $n = 100$). To better understand the factors driving the ordination patterns, we also fit our site variables (facies and age) to the NMDS axes and calculated the weight of these variables to each axis (envfit function in the vegan package using 1,000 permutations; Okansen et al. 2019). Finally, we quantified the differences in taxonomic composition between HC and TM floras through an analysis of similarity (ANOSIM). ANOSIM utilizes rank dissimilarity and is therefore well suited to be paired with an NMDS ordination (Clarke and Warwick 1994); we used the relative abundance of taxa in Dataset 1 and the Bray-Curtis distance metric to compare directly with NMDS results.

We investigated which taxa might be driving shifts in taxonomic composition from HC to TM floras through several species-centered analyses. We examined the distribution of species in the NMDS ordination. We also compared how conifers versus angiosperms changed from HC to

TM floras through a Mantel test (Mantel 1967). This test is based on Pearson's correlation of the Bray-Curtis distances between our localities; we used the abundance data of conifer or angiosperm vegetative morphotypes for this analysis (Dataset 3) as a conservative estimate of species abundance.

Taxonomic Turnover and Diversity

We further examined our first and second hypotheses (H1, H2) that plant communities changed across the KPB in both taxonomic composition and diversity by examining patterns of turnover (appearances and disappearances) as well as diversity (taxonomic richness) across this interval. We first calculated the percent disappearance from HC to TM floras as a measure of extinction magnitude, using range-through occurrences. Following Wilf and Johnson (2004), we excluded singleton taxa (Dataset 2) when tabulating biostratigraphic ranges because of potential sampling biases. We grouped our localities into 15-m stratigraphic bins to minimize sampling bias in our composite section (again following Wilf and Johnson 2004). We then calculated 50% stratigraphic confidence intervals for each of the biostratigraphic ranges, following Wilf and Johnson's (2004) expansion of the Strauss and Sadler (1989) method as outlined by Wilson (2005; 2014). This method uses the abundance and range of a given taxon to estimate the uncertainty in its record (i.e., an abundant taxon found in only a short range has a higher uncertainty on the upper and lower bounds of that range); further, the method calculates the upper and lower confidence intervals by incorporating the sample size in the bins above and below the taxon's observed range (i.e., if the bin above the taxon's observed range is particularly well-sampled, it is less likely the taxon is present in that bin). These confidence intervals are provided for observation and were not incorporated into calculations of percent appearances or disappearances.

Previous researchers have calculated per-capita origination and extinction rates to test hypotheses about patterns of turnover (e.g., Wilf and Johnson 2004). However, given that our floras are unevenly spaced through this time interval, per-capita rates would likely have low accuracy (i.e., large time gaps over which we cannot infer rates). Instead, to test our second hypothesis (H2), we used proportional disappearances and appearances to evaluate turnover through time. Proportional disappearances in each flora were calculated as the percentage of taxa with their last occurrence in that flora, whereas proportional appearances were calculated as the percentage of taxa with their first occurrence in that flora, both out of the total raw richness of that flora. Approaching the upper or lower bounds of our record, our ability to accurately detect a taxon's presence and therefore accurately measure appearances or disappearances declines due to sampling biases (edge effects; Foote 2000). Therefore, we omit the oldest and youngest floras in our calculations where appropriate. We also subsampled our abundance data (Dataset 1) to n = 173 specimens (our smallest sample size) for n = 50 replicates and calculated 95% confidence intervals on the proportions of disappearances and appearances.

Finally, to test our third hypothesis (H3) that Paleocene floras remained depauperate through our section, we calculated taxonomic diversity through time using (a) taxonomic richness and (b) rarefaction curves that employ both extrapolation and interpolation.

Taxonomic richness is commonly used as a metric for diversity in paleoecology, but it does not consider the contribution of relative abundance and is heavily impacted by the often-low sample size in fossil assemblages (Gotelli and Colwell 2001). We used two measures of richness to account for this bias: 1) range-through (standing) richness and 2) rarefied richness. Range-through richness is calculated by assuming that if a taxon is present in the preceding and succeeding time intervals (floras), then its absence from a given time interval (flora) represents a

sampling error and not true absence. For fossil data, this assumption is considered reasonable as a means of estimating maximum diversity and to accommodate uneven temporal sampling effort (Foote 2000; Wilf and Johnson 2004). We note that sampling biases result in low range-through richness at the beginning and end of our record (edge effect; Foote 2000). We used Dataset 3 (vegetative morphotypes) and calculated 95% confidence intervals on range-through richness in the same manner as for proportional disappearances and appearances (described above). Rarefied richness, which has become standard in paleoecology (Siegel and German 1982; Foote 2000), uses subsampling of abundance data to estimate taxonomic richness at a lower sample size through interpolation, thereby allowing for the direct comparison of fossil assemblages with varying sample size. We rarefied our abundance data to the smallest sample size (see Table 3.3) and calculated standard error. We used Dataset 3 (vegetative morphotypes) for a more conservative estimate of taxonomic richness and Dataset 1 to enable comparison with other studies in which a similar approach was used. To quantify differences in diversity through time, we used a Mann-Whitney *u*-test to compare taxonomic richness at different time intervals. This test is non-parametric and therefore does not assume that samples are normally distributed (McKnight and Najab 2010). We compared floras both by age (HC, TM1, and TM2) and by depositional environment (channel versus overbank) to investigate the potential confounding influence of taphonomy.

Rarefaction and extrapolation curves were calculated using an interpolative-extrapolative richness metric (R package iNEXT package; Hsieh et al. 2016). Rarefaction and extrapolation curves allow for the analysis of taxonomic richness across assemblages of variable sample size as well as observation of sample evenness, another component of diversity (Gotelli and Colwell 2001). Although extrapolated richness has been criticized for its low accuracy when sample sizes

are low (i.e., Melo et al. 2003), recent work has pointed to its utility, particularly because interpolative richness may compress richness ranges (Close et al. 2018). Especially for highly variable sample sizes such as ours, interpolative-only richness subsampled to the lowest sample size may flatten the range of estimated richness, thereby compressing the differences between floras. We present both rarefaction (interpolation) and prediction (extrapolation) to compare results from these different approaches. We calculated curves for each floral assemblage as well as for floral assemblages grouped by temporal interval (HC, TM1, or TM2) with 95% confidence intervals. We used our vegetative morphotypes only (Dataset 3) as a conservative estimate of richness.

All analyses were conducted in R version 4.0.2 (R Core Team, 2020; http://www.r-project.org) using the community ecology package vegan version 2.5–7 (Okansen et al. 2019), the fossil diversity dynamics package divDyn (Kocsis et al. 2019), and the species diversity package iNEXT (Hsieh et al. 2016). See Supplementary Material for code.

3.4 RESULTS

3.4.1 Taxonomic Composition

Taxonomic composition is significantly different between HC and TM floras. Our NMDS ordination is a relatively good fit to the underlying data; stress is low (0.0815) and significant based on Monte Carlo simulation ($p = 0.010$), indicating that this ordination is a good representation of the variance in our data (Clarke and Warwick 1994). In the NMDS biplot (Fig. 3.3), HC floras cluster low on the first and second NMDS axes, whereas TM1 and TM2 floras cluster higher on both axes, with the TM2 floras intermediate between HC and TM1 floras. Using age as a predictor of distribution in the ordination, we found that age significantly correlates with the ordination results (envfit $R^2 = 0.4599$, $p = 0.0070$), loading mostly on axis 1 (Fig. 3.3). Furthermore, the differences in taxonomic composition between HC and TM floras and between HC, TM1, and TM2 floras are significant (ANOSIM $p = 0.003$ and $p = 0.001$, respectively). In contrast, sedimentary facies does not significantly correlate with floral composition (envfit $R^2 = 0.1230$, $p = 0.2877$), and there are not significant differences in taxonomic composition between channel and overbank floras (ANOSIM $p = 0.362$).

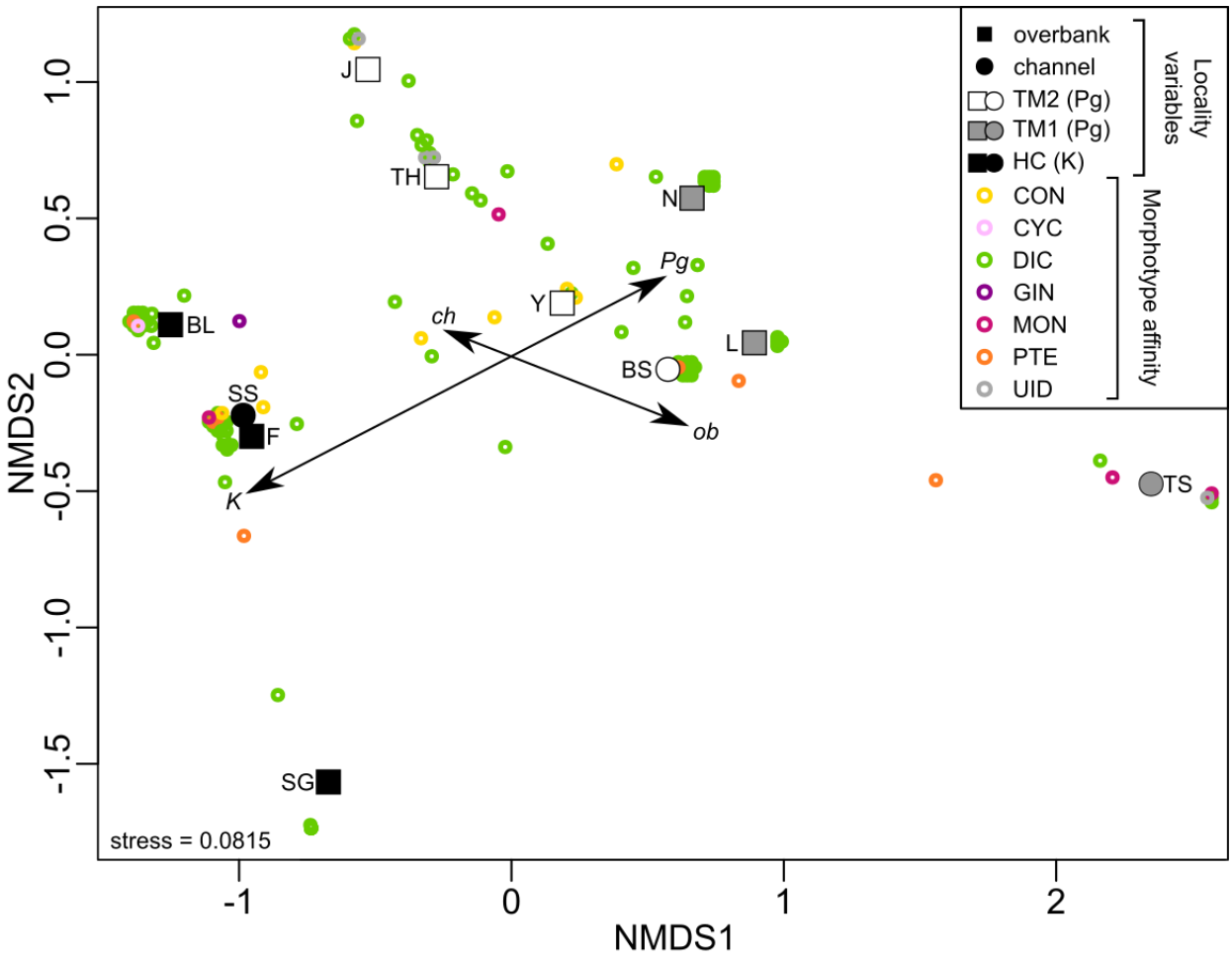

Figure 3.3: Biplot of NMDS ordination of morphotype abundance at the 11 localities. Distance was measured using Bray-Curtis dissimilarity. Stress (0.0815) is relatively low and significant based on Monte Carlo simulation (p = 0.010). Symbols represent taxa (colors correspond to major plant group affinity) and floral assemblages (colors and shapes represent age and sedimentary facies). Age and sedimentary facies were fit to NMDS axes, and the centroids of these groupings are plotted as vectors. Age explains significant variation in the analysis (envfit p = 0.0070) whereas facies does not (envfit p = 0.2877). Abbreviations: CON = conifer, CYC = cycad, DIC = non-monocotyledonous angiosperm, GIN = ginkgo, MON = monocotyledonous angiosperm, PTE = non-seed vascular plant (pteridophyte), UID = indeterminate, K = Cretaceous, Pg = Paleogene, ob = overbank, ch = channel. Floral assemblage abbreviations as in Fig. 3.1.

The NMDS analysis shows that distinct suites of mostly non-monocotyledonous angiosperm taxa plot with HC or TM floras. Conifer taxa are more likely to be shared across HC and TM floras, plotting between them in ordination space (Fig. 3.3). Furthermore, conifers and

angiosperms are not significantly correlated in their distribution across the localities (Mantel statistic r = 0.1528, $p = 0.17$). However, whereas conifers are more likely to be shared between HC and TM floras, the relative abundance of these conifer taxa dramatically declined from HC (35%) to TM1 (6%) floras and then increased again in TM2 floras (25%; Dataset 1). Other non-angiosperms (e.g., the cycad *Nilssonia comtula* MT103, and *Ginkgo adiantoides* MT007) are rare in the sampled floras, and their distributions are therefore harder to characterize. Several monocotyledonous angiosperm and pteridophyte taxa plot close to the TM localities in ordination space; these represent common wetland or aquatic taxa such as *Equisetum* sp. (MT127), *Azolla* sp. (MT034), and *Limnobiophyllum scutatum* (MT106). Figure 3.4 shows images of a selection of taxa from the HC and TM floras.

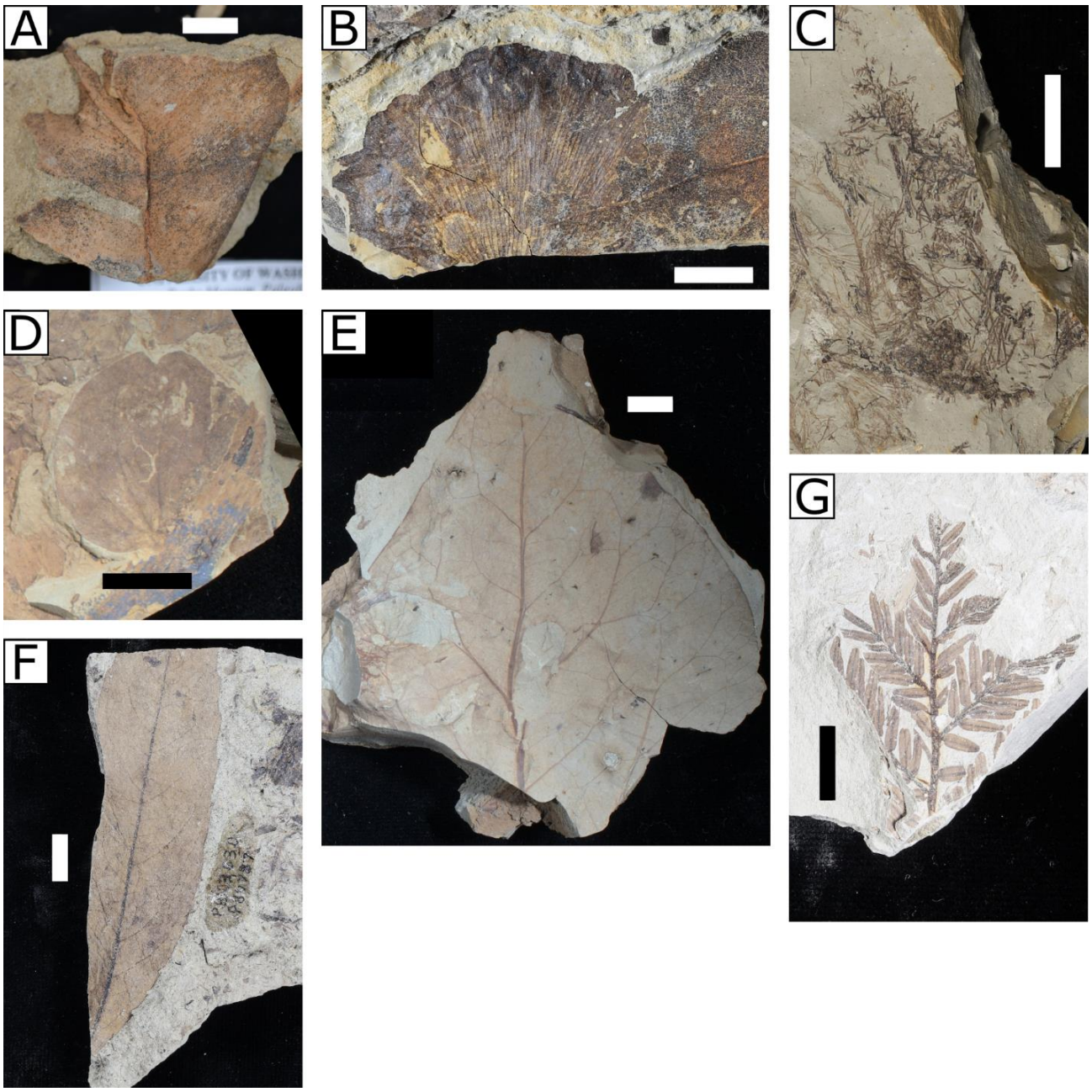

Figure 3.4: Examples of taxa sampled in the HC and TM floras of this study; (A) MT103 *Nilssonia comtula*, University of Washington Burke Museum (UWBM PB 105816.1; (B) MT007 *Ginkgo adiantoides*, UWBM PB 96540; (C) MT034 *Azolla* sp., UWBM PB 97843; (D) MT106 *Limnobiophyllum scutatum*, UWBM PB 99364; (E) MT037 unnamed dicot, UWBM PB 103656; (F) MT023 *"Dryophyllum" subfalcatum*, UWBM PB 103630; (G) MT002 *Metasequoia occidentalis*, UWBM PB 103535.2. Scale bar equals 1 cm.

3.4.2 Taxonomic Turnover and Diversity

Analysis of taxonomic turnover shows that a large proportion of plant morphotypes disappeared across the KPB. Of the 63 HC morphotypes (Dataset 1), 48 (76%) disappeared at the KPB, whereas 41 of 52 (79%) vegetative HC taxa (Dataset 3) were lost at the KPB. Most of the taxa that disappeared at the KPB are singletons; only eight of 23 (35%) non-singleton morphotypes (Dataset 2) disappeared at the KPB (Fig. 3.5). When we restrict the analysis to the uppermost 15 m of the HCF (i.e., Bruce Leaf flora), which corresponds to the last ca. 110 kyr of the Late Cretaceous, 17 of 27 (63%) morphotypes were lost at the KPB. By restricting our analysis to the uppermost HCF, we exclude any earlier disappearances that were not associated with the mass extinction event and reduce the chance of artificially inflating our estimate of extirpation at the KPB. On the other hand, by restricting our analysis to the uppermost 15 m of the HCF we acknowledge that our sample size is very low (a single HC flora) and therefore we may not be accurately reflecting the diversity of pre-KPB vegetation. In general, disappearance rates were high throughout the HC interval; whereas the overall loss of taxa from the HC to TM was ~76% (Fig. 3.5), proportional disappearances from one HC flora to the next ranged from 35–63% (Fig. 3.6A). Disappearances peaked in the latest HC flora and dropped just after the KPB, but there is no distinct spike in disappearances at the KPB (Fig. 3.6A).

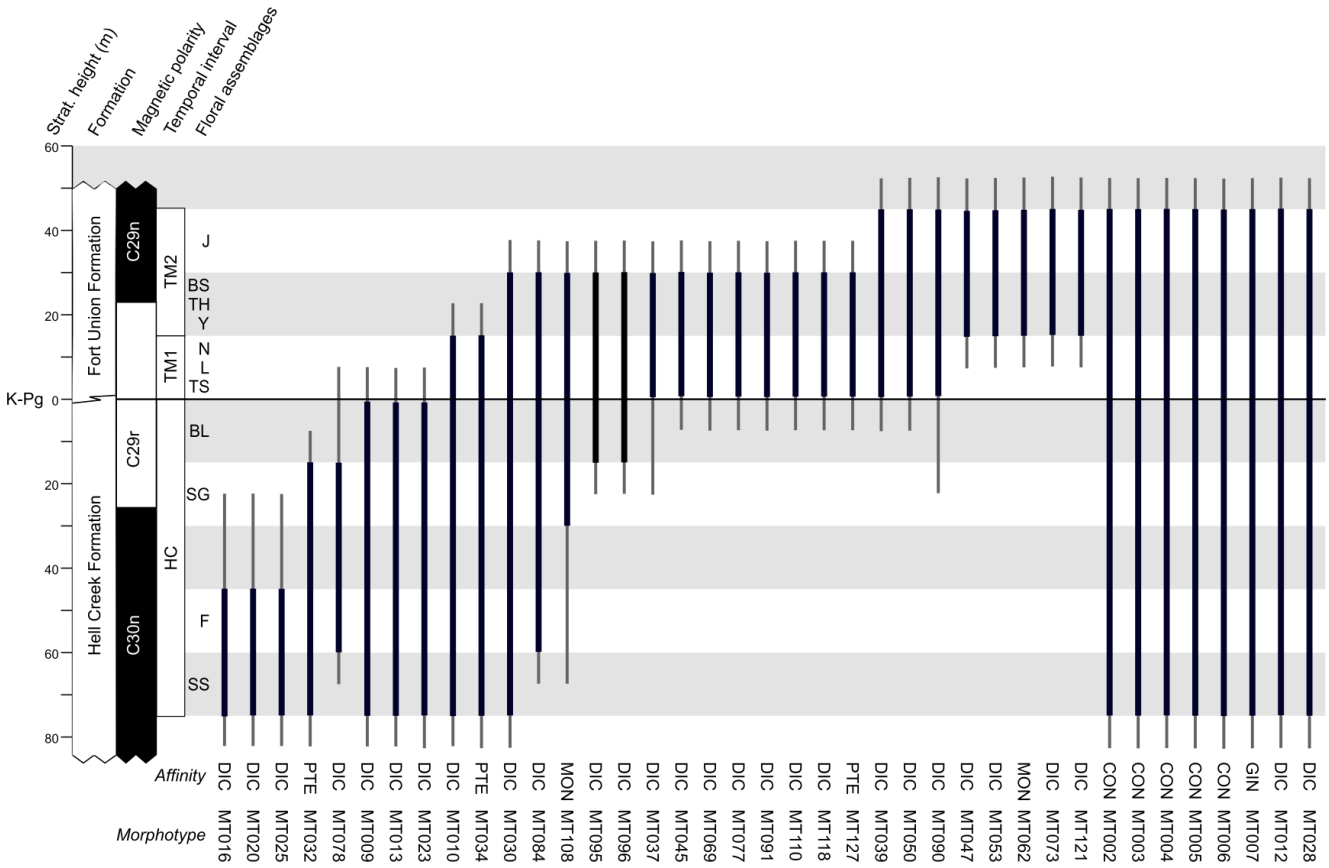

Figure 3.5: Stratigraphic ranges for non-singleton taxa in this study. The ranges (thick, vertical black bars) are based on occurrences at the 11 floras, which are grouped into 15-m bins. The stratigraphic section at the left shows the stratigraphic height relative to the K-Pg boundary, geologic formations, paleomagnetic polarity chrons, temporal intervals (HC, TM1, TM2), and localities included in each stratigraphic bin (marked by alternating white and gray horizontal bands). Floral assemblage abbreviations as in Fig. 3.1. Light gray vertical lines indicate 50% confidence intervals. Note that taxa which are found in the uppermost or lowermost bin in our section may be found before or after, but we do not have records of their occurrences outside of this section. Morphotype and major plant group affinity of the taxon shown at bottom (abbreviations: CON = conifer, DIC = non-monocotyledonous angiosperm, GIN = ginkgo, MON = monocotyledonous angiosperm, PTE = pteridophyte).

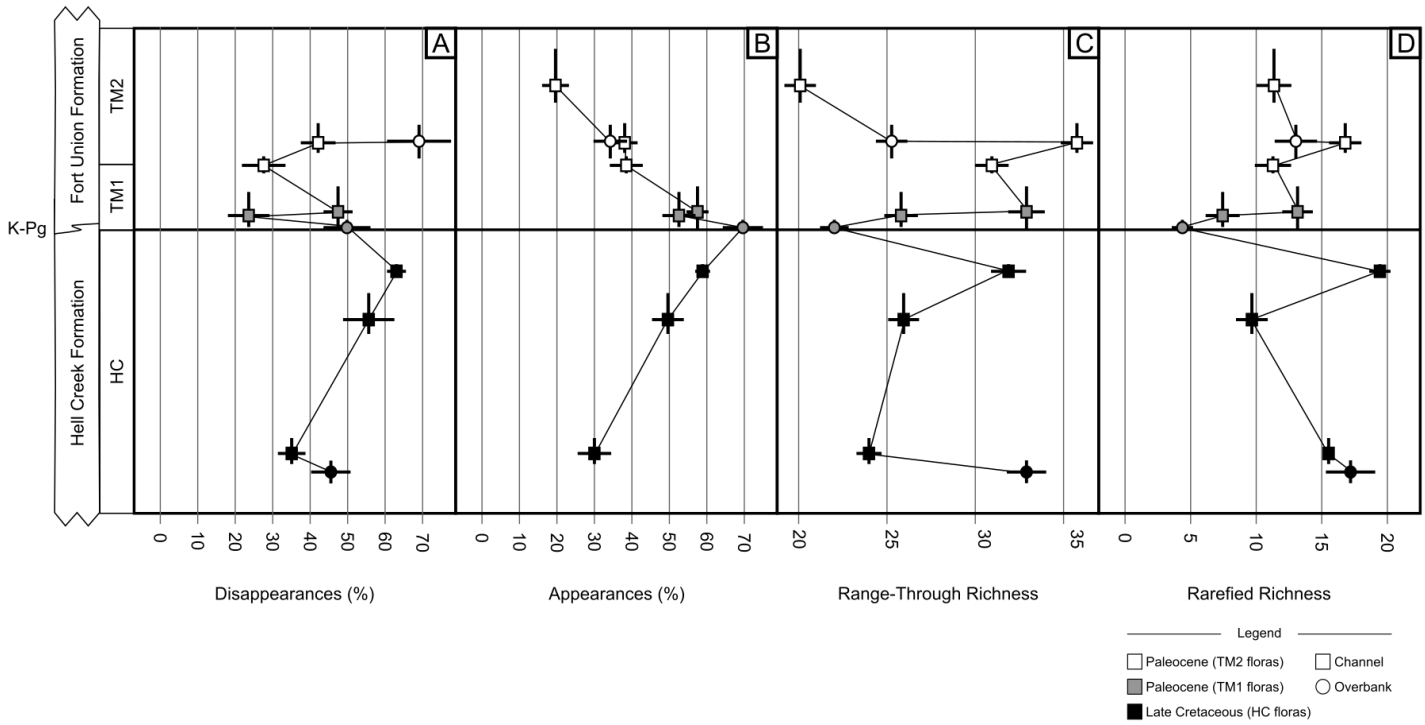

Figure 3.6: Taxonomic turnover and diversity through our study interval at each of the 11 floras. Disappearance (A) is the percentage of taxa that end their stratigraphic range in that flora and appearance (B) is the percentage of taxa that begin their stratigraphic range in that flora. Range-through richness (C) is the number of taxa with range-through occurrences in that time interval. Because the proportion of disappearances and appearances (A–B) are influenced by the start and end of our sequence, we have excluded the oldest and youngest floras where appropriate. On the left, the formations are indicated along with the temporal intervals used in this study (HC, TM1, and TM2). Turnover and diversity values are plotted at the stratigraphic height of the corresponding flora. Marker shape represents sedimentary facies, vertical lines on markers represent stratigraphic uncertainty, and horizontal lines represent 95% confidence intervals based on subsampling of data to N = 173 specimens (A–C) or N = 143 specimens (D). Values for A–C were calculated using all taxa (Dataset 1) and values for D were calculated using vegetative morphotypes only (Dataset 3).

Our analysis further indicates that a high proportion of appearances in the TM1 interval contributed to the KPB turnover to an even higher degree than disappearances (Fig. 3.6B). Proportional appearances increased throughout the HC and reached a peak (70%) in the oldest TM1 flora (Fig. 3.6B). This peak in appearances in the TM1 coincides with the taxonomic turnover we observed between HC and TM1 floras (Fig. 3.3).

Rarefied taxonomic richness was 28% greater in HC floras, on average, than in TM floras (vegetative morphotypes only; Table 3.3), although the difference is not significant (HC average rarefied richness 15.9; TM average rarefied richness 11.5; *u*-test $p = 0.1636$; Table 3.3). The same pattern holds true when all morphotypes are considered (Dataset 1; Table 3.3), but there is no difference in rarefied richness by sedimentary facies (*u*-test $p = 1.000$; Dataset 3; Table 3.3). Specifically, rarefied richness dropped 45% from HC to TM1 floras (TM1 flora average rarefied richness 8.8, *u*-test $p = 0.0571$; Table 3.3); range-through richness also dropped immediately across the KPB (Fig. 3.6C–D). Rarefied richness then increased by 55% from TM1 to TM2 floras (*u*-test $p = 0.2000$; Table 3.3); range-through richness exceeded HC levels during the TM2 interval (Fig. 3.6C–D). Although none of these differences are statistically significant, the changes in both range-through and rarefied richness through time are large (Fig. 3.6C–D).

Dataset	Rarefied Sample Size	Floras in Comparison	Average rarefied richness	*u*-test *p*-value
Dataset 3 (vegetative)	143	TM	11.5 (28% decrease)	0.0818
		HC	15.9	
		TM1	8.8 (45% decrease)	0.0571
		HC	15.9	
		TM2	13.6 (55% increase)	0.2000
		TM1	8.8	
		Channel	13.6	1.0000
		Overbank	12.0	
Dataset 1 (all taxa)	173	TM	15.5 (24% decrease)	0.1152
		HC	20.3	

Table 3.3: Comparison of average rarefied richness of floras by temporal interval and sedimentary facies.

Rarefaction and extrapolation curves for these floras also point to a large drop in taxonomic richness at the KPB (Fig. 3.7). Average richness is higher in the HC than in the TM; in addition, TM2 floras are slightly richer than TM1 floras (Fig. 3.7A). However, richness is

highly variable among individual floras within these temporal intervals (Fig. 3.7B); this variability in richness among individual floras likely contributes to the non-significance of our results comparing rarefied richness grouped by temporal interval (Table 3.3). One HC flora in particular has extremely low taxonomic richness (Smurphy's Guess rarefied richness is 10.1; Fig. 3.7B). When we exclude this anomalous HC flora, the difference in rarefied richness between HC (average rarefied richness 17.9) and TM (average rarefied richness 11.5) floras is significant (*u*-test $p = 0.0167$; Dataset 3). Furthermore, richness rebounds relatively quickly in the earliest Paleocene, and our youngest TM1 flora has similar richness to many TM2 floras (Figs. 3.6–7). Given this rapid increase in taxonomic richness in the TM1 interval, comparing average HC to TM1 taxonomic richness may not accurately capture the interval of greatest change in richness across the KPB. Considering just the immediate change across the KPB, rarefied richness dropped by 75% from the oldest HC flora to the youngest TM1 flora (Figs. 3.6–7).

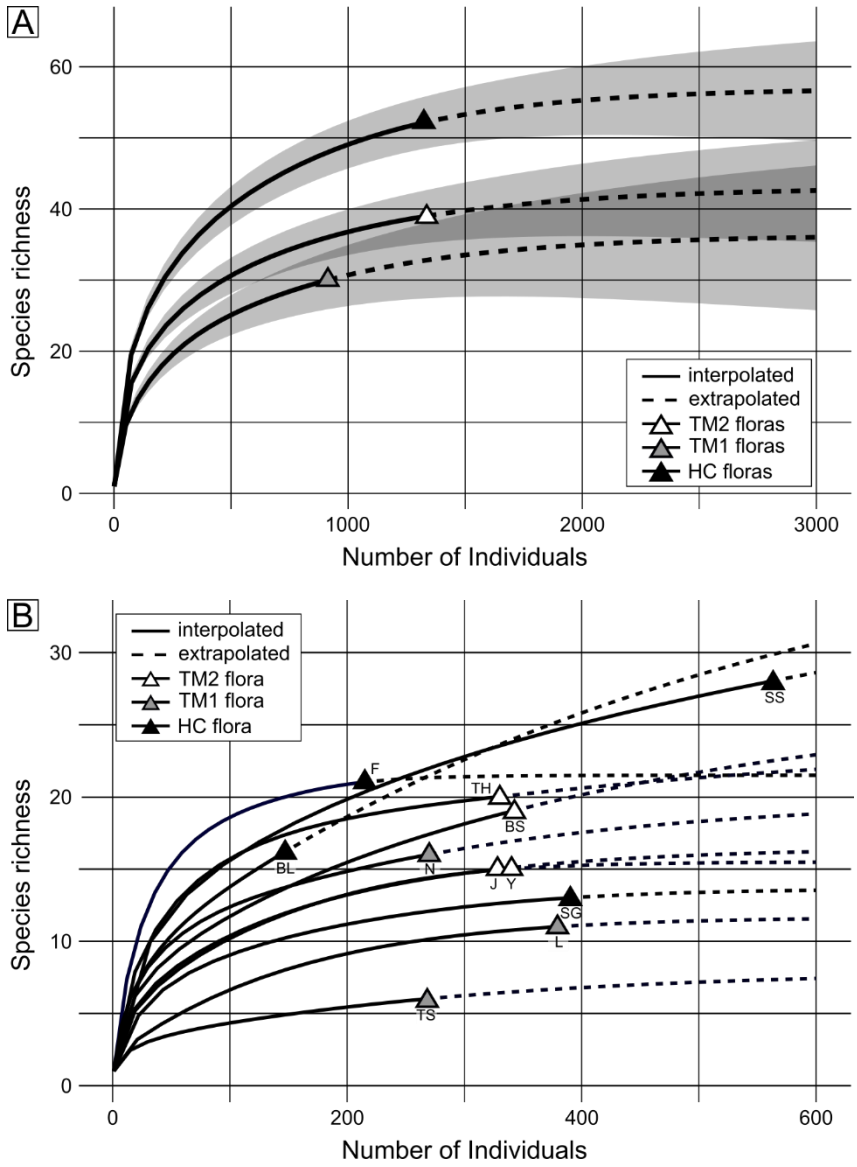

Figure 3.7: Rarefaction and extrapolation curves for each time interval and for each individual flora. (A) Combined rarefaction and extrapolation curves based on species abundance data for floras in the HC, TM1, and TM2 intervals. Shaded regions represent 95% confidence intervals to a target sample size of 3,000 (darker shading indicates overlap). (B) Combined rarefaction and extrapolation curves for each floral assemblage to a target sample size of 600. Marker colors correspond to temporal interval (HC, TM1, or TM2); floral assemblage abbreviations as in Fig. 3.1. In all analyses, we used only vegetative morphotypes (Dataset 3).

3.5 DISCUSSION

3.5.1 Pattern of floral turnover across the KPB

Our results show that the K-Pg mass extinction led to a distinct change in the taxonomic composition and diversity of floras in the Hell Creek study area of NE Montana, as we hypothesized (H1). Floras from the last ca. 1.3 Myr of the Cretaceous were, on average, taxonomically rich (high alpha diversity) and heterogeneous (high beta diversity), either spatially, temporally, or both. Cretaceous vegetation was characterized by a distinct suite of taxa consisting mostly of angiosperms as well as several conifers and pteridophytes (e.g., 'ferns').

At the KPB we find evidence for a substantial drop in taxonomic richness and a significant loss of plant taxa, either due to extirpation or extinction. Between our HC and TM floras, there was a ~28% drop in rarefied richness (Fig. 3.6D). Although this drop in average richness is not statistically significant, it is large, and we suggest the lack of statistical significance may be due to variability in richness among HC floras (Fig. 3.7B) as well as the relatively rapid increase in taxonomic richness during the TM1 interval (Fig. 3.6C–D). Removing the anomalously low-richness mid-HC flora results in a statistically significant 36% drop in rarefied richness from HC to TM floras, and comparisons of the drop in richness immediately across the KPB (75%) unequivocally show that taxonomic diversity declined across the KPB. We also document the disappearance of ~63% of latest Cretaceous taxa (from ca. 110 kyr before the KPB). We view this 63% disappearance figure as the best estimation of extinction magnitude, as this excludes any earlier Cretaceous disappearances which were not associated with the mass extinction event. These changes in taxonomic composition observed across the KPB were driven by a high proportion of appearances in the earliest Paleocene combined with elevated disappearances in the latest Cretaceous (Fig. 3.6). We find no evidence that depositional

taphonomic biases affected the taxonomic composition of our fossil assemblages (comparison of overbank versus channel facies; Fig. 3.3, Table 3.3), and instead interpret the changes observed through this succession of floras as representative of local vegetation change through time. These results provide support for our hypothesis that turnover was driven by high disappearances (H2). Importantly, however, we do not find a pronounced peak in disappearances just before the KPB. This may indicate that turnover was generally high throughout the last ca. 1.3 Myr of the Cretaceous, culminating in major compositional changes by the end of the Cretaceous, rather than a concentrated event at the KPB.

3.5.2 Post-KPB floras and taxonomic recovery in the early Paleocene

Earliest Paleocene (TM1) plant communities in NE Montana were species-poor (Figs. 3.6–7) and were also distinct in terms of the overall taxonomic composition and representation of functional groups (Figs. 3.3, 3.5). Even as many conifers persisted across the KPB, the relative abundance of those conifer taxa declined from 35% in the Late Cretaceous (HC) to 6% in the early Paleocene (TM1), with angiosperms becoming increasingly abundant in the relatively low-diversity TM1 floras. TM1 vegetation also includes several weedy or aquatic angiosperm taxa (e.g., *Limnobiophyllum scutatum*) (Figs. 3.3–4), suggesting either local environmental change in the Paleocene or that the mass extinction led to selection for wet-adapted taxa. Johnson (2002) similarly pointed to the selective survival of mire-adapted taxa across the KPB in North Dakota. The change in lithology from the HCF to the FUF has been interpreted as having resulted from changes in the local hydraulic flux (see Geologic Setting); the abundance of wet-adapted taxa may therefore be an indication of local environmental pressures.

Although TM1 floras were low in alpha and beta taxonomic richness, the relatively high species richness of TM2 floras does not support our hypothesis (H3) that the Paleocene was

depauperate and homogeneous for an extended period. Rather, this pattern suggests that taxonomic recovery after the KPB occurred relatively early in the Paleocene. Within 80 to 900 kyr after the KPB (TM2 floras), there was a change in taxonomic composition (novel angiosperms as well as the relative abundance of conifers rebounding to 25%) along with a ~55% increase in richness (returning to pre-mass extinction diversity levels). Moreover, even the youngest TM1 flora was relatively species-rich, indicating that taxonomic recovery may have begun already during the TM1 interval (Figs. 3.6–7). Overall, NE Montana vegetation recovered relatively quickly in the aftermath of the K-Pg mass extinction, at least in terms of taxonomic diversity (Figs. 3.6–7). This resembles the pattern of recovery among vertebrate faunas from NE Montana. For example, mammalian taxonomic richness and heterogeneity began increasing within 320 kyr of the K-Pg boundary (Smith et al. 2018) and modern lineages (e.g., plesiadapiforms) arrived in NE Montana within ca. 150 kyr post-KPB, becoming a major component of the 'fully recovered' mammalian fauna by ca. 847 kyr post-KPB (Wilson Mantilla et al. 2021).

Taxonomic richness is only one measure of biotic recovery from the K-Pg mass extinction. Previous authors have investigated whether plant ecological strategies were diversifying during the early Paleocene to test for different signals of recovery. Studies in North Dakota and Colorado point to a drop in leaf mass per area across the KPB, indicating a shift to more fast growing, weedy habits (Blonder et al. 2014; Lyson et al. 2019). In Colorado, Lyson et al. (2019) further trace leaf mass per area into the Paleocene and find potential signs of ecological recovery (increasing leaf mass per area) ca. 300 kyr after the KPB. Further research into these additional measures of plant diversity across the KPB in NE Montana might point to

alternative signs of recovery among plant communities and help evaluate drivers of post-KPB vegetation change.

3.5.3 Comparison with Global K-Pg Records

Overall, these results indicate that plant communities in NE Montana experienced substantial taxonomic turnover during the K-Pg mass extinction, similar to other studied regions of WINA (Fig. 3.8). In the Williston Basin of North Dakota (ND) and the Denver Basin in Colorado (CO), extinction rates have been estimated at 46–57% based on megafloras (Wilf and Johnson 2004; Lyson et al. 2019; Fig. 3.8), to be compared to our 63% disappearance rate, based on just the latest Cretaceous. Even though our study has fewer floras from this latest Cretaceous interval, our median sample size per flora is much greater than in ND or CO (Fig. 3.8), and our latest Cretaceous flora (Bruce Leaf; ca. 110 kyr before the KPB) is particularly well-sampled (Fig. 3.7B). Therefore, our sample size should be sufficiently large for a robust comparison among north-central WINA study areas. Relative to WINA, vegetation in Patagonian Argentina experienced an exceptionally high extirpation or extinction rate (up to 90%; Stiles et al. 2020). However, the studies in Patagonia, as well as those in Colombia (Carvalho et al. 2021), are based on floras distributed across large geographic distances (ca. 300–400 km) and are only coarsely dated to the Maastrichtian/Late Cretaceous and Danian/early Paleocene (Fig. 3.8). Therefore, we cannot exclude the possibility that this difference in estimated extinction magnitude between WINA and South America is due to differences in the scale of spatial and temporal sampling.

The drop in taxonomic richness we observe from the HC to TM1 temporal interval, although substantial (~28%), was notably less severe than in Argentinian Patagonia (40%; Stiles et al. 2020), North Dakota (~49% comparing Paleocene floras to the latest 15 m of Cretaceous strata; Wilf and Johnson 2004), or the Denver Basin in Colorado (~50%; Lyson et al. 2019).

Given the small sample size of individual floras in ND and CO compared with this study in NE Montana (Fig. 3.8), it is possible that the diversity estimates from these studies are not truly comparable to ours at the level of individual floras. Alternatively, the lower drop in richness in NE Montana may be a real biological pattern that reflects local vegetation resilience during the mass extinction event.

Our NE Montana floras also point to differences in the rate of taxonomic recovery within the WINA. NE Montana floras returned to pre-mass extinction levels of taxonomic richness quickly, between 80 and 900 kyr after the KPB, on par with the Denver Basin of Colorado (Lyson et al. 2019). In contrast, North Dakota floras remained depauperate for 10 Myr after the KPB (Wilf and Johnson 2004), even as they changed taxonomically during the early and middle Paleocene (Peppe 2010). In other basins of north-central WINA (e.g., Bighorn and Hanna Basins) Paleocene diversity was generally low, similar to in North Dakota (Hickey 1980; Wing et al. 1995; Dunn 2003).

The differences in floral recovery across WINA may have been due to differences in environment (e.g., local climate) or biotic factors (e.g., variation in resilience of vegetation). For example, in the Denver Basin recovery rates have been linked to elevation (Johnson et al. 2003). In this scenario, higher elevation areas may have served as refugia for Cretaceous taxa (e.g., Johnson and Ellis 2002) and/or topographic (hence ecological) variation in high elevation areas may have promoted rapid speciation (see e.g., Antonelli et al. 2018). Based on the relative position of the Western Interior Seaway at this time (although we acknowledge this positioning is debated, see e.g., Slattery et al. 2015 and references therein), we suggest that NE Montana would have been at a slightly higher elevation than North Dakota during this time. If true, heterogeneous microhabitats in the upland may have allowed NE Montana vegetation to persist

during the mass extinction. However, without quantitative estimates of the paleoelevation in these study areas, this inference remains speculative. Alternatively, some aspect of plant community diversity and composition (e.g., in functional groups) may have allowed for higher resilience in NE Montana as compared with North Dakota. For example, the abundance of persistent conifer taxa in NE Montana may have lent resiliency to the local vegetation (see further discussion below). While conifer taxa in North Dakota did decline in abundance from the HCF (17%) to the FUF (4%; Wilf and Johnson 2004), conifers were consistently more abundant in NE Montana during this time period (35% of HC, 6% of TM1, and 25% of TM2 interval specimens). More detailed ecological information about HC floras is necessary to evaluate this hypothesis. Local NE Montana palynofloral records, which sample a broader spatial area and therefore may capture the upland environments, document a large increase in the proportion of conifer pollen after the KPB (Hotton 2002). This pattern would suggest that perhaps conifers, which declined in NE Montana megafloras during the TM1 interval, were restricted to upland or other refugia before rebounding in abundance in TM2 megafloras. Thus, the K-Pg mass extinction may have resulted in different patterns of survival in upland versus lowland environments and among conifers versus angiosperms, although further investigation of these patterns is necessary.

Similar to WINA, floral records in South America show variation in rates of recovery. In Patagonia, Paleocene floras from within ca. 5 Myr after the KPB were more morphologically diverse than Cretaceous floras, indicating a relatively fast recovery among Patagonian plant communities in terms of ecological and taxonomic diversity, even as they remained taxonomically homogeneous (Iglesias et al. 2007, 2021; Stiles et al. 2020). However, both Cretaceous and Paleocene floras from Patagonia were more taxonomically rich than WINA

floras of the same ages (Iglesias et al. 2007, 2021; Stiles et al. 2020). In contrast, plant communities in Colombia did not fully recover for ca. 6 Myr after the KPB (Carvalho et al. 2021). These differences in global patterns of recovery may be attributable to varying devastation caused by the bolide impact in Mexico, regional environmental conditions or vegetation composition leading to resiliency or vulnerability in floral communities, or other factors. Our view of the K-Pg mass extinction remains limited by the few regions where consistent plant fossil records occur; therefore, further work to elucidate global patterns in extinction magnitude and recovery is required to understand what led to these widely differing floral responses to the K-Pg mass extinction.

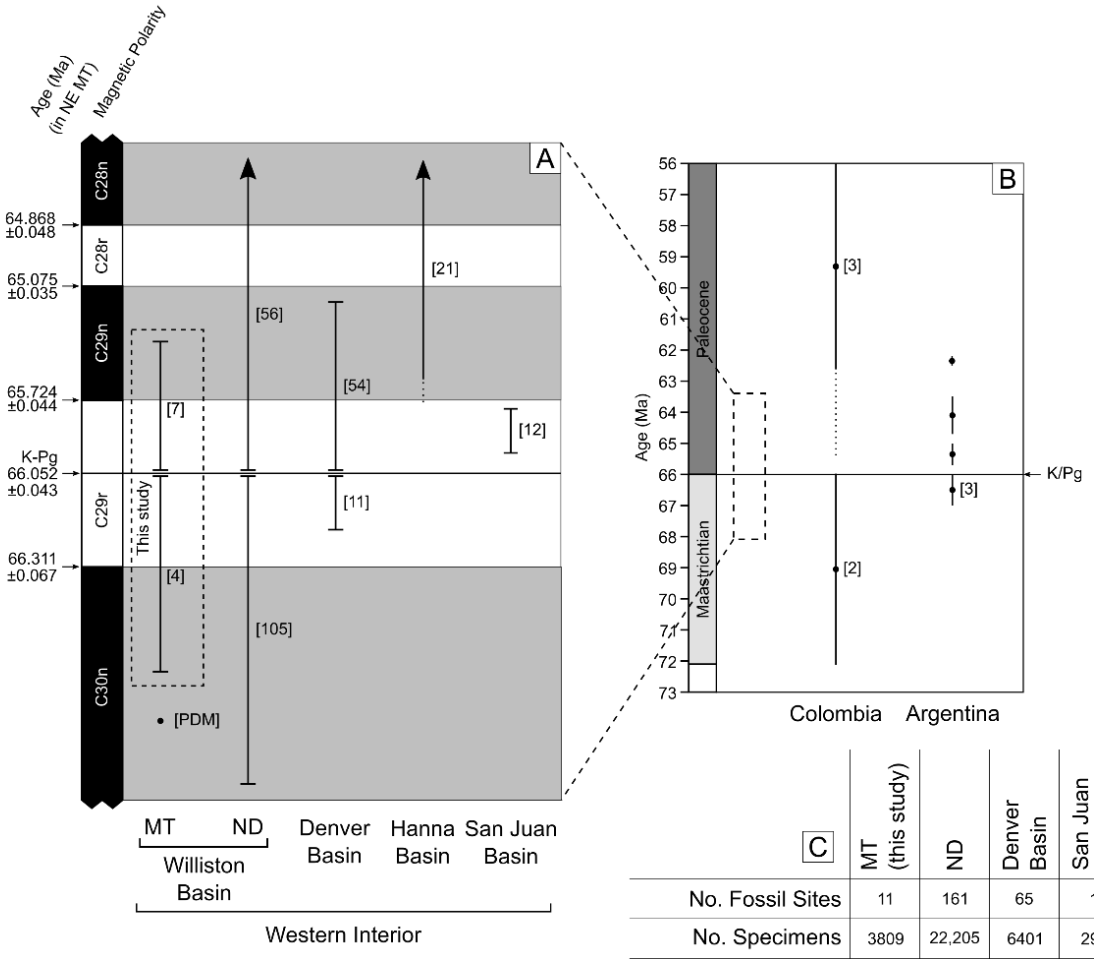

C

	MT (this study)	ND	Denver Basin	San Juan Basin	Hanna Basin	Colombia	Argentina
No. Fossil Sites	11	161	65	12	21	9	6
No. Specimens	3809	22,205	6401	2939	4845	6951	3744
Median Spec./Site	357	34	30	205	110	523	563
Extinction magnitude	63%	57%	46%	N/A	N/A	N/A	90%
Change in richness	-28%	-49%	-50%	N/A	N/A	N/A	-40%

Figure 3.8: Summary of global studies of megaflora from the K-Pg boundary interval. (A) Temporal range and density of megafloral sampling from WINA including NE Montana (MT; this study and PDM flora described by Arens and Allen 2014), North Dakota (ND; Wilf and Johnson 2004, Peppe 2010), Denver Basin (CO; Lyson et al. 2019), San Juan Basin (NM; data from Flynn and Peppe 2019), and Hanna Basin (WY; Dunn 2003). (B) Temporal range and density of megafloral sampling from outside North America including Colombia (Carvalho et al. 2021) and Patagonian Argentina (Stiles et al. 2020) with inset box showing the extent of WINA sampling in A. (C) Summary of sampling and estimations of extinction magnitude from each of these study systems (where available). The sample size from WY is approximated from Dunn (2003) Figure 5.3. In A and B, vertical bars show the estimated age range of the floral assemblages with the number of floras from that time interval shown at right. The age of the K-Pg boundary and polarity chrons measured in NE Montana are taken from Sprain et al. (2015, 2018), Swisher et al. (1993), and LeCain et al. (2014).

3.5.4 Implications of the Floral Record from NE Montana for the Study of Mass Extinctions

Our study points to regional and global variability in the impact of mass extinctions on plant communities. Whereas the magnitude of disappearances across the KPB is relatively consistent throughout WINA (ca. 50%), there are large discrepancies in the timing of recovery after the K-Pg mass extinction within this region. Furthermore, the global magnitude of plant species disappearance at the KPB is variable (43–90%). Susceptibility to the mass extinction as well as the recovery may have been shaped by local factors, both extrinsic (e.g., climate) or intrinsic (e.g., plant ecological strategies). Our results therefore suggest that modern biodiversity loss must be assessed and addressed at a local level in order to predict species loss as well as potential for future diversity recovery.

The proposition that plant communities respond differently compared to animals during mass extinctions is also generally supported in our data. Our results are consistent with the framework described by McElwain and Punyasena (2007) and Green et al. (2011) in which plants respond to mass extinctions by shifts in relative abundance and species-level extinction or extirpation, rather than global, family-level extinction. Specific ecological strategies (e.g., fast

growth, seed dormancy), common among many plant clades, may have conferred resiliency for some, if not many, taxa.

Our NE Montana record offers an example of broad ecological and physiological differences between plant groups that appear to have affected how they responded during and after the K-Pg mass extinction. In this region, conifers seem to have survived the K-Pg mass extinction more readily than angiosperms, even though their abundance decreased in the earliest Paleocene (TM1). We suggest that this difference in abundance loss and recovery is likely driven by broad differences in the ecology of these two groups. Conifer taxa, having longer times between regeneration as well as specific adaptations (e.g., thicker skin) to disturbance (Brodribb et al. 2012) may have been more frequent survivors during the immediate environmental stressors at the KPB, even though they declined in abundance (perhaps restricted to refugia). In contrast, the lower abundance (smaller population size, smaller geographic range) of Late Cretaceous angiosperm taxa may have led to their higher disappearance rate at the KPB (Jablonski 2005; Payne and Finnegan 2007; Jablonski 2008; Heim and Peters 2011). Later, during the TM1 interval, angiosperms may have increased in abundance as a result of numerous ecological advantages: e.g., faster seedling growth rates (Bond 1989), rapid reproduction (Bond 1989; Doyle and Hickey 1976; Hickey and Doyle 1977; Verdu 2002), higher hydraulic capacity and vein density (Lusk et al. 2003; Boyce et al. 2009; Brodribb and Feild 2010; Feild et al. 2011), the ability to spread vegetatively (Boyce and Leslie 2012). These characteristics, which are thought to have promoted angiosperms' success generally during the Cretaceous (Bond 1989; Augusto et al. 2014), may have been crucial during the period just after the mass extinction event. Previous authors (e.g., Wing and Tiffney 1987) have similarly suggested that the environmental crisis at the KPB disturbed the dominance of stress-tolerant and competitive

taxonomic groups (i.e., conifers) allowing for ruderal groups (i.e., angiosperms) to flourish (Wing and Boucher 1998). These results suggest fundamental differences in the response of conifers and angiosperms to disturbance and biodiversity crises. Future research on K-Pg plant ecology will help to elucidate the potential for differential impacts on different plant taxa or functional groups during mass extinctions, with important implications for mitigating the ongoing biodiversity crisis.

3.6 CONCLUSIONS

Our study indicates that plant community composition changed markedly across the K-Pg boundary in NE Montana. This turnover culminated in the extirpation or extinction of 63% of latest Cretaceous plant taxa (from the last ca. 110 kyr of the Cretaceous) and the appearance of a novel suite of Paleocene plan taxa. Floras from the first 80 kyr of the Paleocene were 28% less rich than Late Cretaceous floras on average, with an increase in the representation of wet-adapted taxa. Between 80 and 900 kyr after the mass extinction, plant taxonomic richness had apparently rebounded to Late Cretaceous levels again. This pattern of rapid recovery echoes what has been described from mammalian communities from the same region.

We find broad accord in terms of extirpation or extinction magnitude (ca. 46–63% disappearance) across WINA, but a lower drop in taxonomic richness at the KPB in NE Montana compared with elsewhere in the region. This variation in extinction magnitude may result from differences in sampling intensity or reflect local variation in vegetation susceptibility to the environmental changes associated with the mass extinction event. Our results also support a growing body of evidence that post-KPB recovery may have varied based on latitude, local paleoenvironment, or underlying vegetation dynamics. Future work to integrate analyses of plant community diversity with plant ecology, local environment, and vertebrate paleontological records from this study area will enable a more nuanced view of how terrestrial communities are impacted by mass extinction events on shorter and longer timescales.

Chapter 4: Environmental and ecological changes among plant communities at the Cretaceous-Paleogene boundary in northeastern Montana

4.1 ABSTRACT

Plant communities were dramatically altered by the Cretaceous-Paleogene (K-Pg) mass extinction. In this study we examine the potential ecological impact of the mass extinction on plant communities in northeastern Montana and interpret their paleoenvironmental context. We test the hypotheses that plant ecomorphology shifted across the K-Pg boundary and that environmental changes were correlated with shifts in plant taxonomic and ecological diversity during the extinction and recovery intervals. Our results indicate that the K-Pg mass extinction led to the selective disappearance of plants with slow-return ecological strategies. Early Paleocene vegetation exhibited changes in the relative abundance of certain ecomorphological groups and decline in the diversity of ecological strategies relative to Cretaceous vegetation which lasted for an extended period, beyond when taxonomic diversity began to recover. At the same time, ecomorphological disparity of the dominant plant group, non-monocotyledonous angiosperms (dicots), did not decline across the K-Pg boundary. Ecomorphological and taxonomic diversity were evidently decoupled during the mass extinction event, leading to long-term shifts in the abundance of certain ecomorphological groups. Paleoclimate records based on leaf physiognomy indicate that northeastern Montana was consistently a temperate forest biozone during this entire interval. However, temperatures varied by as much as ~10 °C during this interval: temperatures peaked in the latest Cretaceous, declined ~5–7 °C across the the K-Pg boundary, and experienced a short-duration increase in temperatures again ca. 328 kyr after the K-Pg boundary. Changes in plant taxonomic diversity as well as broader terrestrial community

diversity appear to correlate with fluctuations in temperature, indicating that climate changes may have played some role in the mass extinction and recovery. These results shed light on the ecomorphological impact of mass extinctions on plant communities, the interaction between plant taxonomic, ecological, and morphological diversity, and the role of local climate change in the mass extinction event.

4.2 INTRODUCTION

The Cretaceous-Paleogene (K-Pg) mass extinction led to massive global taxonomic turnover, diversity loss, and ultimately the establishment of modern ecosystems (McGhee et al. 2004, Nichols and Johnson 2008, Krug et al. 2009, Schulte et al. 2010). Despite this significant role in Earth's history, the effect of this event on vegetation is still poorly understood. Local records from northeastern (NE) Montana point to massive (~63%; Wilson Deibel et al. in prep) species-level plant disappearances, but higher-level plant taxa (e.g., families) did not go extinct (McElwain and Punyasena 2007). Researchers have also posited that K-Pg plant extinctions had cascading ecological impacts on animal communities, for example having caused selective extinctions among birds (Longrich et al. 2011, Field et al. 2018), insects (Labandeira et al. 2002, Wilf et al. 2006, Donovan et al. 2014), and mammals (Wilson 2013, DeBey and Wilson 2017, Hughes et al. 2021). Later, the post K-Pg recovery and evolution of angiosperms may have propelled ecomorphological diversification in some vertebrate groups, e.g., certain mammal clades (Grossnickle et al. 2019, Lyson et al. 2019, Wilson Mantilla et al. 2021). Nevertheless, only a few studies have comprehensively quantified patterns of plant ecology (i.e., functional traits) across the K-Pg boundary (KPB; e.g., Blonder et al. 2014, Lyson et al. 2019). Here, we aim to further illuminate the broad ecomorphological changes in floras leading up to and across the KPB and their implications for our understanding of the K-Pg mass extinction.

Although the precise cause of the K-Pg mass extinction is still debated, each proposed causal mechanism has bearing on the specific ecological responses we would predict in local vegetation. The ultimate cause of the K-Pg mass extinction was likely some combination of bolide impact in the Yucatan Peninsula of Mexico (Alvarez et al. 1980, Schulte et al. 2010) and climate change resulting from volcanic activity at the Deccan Traps in India (Keller et al. 2009).

The combined effects of which would have caused profound global environmental changes: a thermal pulse igniting wildfires (Robertson et al. 2004, 2013), prolonged cold winter conditions (Chiarenza et al. 2020, Tabor et al. 2020), atmospheric soot or dust cutting off sunlight (Kaiho et al. 2016, Tabor et al. 2020), and both short- and long-term climate change (Keller et al. 2009, Self et al. 2014). Some researchers posit a combined effect whereby volcanically induced warming altered community structure and left those communities vulnerable to the effects of the bolide impact (the "press-pulse" hypothesis; Arens and West 2008, Mitchell et al. 2012). We do not directly address these causal mechanisms in our study, but each informs our predictions of specific ecological responses from the local vegetation.

In this study, we focus on functional or ecological diversity of plants, which can be measured through the morphological disparity of functionally meaningful traits and the reconstruction of particular ecological or functional roles. Whereas taxonomic diversity is a measure of the number and relative abundance of species, functional or ecological diversity reflects broader ecosystem roles and functions. Thus, it may better reflect the resilience of the ecosystem to environmental perturbation than taxonomic diversity does (Petchey and Gaston 2006). Moreover, ecological diversity may respond differently than taxonomic diversity during times of environmental stress due to the selective extinction of certain groups and ecological turnover (Jablonski 2005). After a mass extinction in particular, a reduction of morphological disparity indicates a nonrandom pattern of extinctions (i.e., selective extinction; Jablonski 2005, Wilson 2013). However, evidence for decoupling of ecological or morphological disparity and taxonomic diversity during environmental crises may be mixed (Foote 1993, Edie et al. 2018, Cole and Hopkins 2021). Among plants in particular, mass extinctions typically result in community restructuring or loss of specific functional groups rather than loss of large

phylogenetic groups (Wing 2004, McElwain and Punyasena 2007, Green et al. 2011), and lead to a period of ecological destabilization (the "disaster" interval; McElwain and Punyasena 2007, see also Erwin 2001) dominated by fast-return, "weedy" taxa. In order to test these hypotheses, ecological diversity can be measured using functionally relevant morphological characters ("ecometrics", see e.g., Vermillion et al. 2018, Chen et al. 2019). In particular, plant ecology is fundamentally tied to leaf morphology due to the function of leaves in photosynthesis (Reich et al. 1997) and plant ecometrics are informative of environmental conditions due to their stationary habit (Peppe et al. 2018). Therefore, leaf morphological diversity may be used to infer ecological diversity (ecomorphological diversity).

Here, we examine the central question whether the K-Pg mass extinction among plants was ecomorphologically selective, resulting in a reduction of plant morphological disparity and ecological diversity across the K-Pg boundary. We specifically examine the morphology of fossil leaves to quantify the morphological disparity, ecological strategies, and paleoenvironmental setting of these floras (Fig. 4.1; see "Leaf Morphology as an Indicator of Plant Ecology and Paleoclimate" for an outline of these approaches). Discordance between ecomorphological and taxonomic diversity may be used to infer patterns of selection during extinction events (Foote 1993). To investigate this, we test the hypothesis H1) that the K-Pg mass extinction led to not only taxonomically but also morphologically less diverse floras in the earliest Paleocene (Fig. 4.1A). We further directly explore the hypothesis H2) that the plant extinctions at the KPB were selective, through the reconstruction of plant ecological strategies. We predict that nonrandom extinction of particular plants (e.g., those with slow-return ecology) would open up ecospace allowing r-selected or fast-return plant taxa to flourish in the aftermath of the mass extinction (Fig. 4.1A). This prediction is linked to both the loss of large vertebrate herbivores (Brusatte et

al. 2015) as well as climate change associated with the bolide impact or volcanism. To further investigate this potential climate driver, we reconstruct local paleoclimate to test our third hypothesis H3) that fluctuating temperatures may have played a role in the magnitude and timing of the mass extinction and recovery (Fig. 4.1). If true, we would predict that periods of changing temperature would be correlated with periods of changing diversity (e.g., increasing temperatures near-coincident with increasing taxonomic diversity; Fig. 4.1A). We test these hypotheses through an analysis of leaf foliar traits in order to examine the paleoclimate and the underlying ecological effects of the K-Pg mass extinction event (Fig. 4.1B–C).

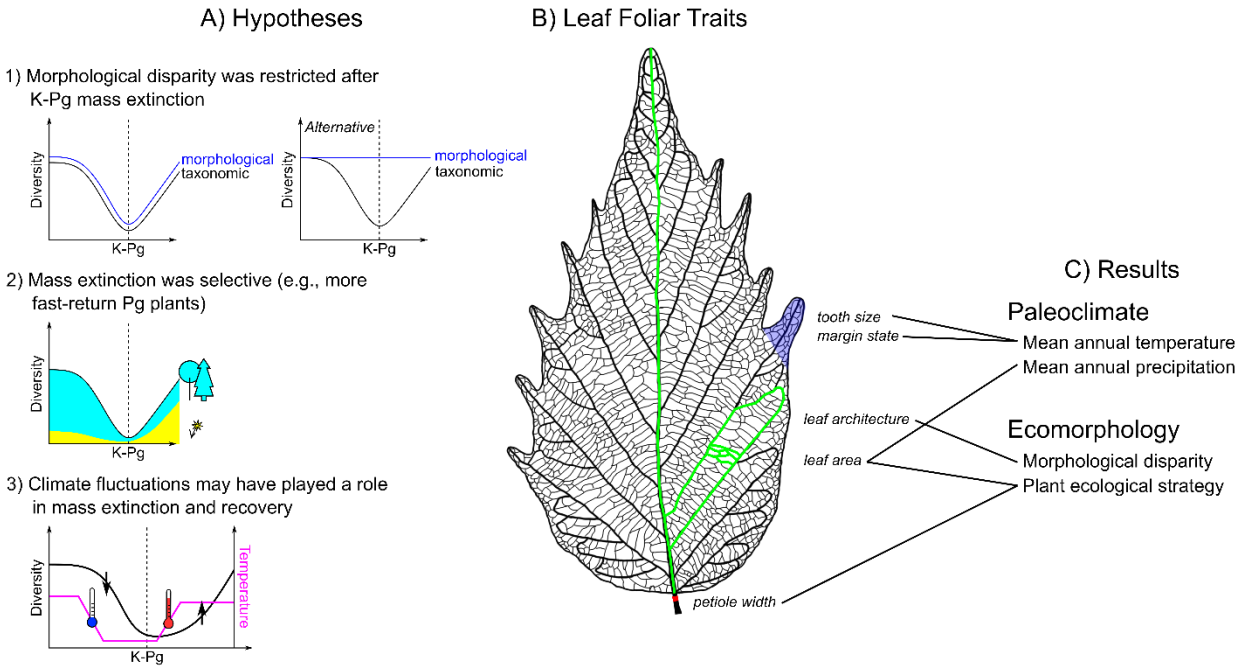

Figure 4.1: Schematic of approach in this study. A) Hypotheses being tested in this study with illustrations of predictions B) Methods revolve around measuring specific leaf foliar traits. C) Results stem from the analysis of those foliar traits to infer paleoclimate and plant ecomorphology.

4.2.1 Leaf Morphology as an Indicator of Plant Ecology and Paleoclimate

In this study, we follow other researchers in using fossil leaf traits to infer aspects of plant diversity and ecology as well as the paleoenvironment (see review by Peppe et al. 2018).

Leaves serve as the primary photosynthetic and respiratory organs of the plant; and as plants are stationary, leaf morphology directly reflects local environmental conditions (i.e., light availability, hydraulic flux, nutrient resources; Peppe et al. 2018). Thus, fossil leaf traits should a) broadly reflect morphological and potentially functional diversity through time (e.g., Green and Hickey 2005, Stiles et al. 2020), b) provide a basis for classifying plant ecological strategies (Royer et al. 2007), and c) enable us to infer paleoclimate variables (e.g., mean annual temperature, precipitation; Bailey and Sinnott 1916, Wolfe 1979, Wolfe 1993, Wilf 1998, Huff et al. 2003, Royer et al. 2005, Peppe et al. 2011b).

Morphological disparity in leaf architecture is one metric to estimate the ecomorphological diversity of plants across the KPB. Leaf foliar traits (i.e., size, shape, toothedness, venation) reflect the balance of photosynthesis, water resources, and temperature regulation for the plant (Peppe et al. 2018); as such, leaf morphology can be used to infer plant paleoecology. A variety of approaches have been used to measure functional diversity and morphological disparity of plants from around the KPB; here, we apply a variety of these measures in order to best describe the paleoecology of these plants and to compare our results with previous studies (see Previous Research into K-Pg Plant Paleoecology and Paleoenvironment). Morphological diversity can be summarized through the assignment of Compendium Index Categories (CIC) to each fossil leaf taxon (e.g., Green and Hickey 2005). Leaf morphology can also be examined through morphological character data whereby discrete foliar characteristics are scored for each taxon and morphospace occupation through time is examined (e.g., Stiles et al. 2020). Fossil leaves can be investigated further to place these plant taxa along the leaf economic spectrum (LES; Reich et al. 1997, Wright et al. 2004). The LES describes a range of plant growth strategies and related functional traits and tradeoffs. On one

end of the LES are “slow-return” plants, associated with high rates of photosynthesis, low leaf nitrogen and phosphorous concentrations, and low rates of respiration; these slow-return plants also have a higher leaf dry mass per area (leaf mass per area or LMpA), representing denser leaves with a longer leaf life span (Wright et al. 2004, Reich 2014). On the opposite end of the LES are “fast-return” plants, associated with lower rates of photosynthesis, high leaf nitrogen and phosphorous concentrations, and high rates of respiration; these fast-return plants have a lower LMpA, representing thinner or less fleshy leaves with a shorter leaf life span (Wright et al. 2004, Reich 2014). At its core, the LES balances productivity-persistence tradeoffs experienced by plants (Reich 2014). LMpA is a core component and predictor of the LES. Generally, LMpA is negatively correlated with leaf life span and therefore linked to deciduousness and weedy habit (Royer et al. 2007, Reich 2014). Recent research has developed a method for estimating LMpA from fossil plants, thus enabling us to broadly categorize fossil plant taxa and communities along the LES. This method utilizes the petiole width and area of fossil leaves to estimate LMpA (Royer et al. 2007). We aim to apply this method to reconstruct species LMpA and thereby generalize leaf ecological strategy along the LES.

In addition, fossil leaf morphology is a reliable proxy for paleoclimate. Bailey and Sinott (1916) initially documented a strong correlation between leaf size and shape (“physiognomy”) and environmental variables (mean annual temperature [MAT] and precipitation [MAP]). From this early work, various methods have been proposed to measure these environmental variables utilizing fossil leaves (e.g., leaf margin analysis [LMA; Wolfe 1979], leaf area analysis [LAA, Wilf 1998], climate leaf analysis multivariate program [CLAMP, Wolfe 1993]). A more recently developed method, digital leaf physiognomy (DiLP; Huff et al. 2003, Royer et al. 2005, Peppe et al. 2011b), utilizes digital images of leaves to measure continuous leaf traits and then uses a

multiple linear regression model to estimate MAT and MAP. DiLP estimates of MAT and MAP appear more accurate than LMA or LAA, and DiLP is more reproducible and functionally meaningful than CLAMP (Peppe et al. 2018). One consideration in all leaf physiognomic methods is the influence of the freshwater margin effect (toothed leaves being more common in locally wet environments; Royer 2012). Flynn and Peppe (2019) suggest that LMA estimates are potentially more susceptible to this effect, whereas DiLP estimates rely upon a variety of leaf foliar characters and are therefore more robust to the effect. Another challenge of applying leaf physiognomic methods to infer paleoclimate is in obtaining sufficient species richness to accurately estimate climate variables. Most studies suggest species richness >20 (Peppe et al. 2018) although various studies have applied these methods with more depauperate floras (e.g., Arens and Allen 2014). Methodological studies indicate that species richness between 10 and 20 generally results in standard deviation of inferred temperature between 0 and 5 °C (Royer et al. 2005). Given the depauperate nature of early Paleocene floras, we also aim to examine the effect of species poor floras on the accuracy of paleoclimate estimates in this study. These methods enable an accurate estimation of paleoclimate to evaluate the potential correlation of changing paleotemperature and plant diversity across the KPB.

4.2.2 Previous Research into K-Pg Plant Paleoecology and Paleoenvironment

Previous research has indicated mixed support for the hypothesis that plant extinctions were selective during the K-Pg mass extinction or that plant ecomorphological diversity declined across the KPB. Ecomorphological and taxonomic diversity in the northern Great Plains declined across the KPB, with the selective extinction of both non-mire adapted taxa and slow-growing taxa (Johnson 2002, Blonder et al. 2014, Lyson et al. 2019). In contrast, Green and Hickey (2005) found no evidence of a change in typical morphology (CIC composition) from the

Cretaceous to the Paleocene among all of North American floras. Outside of North America, the evidence for ecomorphological diversity declining at the KPB is also mixed. Colombian forests shifted in vegetation structure (becoming more closed canopy) but remained taxonomically depauperate for millions of years after the KPB (Graham et al. 2019, Carvalho et al. 2021). Patagonian floras were also taxonomically depauperate for an extended period but evidently did not decline in morphological disparity at the KPB (Stiles et al. 2020). Significantly, these analyses employ a variety of different metrics to infer taxonomic or ecological recovery (e.g., dicot foliar character data, plant functional traits). These varied results and varying methods leave open the question of whether ecomorphological and taxonomic diversity were coupled during the K-Pg interval; in this study, we employ a suite of ecomorphological proxies to allow a comparison of patterns in NE Montana with elsewhere around the globe.

In addition to the short-term environmental changes associated with the K-Pg event, longer-term climate changes during the Late Cretaceous and early Paleocene may have shaped ecological responses. Specifically, in the northern Great Plains the K-Pg mass extinction co-occurred with both a) local temperatures dropping ~5–8 °C (Wilf et al. 2003, Tobin et al. 2014) and b) a rise in the local water table resulting in more widespread floodplains (Fastovsky 1987, Fastovsky and Bercovici 2016). Local changes in plant ecomorphology (i.e., the proliferation of mire-adapted taxa post-KPB in North Dakota; Johnson 2002, Wilf and Johnson 2004) have been attributed to local, long-term climatic trends, as opposed to global effects of the mass extinction event. In contrast, short-term ecomorphological changes (i.e., the proliferation of fast-growing plant taxa post-KPB in North Dakota and Colordao; Blonder et al. 2014, Lyson et al. 2019) have been attributed to biotic effects of the global mass extinction event. Thus, our goal in this study

is to disentangle the impact of environment, biological pressures, and ecological strategies on plant communities through the study of leaf morphology.

4.3 MATERIALS AND METHODS

4.3.1 Fossil Collection and Materials

In this study we analyze a set of 11 fossil floras (3,809 identifiable specimens from 37 quarries) from the Hell Creek area in NE Montana, reposited at the University of Washington Burke Museum of Natural History and Culture (UWBM). Specimens were collected on Bureau of Land Management lands (permits MTM 108226, MTM108766, MTM 109605, and MTM 110439; UWBM localities P7112-7114, P8091-8095, P8527, P7135, P85442, P8086, P8087, P7137, P7136, P8079, P7144, P7145, P8084, P8536, and P8537), the Charles M. Russell Wildlife Refuge administered by U.S. Fish and Wildlife and the Army Corps of Engineers (permits 15-2, DACW45-3-16-6023, 17-007, and 18-008; UWBM localities P8526, P8080, P6909, P6910, P8543, B8198, P8544, P8077, P8078, P7152, P8088, and P8545), as well as private lands (UWBM localities B8202, P7125, P7126, P8075, P8076, B8201, P6911, P7142, and P8098). Of these 11 floral assemblages, four are Late Cretaceous (HC floras) and seven are Paleocene (TM floras). For some analyses, we further subdivide the Paleocene interval into the TM1 interval (the first ca. 80 kyr after the KPB which includes three floras) and the TM2 interval (ca. 80 and 900 kyr after the KPB which includes four floras; Wilson Deibel et al. in prep). In other analyses, we bin localities into 15-m stratigraphic intervals to examine finer-scale trends through time (Table 4.1).

These collections are voucher collections, with all identifiable fossils collected and brought to the UWBM. The fossils include vegetative and reproductive plant structures, primarily preserved as compression and impression fossils. We assigned each specimen to a morphotype (referred to as species or morphospecies). Morphotypes assigned in this study are described by Wilson et al. (2021) and Wilson Deibel et al. (in prep). These morphotypes are assigned a unique alphanumeric code (e.g., MT001) to distinguish from previous studies in North

Dakota (which used FH, HC, and FU prefixes; Johnson 1989, Peppe et al. 2007) and at other locations in Montana (which used FP prefix; Arens and Allen 2014). While we generally follow the morphotypes outlined by Wilson Deibel et al. (in prep) we also erected a few new morphotypes and sub-morphotypes (i.e., splitting morphotypes which had substantial morphological variation) to more accurately score the foliar characters and represent the morphological disparity within and between morphotypes.

Wilson Deibel et al. (in prep) describe additional details on collection, description, and lithologic analyses.

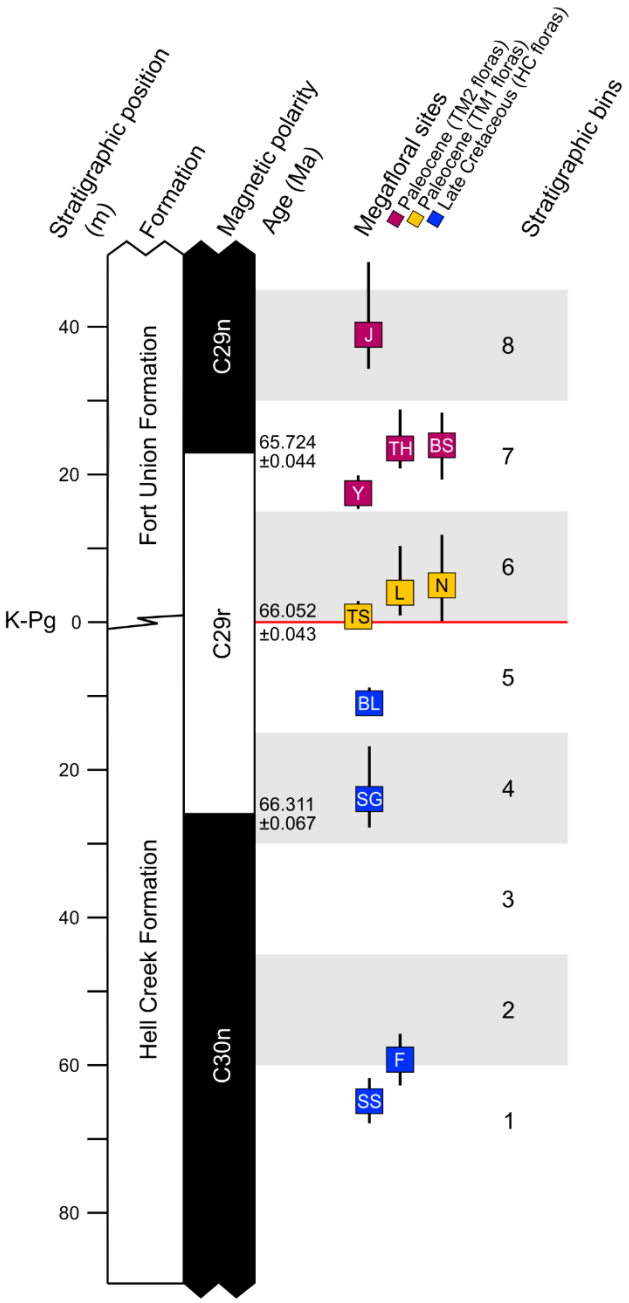

Figure 4.2: Chronostratigraphic framework of fossil floras (modified from Wilson Deibel et al. in prep.). Magnetostratigraphy and stratigraphic section based on the work of LeCain et al. (2014) and Sprain et al. (2015, 2018). Floras in this study are shown in position relative to observed marker beds and colored according to temporal zone (HC, TM1, TM2); abbreviations as in Table 4.1. Uncertainty associated with stratigraphic position of each flora is indicated by vertical lines. Floras are also binned into 15-m stratigraphic bins shown at right.

Fm	Temporal Interval	Bin	Flora	Number of Specimens	Woody Dicot Morphospecies Richness
Fort Union (Tullock Member)	TM2	8	Jane's (J)	103 (23)	10
		7	Biscuit Springs (BS)	102 (33)	14
			Tharp's Market (TH)	101 (7)	19
			Yabba Dabba Do (Y)	64 (26)	10
	TM1	6	New York (N)	65 (19)	15
			Lerbekmo N (L)	62 (24)	11
			The Swamp (TS)	31 (9)	6
Hell Creek	HC	5	Bruce Leaf (BL)	106 (33)	17
		4	Smurphy's Guess II (SG)	89 (6)	9
		2	Fisk I (F)	48 (10)	15
		1	Seafood Salad (SS)	88 (7)	19
Total				859 (197)	94

Table 4.1: Sampling and richness data for the fossil floras in this study. Floras are arranged in stratigraphic order and grouped according to temporal interval and bin. Abbreviations for each flora are in parentheses. Specimen counts refer to the number of specimens measured for paleoclimate analyses (number of specimens measured for LMpA in parentheses) and morphospecies richness values are for woody non-monocotyledonous angiosperm (dicot) taxa only.

4.3.2 Plant Morphology

To evaluate morphological diversity through this time interval, we investigated 1) the distribution of Compendium Index Categories (CIC; Green and Hickey 2005) represented through time and 2) morphospace occupation of floras at different time intervals. The analysis of CIC data a) includes all phylogenetic groups found in our study, b) examines the relative abundance of taxa, and c) provides a less granular categorization of leaf morphology. The analysis of morphospace occupation a) is restricted to dicot taxa, b) examines presence/absence of taxa, and c) provides a more granular categorization of leaf morphology. Thus, these analyses

complement each other to evaluate not just the overall morphological disparity of plant communities, but also the relative abundance structure of those communities.

We use morphological diversity as a proxy for ecological diversity. The implicit assumption is that morphological diversity correlates with ecological diversity. This assumption has been frequently invoked in paleontological studies (see review by Ciampaglio et al. 2001) and more specifically, the use of leaf architecture has been used in this way by previous researchers (e.g., Green and Hickey 2005, Stiles et al. 2020). Nevertheless, we acknowledge that leaf architecture is an imperfect proxy for ecological diversity and is influenced by phylogeny (e.g., Little et al. 2010). Morphospecies are defined based on leaf architecture, and therefore our results may confound differences in taxonomic and ecological diversity (if differences exist). We discuss our results in light of these concerns (see "Ecomorphological and Taxonomic Diversity Across the K-Pg Boundary") and couple our morphological analyses with additional tests for ecological diversity (i.e., LMpA) to further investigate the differences between taxonomic, morphological, and ecological diversity in these floras.

Compendium Index Categories.—We evaluated the morphological diversity of our floras using Compendium Index Categories (CIC). We classified each of our 122 morphospecies into CIC, identified by a number between 100 and 990. CIC group morphospecies according to the plant organ's morphological or architectural features; for instance, CIC 128 includes all morphotypes with simple, pinnately veined, unlobed, obovate angiosperm leaves (Green and Hickey 2005). Distinguishing some CIC from each other was sometimes difficult or impossible (e.g., where one morphotype included variation in tooth shape spanning multiple CIC); in these cases, we binned CIC for our analyses. For example, CIC 113–115 include all simple, pinnately veined, unlobed, ovate, symmetrical, toothed angiosperm leaves and differ only in the shape of

their teeth; for our analyses, we treat these as one CIC group. We tabulated the relative abundance of CIC in each flora (Table 4.S1) to examine the pattern of morphological diversity through time. Floras with higher numbers of CIC represent more morphologically diverse vegetation. We also examine morphological diversity through time using an unconstrained nonmetric multidimensional scaling (NMDS) ordination of the CIC relative abundance data. We chose an NMDS ordination based on Bray-Curtis distances, reducing to k = 2 and running the analysis 100 times to find the minimum stress solution. This method is well suited to abundance data, avoids any assumption of linearity among variables, and is relatively robust to the arch effect (Minchin 1987, Clarke 1993). Although there are drawbacks to NMDS (e.g., see discussion in Donohue et al. 2013), careful selection of ordination and vetting of stress for significance can alleviate these concerns. We generated 95% confidence intervals around the HC, TM1, and TM2 interval floras to evaluate potential changes in morphology through time. Finally, we quantitatively assessed the compositional differences between the HC, TM1, and TM2 intervals through an analysis of similarity (ANOSIM), comparing within versus between group (temporal interval) differences in Bray-Curtis distances of the relative abundance of CIC in each flora. ANOSIM allows us to quantitatively evaluate patterns observed in our ordination and is complementary to NMDS as both utilize rank dissimilarity to quantify distance (Clarke 1993). We apply an unconstrained ordination analysis and analysis of similarity (ANOSIM) to analyze CIC abundance through time, rather than regression or correlation analyses as Green and Hickey (2005) applied because our relatively few temporal intervals are not conducive to correlation.

Morphospace Occupation.—We mapped morphospace occupation through time using leaf architectural characters. We largely follow the methods of Stiles et al. (2020). We classified

the 88 dicot morphospecies using a suite of 39 leaf foliar characters that are based on the character states in Ellis et al. (2009) (Table 4.S4–5). We chose these characters because they meaningfully capture the morphological diversity of our taxa (e.g., primary vein framework, laminar shape) and were identifiable in over half of our taxa (largely following the characters used by Stiles et al. [2020]). We classified each morphospecies using a few (1–5) of its most exemplary specimens. Missing characters were left blank.

From this leaf foliar character matrix, we computed Gower distances (Gower 1971) between each taxon pair using the R package cluster (Maechler et al. 2021). These distances were used in a principal coordinates analysis (PCoA) using the R package stats (R Core Team, 2020; http://www.r-project.org). Gower distance can measure dissimilarity in records that contain multiple data types (e.g., binary, categorical) such as we have in our dataset. PCoA can be used with a variety of distance metrics, has been used in similar analyses (e.g., Stiles et al. 2020), and performs well with missing character data (Foote 1994, Roy and Foote 1997). We plotted both species scores and character loadings for the first four axes of the analysis to visualize 1) the distribution of species in the morphospace and 2) the influence of each character on the distribution of species in morphospace. To evaluate how morphospace occupation changed through time, we plotted the morphospecies from HC, TM1, and TM2 intervals separately. We also measured morphological disparity as the area of morphospace occupied during each of these intervals. Morphospace occupations is frequently measured in paleontological analyses of character data (e.g., Foote 1991, reviews by Lloyd 2016 and Gerber 2019) as both the size and density of morphospace (Guillerme et al. 2020). We calculated the sum of variance among taxa (SoV; Foote 1992), which quantifies morphospace size, as well as the average distance to nearest neighbor (NND; Foote 1992), which quantifies morphospace

density. We compared the distribution of SoV and NND for taxa during each time interval (HC, TM1, TM2, and TM) using a Wilcoxon signed-rank test to examine whether changes in morphospace occupation through time were significant. These calculations were performed using the dispRity package in R (Guillerme 2018).

4.3.3 Image Processing and Measurement

We generally apply the protocols of Royer et al. (2005, 2007) and Peppe et al. (2011b) in preparing specimens for both LMpA and DiLP (or other paleoclimate) analyses. We selected specimens of woody dicot taxa which preserve reasonably complete leaf fossils with >25% of the margin or blade intact. We restrict these analyses (LMpA and paleoclimate) to woody dicot taxa, as they are a) most abundant in our study and b) more useful in the study of petiole width, leaf area, and LMpA (Royer et al. 2007) and in climate and leaf physiognomy (Peppe et al. 2018). The image processing and specimen measurement described below was carried out by a team of researchers led by P.W.D. We trained researchers on a single suite of ten training specimens to evaluate inter-investigator bias and overlapped researchers on approximately 10% of the specimens used in this study to continuously monitor this bias.

We imaged each specimen using a Nikon D3100 camera equipped with an 18–55 mm lens. Each image was digitally manipulated in the GNU Image Manipulation Program (GIMP version 2.10.20; The GIMP Development Team, 2020; https://www.gimp.org) to separate the petiole and blade from the surrounding matrix in the image. We digitally removed teeth from the blade of the specimen to estimate the size of those teeth. We then measured a suite of 11 variables from each specimen including the petiole width (PW), leaf area (A), feret length, margin state, and several variables related to tooth size in the program ImageJ (ImageJ version

1.53c: Rasband, 1997; https://imagej.nih.gov/ij/). Additional variables such as perimeter ratio were calculated from these measurements (Table 4.S6).

4.3.4 Plant Ecological Strategies

We estimate plant ecology along the leaf economic spectrum (LES) by evaluating the leaf mass per area (LMpA) of each woody dicot taxon. We estimate LMpA in fossil taxa using the mechanical relationship between the cross-sectional area of the petiole and the mass of the leaf (Royer et al. 2007). We chose specimens that preserved both the petiole insertion to the base of the leaf blade and enough of the leaf for faithful measurement or estimation of its area. For those specimens in which the complete leaf area could not be measured, we evaluated the Raunkiaer-Webb size category of the leaf (Raunkiær 1934, Webb 1959) and used the mean leaf area for that size category. Leaves for which this approximation was used are indicated in Table 4.S6. We acknowledge that approximation could introduce error into our calculation of LMpA; however, given that we approximated leaf area for only 13% of our specimens, the impact on our results is likely negligible.

We measured petiole width (PW) and area (A) of 197 specimens (Table 4.S6) and used the regression in Royer et al. (2007) to estimate LMpA in woody dicot species (Table 4.S8):

$$log_{10}LMpA = 3.070 + 0.382\ x\ log_{10}\left(\frac{PW^2}{A}\right) \quad \text{Eq. 1}$$

We used those specimen LMpA values to calculate the mean species LMpA values at three different levels of temporal resolution (species-site, species-bin, and species-interval means) for morphospecies with greater than two specimens in a given site (flora), bin, or interval (Table 4.S9). In another iteration we calculated species-LMpA values for all morphospecies (including those with less than 2 specimens). We then calculated the mean, median, and range of species LMpA for each site (flora), bin, or interval. This strategy enables us to estimate LMpA

accurately and to present LMpA estimates that are comparable with other studies from the western interior of North America (e.g., studies in which average species LMpA was calculated for an entire formation). In our results, we present LMpA results for each temporal interval (HC, TM1, TM2) as the mean and range species-interval LMpA. The mean LMpA value can be used to infer the overall ecology of plants at that time interval, whereas the range of LMpA values can be used to infer the ecological diversity of plants at that time interval (Royer et al. 2007, Blonder et al. 2014, Lyson et al. 2019).

4.3.5 Paleoclimate

We obtained measurements of leaf foliar characters from 859 specimens representing 94 morphospecies (Table 4.S6). We excluded specimens that had less than ~25% of the lamina preserved, because they cannot accurately be measured (Peppe et al. 2018). We measured foliar traits on 1–56 (median 2) specimens per morphospecies in each flora; Royer et al. (2005) indicates that 1–6 specimens per species is sufficient. For taxa that can variably have toothed or untoothed leaves, we applied several filters. For cases in which the specimens could represent distinct morphospecies, we subdivided some morphospecies into sub-morphospecies to analyze separately in our analyses. For cases in which the specimens plausibly represent a morphological continuum within a single morphospecies, we included both the toothed and untoothed specimens in calculating the species averages. However, for these variably toothed taxa, we excluded entire margined specimens that had less than 50% of the lamina preserved, because it is uncertain whether teeth were present on the missing part of the lamina. We then averaged our specimen measurements to calculate species-site, species-bin, and species-interval mean leaf foliar measurements (Table 4.S10). We finally averaged species LMpA at each site, bin, or interval for use in the climate regression models. We calculated mean foliar measurements using

either range-through occurrences (following the methods of Wilf et al. 2003 and Lyson et al. 2019) or only specimens from that site (flora); the latter approach may more accurately reflect the leaf physiognomy (and therefore climate) at a particular time.

We estimated mean annual temperature (MAT) and mean annual precipitation (MAP) as well as standard error for both climate parameters. We estimated MAP and MAT using 1) univariate climate models (leaf margin analysis [LMA] and leaf area analysis [LAA]) and 2) multivariate climate models (digital leaf physiognomy [DiLP]). Although DiLP purportedly produces more accurate climate estimates (Royer et al. 2005), previous researchers have variably used multivariate and univariate approaches (e.g., Wilf et al. 2003). Therefore, we utilized DiLP, LMA, and LAA to compare our results with previous work and to investigate differences in these approaches. To minimize phylogenetic signal in our results, we used the DiLP North American (NA) regression model, which is based on modern floras from our geographic region of study. We used the following regression models:

LAA (Peppe et al. 2011b):

$$\ln(MAP) = 0.283\, x \ln(A) + 2.92 \qquad \text{Eq. 2}$$

LMA (Peppe et al. 2011b):

$$MAT = 0.204\ (E) + 4.6 \qquad \text{Eq. 3}$$

DiLP NA regional regression for MAT (Peppe et al. 2011b, D. Peppe pers. comm. 2019):

$$MAT = 0.233\ (E) - 1.547\ (T{:}\,IP) + 8.161 \qquad \text{Eq. 4}$$

DiLP global regression for MAP (Peppe et al. 2011b):

$$\ln(MAP) = 0.298\, x\, ln(A) + 0.279\ ln(T{:}\,IP) - 2.717\ ln(PR) + 3.033 \qquad \text{Eq. 5}$$

where A is the leaf area, E is the proportion of species at the site with entire margins, T:IP is the ratio of the number of teeth to the internal perimeter (for toothed taxa), and PR is the ratio of the internal perimeter to the actual perimeter (for toothed taxa).

Whereas most studies indicate that floras with >20 taxa are most appropriate for use in leaf physiognomic climate estimates (Peppe et al. 2018), the floras in this study range from 6 to 19 woody dicot species (Table 4.1). Recognizing that the low number of species may add error to our estimates, we applied bootstrapping methods to quantify the precision of our paleoclimate estimates at these depauperate sites. We took the calibration data from Peppe et al. (2011b) and selected a diverse site from the temperate northern hemisphere to approximate our study conditions. We then subsampled this site from n = 1 species to the maximum measured species richness at that site (55) and input the newly derived site-species average physiognomic traits into the DiLP, LMA, and LAA regressions reported above. We repeated this subsampling for 1,000 repetitions at each simulated species richness (n = 1–55). From this simulation, we were able to estimate the range of inferred MAT and MAP for a poorly sampled (or species poor) assemblage versus a very well sampled (or species rich) assemblage.

All analyses described above were conducted in R version 4.0.2 (R Core Team, 2020; http://www.r-project.org) using appropriate functions from the community ecology package vegan version 2.5–7 (Okansen et al. 2019), the multivariate ordination package cluster (Maechler et al. 2021), and the disparity package dispRity (Guillerme 2018). See Supplementary Material for code.

4.4 RESULTS

4.4.1 Ecomorphology

Analysis of CIC Relative Abundance.—The distribution of CIC morphologies in NMDS ordination space (Fig. 4.3) show that the distribution and abundance of specific CIC changed through the interval of study. The low stress of this ordination (0.0900) indicates a good fit of this solution in capturing the underlying variance in our abundance data (Clarke and Warwick 1994). HC, TM1, and TM2 floras occupy distinct spaces of this ordination, with TM2 floras generally falling intermediate between HC and TM1. Results of our ANOSIM support this pattern; between-group differences in the abundance distribution of CIC are significant when comparing HC, TM1, and TM2 floras (ANOSIM R = 0.42, *p*-value = 0.006). The changes in CIC abundance were largely driven by the dramatic reduction in relative abundance of short needle conifers (CIC 232) in the earliest Paleocene TM1 interval. Conifers dropped from 40% in HC assemblages to <5% in TM1 assemblages before rebounding to 25% in TM2 assemblages (Fig. 4.4). More broadly, HC floras exhibit relatively large CIC richness (*N* = 29 CIC), with short-needle conifers (CIC 232) and pinnate/elliptical leaves (CIC 108–110) having the highest relative abundance (Fig. 4.4). TM1 floras had fewer morphological categories (*N* = 23 CIC), with notably few conifers (CIC 232) and an abundance of pinnate/obovate leaves (CIC 128) and acrodromous/ovate leaves (CIC 131; Fig. 4.4). By the TM2 interval, conifers (CIC 232) became more common again, acrodromous/ovate leaves (CIC 131) remained relatively common, and acrodromous/elliptic leaves (CIC 129) as well as actinodromous/ovate leaves (CIC 137) became common (Figs. 4.3–4). Overall, the TM2 interval saw a modest increase in terms of CIC richness (*N* = 26 CIC).

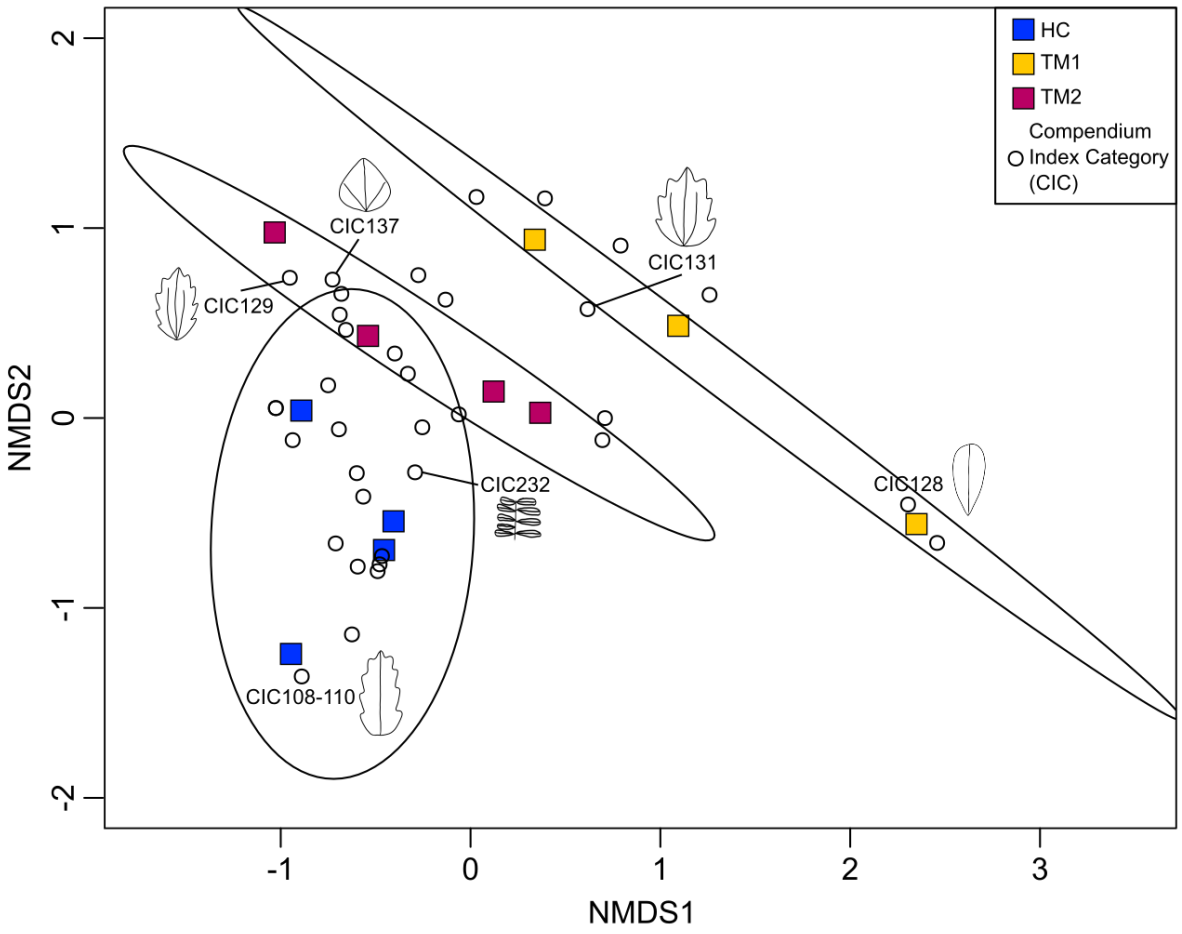

Figure 4.3: NMDS ordination of CIC relative abundance data of the 11 Late Cretaceous and early Paleocene floras. Ordination based on Bray-Curtis distance; stress (0.0900) is low, indicating a good representation of the underlying variance captured by these two dimensions. Closed symbols are floras; symbol color corresponds to temporal interval (HC, TM1, TM2). Confidence ellipses (95%) are drawn for each temporal interval (HC, TM1, TM2). Black circles are CIC; those which are particularly abundant are labelled with an outline showing the generalized morphology of that CIC.

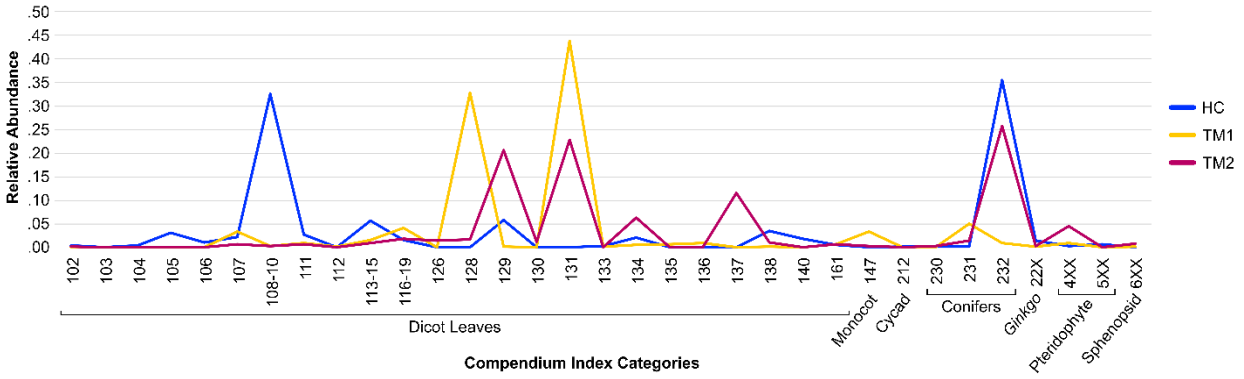

Figure 4.4: Distribution of CIC in the HC, TM1, and TM2 floras. Proportional abundance for each CIC plotted with lines colored according to temporal interval (Late Cretaceous HC or Paleocene TM1 or TM2).

PCoA of Dicot Foliar Character Data.—We further tested the hypothesis that the mass extinction restricted morphological disparity as well as taxonomic diversity by examining the morphospace of leaf architecture through this time interval. The first four axes of our PCoA explain <20% of the variance in the dicot foliar character data. We examined the morphospace occupied during the HC, TM1, and TM2 intervals, first by plotting the external hulls occupied by each temporal interval in morphospace across the first four axes (Fig. 4.5). There are no clear differences either in the size of morphospace occupation nor the region of morphospace occupied during each interval (measured below). The HC floras broadly overlap with both TM1 and TM2 floras in morphospace, but TM1 floras include more orbiculate and peltate-eccentric taxa and TM2 floras include more elliptic taxa (Fig. 4.5). We also quantified morphospace occupation by calculating the sum of variance (SoV; a measure of morphospace size) and mean distance to nearest neighbor (NDD; a measure of morphospace density) for each temporal interval (HC, TM1, TM2, TM) across all PCoA axes. Our results indicate no decrease in morphological disparity (no decline in SoV or NDD) from the Cretaceous to the Paleogene; in fact, there was a

significant expansion in morphospace size (SoV) but a decrease in the density of morphospace occupation (NDD) during the HC versus TM1/TM2 intervals (Table 4.3).

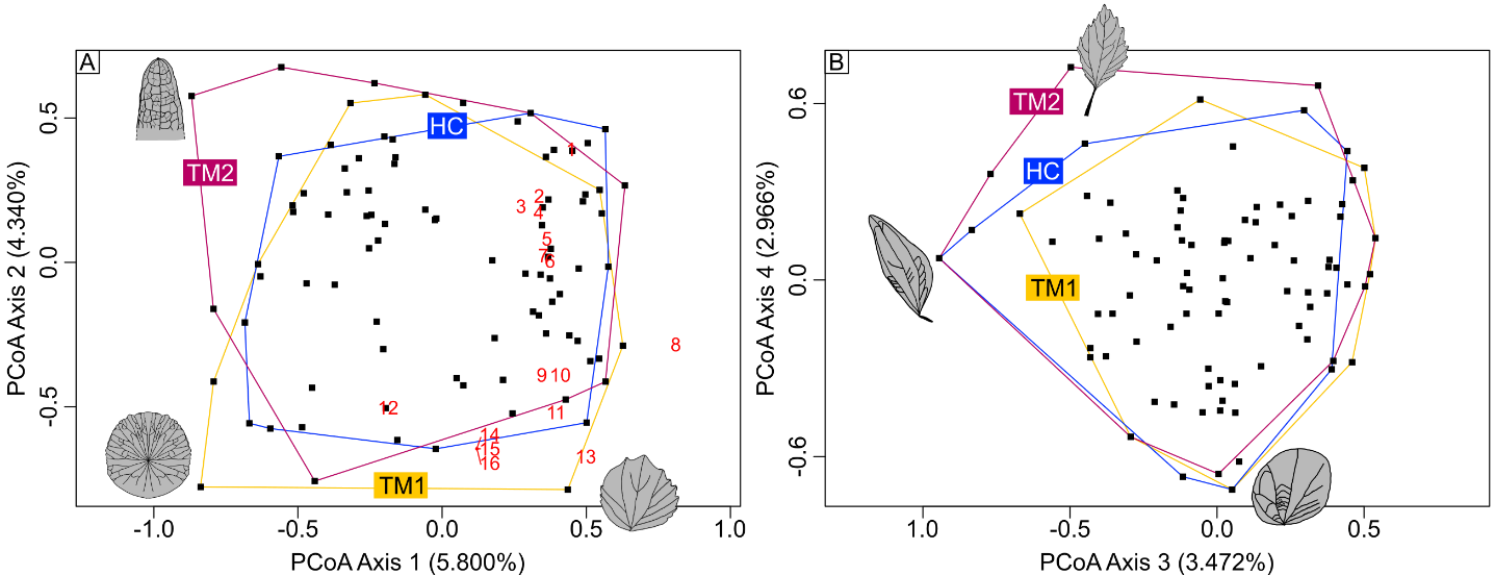

Figure 4.5: Plots of the first four axes of the PCoA of 39 leaf foliar characters across 88 morphospecies from HC, TM1, and TM2 floras. A) PCoA axes 1 and 2 and B) PCoA axes 3 and 4. Black symbols represent individual taxa. Exemplar taxa are illustrated in outline where they plot in the morphospace. Statistically significant characters are plotted as red numbers in A representing the endpoint of vectors which show the correlation of each character with the axes (see Table 4.2 for identification of each character). Morphospace occupied for each time interval (HC, TM1, TM2) is outlined.

Character	***p*-value**	**Character State**	**Identifying Number (Fig. 4.5)**
Major Secondary Spacing	0.0171	Decreasing proximally	1
		Irregular	3
		Gradually increasing proximally	5
		Abruptly increasing proximally	11
		Regular	12
Agrophic Veins	0.0287	Absent	2
		Simple	6
		Present (type uncertain)	9
		Compound	14
Primary Vein Framework	0.0054	Pinnate	4
		Palmate (type uncertain)	10
		Basal actinodromous	16
Secondary Attachment to Midvein	0.0307	Excurrent	7
		Decurrent	15
Orders of Teeth	0.0036		8
Number of Veins at Base	0.0155		13

Table 4.2: Dicot foliar characters that significantly correlate with PCoA results.

	Taxa (n)	Mean sum of variance (SoV)	Mean distance to nearest neighbor (NND)	*p*-values of pairwise Wilcoxon test of SoV values			*p*-values of pairwise Wilcoxon test of NND values		
				TM2	TM1	HC	TM2	TM1	HC
TM	47	0.598	0.341	--	--	--	--	--	--
TM2	33	0.568	0.384	--	--	--	--	--	--
TM1	26	0.581	0.349	0.09	--	--	0.60	--	--
HC	46	0.464	0.298	<0.01	<0.01	--	<0.01	<0.01	--

Table 4.3: Morphospace occupied during each temporal interval (HC, TM1, and TM2) as measured by PCoA of dicot foliar character data.

Analysis of Leaf Mass per Area.— Mean species-interval LMpA (considering taxa with >2 specimens from a given interval) did not clearly change between HC, TM1, or TM2 floras (colored lines; Fig. 4.6A). However, the range of species-interval LMpA decreased from the HC to TM floras; TM floras generally have taxa with lower LMpA values (colored lines; Fig. 4.6A). HC floras contain a handful of taxa with high LMpA values that disappear in TM floras (darker shading; Fig. 4.6B). These results likely indicate both a reduction in the diversity of ecological strategies (reduction in the range of LMpA) of plants from the HC to TM floras as well as an increase in the abundance of fast-growing taxa in TM floras (loss of high-LMpA taxa in the TM intervals).

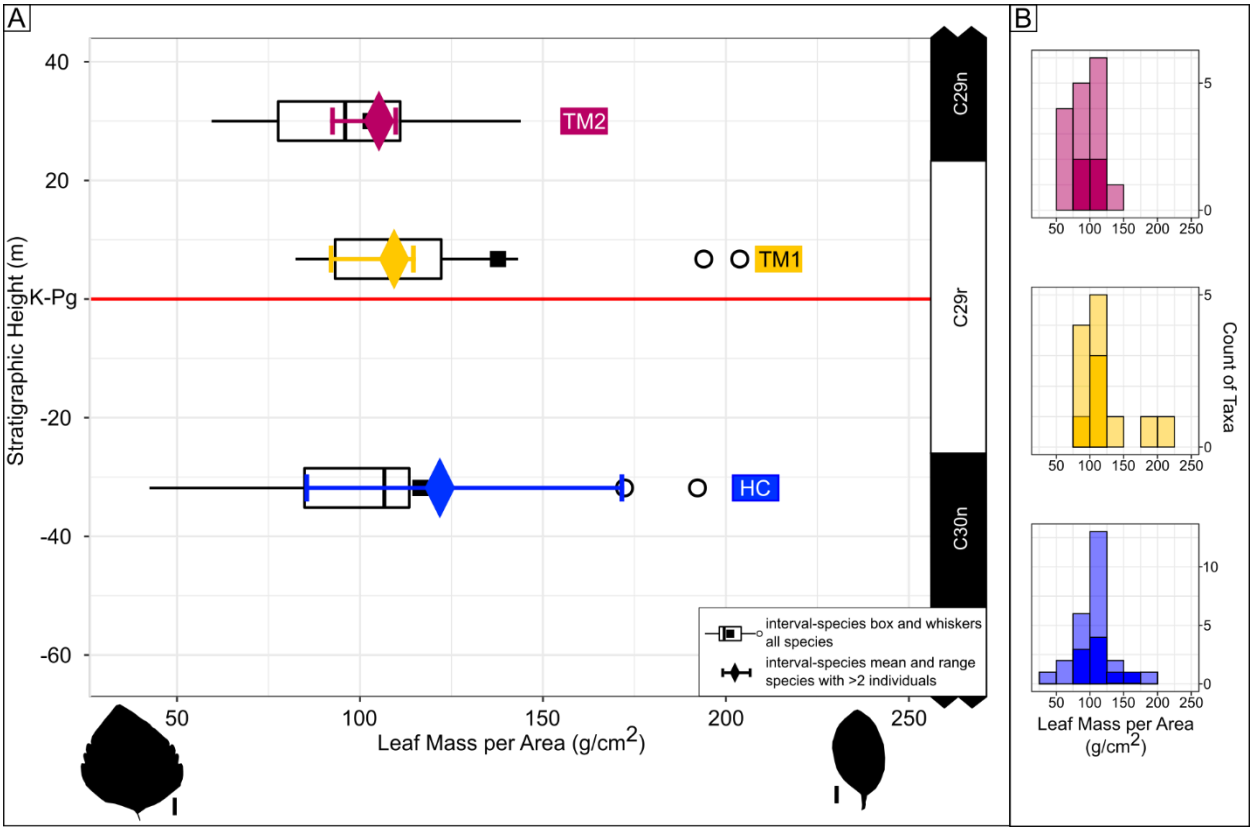

Figure 4.6: Leaf Mass per Area (LMpA) species-interval average and range of values as well as histograms of species-interval LMpA in each interval. A) LMpA data plotted as mean and range of species-interval data for taxa with >2 specimens of that taxon in that interval (colored lines) as well as box and whiskers plot of species-interval data for all taxa in that interval (black box and whiskers plots). The HC interval had nine, TM1 had four, and TM2 had four taxa with >2 specimens in that interval. Example specimens with high and low reconstructed LMpA shown in outline below alongside 1 cm scale bar. B) Histogram of species-interval LMpA distribution. Lighter shading represents histogram of all taxa in that interval, whereas darker shading represents only taxa with >2 specimens in that interval.

The low sample sizes of floras used in our LMpA analyses hamper our ability to unequivocally conclude that the range of species LMpA was reduced through the TM1 and TM2 intervals. We recognize that restricting our analysis to only better-sampled species (with >2 specimens measured) does limit the sample sizes in each interval (HC floras $N = 9$, TM1 floras $N = 4$, and TM2 floras $N = 4$ species). When we include all taxa, there is no reduction in the range of species LMpA from HC to TM1 intervals (black box and whiskers plots; Fig. 4.6A) and there are a few high LMpA species remaining in the TM1 interval (lighter shading; Fig. 4.6B). This is

likely due to high variation in reconstructed LMpA among individual specimens measured in this study; the range of individual specimen LMpA measurements is broad from the HC through TM2 floras (Fig. 4.S1). Further, we found that within-taxon ranges of LMpA can be relatively high (Fig. 4.S2), indicating that intra-specific variation in LMpA may be high; therefore, large sample sizes are needed to accurately estimate the average LMpA for a given taxon.

4.4.2 Paleoclimate

The results of our subsampling exercise indicate that samples with 10–20 species do not introduce a significant amount of error. At ~10 species and above, the spread of MAP and MAT estimates in our bootstrapped samples are not markedly greater than in our bootstrapped samples with >20 species (Fig. 4.S3). Of floras with 10–20 species, the average standard error of our MAP estimates is 0.39 cm and of our MAT estimates is 0.07 °C (using the LMA regression) or 0.08 °C (using the DiLP NA regional regression). This error is less than 1% of the minimum error associated with these paleoclimate methods (± 3.3 °C DiLP NA regional regression [Peppe et al. 2011b], ± 4.8 °C LMA regression [Peppe et al. 2011b], average ± 100 cm LAA regression [Peppe et al. 2011b]). Therefore, the error added by using depauperate floras with 10–20 woody dicot species is negligible. We exclude the two floras (Smurphy's Guess II and The Swamp) with less than 10 woody dicot species from our site-specific paleoclimate estimates.

The resulting paleoclimate estimates from the three approaches (LMA, LAA, or DiLP) are broadly in agreement (Table 4.S11, Fig. 4.7B). However, for each flora, DiLP estimates were consistently ~2.5 °C higher than our LMA estimates (Fig. 4.7B; Table 4.S11). This offset in estimated MAT values may be due to differences in the foliar characters used in LMA versus DiLP (see Introduction). Our DiLP MAP estimates are also lower than our LAA MAP estimates (Table 4.S11). This discrepancy may be because our specimens tend to be very partial. DiLP

methods require a near-complete specimen to estimate leaf area whereas LAA methods allow leaf area to be estimated using other means such as size category (see Materials and Methods). Given this difference and the use of LAA in most previous research, we present only the LAA MAP estimates in Figure 4.8 but report both LAA and DiLP MAP estimates in Table 4.S11 for comparison.

Our results indicate that local temperatures fluctuated in the latest Cretaceous HC interval and during the earliest Paleocene TM interval in NE Montana. There was an increase of ~5–7 °C in the HC interval around the C30n/C29r boundary (66.311 ± 0.067 Ma; Sprain et al. 2018) followed by a decrease of ~5–7 °C at or just before the KPB (66.052 ± 0.043 Ma; Sprain et al. 2018). Temperatures varied through the TM interval, between 13.7 and 20.1 °C (DiLP results; Table 4.S11). There was a slight (3–5 °C) increase in temperature in the earliest Paleocene just before the C29r/C29n boundary (65.724 ± 0.044 Ma; Sprain et al. 2018). When we bin our floras into 15-m intervals, the resultant temperature curve generally follows the same pattern as our individual flora-derived estimates (Fig. 4.7). We also compare these results with previous paleoclimate estimates from the northern Great Plains (Fig. 4.7A). Paleoclimate reconstruction methods used in previous work varied: Wilf et al. (2003) used LMA based on range-through occurrences of fossil plant taxa from stratigraphic section spanning the entire interval, Tobin et al. (2014) use clumped isotope paleothermometry based on bivalve fossil material, and Arens and Allen (2014) use CLAMP based on a single Late Cretaceous leaf assemblage. Tobin et al. (2014) interpret their paleotemperature estimates as mean summer temperature, and therefore suggest these temperatures are likely ~15 °C higher than MAT; therefore, we have subtracted 15 °C from the results of Tobin et al. (2014) to approximate MAT (following the approach of those authors). We use our binned floral data and report LMA MAT estimates here, as this sampling

and analytical approach matches that used by Wilf et al. (2003), making our results more easily comparable (Fig. 4.7A).

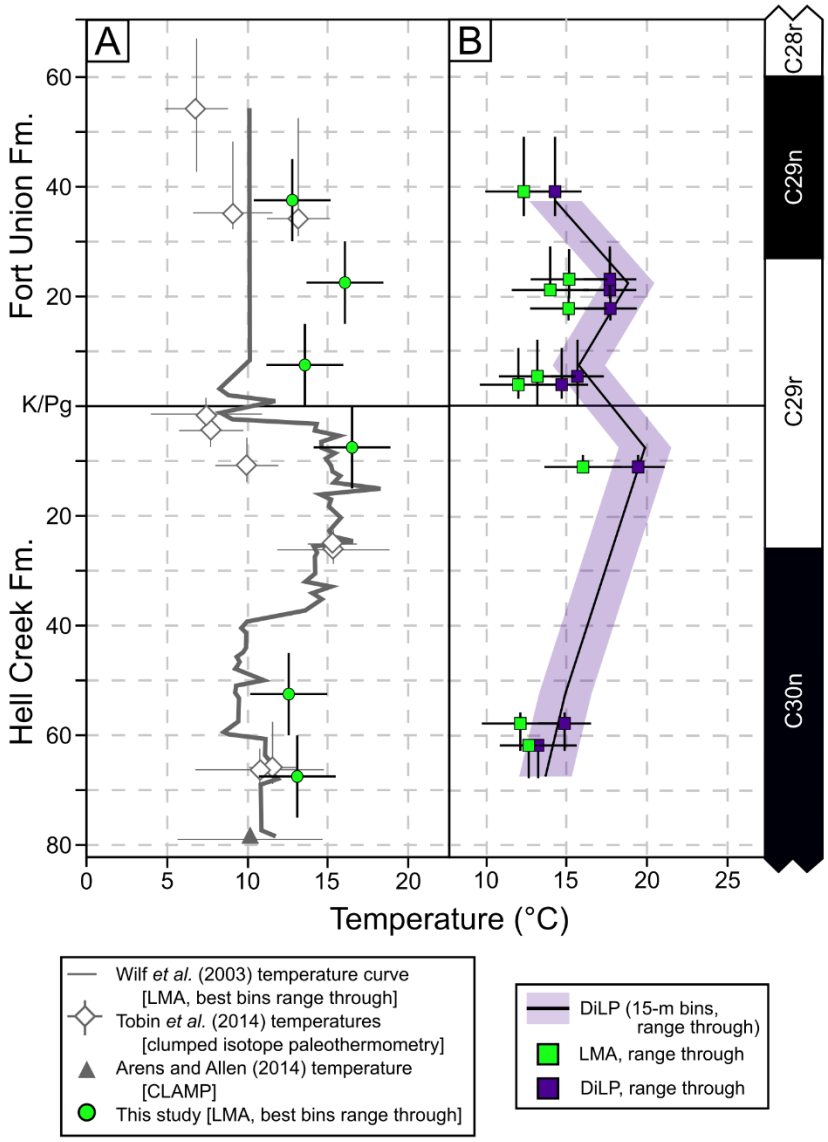

Figure 4.7: Paleotemperature reconstruction. A) MAT records from Tobin et al. (2014), Wilf et al. (2003), Arens and Allen (2014), and this study. As noted in the legend, paleothermometry methods as well as floral sampling strategies differ among studies. Clumped isotope paleothermometry of fossil bivalve material (Tobin et al. 2014) likely records growing season temperature, therefore temperature estimates are adjusted down 15 °C to compare with the MAT estimates reported in other studies. B) Comparison of MAT estimates in this study from leaf margin analysis (LMA) versus digital leaf physiognomy (DiLP) at each site (closed symbols) versus DiLP for each 15-m bin (line).

Based on our MAP and MAT estimates and the Whittaker (1975) ecozones, the biome in NE Montana was likely a temperate to tropical seasonal forest during the HC and TM intervals (Fig. 4.8). Reconstructed MAP was mostly stable throughout this interval, 154 cm/yr on average (Table 4.S11). The range of error on these MAP estimates is large (in some cases doubling the estimated MAP), so we cannot discount the possibility that these floras represent vegetation in a temperate rainforest environment (Fig. 4.8). We also plotted paleoclimate estimates (Fig. 4.8) from the early Paleocene in the San Juan Basin, New Mexico (SJB), the Denver Basin, Colorado (DB), and the Williston Basin, North Dakota (ND). The SJB and ND reconstructions are based on DiLP paleothermometry whereas the DB reconstruction is based on LMA and LAA models (Fig. 4.8; data reported by Flynn and Peppe 2019). We present our DiLP MAT and our LAA MAP estimates because these regressions have the lowest error and produce results which are also broadly comparable with these previous works (Fig. 4.8). The results show general agreement in reconstructing a temperate forest ecozone in the northern Great Plains (ND, DB, and this study) during the earliest Paleocene; the SJB was warmer during this interval, and likely hosted a tropical seasonal forest (Fig. 4.8; see Discussion). The range of error on MAP estimates also leaves open the possibility that there was a temperate rainforest in the northern Great Plains and a tropical rainforest in the SJB (Fig. 4.8).

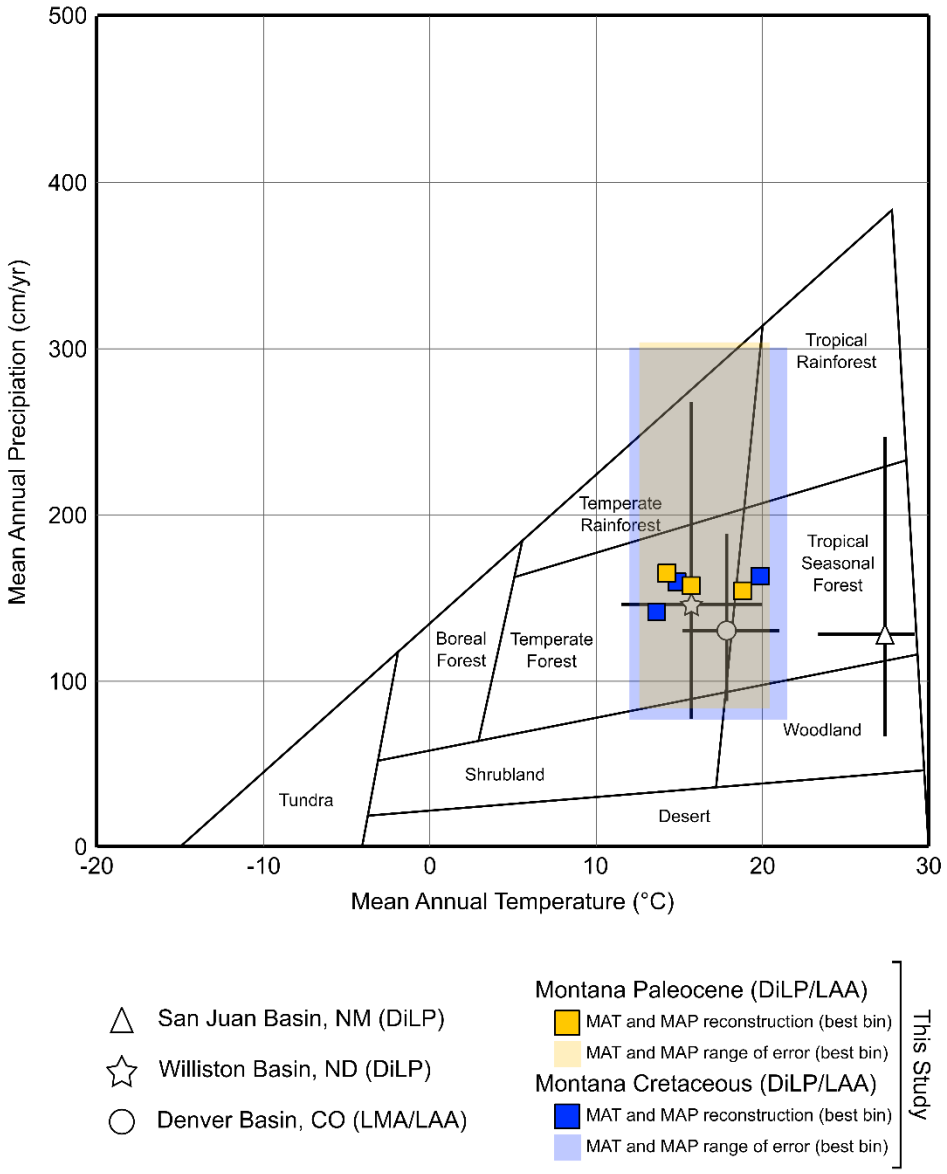

Figure 4.8: Paleoclimate proxy data from the western interior of North America plotted on the Whittaker (1975) ecozones. Paleoclimate proxies from this study were calculated for each 15-m stratigraphic bin using range-through data (closed symbols) with uncertainty shown in shaded regions, comparing the Late Cretaceous (blue) with the Paleocene (yellow). MAP was calculated using LAA, and MAT was calculated using the DiLP NA regression. Paleocene paleoclimate proxy data from other regions in the western interior of North America were plotted for comparison. Horizontal and vertical bars indicate uncertainty (data compiled by Flynn and Peppe 2019: Williston Basin ND data from Peppe et al. 2011a, San Juan Basin NM data from Flynn and Peppe 2019, and Denver Basin CO data from Barclay et al. 2003).

4.5 DISCUSSION

The effects of the K-Pg mass extinction on the ecomorphology of plants and the paleoenvironment during this time are central to understanding this critical event. We tested three hypotheses: H1) the K-Pg mass extinction led to not only taxonomically but also morphologically less diverse vegetation in the earliest Paleocene; H2) the plant extinctions at the KPB were selective, opening up ecospace to allow fast-return plant taxa to flourish in the aftermath of the mass extinction; and H3) fluctuations in latest Cretaceous and earliest Paleocene paleo-temperatures contributed to the pattern of the mass extinction and biotic recovery.

4.5.1 Ecomorphological and Taxonomic Diversity Across the K-Pg Boundary

Our results support the hypothesis that the mass extinction led to the selective extinction of certain plant taxa (resulting in a shift in morphology or the abundance distribution of CIC) in plant communities as a whole (Figs. 4.3–4) but not necessarily a restriction in morphological disparity among dicots (no change in morphospace occupation; Fig. 4.5, Table 4.3). We document a large reduction in the abundance of short needle conifers in the earliest Paleocene along with changes in the abundance of various dicot morphologies, although few of these ecomorphological groups disappeared completely during the mass extinction (Figs. 4.3–4). This corresponds to a restructuring of plant community ecomorphology but not a decline in ecomorphological disparity.

We examined several reasons for this difference between ecomorphological abundance structure and disparity, beginning with taphonomic or methodological concerns. Our morphospace analysis was only able to summarize a fraction of the variance in our dicot foliar character data (<20% in the first four PCoA axes; Fig. 4.5); therefore, these results may not be capturing the shift in morphology we find in our CIC results. This low variance explained may

be due to the complexity in our dicot foliar character data (we are examining 26 characters, some of which have up to 20 states) as well as the high proportion of missing data (data was missing for as many as 50% of taxa for some characters; Table 4.S5). However, we also note that this level of variance explained is typical in ordination analyses of discrete character data (Lloyd 2016). Stiles et al. (2020) do not report percent variance explained in their PCoA, so it is difficult to assess whether our analysis is performing similarly. In addition, because we use leaf architecture to define our morphotype scheme, we may be conflating taxonomic and ecological diversity at some level. However, recent work on these floras indicates that taxonomic richness decreased from the Late Cretaceous to the Paleogene by ~28% (Wilson Deibel et al. in prep), even as we report that dicot morphological disparity did not change. Therefore, the trends in leaf architecture reported in this study appear to capture aspects of plant ecomorphology distinct from taxonomy, and moreover indicate that plant taxonomic and morphological diversity were decoupled during the K-Pg mass extinction.

We interpret this discrepancy between ecomorphological relative abundance structure, ecomorphological disparity, and taxonomic richness as an indication of underlying biotic trends: changes in community structure (relative abundance) without the total disappearance of particular ecomorphological groups. The CIC analysis captures changes in relative abundance and includes conifer taxa, whereas the morphospace analysis only considers presence/absence and is exclusive to dicots. Therefore, the discrepancy in results of these two analyses may indicate that the relative abundance of specific functional groups (e.g., short needle conifers as well as several dicot groups; Fig. 4.4) shifted after the mass extinction, even as overall morphological disparity of dicots remained relatively unchanged (Fig. 4.5). These results support the framework of previous authors (e.g., McElwain and Punyasena 2007) who suggested that

mass extinctions impact plant communities more in shifts of relative abundance (here, in ecomorphological groups) rather than in large proportions of extinction or extirpation. In addition, this pattern may also exist in vertebrate groups where functional redundancy buffers communities from loss of ecological diversity during periods of extinction (Pimiento et al. 2020).

These results also point to local-scale variability in plant ecomorphological changes across the KPB. Stiles et al. (2020) found that floras in Patagonia experienced no restriction in dicot morphospace occupation from the Cretaceous to the Paleocene, just as we find here from Montana (Fig. 4.5, Table 4.3). However, we find a shift in the relative abundance of morphological categories from the Late Cretaceous to Paleocene (estimated through CIC; Figs. 4.3–4), which was not directly addressed by Stiles et al. (2020). Green and Hickey (2005) analyzed CIC in North America during this time interval and suggested that there was no morphological change in floral architecture across the KPB. Our analytical methods differ from Green and Hickey (2005), but our results contradict their findings. Our results likely reflect local-scale changes in plant morphology which are not reflected in the continent-scale analysis of Green and Hickey (2005).

4.5.2 Selectivity of Extinctions at the K-Pg Boundary

Our LMpA results support the hypothesis that the K-Pg event led to the selective extinction of slow-return plants and to a restriction of ecological strategies after the KPB (Fig. 4.6). Mean taxon-LMpA was relatively constant throughout our time series (100–125 g/m^2; Fig. 4.6A), consistent with temperate vegetation (Royer et al. 2010), but the range of species LMpA values decreased across the KPB (Fig. 4.6A). Reconstructed LMpA is more clearly divorced from taxonomy, and therefore we feel confident that the shifts we report reflect underlying ecological changes in the plant community. However, we also note that small sample sizes in our

LMpA results hinder our ability to provide unequivocal conclusions. Whereas there is a reduction in the range of average species LMpA when we exclude poorly sampled species (with <2 specimens), there is no reduction when we consider all taxa (Fig. 4.6). Given the intra-specific variation we observe in LMpA (Fig. 4.S2) as well as following the methods of previous authors (e.g., Royer et al. 2007, Lyson et al. 2019), we believe that restricting our analysis to taxa with >2 specimens is the best approach to minimize erroneous data due to small sample sizes for a given taxon, even though this limits the number of taxa we consider from each interval. In addition, this analysis of LMpA is restricted to woody dicot taxa. We anticipate that if conifers, which typically have LMpA values 19–58% higher than dicots (Royer et al. 2010), were included they would reinforce the observed pattern (increase the mean and range of LMpA values in the HC and TM2 intervals). These results suggest that plants with high LMpA values selectively disappeared at the KPB in NE Montana. In context of the leaf economic spectrum (LES), the K-Pg mass extinction led to selection against slow-return (longer leaf life span) plants. These results are broadly in accord with findings from Lyson et al. (2019) and Blonder et al. (2014) and support our hypothesis that the environmental disaster at the KPB led to the selective extinction of plants with long leaf lifespans and slow-return strategies.

However, our LMpA results do not indicate any clear signs of ecological recovery through our study section. In contrast to Lyson et al. (2019) who indicate that by ca. 300 kyr after the KPB woody dicot LMpA values had rebounded to pre-KPB levels, we find no clear change in the average or range of species LMpA throughout our Paleocene section (covering ca. 900 kyr post-KPB). Recent taxonomic study of these floras (Wilson Deibel et al. in prep) indicate that Montana vegetation was taxonomically recovering by the time of our TM2 floras. Therefore, taxonomic and ecomorphological diversity in NE Montana continued to be decoupled

during the recovery from the mass extinction. Further collection of Paleocene (TM) specimens from NE Montana to boost sample size for LMpA analysis will help to elucidate the pattern of ecological diversity in the post-KPB interval.

4.5.3 Paleoclimate Reconstruction

We find evidence that temperatures were fluctuating during the latest Cretaceous and early Paleocene (Figs. 4.7–8), coincident with intervals of diversity change among communities in NE Montana. During the latest Cretaceous (near the C30n/29r boundary ca. 66.311 ± 0.067 Ma; Sprain et al. 2018), temperatures increased by ~5–7 °C and then declined by ~5–7 °C near the KPB (66.052 ± 0.043 Ma, Sprain et al. 2018; Fig. 4.7). The rise in temperatures in the latest Cretaceous is coeval with maximum floral richness and mammalian body size in NE Montana (Fig. 4.9). The decline in temperatures near the KPB is coincident with the mass extinction event and the decline in taxonomic richness of plants, mammals, and many other local populations (Fig. 4.9). These results also agree with previous paleoclimate records from the region: Wilf et al. (2003) and Tobin et al. (2014) report a similar magnitude temperature increase in the latest Cretaceous (Fig. 4.7A) and Johnson (2002) found that North Dakota floras from this interval display thermophilic characters. Although we are not able to directly address the cause of the K-Pg mass extinction with this local record, the decline in temperatures coincident with the KPB supports the theories of previous authors who suggest that fluctuating temperatures may have played a role in the mass extinction magnitude and timing (MacLeod et al., 1997, Wilson 2014).

This work also helps to fill in the knowledge gap regarding earliest Paleocene temperatures in the Williston Basin, indicating a warm period just before the C29r/C29n boundary (ca. 328 kyr after the KPB; Fig. 4.7). Previously, there were sparse MAT records from the TM interval in Montana and North Dakota, with some studies suggesting temperatures were

relatively cool and unchanging for ca. 1 Myr after the KPB (Wilf et al. 2003). In contrast, we find that temperatures were changing during this period, with periods of warming and cooling (Fig. 4.7). We also find that overall climate reconstructions in the earliest Paleocene from the northern Great Plains reflect a temperate forest ecozone (MT, ND, DB; Fig. 4.8) while southern North America has been reconstructed as a tropical seasonal rainforest (SJB; Fig. 4.8). These results corroborate the findings of Flynn and Peppe (2019) that there was evidently a latitudinal temperature gradient in the earliest Paleocene, with the northern Great Plains (DB, ND, and MT) representing a more temperate vegetation than the SJB (Fig. 4.8). Rose et al. (2011) also found evidence for a latitudinal temperature gradient in the earliest Paleocene but suggest that mammalian diversity was decoupled from latitudinal climate. Future work to explore the relationship between floral diversity, climate, and latitude may help to elucidate local-scale differences in diversity.

The temperature spike in the earliest Paleocene is also coincident with signs of floral and faunal recovery, indicating that climate may have played a role in driving ecosystem recovery post-KPB. Previous research had suggested a discrepancy between research in Montana, which indicated mammalian communities were recovering by ca. 150–847 kyr after the KPB (Fig. 4.9F; Wilson, 2014, Smith et al. 2018, Wilson Mantilla et al. 2021) versus research in North Dakota which indicated that plant communities remained depauperate for at least 1 myr after the KPB (Wilf and Johnson 2004). These disparate records left open the question of whether plant and animal recovery from the K-Pg mass extinction was decoupled, or whether local (Montana versus North Dakota) differences in recovery timing were at play. Our findings indicate that not only were plant communities in Montana taxonomically recovering coeval with mammalian communities (Fig. 4.9B; Wilson Deibel et al. in prep) but also that increasing temperatures at this

time may have played a role this recovery (Fig. 4.9D). Lyson et al. (2019) similarly reported a period of warming around the C29r/C29n boundary in the DB coincident with recovering plant taxonomic/ecological diversity and increasing mammalian body size, interpreted as signs of recovery in these communities. In NE Montana, mammalian body size does appear to track paleotemperature: mean individual body size increased during the Late Cretaceous warming interval and decreased during the cooling interval at the KPB (Fig. 4.9E; Wilson 2005). Specimen-level records from the Paleocene of NE Montana are currently insufficient to estimate mammalian body size through the earliest Paleocene, so we are unable to fully evaluate whether body size increased during the warming at the C29r/C29n boundary as has been found in the DB (Lyson et al. 2019). This growing body of evidence suggests that local climate may have played a role in ecosystem recovery, and future work to reconstruct local-scale paleotemperature records may help to explain differences in recovery timing around the globe.

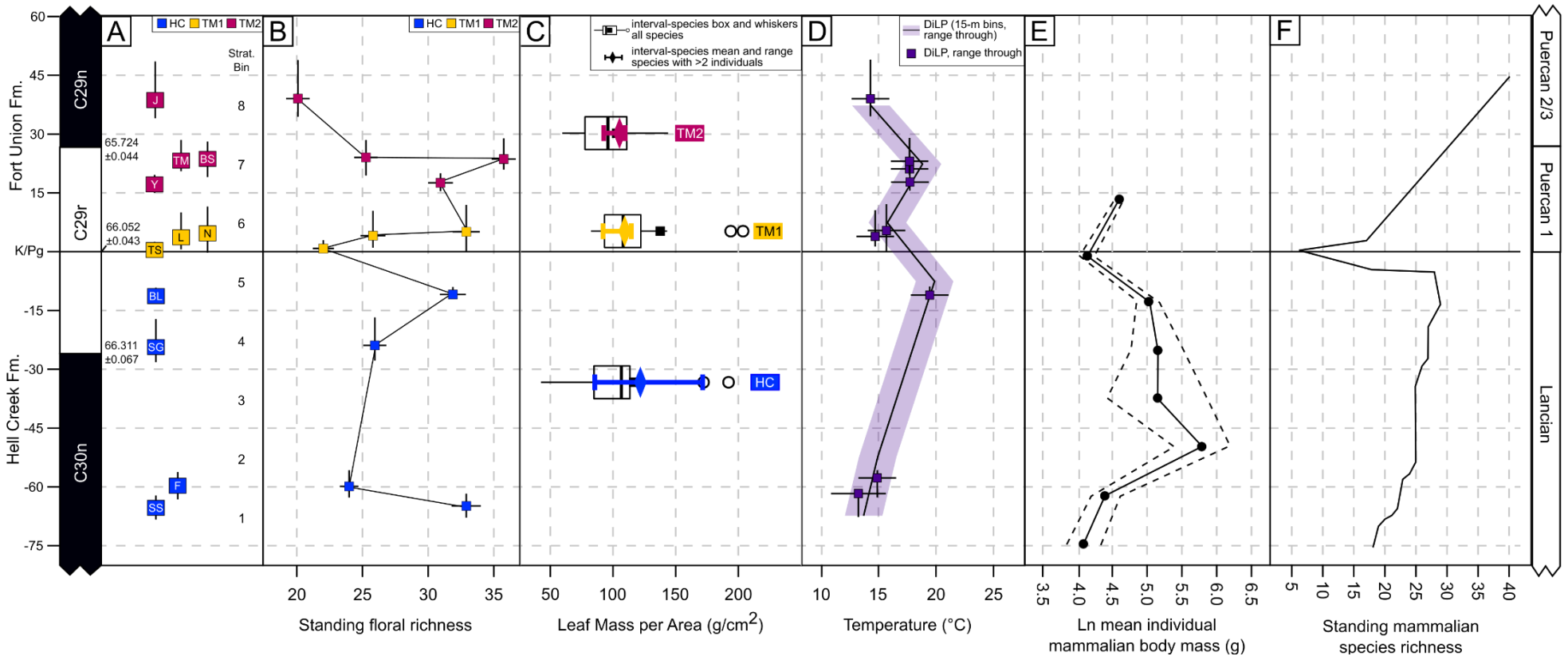

Figure 4.9: Correlated stratigraphic, floral, and faunal data from the K-Pg interval in NE Montana. A) Stratigraphic position of floral assemblages (vertical bars represent uncertainty) and magnetostratigraphy (dates from Sprain et al. 2018) in the study area. Horizontal dashed lines designate the eight 15-m stratigraphic bins used to combine floral data for some analyses in this study. Floras are identified by abbreviation of name (see Table 4.1) and colored according to temporal interval (Fig. 4.1). B) Standing floral richness through time taken from Wilson Deibel et al. in prep. C) Average leaf mass per area (LMpA) in each temporal interval (Fig. 4.6). D) Paleoclimate estimates based on dicot foliar characters (Fig. 4.7). MAT estimated using DiLP NA regression model and using either individual floras or binned data. E) Mean individual mammalian body mass (ln-scale) from NE Montana from Wilson (2005). F) Standing mammalian species richness in NE Montana from Wilson (2014). North American Land Mammal Age (NALMA) shown at right.

4.6 CONCLUSIONS

During the K-Pg mass extinction in NE Montana, we find evidence that plant ecomorphology was changing and likely became more restricted. There was evident selection for fast-return plant ecological strategies at the KPB: average dicot LMpA declined and conifers became rare. In contrast, dicot morphological disparity did not decline, even as the relative abundance of specific morphologies shifted. During the aftermath of the K-Pg mass extinction, taxonomic richness rebounded relatively quickly (Wilson Deibel et al. in prep), even though ecological diversity does not appear to have increased in the ca. 900 kyr after the KPB captured in our record.

The contrasting and complimentary results of our ecomorphological analyses have significant implications for our understanding of plant taxonomic and ecological diversity during environmental crises. Ecomorphological relative abundance, ecomorphological disparity, and taxonomic richness were decoupled during both the mass extinction and recovery intervals. These results largely support the framework of previous authors (e.g., Wing 2004; McElwain and Punyasena 2007; Green et al. 2011) who proposed that plant communities respond to mass extinctions through shifts in abundance structure and the unseating of dominant groups, rather than in high-level (e.g., family-level) extinction or extirpation. Moreover, these results point to the fundamental differences in angiosperm and conifer response during mass extinctions; conifers declined in the initial "disaster" interval post-KPB (TM1) but rebounded in abundance relatively soon after the mass extinction coincident with increases in taxonomic richness (Wilson Deibel et al. in prep). In this study, we find that slow-return dicots did not rebound along with conifers during this "recovery" phase (TM2). These results indicate that angiosperm taxa remained restricted to more fast-growing, "weedy" habits for an extended period post-KPB. The

mass extinction served not only to unseat the abundant conifer taxa, but also the more slow-return angiosperm taxa (Wing and Boucher 2997; see discussion by Wilson Deibel et al. in prep).

Furthermore, our results suggest that ecomorphological diversity cannot be summarized through ecological strategy (LMpA), morphological disparity (dicot foliar character data), or functional groups (CIC abundance) alone, as previous studies of KPB vegetation have done (e.g., Green and Hickey 2005, Blonder et al. 2014, Lyson et al. 2019, Stiles et al. 2020). Rather, each of these analyses (LMpA, dicot foliar character data, CIC abundance) lend particular insight into components of ecomorphological diversity. Therefore, we suggest that future studies of K-Pg vegetation work to integrate multiple of these measures to capture the patterns of plant diversity during environmental crises.

These changes in vegetation structure also co-occurred with shifts in climate that may elucidate some of the drivers behind plant diversity and ecology. Latest Cretaceous temperatures peaked near the C30n/C29r boundary, just as plant species richness was rising, and dropped at the KPB coincident with major biotic turnover in NE Montana. During the earliest Paleocene, we also find evidence for shifting temperatures, including a small peak ca. 328 kyr after the KPB, at the same time we find some signals of ecosystem recovery (increasing plant taxonomic richness).

Overall, taxonomic and ecomorphological plant diversity were decoupled during the K-Pg mass extinction, and the selective extinction of slow-return plant taxa had long-lasting impacts on plant communities independent of taxonomic richness. Our results also support the hypothesis that temperature fluctuations contributed, locally, to the timing and magnitude of diversity loss and recovery. Future work to explore the whole-ecosystem impact of the mass extinction will help to further explore the connection between climate and ecosystem stability.

Chapter 5: Summary

In this dissertation, I set out to investigate how paleovegetation changed during the Cretaceous-Paleogene (K-Pg) mass extinction. Specifically, I tested five hypotheses related to plant response during the mass extinction event (Fig. 1.1) using a suite of megafloras spanning 2.3 Myr across the K-Pg boundary (KPB) in northeastern (NE) Montana: 1) that there was significant turnover of local floras at the KPB, 2) that regional floral associations would be reflected in the local NE Montana vegetation, 3) that changes in faunal diversity would be contemporaneous with floral diversity during the mass extinction and recovery, 4) that plant ecological diversity would also decline across the KPB, and 5) that local environmental changes were correlated with the mass extinction.

In chapter 2 I found support for hypothesis 2 (Fig. 1.1) that regional floral associations are reflected in the local NE Montana floras. Specifically, the Seafood Salad flora preserves a diverse suite of plant taxa which share several taxa in common with assemblages from the HCI interval in North Dakota (13 out of 34 taxa) (Johnson 2002). The conifer taxa were apparently more cosmopolitan (i.e., found in both North Dakota and Montana); among angiosperms, most taxa (10 out of 19) are unique to NE Montana. Thus, the floras in Montana are broadly comparable to regional vegetation, but also contain a large proportion of endemic taxa. Furthermore, I described the taxonomy of the Seafood Salad flora and found that vegetation in NE Montana during the Late Cretaceous was diverse, angiosperm-dominated (in terms of species richness), but with an unusually high (>50%) abundance of conifers.

In chapter 3 I quantified the magnitude and rate of vegetation change during the mass extinction and recovery intervals. Local NE Montana vegetation experienced a ~28% drop in taxonomic richness from the Late Cretaceous to earliest Paleocene as well as the disappearance

of ~63% of local plant taxa. Although the drop in richness was less than most other studies around the globe (40–50%; Wilf and Johnson 2004; Lyson et al. 2019; Stiles et al. 2020), the proportion of disappearances is similar to elsewhere in the western interior of North America (46–57%; Wilf and Johnson 2004; Lyson et al. 2019). In comparison, Patagonia experienced a seemingly higher rate of disappearance at the KPB (up to 90%; Stiles et al. 2020). Thus, my results reinforce the notion that there was global variability in the magnitude of extinction and regional variability in the impact on vegetation diversity at the KPB. In addition, my results suggest that the pattern of recovery was heterogeneous. NE Montana vegetation shows signs of taxonomic diversity recovering within 900 kyr after the KPB, significantly faster than reported in North Dakota (Wilf and Johnson 2004), but coincident with signals of terrestrial faunas recovering in NE Montana (e.g., mammals; Smith et al. 2018; Wilson Mantilla et al. 2021). These results support my hypotheses 1 and 3 (Fig. 1.1), but also point to a nuanced view of vegetation change across the KPB.

Finally, in chapter 4 I investigated the ecological and environmental implications of these megafloral records. The K-Pg mass extinction led to a restructuring of plant ecomorphology: slow-return plant ecological strategies became less common, specific ecomorphological groups became less abundant (e.g., conifers), and even within the dicot angiosperms I found evidence for changes in the relative abundance of specific ecomorphological groups. In contrast, dicot morphological disparity remained constant across the KPB. These results suggest that the KPB led to the selective extinction of plants with slow-return ecological strategies. At the same time, few to no major ecomorphological categories were entirely lost across the KPB. These findings support the framework put forward by McElwain and Punyasena (2007) and Green et al. (2011) that plants tend to experience mass extinctions through restructuring and the diminishment of

particular ecological groups while few major plant taxonomic groups go extinct. These results also support my hypothesis 4 (Fig. 1). However, NE Montana vegetation remained ecologically less diverse (restricted to more fast-growth strategies) for at least 900 kyr after the KPB, even as taxonomic richness was recovering. Furthermore, conifers returned in abundance ca. 80 to 900 kyr after the KPB while slow-return angiosperms remained uncommon. These results suggest that taxonomic and ecological recovery may have been decoupled, and that angiosperm and conifer taxa responded differently both to the pressures of the mass extinction event and during the recovery.

Results of my paleoclimate analysis support hypothesis 5 (Fig. 1.1), that climate was fluctuating across this interval and can potentially be tied to the changes in taxonomic diversity reported here. Specifically, I find evidence for a latest Cretaceous warming interval, corroborating previous reports from the region (Wilf et al. 2003; Tobin et al. 2014) and coincident with the period of highest floral and mammalian taxonomic diversity. Furthermore, this study presents novel paleotemperature records from the earliest Paleocene which suggest a period of warming ca. 328 kyr after the KPB coincident with increasing plant taxonomic richness post K-Pg mass extinction. This Paleocene warm interval correlates with the temperature record from the Denver Basin (Lyson et al., 2019), suggesting that local or regional climate changes may have influenced the pattern of recovery after the mass extinction in North America.

These results also have bearing on our understanding of ecosystem response to mass extinctions more broadly. Whereas the magnitude of diversity loss and taxonomic turnover was much lower in plants than other vertebrate groups (e.g., mammals; Wilson 2005, 2014) the timing of disappearances as well as recovery is similar. Even though plant ecological diversity remained relatively low for at least 1 myr after the KPB, both plants and animal taxonomic

diversity rebounded within 1 Myr after the mass extinction. These results suggest a coupled response of terrestrial communities in both extinction and recovery timing, despite the apparent lag in plant ecological diversity during the recovery. These results provide some support for hypothesis 3 (Fig. 1) but also suggest that ecosystem recovery after a mass extinction may involve multiple phases (i.e., taxonomic, ecological).

Ultimately, this study provides a novel view of terrestrial communities during one of the most pivotal events in Earth history. The results presented herein suggest a model for understanding plant response to mass extinction events and can potentially provide insight into how our planet will respond to the current biodiversity crisis. Moreover, this study underscores the importance of studying communities at multiple taxonomic (e.g., plants, mammals), spatial (local, regional, and global), and biological (e.g., taxonomic, ecologic) levels.

References

Alvarez, L. W., W. Alvarez, F. Asaro, and H. V. Michel. 1980. Extraterrestrial Cause for the Cretaceous-Tertiary Extinction: Experimental results and theoretical interpretations. Science 208:1095–1108.

Antonelli, A., W. D. Kissling, S. G. A. Flantua, M. A. Bermúdez, A. Mulch, A. N. Muellner-Riehl, H. Kreft, H. P. Linder, C. Badgley, J. Fjeldså, S. A. Fritz, C. Rahbek, F. Herman, H. Hooghiemstra, and C. Hoorn. 2018. Geological and climatic influences on mountain biodiversity. Nature Geoscience 11:718–725.

Archibald, J. D. 1982. A study of Mammalia and geology across the Cretaceous-Tertiary boundary in Garfield County, Montana. Univ. Calif. Publ. Geol. Sci. 122:1–286.

Archibald, J. D., R. F. Butler, E. H. Lindsay, W. A. Clemens, and L. Dingus. 1982. Upper Cretaceous-Paleocene biostratigraphy and magnetostratigraphy, Hell Creek and Tullock Formations, northeastern Montana. Geology 10:153–159.

Archibald, J. D., W. A. Clemens, K. Padian, T. Rowe, N. Macleod, P. M. Barrett, A. Gale, P. A. T. Holroyd, N. A. N. C. Arens, J. R. Horner, G. P. Wilson, B. Mark, C. A. Brochu, D. L. Lofgren, S. H. Hurlbert, J. H. Hartman, D. A. Eberth, P. B. Wignall, P. J. Currie, G. V. R. Prasad, L. Dingus, V. Courtillot, N. MacLeod, P. M. Barrett, A. Gale, and P. A. T. Holroyd. 2010. Cretaceous Extinctions: Multiple Causes. Science 328:973.

Arens, N. C., and S. E. Allen. 2014. A florule from the base of the Hell Creek Formation in the type area of eastern Montana: Implications for vegetation and climate. Geological Society of America Special Paper 503:173–207.

Arens, N. C., and I. D. West. 2008. Press-Pulse: A General Theory of Mass Extinction? Paleobiology 34:456–471.

Arens, N. C., A. H. Jahren, and D. C. Kendrick. 2014a. Carbon isotope stratigraphy and correlation of plant megafossil localities in the Hell Creek Formation of eastern Montana, USA. Geological Society of America Special Paper 503:149–171.

Arens, N. C., A. Thompson, and A. H. Jahren. 2014b. A preliminary test of the press-pulse extinction hypothesis: Palynological indicators of vegetation change preceding the Cretaceous-Paleogene boundary, McCone County, Montana, USA. Geological Society of America Special Paper 503:209–227.

Ash, A., B. Ellis, L. J. Hickey, K. R. Johnson, P. Wilf, S. L. Wing, D. C. Daly, L. J. Hickey, J. D. Mitchell. 1999. Manual of leaf architecture. Ithaca, NY, Cornell University Press, 67 p.

Augusto, L., T. Davies, S. Delzon, and A. De Schrijver. 2014. The enigma of the rise of angiosperms: can we untie the knot? Ecology Letters 17:1326–1338.

Badgley, C., T. M. Smiley, R. Terry, E. B. Davis, L. R. G. Desantis, D. L. Fox, S. S. B. Hopkins, T. Jezkova, M. D. Matocq, N. Matzke, J. L. McGuire, A. Mulch, B. R. Riddle, V. L. Roth, J. X. Samuels, C. A. E. Strömberg, and B. J. Yanites. 2017. Biodiversity and Topographic Complexity: Modern and Geohistorical Perspectives. Trends in Ecology and Evolution 32:211–226.

Bailey, I. W., and E. W. Sinnott. 1916. The Climatic Distribution of Certain Types of Angiosperm Leaves. American Journal of Botany 3:24–39.

Barclay, R. S., and Johnson, K. R. 2004. West Bijou Site Cretaceous-Tertiary boundary, Denver Basin, Colorado. Geological Society of America Field Guide 5:59–68.

Barclay, R. S., K. R. Johnson, W. J. Betterton, and D. L. Dilcher. 2003. Stratigraphy and megaflora of a K-T boundary section in the eastern Denver Basin, Colorado. Rocky Mountain Geology 38:45–71.

Barnosky, A. D., N. Matzke, S. Tomiya, G. O. U. Wogan, B. Swartz, T. B. Quental, C. Marshall, J. L. McGuire, E. L. Lindsey, K. C. Maguire, B. Mersey, and E. A. Ferrer. 2011. Has the Earth's sixth mass extinction already arrived? Nature 471:51–57.

Bell, W. A. 1949. Uppermost Cretaceous and Paleocene Floras of Western Alberta. Geological Survey of Canada Bulletin 13:231 p.

Benton, M. J. 1995. Diversification and extinction in the history of life. Science 268:52–58.

Berry, E. W. 1911. The Flora of the Raritan Formation. Trenton, NJ, US Geological Survey of New Jersey.

Berry, E. W. 1925. The flora of the Ripley formation. US Geological Survey Professional Paper 136.

Berry, E. W. 1934. A Lower Lance Florule From Harding County, South Dakota. US Geological Survey Professional Paper 185-F:127–133.

Blonder, B., D. L. Royer, K. R. Johnson, I. Miller, and B. J. Enquist. 2014. Plant ecological strategies shift across the Cretaceous-Paleogene boundary. PLoS Biology 12.

Bond, W. J. 1989. The tortoise and the hare: ecology of angiosperm dominance and gymnosperm persistence. Biological Journal of the Linnean Society 36:227–249.

Bond, D. P. G., and S. E. Grasby. 2017. On the causes of mass extinctions. Palaeogeography, Palaeoclimatology, Palaeoecology 478:3–29.

Boyce, C. K., and A. B. Leslie. 2012. THE PALEONTOLOGICAL CONTEXT OF ANGIOSPERM VEGETATIVE EVOLUTION. International Journal of Plant Sciences 173:561–568.

Boyce, C. K., T. J. Brodribb, T. S. Feild, and M. A. Zwieniecki. 2009. Angiosperm leaf vein evolution was physiologically and environmentally transformative. Proceedings of the Royal Society B 276:1771–1776.

Bray, J. R., and J. T. Curtis. 1957. An Ordination of the Upland Forest Communities of Southern Wisconsin. Ecological Monographs 27:325–349.

Brodribb, T. J., and T. S. Feild. 2010. Leaf hydraulic evolution led a surge in leaf photosynthetic capacity during early angiosperm diversification. Ecology Letters 13:175–183.

Brodribb, T. J., J. Pittermann, and D. A. Coomes. 2012: ELEGANCE VERSUS SPEED: EXAMINING THE COMPETITION BETWEEN CONIFER AND ANGIOSPERM TREES. International Journal of Plant Sciences 173:673–694.

Brongniart, A. 1833. Notice sur une conefère fossil du terrain d'eau douce de l'ile Iliodroma. Annales des sciences naturelles:168–176.

Brown, R. W. 1936. The genus *Glyptostrobus* in America. Journal of the Washington Academy of Sciences 26:353–357.

Brown, R. W. 1939. Fossil Plants from the Colgate Member of the Fox Hills Sandstone and Adjacent Strata. US Geological Survey Professional Paper 189–I:239–275.

Brown, R. W. 1962. Paleocene Flora of the Rocky Mountains and Great Plains. US Geological Survey Professional Paper 375.

Brusatte, S. L., R. J. Butler, P. M. Barrett, M. T. Carrano, D. C. Evans, G. T. Lloyd, P. D. Mannion, M. A. Norell, D. J. Peppe, P. Upchurch, and T. E. Williamson. 2015. The extinction of the dinosaurs. Biological Reviews 90:628–642.

Butala, J. R., and A. A. Cridland. 1978. Nomenclature of Fossil *Glyptostrobus* in North America. Taxon 27:15–20.

Carvalho, M. R., C. A. Jaramillo, F. de la Parra, D. Caballero-Rodriguez, F. Herrera, S. Wing, B. L. Turner, C. D'Apolito, M. Romero-Baez, P. Narvaez, C. Martinez, M. Gutierrez, C. Labandeira, G. Bayona, M. Rueda, M. Paez-Reyes, D. Cardenas, A. Duque, J. L. Crowley, C. Santos, and D. Silvestro. 2021. Extinction at the end-Cretaceous and the origin of modern Neotropical rainforests. Science:63–68.

Ceballos, G., P. R. Ehrlich, and P. H. Raven. 2020. Vertebrates on the brink as indicators of biological annihilation and the sixth mass extinction. PNAS 117:13596–13602.

Chandrasekharam, A. 1974. Megafossil flora from the Genesee locality, Alberta, Canada.

Chaney, R.W. 1951. A Revision of Fossil *Sequoia* and *Taxodium* in Western North America Based on the Recent Discovery of *Metasequoia*. Transactions of the American Philosophical Society 40:171–263.

Chen, M., C. A. E. Strömberg, and G. P. Wilson. 2019. Assembly of modern mammal community structure driven by Late Cretaceous dental evolution, rise of flowering plants, and dinosaur demise. PNAS 116.20:9931–9940.

Chiarenza, A. A., A. Farnsworth, P. D. Mannion, D. J. Lunt, P. J. Valdes, J. V. Morgan, and P. A. Allison. 2020. Asteroid impact, not volcanism, caused the end-Cretaceous dinosaur extinction. PNAS 117.29:17084–17093.

Ciampaglio, C. N., M. Kemp, and D. W. McShea. 2001. Detecting changes in morphospace occupation patterns in the fossil record: characterization and analysis of measures of disparity. Paleobiology 27:695–715.

Clarke, K. R. 1993. Non-parametric multivariate analyses of changes in community structure. Australian Journal of Ecology 18:117–143.

Clarke, K. R., and R. M. Warwick. 1994. Similarity-based testing for community pattern: the two-way layout with no replication. Marine Biology 118:167–176.

Clemens, W.A. 2002. Evolution of the mammalian fauna across the Cretaceous-Tertiary boundary in northeastern Montana and other areas of the Western Interior: Geological Society of America Special Paper 361: 217-245.

Clemens, W. A., and J. H. Hartman. 2014. From *Tyrannosaurus rex* to asteroid impact: Early studies (1901 – 1980) of the Hell Creek Formation in its type area. Geological Society of America Special Paper 503:1–87.

Close, R. A., S. W. Evers, J. Alroy, and R. J. Butler. 2018. How should we estimate diversity in the fossil record? Testing richness estimators using sampling-standardised discovery curves. Methods in Ecology and Evolution 9.

Cole, S. R., and M. J. Hopkins. 2021. Selectivity and the effect of mass extinctions on disparity and functional ecology. Science Advances 7.

Crane, P. R., S. R. Manchester, D. L. Dilcher. 1991. Reproductive and Vegetative Structure of *Nordenskioldia* (Trochodendraceae), a Vesselless Dicotyledon from the Early Tertiary of the Northren Hemisphere. American Journal of Botany 78:1311–1334.

D'Hondt, S. 2005. Consequences of the Cretaceous/Paleogene Mass Extinction for Marine Ecosystems. Annual Review of Ecology, Evolution, and Systematics 36:295–317.

Davies-Vollum, K. S. 1997. Early Palaeocene palaeoclimatic inferences from fossil floras of the western interior, USA. Palaeogeography, Palaeoclimatology, Palaeoecology 136:145–164.

DeBey, L. B., and G. P. Wilson. 2017. Mammalian distal humerus fossils from eastern Montana, USA with implications for the Cretaceous-Paleogene mass extinction and the adaptive radiation of placentals. Palaeontologia Electronica 20:1–93.

Donohue, S. L., G. P. Wilson, and B. H. Breithaupt. 2013. Latest Cretaceous multituberculates of the Black Butte Station local fauna (Lance Formation, southwestern Wyoming), with implications for compositional differences among mammalian local faunas of the Western Interior. Journal of Vertebrate Paleontology 33:677–695.

Donovan, M. P., P. Wilf, C. C. Labandeira, K. R. Johnson, and D. J. Peppe. 2014. Novel insect leaf-mining after the end-Cretaceous extinction and the demise of Cretaceous leaf miners, Great Plains, USA. PLoS ONE 9.

Dorf, E. 1940. Relationship between floras of type Lance and Fort Union formations. Bulletin of the Geological Society of America 51:213–235.

Dorf, E. 1942. Upper Cretaceous floras of the Rocky Mountain region. Carnegie Institution of Washington publication 508.

Doyle, J. A., and L. J. Hickey. 1976. Pollen and leaves from the mid-Cretaceous Potomac Group and their bearing on early angiosperm evolution. *in* C.B. Beck (editor) Origin and early evolution of angiosperms. Columbia Univ. Press, New York. 139-206.

Dunn, R. E. 2003. Correlation of Leaf Megafossil and Palynological Data with North American Land Mammal Ages from Paleocene Strata of the Ferris and Hanna Formations, Hanna Basin, South-Central Wyoming. The University of Wyoming, 223pp.

Ellis, B., D. C. Daly, L. J. Hickey, K. R. Johnson, J. D. Mitchell, P. Wilf, and S. L. Wing. 2009. Manual of leaf architecture. Cornell University Press, Ithaca.

Erwin, D. H. 2001. Lessons from the past: Biotic recoveries from mass extinctions. PNAS 98:5399–5403.

Fastovsky, D. E. 1987. Paleoenvironments of Vertebrate-Bearing Strata during the Cretaceous-Paleogene Transition, Eastern Montana and Western North Dakota. PALAIOS 2:282–295.

Fastovsky, D. E., and A. Bercovici. 2016. The Hell Creek Formation and its contribution to the Cretaceous-Paleogene extinction: A short primer. Cretaceous Research 57:368–390.

Fastovsky, D. E., and K. McSweeney. 1987. Paleosols spanning the Cretaceous-Paleogene transition, eastern Montana and western North Dakota. Bulletin of the Geological Society of America 99:66–77.

Fastovsky, D. E. and P. M. Sheehan. 2005. The extinction of the dinosaurs in North America. GSA Today 15:4–10.

Feild, T. S., T. J. Brodribb, A. Iglesias, D. S. Chatelet, A. Baresch, G. R. J. Upchurch, B. Gomez, B. A. R. R. Mohr, C. Coiffard, J. Kvacek, and C. Jaramillo. 2011. Fossil evidence for Cretaceous escalation in angiosperm leaf vein evolution. PNAS 108:8363–8366.

Field, D. J., A. Bercovici, J. S. Berv, R. E. Dunn, D. E. Fastovsky, T. R. Lyson, V. Vajda, and J. A. Gauthier. 2018. Early evolution of modern birds structured by global forest collapse at the end-Cretaceous mass extinction. Current Biology:1–7.

Flight, J. N. 2004. Sequence stratigraphic analysis of the Fox Hills and Hell Creek Formations (Maastrichtian), eastern Montana and its relationship to dinosaur paleontology. Unpublished Master Thesis - Montana State University, Bozeman:164.

Flynn, A., and D. Peppe. 2019. Early Paleocene tropical forest from the Ojo Alamo Sandstone, San Juan Basin, New Mexico, USA. Paleobiology 45:612–635.

Foote, M. 1991. Morphological and taxonomic diversity in clade's history: The blastoid record and stochastic simulations. Contributions From the Museum of Paleontology 28:101–140.

Foote, M. 1992. Rarefaction Analysis of Morphological and Taxonomic Diversity. Paleobiology 18:1–16.

Foote, M. 1993: Discordance and Concordance Between Morphological and Taxonomic Diversity. Paleobiology 19:185–204.

Foote, M. 1994: Morphological Disparity in Ordovician-Devonian Crinoids and the Early Saturation of Morphological Space. Paleobiology 20:320–344.

Foote, M. 2000. Origination and extinction components of taxonomic diversity: General problems. Paleobiology 26:74–102.

Fowler, D. 2020. The Hell Creek Formation, Montana: A Stratigraphic Review and Revision Based on a Sequence Stratigraphic Approach. Geosciences 10.

Gerber, S. 2019. Use and misuse of discrete character data for morphospace and disparity analyses. Palaeontology 62:305–319.

Gotelli, N. J., and R. K. Colwell. 2001. Quantifying biodiversity: procedures and pitfalls in the measurement and comparison of species richness. Ecology Letters 4:379–391.

Gould, S. J. 1985. The Paradox of the First Tier: An Agenda for Paleobiology. Paleobiology 11:2–12.

Gower, J. C. 1971. A general coefficient of similarity and some of its properties. Biometrics 27:857–874.

Graham, H. V, F. Herrera, C. Jaramillo, S. L. Wing, K. H. Freeman, and N. Goddard. 2019. Canopy structure in Late Cretaceous and Paleocene forests as reconstructed from carbon isotope analyses of fossil leaves. Geology 47:977–981.

Green, W. A., and L. J. Hickey. 2005. Leaf architectural profiles of angiosperm floras across the Cretaceous/Tertiary boundary. American Journal of Science 305:983–1013.

Green, W. A., G. Hunt, S. L. Wing, and W. A. Dimichele. 2011. Does extinction wield an axe or pruning shears? How interactions between phylogeny and ecology affect patterns of extinction. Paleobiology 37:72–91.

Grossnickle, D. M., S. M. Smith, and G. P. Wilson. 2019. Untangling the Multiple Ecological Radiations of Early Mammals. Trends in Ecology & Evolution 11:1–14.

Guillerme, T. 2018. dispRity. A modular R package for measuring disparity. Methods in Ecology and Evolution 9:1755–1763.

Guillerme, T., M. N. Puttick, A. E. Marcy, and V. Weisbecker. 2020. Shifting spaces: Which disparity or dissimilarity measurement best summarize occupancy in multidimensional spaces? Ecology and Evolution 10:7261–7275.

Guo, S. X., Z. Sun, H. Li, and Y. Dou. 1984. Palaeocene flora from Altai in Xinjiang, Northwest China. Bull. Nanjing Inst. Geo. Palaeont., Academia Sinica 8:119–146.

Guo, S. X., Z. Kvaček, S. R. Manchester, and Z. K. Zhou. 2012. *Ditaxocladus* (extinct Cupressaceae, cupressoideae) from the Upper Cretaceous and Paleocene of the Northern Hemisphere. Palaeontographica Abteilung B 288:135-159.

Hammer, O., D. Harper, and P. Ryan. 2001. PAST: Paleontological Statistics Software Package for education and data analysis. Palaeontologia Electronica 4:1–9.

Hartman, J. H., R. D. Butler, M. W. Weiler, and K. K. Schumaker. 2014. Context, naming, and formal designation of the Cretaceous Hell Creek Formation lectostratotype, Garfield County, Montana. Geological Society of America Special Paper 503:89–121.

Heer, O. 1855. Flora tertiaria helvetiae (J. Wurster, Ed.). v. 1.

Heer, O. 1868. K. svenska vet.-akad Ütvers. Führ, v. 25.

Heer, O. 1878. Miocene Flora der Insel Sachalin. Mémoires de L'Acadadémie Impériale des Sciences de St.-Petersbourg *in* Die fossile Flora der Polarländer: 1–61.

Heim, N. A., and S. E. Peters. 2011. Regional Environmental Breadth Predicts Geographic Range and Longevity in Fossil Marine Genera. PLoS ONE 6.

Hickey, L. J. 1977. Stratigraphy and Paleobotany of the Golden Valley Formation (Early Tertiary) of Western North Dakota. Washington, D.C., The Geological Society of America.

Hickey, L. J. 1980. Paleocene stratigraphy and flora of the Clark's Fork Basin. Pp. 33–49 *in* P. D. Gingerich, ed. Early Cenozoic paleontology and stratigraphy of the Bighorn Basin, Wyoming: 1880–1980. University of Michigan Papers on Paleontology 24.

Hickey, L. J. 2001. On the Nomenclatural Status of the Morphogenera, *Quereuxia* and *Trapago*. Taxon 50:1119–1124.

Hickey, L. J., and J. A. Doyle. 1977. Early Cretaceous Fossil Evidence for Angiosperm Evolution. Botanical Review 43:2–104.

Hicks, J. F., K. R. Johnson, J. D. Obradovich, L. Tauxe, and D. Clark. 2002. Magnetostratigraphy and geochronology of the Hell Creek and basal Fort Union Formations of southwestern North Dakota and a recalibration of the age of the Cretaceous-Tertiary boundary. Geological Society of America Special Paper 361:35–55.

Hill, M. O., and H. G. Gauch. 1980. Detrended Correspondence Analysis: An Improved Ordination Technique. Classification and Ordination:47–58.

Hollick, C. A. 1936. The tertiary floras of Alaska. US Government Printing Office.

Hotton, C. L. 1988. Palynology of the Cretaceous-Tertiary boundary in central Montana, U.S.A., and its implications for extraterrestrial impact. University of California, Davis, p. 732.

Hotton, C. L. 2002. Palynology of the Cretaceous-Tertiary boundary in central Montana: evidence for extraterrestrial impact as a cause of the terminal Cretaceous extinctions. Geological Society of America Special Paper 361:473–501.

Hsieh, T. C., K. H. Ma, and A. Chao. 2016. iNEXT: an R package for rarefaction and extrapolation of species diversity (Hill numbers). Methods in Ecology and Evolution 7:1451–1456.

Huff, P. M., P. Wilf, and E. J. Azumah. 2003. Digital Future for Paleoclimate Estimation from Fossil Leaves? Preliminary Results. PALAIOS 18:266–274.

Hughes, J. J., J. S. Berv, S. G. B. Chester, E. J. Sargis, and D. J. Field. 2021. Ecological selectivity and the evolution of mammalian substrate preference across the K–Pg boundary. Ecology and Evolution 11:14540–14554.

Iglesias, A., P. Wilf, K. R. Johnson, A. B. Zamuner, N. R. Cúneo, S. D. Matheos, and B. S. Singer. 2007. A Paleocene lowland macroflora from Patagonia reveals significantly greater richness than North American analogs. Geology 35:947–950.

Iglesias, A., P. Wilf, E. Stiles, and R. Wilf. 2021. Patagonia's diverse but homogeneous early Paleocene forests: Angiosperm leaves from the Danian Salamanca and Peñas Coloradas formations, San Jorge Basin, Chubut, Argentina. Palaeontologia Electronica 24:1–88.

Iljinskaja, J. 1974. *Trochodendroides* Berry, *Nordenskioldia* Heer, *Nyssidium* Heer *in* Takhtajan,

A. ed., Magnoliophyta Fossilia U.R.S.S. I. Magnoliaceae-Eucommiaceae. Nauka, Leningrad.

Jablonski, D. 1986. Causes and consequences of mass extinctions: a comparative approach *in* Elliott, D. K. ed., Dynamics of extinction:183–229.

Jablonski, D. 2005. Mass extinctions and macroevolution. Paleobiology 31:192–210.

Jablonski, D. 2008. Extinction and the spatial dynamics of biodiversity. PNAS 105:11528–11535.

Jablonski, D., K. Roy, J. W. Valentine, R. M. Price, and P. S. Anderson. 2003. The Impact of the Pull of the Recent on the History of Marine Diversity. Science 300.

Johnson, K. R. 1989. A high-resolution megafloral biostratigraphy spanning the Cretaceous-Tertiary boundary in the northern Great Plains. Yale University.

Johnson, K. R. 1992. Leaf-fossil evidence for extensive floral extinction at the Cretaceous-Tertiary boundary, North Dakota, USA. Cretaceous Research 13:91–117.

Johnson, K. R. 1996. Description of Seven Common Fossil Leaf Species from the Hell Creek Formation (Upper Cretaceous: Upper Maastrichtian), North Dakota, South Dakota, and Montana. Proceedings of the Denver Museum of Natural History 3.

Johnson, K. R. 2002. Megaflora of the Hell Creek and lower Fort Union Formations in the western Dakotas: Vegetational response to climate change, the Cretaceous-Tertiary boundary event, and rapid marine transgression. Geological Society of America Special Paper 361:329-391.

Johnson, K. R., and B. Ellis. 2002. A Tropical Rainforest in Colorado 1.4 Million Years After the Cretaceous-Tertiary Boundary. Science 296:2379–2383.

Johnson, K. R., and L. J. Hickey. 1990. Megafloral change across the Cretaceous/Tertiary

boundary in the northern Great Plains and Rocky Mountains, U.S.A. Geological Society of America Special Paper 247:433–444.

Johnson, K. R., D. J. Nichols, M. J. Attrep, and C. J. Orth. 1989. High-resolution leaf-fossil record spanning the Cretaceous/Tertiary boundary. Nature 340:708–711.

Johnson, K. R., D. J. Nichols, and J. H. Hartman. 2002. Hell Creek Formation: A 2001 synthesis. Geological Society of America Special Paper 361:503–510.

Johnson, K. R., M. L. Reynolds, K. W. Werth, and J. R. Thomasson. 2003. Overview of the Late Cretaceous, early Paleocene, and early Eocene megafloras of the Denver Basin, Colorado. Rocky Mountain Geology 38:101–120.

Kaiho, K., N. Oshima, K. Adachi, Y. Adachi, T. Mizukami, M. Fujibayashi, and R. Saito. 2016. Global climate change driven by soot at the K-Pg boundary as the cause of the mass extinction. Scientific Reports 6:1–13.

Keller, G., A. Sahni, and S. Bajpai. 2009. Deccan volcanism, the KT mass extinction and dinosaurs. Journal of Biosciences 34:709–728.

Keller, G., T. Adatte, A. Pardo, S. Bajpai, A. Khosla, B. Samant, P. Schulte, L. Alegret, I. Arenillas, J. A. Arz, P. J. Barton, P. R. Bown, T. J. Bralower, G. L. Christeson, P. Claeys, C. S. Cockell, G. S. Collins, A. Deutsch, T. J. Goldin, K. Goto, J. M. Grajales-nishimura, R. A. F. Grieve, S. P. S. Gulick, K. R. Johnson, and W. Kiessling. 2010. Cretaceous Extinctions: Evidence Overlooked. Science 328:974–976.

Kennedy, E. M. 2003. Late Cretaceous and Paleocene terrestrial climates of New Zealand: Leaf fossil evidence from South Island assemblages. New Zealand Journal of Geology and Geophysics 46:295–306.

Knowlton, F. H. 1917. Fossil floras of the Vermejo and Raton formations of Colorado and New

Mexico.

Knowlton, F. H. 1930. The flora of the Denver and associated formations of Colorado. US Government Printing Office.

Kocsis, Á. T., C. J. Reddin, J. Alroy, and W. Kiessling. 2019. The R package divDyn for quantifying diversity dynamics using fossil sampling data. Methods in Ecology and Evolution 10:735–743.

Kovach, W. L. 1989. Comparisons of multivariate analytical techniques for use in pre-Quaternary plant paleoecology. Review of Palaeobotany and Palynology 60:255–282.

Kowalczyk, J. B., D. L. Royer, I. M. Miller, C. W. Anderson, and D. J. Beerling. 2018. Multiple Proxy Estimates of Atmospheric CO_2 From an Early Paleocene Rainforest. Paleoceanography and Paleoclimatology:1427–1438.

Krassilov, V. A. 1979. The Cretaceous floras of Sakhalin. Nauka, Moscow:183.

Krug, A. Z., D. Jablonski, and J. W. Valentine. 2009. Signature of the End-Cretaceous Mass Extinction in the Modern Biota. Science 323:771.

Kryshtofovich, A. N. 1953. Some enigmatic plants of the Cretaceous flora and their phylogenetic significance, *in* Paleontologiya i stratigrafiya. Moscow, State Publishing House for Geological Literature:17–37.

Labandeira, C. C., K. R. Johnson, and P. Lang. 2002. Preliminary assessment of insect herbivory across the Cretaceous-Tertiary boundary: Major extinction and minimum rebound. Geological Society of America Special Paper 361:297–327.

LeCain, R., W. C. Clyde, G. P. Wilson, and J. Riedel. 2014. Magnetostratigraphy of the Hell Creek and lower Fort Union Formations in northeastern Montana. Geological Society of America Special Paper 503:137–147.

Lee, H., and H. Li. 1959. *Trapa? microphylla* Lesq., the first occurrence from the upper Cretaceous formation of China. Acta Palaeontologica Sinica 7:33–40.

Lesquereux, L. 1876. On the Tertiary flora of the North American Lignitic, considered as evidence of the age of the formation., *in* Hayden, F.V. ed., U.S. Geological and Geographical Survey of the Territories, embracing Colorado and parts of adjacent territories; being a report of the exploration for the year 1874. Annual Report of U.S. Geological Survey of the Territories:275–315.

Lesquereux, L. 1878. The fossil flora of the Western Territories, *in* U.S. Geological Survey of the Territories.

Lesquereux, L. 1883. Contributions to the flora of the Western Territories III. The Cretaceous and Tertiary floras. US Government Printing Office.

Li, L., and G. Keller. 1998. Abrupt deep-sea warming at the end of the Cretaceous. Geology 26:995–998.

Little, S. A., S. W. Kembel, and P. Wilf. 2010: Paleotemperature proxies from leaf fossils reinterpreted in light of evolutionary history. PLoS ONE 5:1–8.

Liu, Y., C. Li, and Y. Wang. 1999. Studies on fossil Metasequoia fiom north-east China and their taxonomic implications. Botanical Journal of the Linnean Society 130:267–297.

Lloyd, G. T. 2016. Estimating morphological diversity and tempo with discrete character-taxon matrices: Implementation, challenges, progress, and future directions. Biological Journal of the Linnean Society 118:131–151.

Lofgren, D. L. 1995. The Bug Creek Problem and the Cretaceous-Tertiary Transition at McGuire Creek, Montana. University of California Publications in Geological Sciences, p. 185.

Longrich, N. R., T. Tokaryk, and D. J. Field. 2011. Mass extinction of birds at the Cretaceous-Paleogene (K-Pg) boundary. PNAS 108:15253–15257.

Longrich, N. R., B. A. S. Bhullar, and J. A. Gauthier. 2012. Mass extinction of lizards and snakes at the Cretaceous-Paleogene boundary. PNAS 109:21396–21401.

Longrich, N. R., J. Scriberas, and M. A. Wills. 2016. Severe extinction and rapid recovery of mammals across the Cretaceous–Palaeogene boundary, and the effects of rarity on patterns of extinction and recovery. Journal of Evolutionary Biology 29:1495–1512.

Lusk, C. H., I. Wright, and P. B. Reich. 2003. Photosynthetic differences contribute to competitive advantage of evergreen angiosperm trees over evergreen conifers in productive habitats. New Phytologist 160:329–336.

Lyson, T. R., I. M. Miller, A. D. Bercovici, K. Weissenburger, A. J. Fuentes, W. C. Clyde, J. W. Hagadorn, M. J. Butrim, K. R. Johnson, R. F. Fleming, R. S. Barclay, S. A. Maccracken, B. Lloyd, G. P. Wilson, D. W. Krause, and S. G. B. Chester. 2019. Exceptional continental record of biotic recovery after the Cretaceous-Paleogene mass extinction. Science 1:1–13.

MacLeod, N., P. F. Rawson, P. L. Forey, F. T. Banner, M. K. Boudagher-Fadel, P. R. Bown, J. A. Burnett, P. Chambers, S. Culver, S. E. Evans, C. Jeffery, M. A. Kaminski, A. R. Lord, A. C. Milner, A. R. Milner, N. Morris, E. Owen, B. R. Rosen, A. B. Smith, P. D. Taylor, E. Urquhart, and J. R. Young. 1997. The Cretaceous – Tertiary biotic transition. Journal of the Geological Society 154:265–292.

Maechler M., P. Rousseeuw, A. Struyf, M. Hubert, K. Hornik. 2021. cluster: Cluster Analysis Basics and Extensions. R package version 2.1.

Mantel, N. 1967. The detection of disease clustering and a generalized regression approach. Cancer Research 27:209–220.

McCune, B., J. B. Grace, and D. L. Urban. 2002. Analysis of ecological communities. Gleneden Beach, OR, MjM software design.

McElwain, J. C., and S. W. Punyasena. 2007. Mass extinction events and the plant fossil record. Trends in Ecology and Evolution 22:548–557.

McGhee, G. R., P. M. Sheehan, D. J. Bottjer, and M. L. Droser. 2004. Ecological ranking of Phanerozoic biodiversity crises: Ecological and taxonomic severities are decoupled. Palaeogeography, Palaeoclimatology, Palaeoecology 211:289–297.

McGhee, G. R., M. E. Clapham, P. M. Sheehan, D. J. Bottjer, and M. L. Droser. 2013. A new ecological-severity ranking of major Phanerozoic biodiversity crises. Palaeogeography, Palaeoclimatology, Palaeoecology 370:260–270.

McIver, E. E., and J. F. Basinger. 1990. Fossil seed cones of *Fokienia* (Cupressaceae) from the Paleocene Ravenscrag Formation of Saskatchewan, Canada. Canadian Journal of Botany. 8:1609–1618.

McKnight, P. E. and J. Najab. 2010. Mann-Whitney U Test. Corsini Encyclopedia of Psychology.

Melo, A. S., R. A. S. Pereira, A. J. Santos, G. J. Shepherd, G. Machado, H. F. Medeiros, R. J. Sawaya. 2003. Comparing species richness among assemblages using sample units: why not use extrapolation methods to standardize different sample sizes? OIKOS 101:398–410.

Minchin, P. R. 1987. An evaluation of the relative robustness of techniques for ecological ordination. Theory and models in vegetation science. Springer, Dordrecht. 89-107.

Mitchell, J. S., P. D. Roopnarine, and K. D. Angielczyk. 2012. Late Cretaceous restructuring of terrestrial communities facilitated the end-Cretaceous mass extinction in North America. PNAS 109:18857–18861.

Moore, J. R., G. P. Wilson, M. Sharma, H. R. Hallock, D. R. Braman, and P. R. Renne. 2014. Assessing the relationships of the Hell Creek-Fort Union contact, Cretaceous-Paleogene boundary, and Chicxulub impact ejecta horizon at the Hell Creek Formation lectostratotype, Montana, USA. Geological Society of America Special Paper 503:123–135.

Murphy, E. C., J. W. Hoganson, and K. R. Johnson. 2002. Lithostratigraphy of the Hell Creek Formation in North Dakota. Geological Society of America Special Paper 361:9–34.

Newberry, J. S. 1861. Fossil plants, *in* Report upon the Colorado River of the West, explored in 1857 and 1858 by Lieutenant Joseph C. Ives. Washington:129–132.

Newberry, J. S. 1863. Descriptions of the Fossil Plants Collected by Mr. George Gibbs: Geologist to the United States Northwest Boundary Commission, Under Mr. Archibald Campbell, United States Commissioner. Boston Journal of Natural History 7:506–525.

Newberry, J. S. 1898. The Later Extinct Floras of North America. US Geological Survey Monograph.

Nichols, D. J., and K. R. Johnson. 2002. Palynology and microstratigraphy of Cretaceous-Tertiary boundary sections in southwestern North Dakota. Geological Society of America Special Paper 361:95–143.

Nichols, D. J., and K. R. Johnson. 2008. Plants and the KT Boundary. Cambridge University Press.

Norris, R. D. 2001. Impact of K-T Boundary Events on Marine Life, *in* Briggs, D. and Crowther,

P. eds., Palaeobiology II:229–231.

Okansen, J., F. G. Blanchet, M. Friendly, R. Kindt, P. Legendre, D. McGlinn, P. R. Minchin, R. B. O'Hara, G. L. Simpson, P. Solymos, M. H. H. Stevens, E. Szoecs, and H. Wagner. 2019. vegan: Community Ecology Package. R package version 2.5-6.

Payne, J. L., and S. Finnegan. 2007. The effect of geographic range on extinction risk during background and mass extinction. PNAS 104:10506–10511.

Peppe, D. 2003. Fox Hills I , a new Upper Maastrichtian megafloral zone within the Williston Basin of North Dakota. St. Lawrence University.

Peppe, D. J. 2010. Megafloral change in the early and middle Paleocene in the Williston Basin, North Dakota, USA. Palaeogeography, Palaeoclimatology, Palaeoecology 298:224–234.

Peppe, D. J., J. M. Erickson, and L. J. Hickey. 2007. Fossil Leaf Species from the Fox Hills Formation (Upper Cretaceous: North Dakota, USA) and Their Paleogeographic Significance. Journal of Paleontology 81:550–567.

Peppe, D. J., K. R. Johnson, and D. A. D. Evans. 2011a. Magnetostratigraphy of the Lebo and Tongue River members of the Fort Union Formation (Paleocene) in the northeastern Powder River Basin, Montana. American Journal of Science 311:813–850.

Peppe, D. J., D. L. Royer, B. Cariglino, S. Y. Oliver, S. Newman, E. Leight, G. Enikolopov, M. Fernandez-Burgos, F. Herrera, J. M. Adams, E. Correa, E. D. Currano, J. M. Erickson, L. F. Hinojosa, J. W. Hoganson, A. Iglesias, C. A. Jaramillo, K. R. Johnson, G. J. Jordan, N. J. B. Kraft, E. C. Lovelock, C. H. Lusk, Ü. Niinemets, J. Peñuelas, G. Rapson, S. L. Wing, and I. J. Wright. 2011b. Sensitivity of leaf size and shape to climate: Global patterns and paleoclimatic applications. New Phytologist 190:724–739.

Peppe, D. J., A. Baumgartner, A. Flynn, and B. Blonder. 2018. Reconstructing paleoclimate and paleoecology using fossil leaves. *in* D. A. Croft, D. F. Su, and S. W. Simpson, eds. Methods in Paleoecology. Springer International Publishing.

Petchey, O. L., and K. J. Gaston. 2006. Functional diversity: Back to basics and looking forward. Ecology Letters 9:741–758.

Petersen, S. V, A. Dutton, and K. C. Lohmann. 2016. End-Cretaceous extinction in Antarctica linked to both Deccan volcanism and meteorite impact via climate change. Nature Communications 7:12079.

Pielou, E. C. 1966. The measurement of diversity in different types of biological collections. Journal of Theoretical Biology 13:131–144.

Pimiento, C., C. D. Bacon, D. Silvestro, A. Hendy, C. Jaramillo, A. Zizka, X. Meyer, and A. Antonelli. 2020. Selective extinction against redundant species buffers functional diversity: Redundancy buffers functional diversity. Proceedings of the Royal Society B: Biological Sciences 287.

R Core Team. 2021. R: A Language and environment for statistical computing. R Foundation for Statistical Computing, Vienna, Austria. https://www.R-project.org/.

Raines, G. L. and B. R. Johnson. 1995: Digital representation of the Montana stage geologic map: a contribution to the Interior Columbia River Basin Ecosystem Management Project. U.S. Geological Survey Open-File Report 95-691. http://pubs.usgs.gov/.

Rasband, W. S. 1997. ImageJ, U. S. National Institutes of Health, Bethesda, Maryland, USA, https://imagej.nih.gov/ij/.

Raunkiær, C. 1934. The life forms of plants and statistical plant geography. The Clarendon Press, Oxford.

Raup, D. M., and J. J. Sepkoski. 1982. Mass Extinctions in the Fossil Record. Science 215:1501–1503.

Reich, P. B. 2014. The world-wide "fast-slow" plant economics spectrum: A traits manifesto. Journal of Ecology 102:275–301.

Reich, P. B., M. B. Walters, and D. S. Ellsworth. 1997. From tropics to tundra: Global convergence in plant functioning. PNAS 94:13730–13734.

Renne, P. R., A. L. Deino, F. J. Hilgen, K. F. Kuiper, D. F. Mark, W. S. Mitchell, L. E. Morgan, R. Mundil, and J. Smit. 2013. Time scales of critical events around the Cretaceous-Paleogene boundary. Science 339:684–687.

Retallack, G. J. 1994. A pedotype approach to latest Cretaceous and earliest Tertiary paleosols in eastern Montana. Bulletin of the Geological Society of America 106:1377–1397.

Reyment, R. 1963. Multivariate Analytical Treatment of Quantitative Species Associations: An Example from Paleoecology. Journal of Animal Ecology 32:535–547.

Rigby, J. K., and K. J. J. Rigby. 1990. Geology of the Sand Arroyo and Bug Creek Quadrangles, McCone County, Montana. Brigham Young University Geology Studies 36:69–134.

Robertson, D. S., M. C. McKenna, O. B. Toon, S. Hope, and J. A. Lillegraven. 2004. Survival in the first hours of the Cenozoic. Bulletin of the Geological Society of America 116:760–768.

Robertson, D. S., W. M. Lewis, P. M. Sheehan, and O. B. Toon. 2013. K-Pg extinction: Reevaluation of the heat-fire hypothesis. Journal of Geophysical Research: Biogeosciences 118:329–336.

Rose, P. J., D. L. Fox, J. Marcot, and C. Badgley. 2011. Flat latitudinal gradient in Paleocene mammal richness suggests decoupling of climate and biodiversity. Geology 39:163–166.

Rothwell, G. W., and R. A. Stockey. 1994. The role of *Hydropteris pinnata* gen. et. sp. nov. in

reconstructing the cladistics of heterosporous ferns. American Journal of Botany 81:479–492.

Roy, K., and M. Foote. 1997. Morphological approaches to measuring biodiversity. Trends in Ecology and Evolution 12:227–281.

Royer, D. L. 2012. Climate Reconstruction from Leaf Size and Shape: New Developments and Challenges. The Paleontological Society Papers 18:195–212.

Royer, D. L., P. Wilf, D. L. Janesko, E. A. Kowalski, and D. L. Dilcher. 2005. Correlations of Climate and Plant Ecology to Leaf Size and Shape: Potential Proxies for the Fossil Record. American Journal of Botany 92:1141–1151.

Royer, D. L., L. Sack, P. Wilf, C. H. Lusk, J. J. Gregory, Ü. Niinemets, I. J. Wright, M. Westoby, B. Cariglino, P. D. Coley, A. D. Cutter, K. R. Johnson, C. C. Labandeira, A. T. Moles, B. Matthew, and F. Valladares. 2007. Fossil Leaf Economics Quantified: Calibration, Eocene Case Study, and Implications. Paleobiology 33:574–589.

Royer, D. L., I. M. Miller, D. J. Peppe, and L. J. Hickey. 2010. Leaf economic traits from fossils support a weedy habit for early angiosperms. American Journal of Botany 97:438–445.

Samylina, V. A. 1988. The Arkagala stratoflora of northeastern Asia.

Scholz, H., and J. H. Hartman. 2007. Paleoenvironmental Reconstruction of the Upper Cretaceous Hell Creek Formation of the Williston Basin, Montana, USA. Implications From the Quantitative Analysis of Unionoid Bivalve Taxonomic Diversity and Morphologic Disparity: PALAIOS 22:24–34.

Schulte, P., L. Alegret, I. Arenillas, J. A. Arz, P. J. Barton, P. R. Bown, T. J. Bralower, G. L. Christeson, P. Claeys, C. S. Cockell, G. S. Collins, A. Deutsch, T. J. Goldin, K. Goto, J. M. Grajales-Nishimura, R. A. F. Grieve, S. P. S. Gulick, K. R. Johnson, W. Kiessling, C.

Koeberl, D. A. Kring, K. G. MacLeod, T. Matsui, J. Melosh, A. Montanari, J. V. Morgan, C. R. Neal, D. J. Nichols, R. D. Norris, E. Pierazzo, G. Ravizza, M. Rebolledo-Vieyra, W. U. Reimold, E. Robin, T. Salge, R. P. Speijer, A.R. Sweet, J. Urrutia-Fucugauchi, V. Vajda, M. T. Whalen, and P. S. Willumsen. 2010. The Chicxulub Asteroid Impact and Mass Extinction at the Cretaceous-Paleogene Boundary. Science 327:1214–1218.

Self, S., A. Schmidt, and T. A. Mather. 2014. Emplacement characteristics, time scales, and volcanic gas release rates of continental flood basalt eruptions on Earth. Geological Society of America Special Paper 505:319–337.

Sepkoski, J. J. 1996: Patterns of Phanerozoic Extinction: A Perspective from Global Data Bases. *in* O. H. Walliser, ed. Springer-Verlag, Berlin Heidelberg.

Seward, A. C. 1963. Fossil Plants: A Text-book for Students of Botany and Geology, Volume IV. New York, NY, Hafner Publishing Company.

Seward, A. C., and V. M. Conway. 1935. Additional Cretaceous plants from western Greenland. Alexander Doweld.

Sheehan, P. M., D. E. Fastovsky, R. G. Hoffmann, C. B. Berghaus, and D. L. Gabrielt. 1991. Sudden Extinction of the Dinosaurs: Latest Cretaceous, Upper Great Plains, U.S.A. Science 254:835–839.

Shoemaker, R. E. 1966. Fossil Leaves of the Hell Creek and Tullock Formations of Eastern Montana. Palaeontographica Abteilung B 119:54–75.

Siegel, A. F., and R. Z. German. 1982. Rarefaction and Taxonomic Diversity. Biometrics 38:235–241.

Simpson, E. H. 1949. Measurement of diversity. Nature 163:688.

Slattery, J. S., W. A. Cobban, K. C. McKinney, P. J. Harries, and A. L. Sandness. 2015. Early Cretaceous to Paleocene Paleogeography of the Western Interior Seaway: The Interaction of Eustasy and Tectonism. Wyoming Geological Association Guidebook:22–60.

Smit, J., and S. Van Der Kaars. 1984. Terminal Cretaceous extinctions in the Hell Creek area, Montana: compatible with catastrophic extinction. Science 223:1177–1179.

Smith, R. Y., J. F. Basinger, and D. R. Greenwood. 2012. Early Eocene plant diversity and dynamics in the Falkland flora, Okanagan Highlands, British Columbia, Canada. Palaeobiodiversity and Palaeoenvironments 92:309–328.

Smith, S. M., C. J. Sprain, W. A. Clemens, D. L. Lofgren, P. R. Renne, and G. P. Wilson. 2018. Early mammalian recovery after the end-Cretaceous mass extinction: A high-resolution view from McGuire Creek area, Montana, USA. Bulletin of the Geological Society of America 130:2000–2014.

Spicer, R. A., and M. E. Collinson. 2014. Plants and floral change at the Cretaceous-Paleogene boundary: Three decades on. Special Paper of the Geological Society of America 505:117–132.

Sprain, C. J., P. R. Renne, G. P. Wilson, and W. A. Clemens. 2015. High-resolution chronostratigraphy of the terrestrial Cretaceous-Paleogene transition and recovery interval in the Hell Creek region, Montana. Bulletin of the Geological Society of America 127:393–409.

Sprain, C. J., P. R. Renne, W. A. Clemens, and G. P. Wilson. 2018. Calibration of chron C29r: New high-precision geochronologic and paleomagnetic constraints from the Hell Creek region, Montana. Bulletin of the Geological Society of America:1–30.

Stiles, E., P. Wilf, A. Iglesias, M. A. Gandolfo, and N. R. Cuneo. 2020. Cretaceous-Paleogene plant extinction and recovery in Patagonia. Paleobiology 46:445–469.

Stockey, R. A., and G. W. Rothwell. 1997. The Aquatic Angiosperm *Trapago angulata* from the Upper Cretaceous (Maastrichtian) St. Mary River Formation of Southern Alberta. International Journal of Plant Sciences 158:83–94.

Stockey, R. A., G. W. Rothwell, and K. R. Johnson. 2007. *Cobbania corrugata* gen. et comb. nov. (Araceae): A floating aquatic monocot from the upper cretaceous of western North America. American Journal of Botany 94:609–624.

Strauss, D., and P. M. Sadler. 1989. Classical confidence intervals and Bayesian probability estimates for ends of local taxon ranges. Mathematical Geology 21:411–427.

Swisher, C. C., L. Dingus, and R. F. Butler. 1993. 40Ar/39Ar dating and magnetostratigraphic correlation of the terrestrial Cretaceous-Paleogene boundary and Puercan Mammal Age, Hell Creek -- Tullock formations, eastern Montana. Canadian Journal of Earth Sciences 30:1981–1996.

Tabor, C. R., C. G. Bardeen, B. L. Otto-Bliesner, R. R. Garcia, and O. B. Toon. 2020. Causes and Climatic Consequences of the Impact Winter at the Cretaceous-Paleogene Boundary. Geophysical Research Letters 47.

Tanai, T., 1970. The Oligocene floras from the Kushiro coal field, Hokkaido, Japan. Journal of the Faculty of Science, Hokkaido University. Series 4, Geology and mineralogy= **北海道大學理學部紀要** 14:383–514.

The GIMP Development Team. 2019. *GIMP*. https://www.gimp.org.

Tobin, T. S., G. P. Wilson, J. M. Eiler, and J. H. Hartman. 2014. Environmental change across a terrestrial Cretaceous-Paleogene boundary section in eastern Montana, USA, constrained by carbonate clumped isotope paleothermometry. Geology 42:351–354.

Tobin, T. S., J. W. Honeck, I. M. Fendley, L. N. Weaver, C. J. Sprain, M. L. Tuite, D. T. Flannery, W. W. Mans, and G. P. Wilson Mantilla. 2021. Analyzing sources of uncertainty in terrestrial organic carbon isotope data: A case study across the K-Pg boundary in Montana, USA. Palaeogeography, Palaeoclimatology, Palaeoecology 574:110451.

Tschudy, R. H., and B. D. Tschudy. 1986. Extinction and survival of plant life following the Cretaceous/Tertiary boundary event, Western Interior, North America. Geology 14:667–670.

Tschudy, R. H., C. L. Pillmore, C. J. Orth, J. S. Gilmore, and J. D. Knight. 1984. Disruption of the Terrestrial Plant Ecosystem at the Cretaceous-Tertiary Boundary: Western Interior. Science 225:1030–1032.

Unger, F. 1850. Genera et species plantarum fossilium, W. Barumuller, Ed. Vienna, 627 p.

Vajda, V., and A. Bercovici. 2014. The global vegetation pattern across the Cretaceous-Paleogene mass extinction interval: A template for other extinction events. Global and Planetary Change 122:29–49.

Vellekoop, J., A. Sluijs, J. Smit, S. Schouten, J. W. H. Weijers, J. S. Sinninghe Damsté, and H. Brinkhuis. 2014. Rapid short-term cooling following the Chicxulub impact at the Cretaceous-Paleogene boundary. PNAS 111:7537–7541.

Verdu, M. 2002. Age at maturity and diversification in woody angiosperms. Evolution 56:1352–1361.

Vermillion, W. A., P. D. Polly, J. J. Head, J. T. Eronen, and A. M. Lawing. 2018. Ecometrics: A trait-based approach to paleoclimate and paleoenvironmental reconstruction. Vertebrate Paleobiology and Paleoanthropology:373–394.

Vilhena, D. A., E. B. Harris, C. T. Bergstrom, M. E. Maliska, P. D. Ward, C. A. Sidor, C. A. E. Strömberg, and G. P. Wilson. 2013. Bivalve network reveals latitudinal selectivity gradient at the end-Cretaceous mass extinction. Scientific Reports 3:1790.

Weaver, L. N., Thomas, T. S., Claytor, J.R., Wilson Deibel, P. K., Clemens, W. A., Wilson Mantilla, G. P. 2022. Revised Stratigraphic Relationships Within the Lower Fort Union Formation (Tullock Member; Garfield County, Montana, U.S.A.) Provide a New Framework for Examining Post K-Pg Mammalian Recovery Dynamics. In revision Palaois.

Webb, L. J. 1959. A physiognomic classification of Australian rain forests. Journal of Ecology 47:551–570.

Whittaker, R. H. 1975. Classification of Natural Communities. Botanical Review 28.1:1-239.

Wilf, P. 1998. Using Fossil Plants to Understand Global Change: Evidence for Paleocene-Eocene Warming in the Greater Green River Basin of Southwestern Wyoming. University of Pennsylvania.

Wilf, P., and K. R. Johnson. 2004. Land plant extinction at the end of the Cretaceous: a quantitative analysis of the North Dakota megafloral record. Paleobiology 30:347–368.

Wilf, P., K. R. Johnson, and B. T. Huber. 2003. Correlated terrestrial and marine evidence for global climate changes before mass extinction at the Cretaceous-Paleogene boundary. PNAS 100:599–604.

Wilf, P., C. C. Labandeira, K. R. Johnson, and B. Ellis. 2006. Decoupled Plant and Insect Diversity After the End-Cretaceous Extinction. Science 313:1112–1116.

Wilson, G. P. 2005. Mammalian faunal dynamics during the last 1.8 million years of the Cretaceous in Garfield County, Montana. Journal of Mammalian Evolution 12:53–76.

Wilson, G. P. 2013. Mammals across the K/Pg boundary in northeastern Montana, U.S.A.: dental morphology and body-size patterns reveal extinction selectivity and immigrant-fueled ecospace filling. Paleobiology 39:429–469.

Wilson, G. P. 2014. Mammalian extinction, survival, and recovery dynamics across the Cretaceous-Paleogene boundary in northeastern Montana, USA. Geological Society of America Special Paper 503:365–392.

Wilson, G. P., W. A. Clemens, J. R. Horner, and J. H. Hartman. 2014. Foreward. Geological Society of America Special Paper 503:29–55.

Wilson Mantilla, G. P., S. G. B. Chester, W. A. Clemens, J. R. Moore, C. J. Sprain, B. T. Hovatter, W. S. Mitchell, W. W. Mans, R. Mundil, and P. R. Renne. 2021. Earliest Palaeocene purgatoriids and the initial radiation of stem primates. Royal Society Open Science 8.

Wilson, P. K., Strömberg, C. A. E., Wilson Mantilla, G. P., 2020. Plant community change across the Cretaceous-Paleogene boundary in northeastern Montana. GSA 2020 Connects Online.

Wilson, P. K., G. P. Wilson Mantilla, and C. A. E. Stromberg. 2021. Seafood Salad: A diverse latest Cretaceous flora from eastern Montana. Cretaceous Research 121.

Wilson Deibel, P. K., G. P. Wilson Mantilla, and C. A. E. Strömberg. *in prep*: Plant taxonomic turnover and diversity across the Cretaceous-Paleogene boundary in northeastern Montana.

Wing, S. L. 2004. Mass extinctions in plant evolution. *in* Extinctions in the History of Life.

Wing, S. L., and L. D. Boucher. 1998. Ecological aspects of the Cretaceous flowering plant radiation. Annual Review of Earth and Planetary Sciences 26:379–421.

Wing, S. L., and B. H. Tiffney. 1987. The reciprocal interaction of angiosperm evolution and tetrapod herbivory. Review of Palaeobotany and Palynology 50:179–210.

Wing, S. L., J. Alroy, and L. J. Hickey. 1995. Plant and mammal diversity in the Paleocene to Early Eocene of the Bighorn Basin. Palaeogeography, Palaeoclimatology, Palaeoecology 115:117–155.

Wing, S. L., C. A. E. Stromberg, L. J. Hickey, F. Tiver, B. Willis, R. J. Burnham, and A. K. Behrensmeyer. 2012. Floral and environmental gradients on a Late Cretaceous landscape. Ecological Monograph 82:23–47.

Wolfe, J. A., 1966. Tertiary plants from the Cook Inlet region, Alaska. US Government Printing Office:1-32.

Wolfe, J. A. 1979. Temperature parameters of humid to mesic forests of eastern Asia and relation to forests of other regions of the Northern Hemisphere. US Geological Survey Professional Paper 1106:1–37.

Wolfe, J. A. 1993. A Method of Obtaining Climatic Parameters from Leaf Assemblages. US Government Printing Office.

Wolfe, J., and G. Upchurch. 1986. Vegetation, climatic and floral changes at the Cretaceous-Tertiary boundary. Nature 324:148–152.

Wolfe, J. A., and G. R. Upchurch. 1987. Leaf Assemblages across the Cretaceous-Tertiary Boundary in the Raton Basin, New Mexico and Colorado. Proceedings of the National Academy of Sciences of the United States of America, v. 84, p. 5096–5100.

Wright, I. J., P. B. Reich, M. Westoby, D. D. Ackerly, Z. Baruch, F. Bongers, J. Cavender-Bares, T. Chapin, J. H. C. Cornellssen, M. Diemer, J. Flexas, E. Garnier, P. K. Groom, J. Gulias, K. Hikosaka, B. B. Lamont, T. Lee, W. Lee, C. Lusk, J. J. Midgley, M. L. Navas, Ü. Niinemets, J. Oleksyn, H. Osada, H. Poorter, P. Pool, L. Prior, V. I. Pyankov, C. Roumet, S. C. Thomas., M. G. Tjoelker, E. J. Veneklaas, and R. Villar. 2004. The worldwide leaf economics spectrum. Nature 428:821–827.

Zhang, Z. 1983. The Upper Cretaceous fossil plants from Jayin Region, Northern Heilongjiang, *in* Professional Paper on Stratigraphy and Palaeontology. vol. II. Beijing, Geological Publishing House:111–132.

Appendices

Chapter 2 SUPPLEMENT: STRATIGRAPHIC DESCRIPTION

The base of the butte exposes a dark gray to purple siltstone unit that is 5-m-thick (Unit 1, Figure 2.S1 A). Unit 2 is a 6.7-m-thick white to tan, very fine, well indurated sandstone that is interrupted by a thin layer of interbedded, very fissile sandstone (2.4 m above the base of the unit) (Unit 2, Figure 2.S1 A). Unit 3 is 1.4-m-thick, fine, yellow to tan sandstone, with a large lithic component (Unit 3, Figure 2.S1 A). Unit 4 consists of purple to green, banded paleosols; each individual bed is tens of centimeters thick (Unit 4, Figure 2.S1 A). At the top of the butte, Unit 5 (shown in detail in Figure 2.S1 B) bears the Seafood Salad I and II fossiliferous horizons, and grades from fine sandstone to claystone.

Seafood Salad II (lower quarry) has a coarser lithology than Seafood Salad I (upper quarry), consisting of a yellow to tan, fissile, very-fine sandstone (Figure 2.S1 B). The plants are preserved as compressions and impressions with preserved third- or fourth- order leaf venation. Much of the plant material from this quarry is highly carbonized, and there is a significant organic component to the sandstone containing the fossils. Seafood Salad I consists of a fine gray, massive, blue siltstone (Figure 2.S1 B). Plants are preserved mostly as compression fossils and represent a diversity of plant taxa. Because of the close vertical proximity (0.75 m) we interpret Seafood Salad I and Seafood Salad II as contemporaneous or penecontemporaneous. For the purposes of the description and analyses, we combine data from both quarries (see Section 2.5.1).

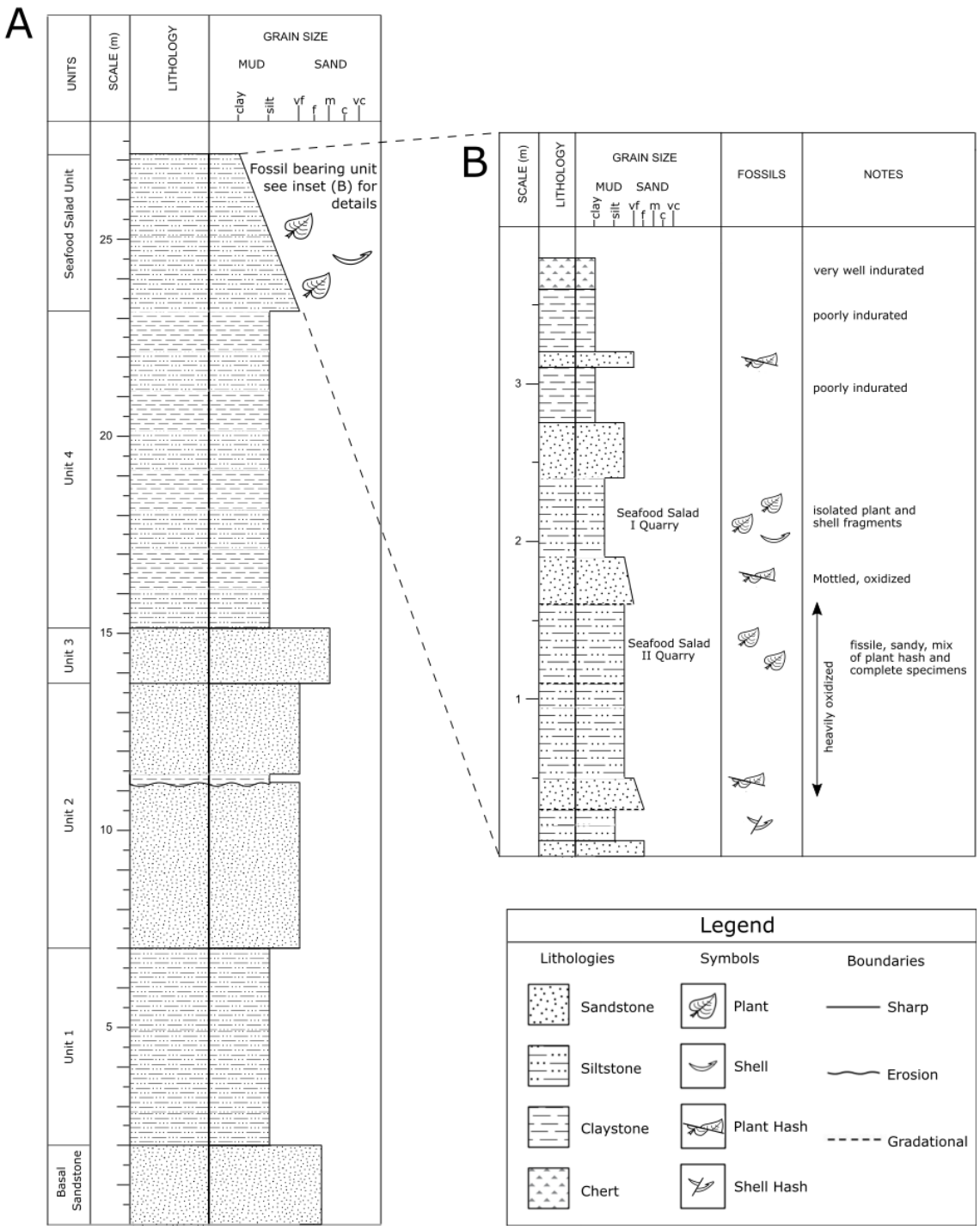

Figure 2.S1: Stratigraphic column of Seafood Salad locality showing relative positions of Seafood Salad I and II quarries. (A) Stratigraphic column at the outcrop level showing strata of the lowest Hell Creek Formation. The upper ca. 4 m at this outcrop preserved the fossiliferous units exposed at our Seafood Salad I and Seafood Salad II quarries. (B) Stratigraphic column at the quarry level showing details of the upper ca. 4 m of stratigraphy exposed at this butte. Section was measured at the Seafood Salad II quarry and the position of the Seafood Salad I quarry was measured in.

Chapter 3 SUPPLEMENT: SITE DESCRIPTIONS

Seafood Salad I and II

The Seafood Salad (SS) site is located in the Charles M. Russell (CMR) Wildlife Refuge north of the town of Jordan within the Maloney Hill Quadrangle in Garfield County, Montana. The locality was discovered while prospecting in the area. Crews from the University of Washington Burke Museum of Natural History and Culture (UWBM) made collections at the site from 2015-2019. Plant fossils were found at two distinct horizons, SS I (UWBM P6909, P6910, P8543, and P8078) and SS II (UWBM B8198, P8544, P8077). For more detail about this locality please see Wilson et al. (2021).

While no dated marker bed was found in the vicinity of the SS locality, the base of the butte at SS exposes a prominent white sandstone, identified as the basal sandstone unit of the Hell Creek Formation. The SSI quarry was measured at 21.1 m above the top of this unit, while the SSII quarry was measured at 22.4 m above the top of this unit. Based on the average thickness of this unit (5.8 m thick at the Flag Butte lectostratotype section; Hartman et al. 2014) we estimate the locality is 28 m above the Fox Hills-Hell Creek Formational contact. This places SS in the lower third of the Hell Creek Formation.

The base of the butte at SS exposes a dark gray to purple siltstone unit that is 5-m-thick. At the top of this butte, 10.5 m above this siltstone unit, the Seafood Salad I and II fossiliferous horizons outcrop. Seafood Salad II (lower quarry) has a coarser lithology than Seafood Salad I (upper quarry), consisting of a yellow to tan, fissile, very fine-grained sandstone (Fig. 3.S1). The plants are preserved as compressions and impressions with preserved third- or fourth- order leaf venation. Much of the plant material from this quarry is highly carbonized, and there is a significant organic component to the sandstone containing the fossils. Seafood Salad I consists of a fine-grained, gray-blue, massive siltstone (Fig. 3.S1). Plants are preserved mostly as

compression fossils and represent a diversity of plant taxa. Because of the close vertical proximity (0.75 m) we interpret Seafood Salad I and Seafood Salad II as contemporaneous or penecontemporaneous.

We interpret SSI and SSII as distinct facies. SSII most likely preserves a crevasse splay or levee deposit based on the thin bedding of sandstones and siltstones and presence of root traces. SSI most likely preserves a pond deposit based on the fine grain size and unoxidized sediments.

Fossils found at SS are mostly angiosperm leaves, although the most common taxon found at this locality is a conifer (*Metasequoia occidentalis*). This plant material is found preserved among the calcium carbonate shells of invertebrates. Please see Wilson et al. (2021) for a more complete description of the flora.

Fisk I

The Fisk I (F) site is located in the CMR within the Maloney Hill Quadrangle north of the town of Jordan in Garfield County, Montana. Workers from the University of California Museum of Paleontology (UCMP) made collections at the site, presumably discovered while working at the nearby vertebrate mcro-fossil site. Subsequently, crews from the University of Washington Burke Museum of Natural History and Culture (UWBM) re-located the site in 2018 and made collections from the site from 2018-2019 (UWBM P8080 and P8526).

The productive horizon at Fisk I is in a well indurated, light gray siltstone. Quarries were dug into a ledge ca. 23 m above the base of this butte. Multiple productive quarries were found north to south along this ledge. Productivity is relatively continuous along this section of outcrop; towards the south as the butte turns, the outcrop becomes more sandy and less productive. Plants were found across ca. 1.5 m of lithology, most productive towards the base of

this ledge. The Fisk vertebrate micro-site is located approximately 5 m below the plant productive horizon along the same outcrop.

This site is placed in the lower third of the Hell Creek Formation. The contact between the Hell Creek and underlying Fox Hills Formation is visible north of F, in the deep east-west ravine which borders the Fisk I butte to the north. This contact is characterized by a prominent, cliff-forming white sandstone unit overlain by a purple paleosol unit. Measuring from the base of this sandstone to the fossiliferous horizon at F, we estimate this site to be 29 m above the formational contact.

The lithology at the Fisk I outcrop transitions from a very fine-grained sandstone to a dark gray very fine-grained sandstone where some vertebrate microfossils (i.e., fish dermal) were found (Fig. 3.S1). This sandstone gradually transitions to a silty sandstone, with increasing coal and iron oxide lenses up section. Plant fossils are found in a section of ca. 30 cm of stratigraphy above this silty sandstone unit, interspersed with common coal and iron oxide lenses. This fossiliferous horizon is capped by a poorly indurated, very fine-grained sandstone which still includes numerous coal and iron oxide lenses.

The lithology at F is interpreted as likely channel deposit. The sandstone beds are frequently inclined and interspersed with siltstone layers. This facies is interpreted as inclined heterolithic stratification (IHS), a deposit commonly associated with point bars in river channels. In addition, the Fisk I vertebrate micro-site is just stratigraphically below F, and has been interpreted as a channel deposit.

Fossils recovered from Fisk I included numerous angiosperm leaves with venation down to fourth order in some cases, abundant conifers (including common *Metasequoia* cones). In addition, several small (<1 cm diameter) nodules were noted in this horizon.

Smurphy's Guess II

The Smurphy's Guess II (SG) site is located in the Maloney Hill Quadrangle in Garfield County, Montana. Fossil plant material was excavated at the site between 2017 and 2019. Previously, a crew from the UCMP had found this site and collected some few plant fossils. Workers from the UWBM have collected at the site between 2017 and 2019. The relationship between the UCMP and UWBM quarries is unclear. UWBM workers found several additional plant fossil sites in the immediate vicinity, but none were very extensive. Additionally, while some vertebrate fossils have been recovered in the vicinity, no extensive collections have been completed.

The site is located in the upper third of the Hell Creek Formation. A nearby hill located north of the site exposes a coal marking the lithologic contact between the Hell Creek and Fort Union Formations (the so-called lower Z or IrZ coal). This contact is roughly coincident with the Cretaceous-Paleogene (K-Pg) boundary locally. Jacob's staff and hand level as well as Trimble GPS receivers with sub-meter accuracy were used to estimate the stratigraphic distance between this marker bed and the SG quarry. The base of the quarry is 27 m below this contact and the top of the quarry is estimated at 25 m below this contact.

In 2017 we developed two separate quarries at the SG site, designated SG IIa (UWBM P7137) and SG IIb (UWBM P7136), respectively. Fossils were also collected in undifferentiated collections combining both quarries (UWBM P8079). The SG IIa site is 1.3m above the SG IIb site and the rock hosting fossils at this quarry is lighter in color and coarser in grain size. More specifically, SG IIa was dug from a horizon of orange banded sandstone with intermittent siltstone lenses where leaves were concentrated. This quarry also tends to preserve abundant *Dryophyllum* specimens, mostly partial. The SG IIb quarry was dug from a gray, dark siltstone

with abundant leaves preserved as black compressions, overall in a much less oxidized environment. The evenness of leaf species and morphotypes also tends to be higher at this quarry, with a more equal distribution of specimens from several taxa. Overall, floristically, this site tends to preserve abundant angiosperm leaves, mostly partial, and almost no gymnosperms, ferns, or reproductive or woody structures.

A detailed stratigraphic section at the site revealed a sequence of organic-rich sandstones, mostly massive and poorly consolidated, interspersed with more well consolidated organic-poor sandstone units (Fig. 3.S1). This transitions gradually to a darker siltstone unit, possibly hosting the SG IIb quarry, with abundant rip up clasts present in the lower part of this unit. The SG IIa fossil bearing unit is above this over a sharp contact, characterized as an oxidized, well indurated, white to tan sandstone unit with lenses of mudstone. Leaf fossils are found within ca. 10cm of this unit, usually in the mudstone lenses or rip ups, and are often contorted or not flat lying. The unit tends to fracture in irregular blocks, so most fossil leaves are partial. Above this fossiliferous unit the lithology gradually becomes rich in organic matter and less oxidized again before being capped by a dark brown, fissile, sandy siltstone unit. These units dip generally to the south at a shallow angle.

The lithology of this site is interpreted as preserving a river channel point bar or IHS (inclined heterolithic stratification). This interpretation is based on the coarse lithology, high oxidation, and chaotic rip up clasts and other features which point to a generally high energy environment with intermittent low-energy periods depositing the mud drapes. In addition, when viewed from the north, this entire exposure appears to show a characteristic slight dip, interpreted as original to deposition due to the inclined surface of the point bar feature.

Bruce Leaf

The Bruce Leaf (BL) site is located on Bureau of Land Management (BLM) property within the Ash Creek West Quadrangle in western Garfield County, Montana. Workers from the UWBM discovered this locality in 2019 while prospecting in the area for fossiliferous horizons. Initial excavations yielded mainly angiosperm leaf fossils with high levels of preservation (detail down to third order venation) and quarries were dug over that field season yielding the assemblages described herein (UWBM P8527).

Fossils were excavated from quarries across a wide outcrop exposure: covering ca. 1-2m of stratigraphy and extending ca. 10m along strike. The so-called iridium Z (IrZ) coal, roughly coincident with the K/Pg boundary locally and marking the contact between the Hell Creek and Fort Union Formations, was identified above the quarries in outcrop. The stratigraphic distance from the quarries to the base of the IrZ coal was measured at 11.23 m. This places the locality in the upper third of the Hell Creek Formation.

The lithology of the outcrop at BL is largely well indurated sandstone, and the fossils of the BL appear as compressions and impressions included in silty drapes within this sandstone complex (Fig. 3.S1). From the base of the outcrop, the lithology is largely blue-gray, massive, blocky, and mottled for approximately 1m before transitioning to a more oxidized, fine-to-very fine-grained sandstone. This more massive sandstone unit includes chaotic layers of fine sand to silt with varying levels of oxidation. Most of the fossils are contained in these silty mud drapes, usually in the more oxidized sections. The unit is intermittently barren, and these drapes are not always continuous nor flat lying. The uppermost fossiliferous unit on this outcrop is more fine-grained, with oxidized, very thin and fissile layers of siltstone with plant material preserved.

Fossils recovered from BL preserve a diverse assemblage of mainly angiosperm fossils with some conifers and one cycad specimen. The fossiliferous horizons were most frequently

found in mud drapes interspersed in sandstone. Leaves are often in overlapping mats, making it difficult to extract single leaves without damage. Some chaotic layers preserve hash and/or leaves orthogonal to bedding planes.

This outcrop is interpreted as a channel deposit, with the fossils preserved in what was likely a point bar or lateral edge of the channel body. The mix of sandstone and siltstone, often deposited as an incline, is interpreted as inclined heterolithic stratification (IHS), a common lithology in this formation interpreted as point bar deposits. Following the outcrop laterally, we found the channel sand pinched out and also found evidence for large ironstone concretionary bodies. Below the fossiliferous horizon at the site, we noted a sequence of sand-mud rip up sequences, likely indicating intermittent drying of the channel body and/or migration of the main channel. These rip up clasts mark the lower bound of the fossiliferous zone at this site.

The Swamp A and B

The Swamp (TS) site is located on BLM land in the Maloney Hill Quadrangle in Garfield County, Montana. Previously, a crew from the UCMP had found this site and collected some few plant fossils in 1997. Workers from the UWBM attempted to relocate the site but were unable to precisely find the UCMP quarry. UWBM workers found a productive horizon in the approximate region described by the UCMP crew and refer to this as The Swamp. UWBM workers collected at the site between 2017 and 2019. However, the exact relationship between the UCMP and UWBM quarries is still unclear; UCMP workers indicated their quarry was on Charles M Russell National Wildlife Refuge land, implying their excavations were some tens of meters north of the UWBM quarry.

Fossils from TS come from two horizons, referred to as TSA (UWBM P7144) and TSB (UWBM P7145, P8084, P8537, P8536). TSA is hosted in a fine-grained, light gray sandstone

just above an upper carbonaceous shale layer. TSB is hosted in a light gray to brown clay/siltstone; exposures of this horizon yielded several quarries in the vicinity of the locality. TSB beds are chaotic with abundant organic material. Fossils were excavated from several quarries over ~0.5 m of stratigraphy and along at least 30 m of outcrop.

The UCMP locality sheet for TS notes that the locality is in sandstone of the Hell Creek Fm but palynologically of Paleocene age. Our investigations yielded plant fossils that are distinctly Paleocene (e.g., presence of a likely *Paranymphaea* species), supporting this conclusion. TS quarries are stratigraphically 3.15 m below the base of the prominent MCZ coal exposed at this outcrop. This places the fossiliferous horizon in the Hell Creek Formation, but locally the K/Pg boundary is believed to be below this lithologic contact (Lofgren 1995). Fossils recovered from TS include mostly angiosperm leaves in thinly bedded siltstone layers. Abundant "typha" layers interspersed throughout, particularly in TSB horizon. Leaves are often partial, with numerous aquatic-associated taxa (e.g., *Limnobiophyllum*) and TSB hosts frequent reproductive and other miscellaneous structures in addition to leaves.

The lithology at TS outcrop exposes a sequence of mainly organic rich siltstone units (Fig. 3.S1). The base of the butte at TS is an organic rich, gray siltstone which is capped by a thin carbonaceous shale unit. Overlying this is a dark gray siltstone, containing abundant organic hash, and coarsening up section. This dark gray to brown siltstone unit hosts TSB quarry. Above this in section is a moderately well indurated white sandstone which hosts TSA quarry, becoming more massive above. This unit transitions to an overlying gray siltstone unit. Overlying this is a gray very fine-grained sandstone unit with abundant organic material which grades into the overlying MCZ coal.

Based on the abundance of aquatic taxa, horizontal, thin bedding planes, and abundance of un-oxidized organic material this lithology is interpreted to preserve a pond or other overbank facies.

Lerbekmo N

The Lerbekmo N (L) site is located on BLM land north of the town of Jordan within the Maloney Hill Quadrangle in Garfield County, Montana. Anecdotally, we have heard of numerous collections made at the Lerbekmo N site, but the first known museum collections at this locality were made by crews from the UWBM in 2015. Subsequent collections from workers at the UWBM have been made from 2015-2019 (UWBM P7130, P8097, P6912, P8540).

The L locality includes several quarries dug over ~0.75 m of stratigraphy around ~15 m of outcrop exposed on a prominent butte. A prominent coal is exposed at the base of this butte and has been positively identified as the IrZ coal. The quarries dug at L are between 2.8 and 4.3 m above the base of the IrZ.

The lithology at L is a mix of blue-gray siltstone and tan, oxidized very fine-grained sandstone. The outcrop (Fig. 3.S1) exposes the IrZ at the base, overlain by a blocky blue gray siltstone which coarsens up to sandstone. The L quarries were dug in a unit of mixed siltstone and sandstone, with leaves frequently preserved in the finer grained beds. This unit transitions to a more oxidized, orange clayey siltstone above, barren of fossils. Overlying these rock units another thin coal is exposed towards the top of the butte.

Plants collected at L are dominated by a handful of common taxa (mostly palmate angiosperm leaves, likely a relative of *Archeampelos*) with some rare examples of other aquatic taxa (*Paranymphaea* and *Nelumbo*) and an abundance of woody, typhaceous material. The plants

recovered from L are almost entirely angiosperm leaves; <10 non-angiosperm taxa (eight conifer specimens) and <10 angiosperm reproductive structures have been recovered at this locality.

The lithology at L is interpreted as representing a point bar deposit. Leaves are hosted in a gray siltstone interbedded with tan sandstone with moderate oxidation. Bedding planes are dipping and sometime chaotic, recognized as inclined heterolithic stratification (IHS).

New York I and II

The New York (NY) site is located on BLM land northwest of the town of Jordan within the Hell Hollow Quadrangle in Garfield County, Montana. We understand that some excavations were made here in the early 2000s, as reported by local ranchers, but we know of no museum collections made at that time. Crews from the UWBM located the site in 2017 and have made significant collections there from 2017-2019. These collections come from one main quarry (NY I; UWBM P7135, P8542, P8086) and one minor quarry from a productive horizon ~2 m below (NY II; UWBM P8087).

NY is located approximately halfway up a prominent butte; at the base of this butte is a coal identified as the IrZ coal. Quarries dug at NY were measured between 2 and 5 m above the base of the IrZ. The lithology at NY is a thick unit of tan sandstone with beds inclined to the SE, interspersed with periodic iron-rich horizons (Fig. 3.S1). Overlying the fossiliferous unit at NY is a thin siltstone unit, bound above and below by ironstone beds.

Plants collected at NY are very similar to those found at Lerbekmo N. The same abundant taxa are present (a likely relative of *Archeampelos*) with a single conifer taxon (different from those found at Lerbekmo N) which is relatively abundant.

The lithology at NY is interpreted as representing a channel point bar deposit. The outcrop is similar in lithology to Lerbekmo N, and we also recognize the presence of IHS

(inclined heterolithic stratification) at NY. Leaves are typically preserved in the unoxidized, fine-grained siltstone beds.

Yabba Dabba Do

The Yabba Dabba Do (YDD) site is located on CMR property northeast of the town of Jordan in Garfield County, Montana. Crews from the UWBM discovered the site while prospecting in 2017. Workers from the UWBM have made collections at YDD from 2017-2019 (UWBM P7152, P8088, P8545).

The section at YDD exposes a prominent coal at the base, identified as the IrZ coal, and a smaller coal at the top, though to perhaps be a Y coal. The quarry at YDD was measured at 17 m above the base of the IrZ coal and 1.5 m below the ?Y coal above. The section at YDD exposes a series of mostly fine-grained sandstone with variable organic content, capped by a prominent coal (Fig. 3.S1). The base of this section is a clayey siltstone with a chaotic mix of very fine-grained sand and hosts abundant organic material. This unit grades into the bright white very fine-to-fine-grained sandstone which hosts the YDD quarry. Overlying this productive horizon is a more thinly bedded very fine-to-fine-grained sandstone, thinly bedded, fissile, with some roots and woody materials. This unit grades to a fine-to-medium-grained sand which is tan and thin. At the top of this stratigraphic section there is exposure of a coal bed.

The lithology at YDD (fine-to-medium-grained, gray sandstone) is interpreted as a likely point bar deposit. The beds appear to be inclined heterolithic stratification (IHS): dipping to the southeast, mixed grain size, sometimes convoluted or chaotic bedding. Fossils were recovered from very thin layers of finer grained material, overlain by salt-and-pepper colored sandstone-dominated strata above. Leaves were sometimes rolled or otherwise convoluted. Root traces

were found cutting through the horizontal or inclined strata, which may signify partial exposure of the point bar during deposition.

Typical plant fossils found at YDD were almost entirely non-monocot angiosperm leaves. Similar to other Paleogene assemblages in this study, this flora is dominated by a taxon likely related to *Archeampelos*. However, this flora is unique compared with early-Paleocene floras in this study in that YDD has abundant conifers (particularly the taxon *Glyptostrobus*).

Tharp's Market

The Tharp's Market (TM) site is located on private land northwest of the town of Jordan within the Hell Hollow Quadrangle in Garfield County, Montana. Crews from the UWBM discovered the site while prospecting on a local rancher's property in 2015. Workers from the UWBM have made collections at TM from 2015-2019 (UWBM B8201, P6911, P7142).

The TM quarry is above the prominent HFZ coal; we measured the distance from the top of this coal to the TM quarry as 6.6 m. The lithology at TM is predominately a mix of very fine-grained sandstone and siltstone (Fig. 3.S1). The base of the butte at TM exposes an organic hash horizon, transitioning to a dark black, organic rich siltstone and thin coal band. Above this organic rich layer is the fossiliferous horizon at TM: a chaotic layering of white very fine-grained sandstone and dark gray clayey siltstone dipping to the south. Leaves are preserved mostly along mud drapes in this unit. Overlying this fossiliferous horizon the lithology gradually becomes more clay rich, capped by a wet logged clay unit which is overlain by another organic rich unit.

Fossils recovered from TM are predominately non-monocot angiosperm leaves. The flora is dominated by a likely *Zizyphoides* relative, but also includes a large conifer component (mostly *Glyptostrobus*).

The outcrop at TM is interpreted as a likely point bar deposit. The lithology is interbedded siltstone and fine-grained sandstone; the sandstone is white with black organic-rich beds whereas the siltstone is dark gray with oxidized bands. This is typical of the IHS (inclined heterolithic stratification) which is common in this study area, and interpreted as channel point bar deposition. Leaves were typically recovered from the medium-gray clayey siltstone beds, massive in some areas and extremely fissile in others.

Biscuit Springs I, II, III, IV, V, VI, and VII

The Biscuit Springs (BS) site is located on BLM land in the Biscuit Butte Quadrangle north of the town of Jordan in Garfield County, Montana. BS encompasses several distinct quarries from the same productive horizon in the vicinity of this spring. Biscuit Springs I (East) is ca. 65 m north-northeast of the springs within a fissile yellow sandstone, cliff-forming unit (UWBM P7112, P8092). Biscuit Springs II (West) is ca. 60 m north-northwest of the springs, on the far side of the drainage from Biscuit Springs I and also in the same fissile, yellow sandstone unit (UWBM P7113). Biscuit Springs III (Red Velvet) is one of the most productive quarries, ca. 100 m northeast of the springs (UWBM P7114, P8538, P8091). The Biscuit Springs III productive horizon is a silicified, massive claystone which forms a prominent, overhung cliff above the drainage and often has a red patina. The Biscuit Springs IV (Matt's Gully) site is located 70 m north of the springs, just stratigraphically below the Biscuit Springs I site, with fossils coming out of a finer silt-claystone unit in a small drainage (UWBM P8094). The Biscuit Springs V (Horsefly Cavern) site is located ca. 85 m east-northeast of the springs at the headwall of the east-west running drainage which Biscuit Springs III is also located along (UWBM P8093). The Biscuit Springs V collections came predominantly from float material eroding from a cliff forming, silicified claystone unit. These collections came from just under the prominent

overhang forming the headwall of this drainage. The Biscuit Springs VII (Lemon Gulch) site is located 113 m east-northeast of the springs, near the junction of a prominent east-west running drainage and the main drainage running north out of the springs (UWBM P8095). The Biscuit Springs VII collections were made from a fissile, yellow siltstone unit outcropping at the top of the walls of this drainage.

BS plants were originally collected by crews from the UCMP in the 1970s and referred to as Biscuit Springs Flora and Biscuit Springs Flora North. However, it is unclear if this Biscuit Springs Flora is from the same horizons or specific areas as the collections described herein. Efforts by crews from the UWBM in 2017 to relocate this UCMP locality found fossils at the above described strata in the Biscuit Springs area. We refer to these floras by names of their distinct quarries given the stratigraphic and geographic distance between each distinct quarry, and cannot say whether these collections were made from precisely the same strata as the UCMP collections.

BS I and II are at the same horizon, ~20 cm above the horizon of BS III and V. BS IV was collected primarily from float material eroded out of the overlying rock; based on observations in the field, we believe BS IV fossils came from approximately the same horizon as BS III and V, however. The quarries dug at BS are < 1 m above a thin coal band, likely one of the Y coals. The stratigraphic distance between the BS quarries and overlying dated coal beds places BS ~57 m below the U coal and ~23 m above the IrZ. Based on the stratigraphic height of the Y coal presented by Sprain et al. (2015) this supports our hypothesis that the thin coal just below BS is a Y coal. Given the short stratigraphic distance between all of the BS localities (<1 m), we combine these collections for analyses here.

Based on cross cutting relationships, the BS plant sites are evidently younger than the Biscuit Springs channel complex, which incises through the BS plant fossiliferous horizons. The lithology at BS ranges from silica rich claystone with massive horizontal bedding to fine-grained sandstone with thin planar bedding. We interpret these strata as representing a distal channel deposit associated with the Biscuit Springs channel complex. As described by Weaver et al. (in revision), this channel complex is in the Y to X stratigraphic zone, just above the Y coal.

A synthetic stratigraphic section was logged at the BS sites (Fig. 3.S1). Above the Y coal the rock is weathered and vegetated in most sections. The first identifiable unit is a blue/gray laminated claystone which is overlain by a more massive, organic rich siltstone. This unit grades to a very thinly bedded siltstone with more frequent plant matter preserved. Above this is the fossiliferous unit which hosts the BSII, BSIV, and BSV quarries, which is a very well indurated, silica rich, red weathering, conchoidally fracturing, and massive siltstone. This prominent unit forms many small cliffs in the area. Overlying this is a massive fine-grained sandstone, mostly barren of fossils. Overlying this is a very fine-grained sandstone, thinly laminated with abundant plant impressions (mostly the conifer *Glyptostrobus*); this unit hosts the BSI and BSII quarries and often overhangs the underlying siltstone cliffs. This entire sequence is capped in places by the main BS channel unit, which incises through these beds and all the way to the Y coal in places.

Common plant fossils recovered from BS are mostly non-monocot angiosperm leaves, along with relatively abundant ferns (of a single taxon) and conifers (mostly *Glyptostrobus*). The most common angiosperm is a likely *Archeampelos* relative. This flora contains numerous singleton taxa (not appearing at any other sites) and is relatively unique among the Paleogene assemblages discussed here.

Jane's II and III

The Jane's (J) site is located on BLM land in the Biscuit Butte Quadrangle north of the town of Jordan in Garfield County, Montana. Collections were made by the UCMP in 1997 and 2005. Workers from the UWBM revisited these sites in 2015 and 2016 and made collections (UWBM B8202). Subsequent collections by UWBM crews in 2017 through 2019 from the Jane's site came from two distinct quarries at slightly different productive horizons; unfortunately, their exact stratigraphic position in relation to the original Jane's collections is unclear, so these collections have been labelled as separate quarry sites (Jane's II and III). The Jane's II site (UWBM P7125, P8075) is located within a gray siltstone unit on a southwest facing outcrop. The Jane's III site (UWBM P7126, P8076) is located ca. 40 m south from Jane's II, approximately 3 m stratigraphically below that site, and within a yellow, massive fine-grained sandstone unit.

JII and JIII are both likely in the Garbani Channel complex outcrop here, based on lithologic comparisons laid out in Weaver et al. (in revision). The stratigraphic height of the J quarries places these localities 80 m below the U coal locally and 39 m above the IrZ. The lithology at JII (gray siltstone with massive horizontal bedding) likely represents either a distal channel deposit or more likely still water deposition in an abandoned channel. The lithology at JIII (tan fine-grained sandstone with moderate oxidation and moderately dipping bedding planes) likely represents a point bar deposit (IHS; inclined heterolithic stratification) associated with the Garbani Channel. Tracing the deposit at JIII, it appears this horizon is entirely below JII. While these strata represent distinct depositional phases, the short stratigraphic distance between the two quarries implies the time elapsed between deposition is likely relatively short. Therefore, we combine these collections for analyses here.

The lithology at the J locality varies from dipping, oxidized sandstone to less oxidized, more massive siltstone (Fig. 3.S1). The JIII quarry is hosted in a thick very fine-to-fine-grained sandstone, striped with oxidized layers, dipping east. Above this the lithology transitions to a more massive, less oxidized sandstone and finally to a more organic rich fine-grained sandstone to siltstone. This organic rich siltstone/sandstone unit hosts the JII quarry. Overlying this unit is a blue gray, very platy siltstone which transitions to a more oxidized, more massive blue-gray clayey siltstone. There is an erosional contact above this, with rip up clasts of the clayey siltstone in the overlying very fine-to-fine-grained sandstone above.

Plant fossils recovered from J are mostly non-monocot angiosperm leaves. The most common taxon is a likely *Zizyphoides* relative, similar to TM. There is a relatively low conifer abundance and some angiosperm reproductive structures as well. There are a few *Ginkgo* specimens, which represents a novel occurrence for the early Paleocene in the Williston Basin.

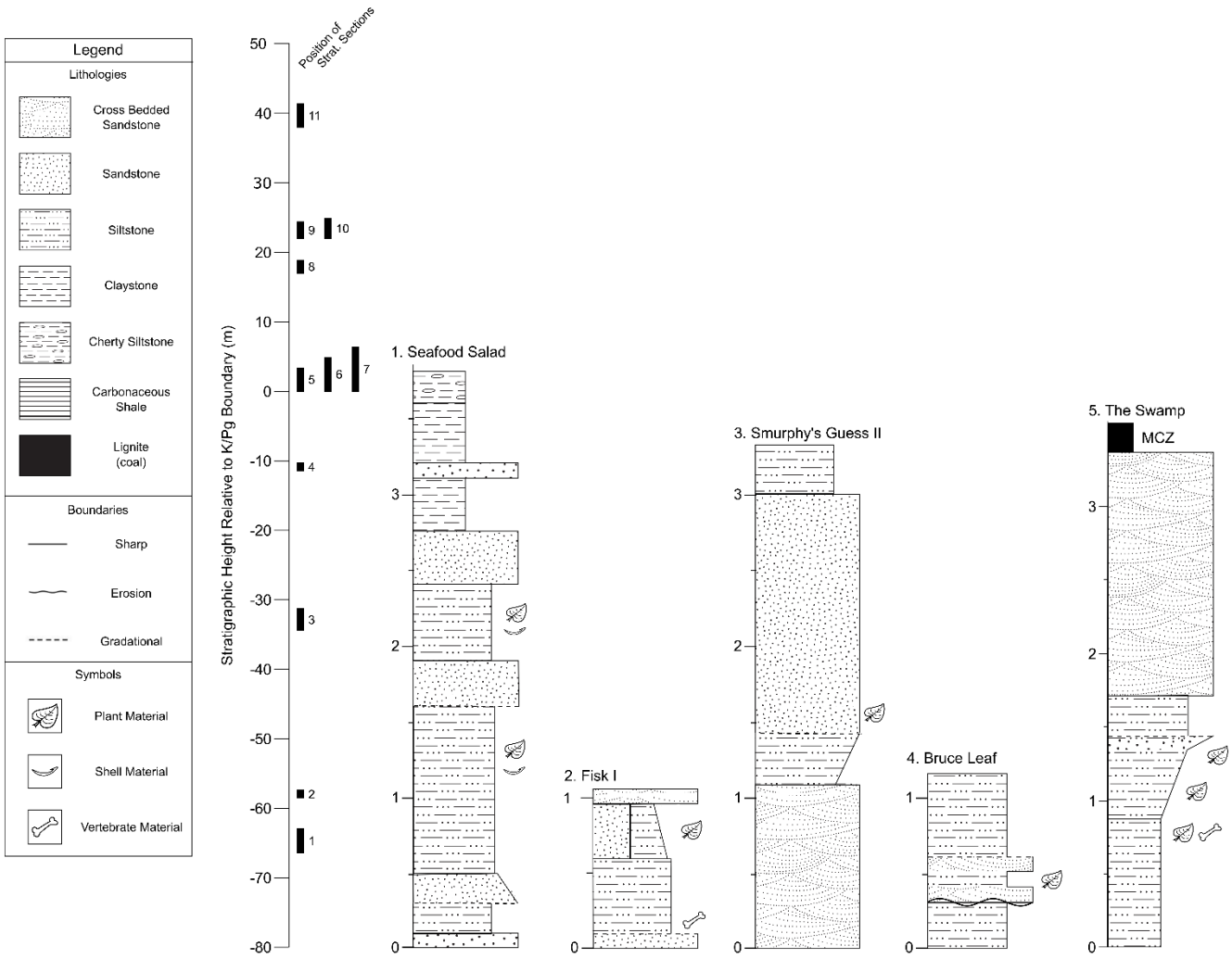

Figure 3.S1: Stratigraphic sections at each floral locality in this study. Lithologic symbols, boundary markers, and sedimentological symbols shown at left. Relative stratigraphic position of each column shown in composite section at left. Stratigraphic sections of the fossiliferous horizon and surrounding 2–7 m of stratigraphy are logged at each of the 11 localities in this study. (continued on next page)

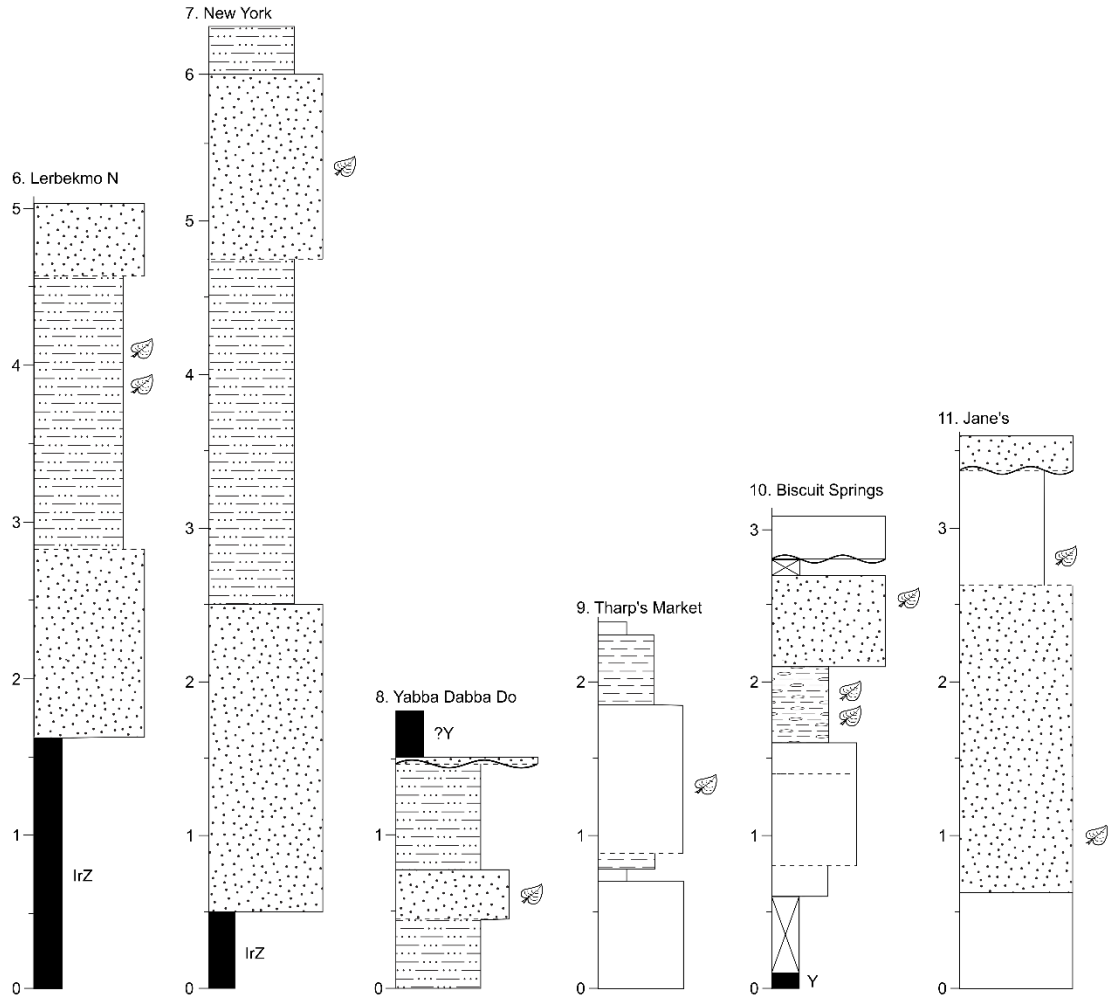
6. Lerbekmo N
7. New York
8. Yabba Dabba Do
9. Tharp's Market
10. Biscuit Springs
11. Jane's
IrZ
IrZ
?Y
Y
0
1
2
3
4
5
6

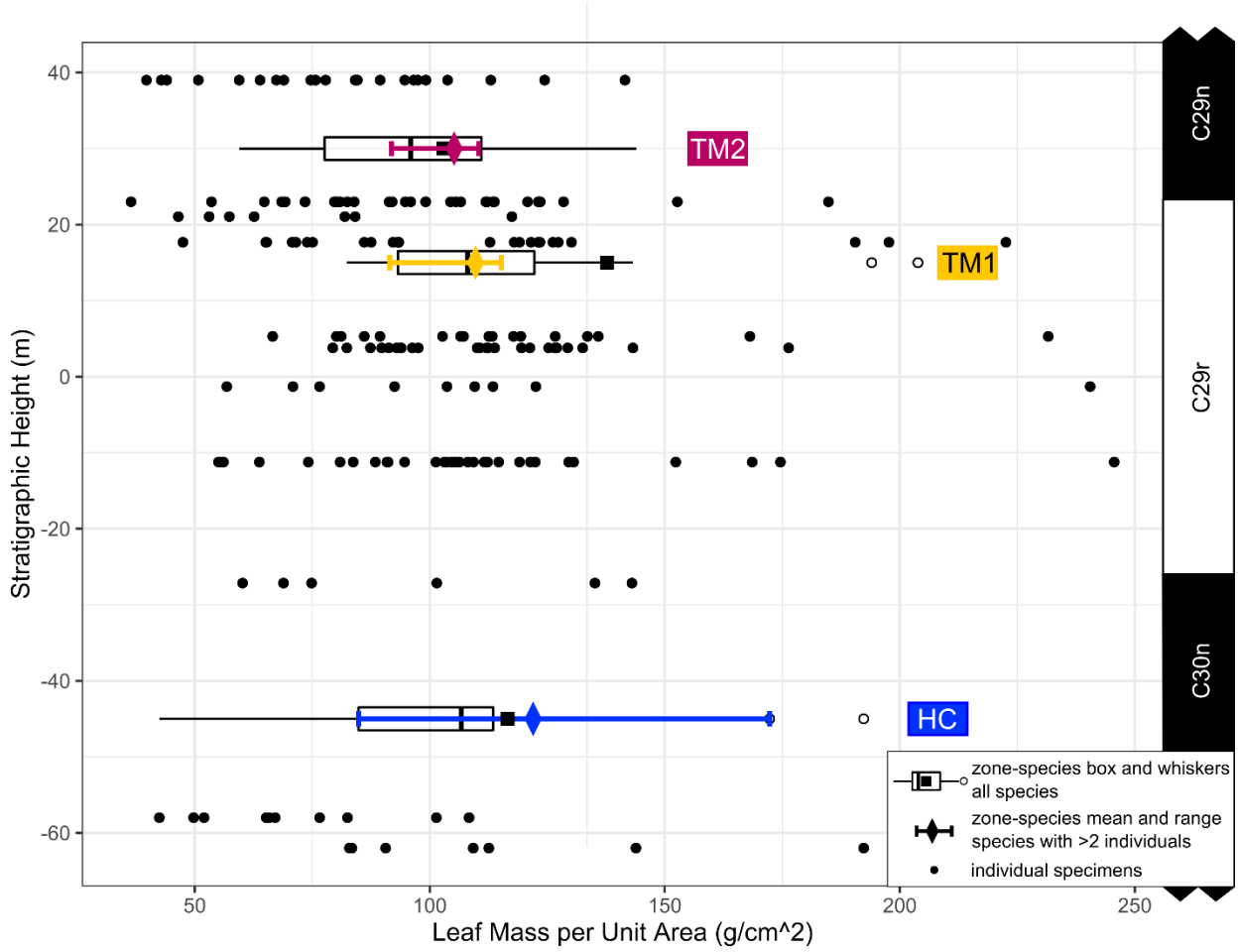

Figure 4.S1: Leaf Mass per Area (LMpA) for individual specimens and averaged by temporal interval. Specimen LMpA values (n = 198 specimens representing 50 morphospecies) are plotted in black at the stratigraphic position of that flora. LMpA was also compiled by interval (Late Cretaceous HC or early Paleocene TM1 or TM2). Interval data are plotted 1) including all species average data represented as box and whiskers of the distribution of species average LMpA in that interval and 2) including only species with >2 specimens of that species in that interval represented as the mean and range of species average LMpA. The HC interval had nine, TM1 had four, and TM2 had four species with >2 specimens in that interval.

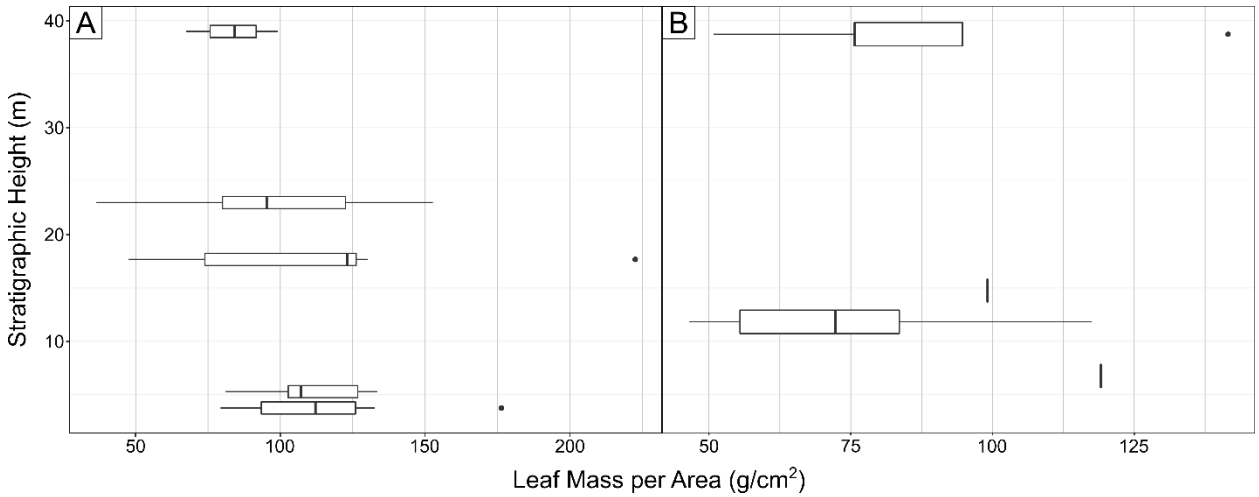

Figure 4.S2: Intra-specific variability of Leaf Mass per Area (LMpA) for two example taxa. Box and whiskers plots of specimen measurements of LMpA at each flora through time for A) morphospecies MT090 and B) morphospecies MT053.

Chapter 4 SUPPLEMENT: SUBSAMPLING RESULTS

As described in our Materials and Methods, we simulated various species richness using one of the modern sites from Peppe et al. (2011a) which were used to calculate the DiLP and LMA regression equations we use in this study (see Supplement for R code). We ran this simulation using several sites from the calibration data collected by Peppe et al. (2011a) and found broadly similar results regardless of which modern site we used. We report our simulation here using the York, PA site as this is the most speciose northern hemisphere, temperate site and therefore presents the best comparison to our study. After subsampling the modern flora from n = 1 to n = 55 species, we estimated MAP and MAT, repeating this subsampling for 1,000 repetitions (Fig. 4.S3). Based on this simulation, we find that the range of estimated MAP and MAT values drops once a threshold of 10 species is reached and continues to decline as larger species richness is achieved. As anticipated, with greater species richness our estimates of MAT and MAP become more precise. However, the benefits above 20 species are not noticeably greater than above ~10 or 15 species.

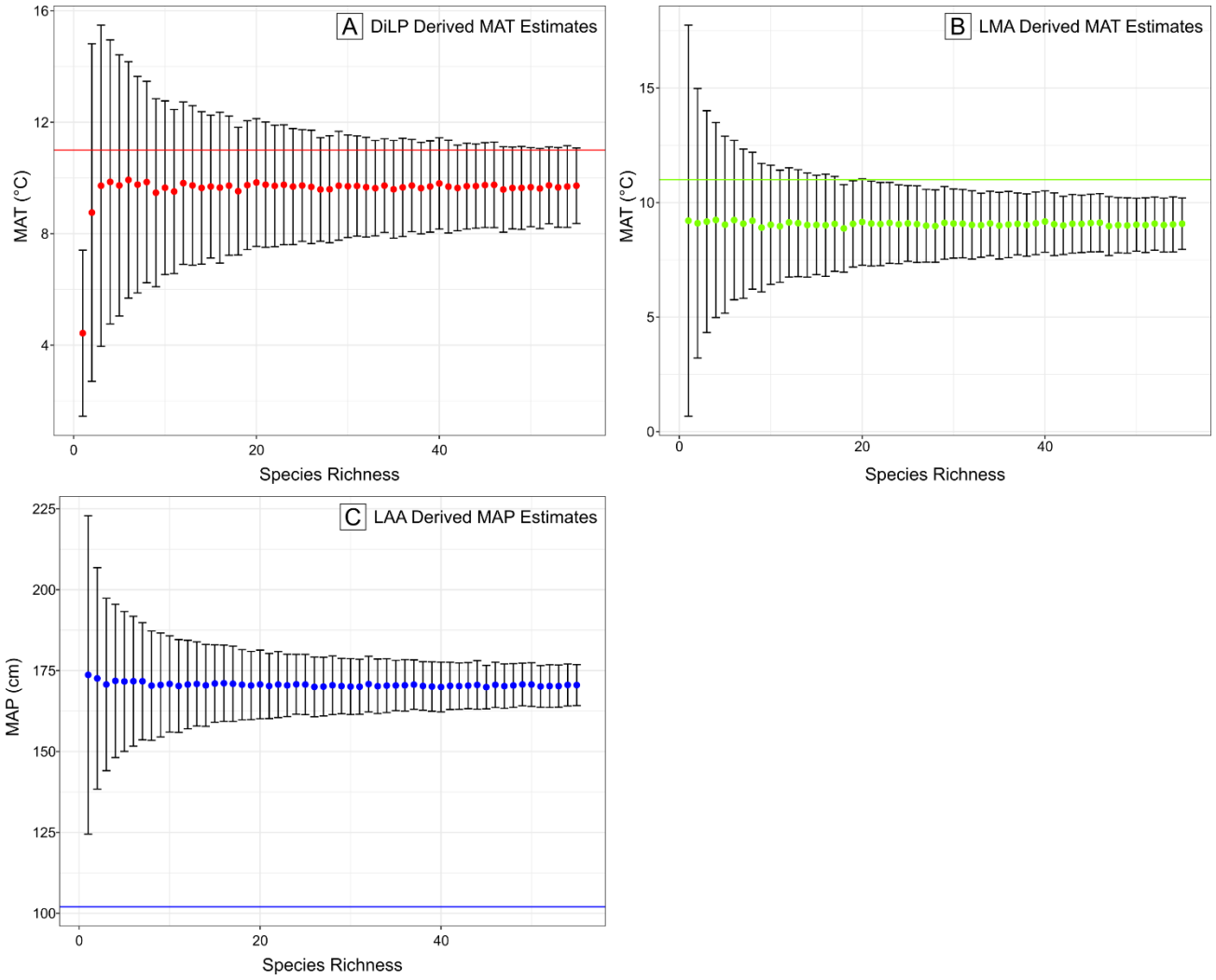

Figure 4.S3: Results of subsampling simulation indicate the uncertainty of MAT and MAP estimates with varying species richness. At each simulated species richness (n = 1–55), we subsampled the data from York, PA (Peppe et al. 2011b) 1,000 times and calculated A) MAT based on the DiLP regression (Peppe et al. 2011b), B) MAT based on the LMA regression (Peppe et al. 2011b), and C) MAP based on the LAA regression (Peppe et al. 2011b). The dots indicate the average MAT or MAP estimated at that simulated species richness, with error bars showing the standard deviation of MAT or MAP estimates among our 1,000 repetitions. In each panel, the horizontal line indicates the measured MAP or MAT at York, PA (Peppe et al. 2011b).

We further use the results of this simulation to inform our estimated error on our MAT and MAP calculations. We use the average standard error of our simulated MAT or MAP estimates using subsamples from 10 to 20 species to incorporate this additional uncertainty into our reported MAT and MAP values. The average standard error of our MAT estimates subsampling

to between 10 and 20 species and using the DiLP regional North American regression (Peppe et al. 2011b) was 0.08 °C. The average standard error of the same simulations using the LMA regression (Peppe et al. 2011b) was 0.07 °C. The average standard error of the same simulations using the LAA regression (Peppe et al. 2011b) was 0.39 cm.

We note that the error introduced by using low-richness floras is much less than the analytical error already incorporated into the LMA, LAA, and DiLP methodologies. The estimated MAT and MAP for York, PA never converge on the actual measured MAT and MAP, even when we use the full dataset of 55 species from this flora (Fig. 4.S1). This imprecision is accounted for in the LMA, LAA, and DiLP methodologies, which all include error calculations. We suggest that the increased error using depauperate floras is minimal.

Our interpretation of these simulation results are that a) the loss of precision using floras with 10-20 species can be quantified and incorporated into our climate estimations b) this loss of precision is not great enough to justify not using these methods with depauperate floras and c) the error associated with low richness floras is minimal particularly in comparison with the methodological uncertainty and inaccuracy already accounted for in these methods.

The following supplemental materials are available through *Cretaceous Research* (https://doi.org/10.1016/j.cretres.2020.104734):

Table 2.S1: Morphotype Taxonomy, Synonyms, and Summary Information
Table 2.S2: Systematic Paleobotany
Table 2.S3: Morphotypes Grouped by Morphology
Table 2.S4: Abundance Data at Seafood Salad
Chapter 2 Supplement: R Code

The following supplemental materials can be found associated with this dissertation online:

Table 3.S1: Quarry information
Table 3.S2: Morphotype Guide
Table 3.S3: Dataset 1 abundance
Table 3.S4: Dataset 2 abundance
Table 3.S5: Dataset 3 abundance
Table 3.S6: Dataset 1 species information
Table 3.S7: Dataset 2 species information
Table 3.S8: Dataset 3 species information
Table 3.S9: Locality information
Table 3.S10: Taxon ID for individual specimens in this study
Chapter 3 Supplement: R Code

Table 4.S1: CIC abundance data
Table 4.S2: CIC taxon data
Table 4.S3: Site data
Table 4.S4: Morphological character states
Table 4.S5: Morphological Character Matrix
Table 4.S6: Raw character measurements on individual specimens for LMpA and paleoclimate analyses
Table 4.S7: Range through occurrences of taxa
Table 4.S8: LMpA calculated for individual specimens
Table 4.S9: LMpA averages
Table 4.S10: Paleoclimate character averages
Chapter 4 Supplement: R Code

Vita

PAIGE K. WILSON DEIBEL

EDUCATION

Ph.D. Earth and Space Sciences (2016 - 2022) *University of Washington (UW), Seattle WA*
Advised by Drs. Greg Wilson Mantilla and Caroline A.E. Strömberg
Passed preliminary exam in Fall 2017; Passed general exam in Fall 2019
Awarded Coombs Teaching Excellence (2019) and Johnston Research Excellence (2020) Fellowships

B.A. Earth Sciences and Biological Sciences (2010 - 2022) *Dartmouth College, Hanover NH*
High Honors in Earth Sciences

RESEARCH SUMMARY

2016 – Present Graduate Research; University of Washington
Investigation into the Cretaceous-Paleogene (K-Pg) mass extinction event; analysis of macrofloral assemblages, microflora, and sedimentology to understand the role of environment and record of ecosystem change through time. Collection and classification of macrofloral taxa. Interpretation of paleoecology and paleoenvironment using digital leaf physiognomy and leaf mass per area methods. Additional projects analyzing palm (Arecaceae) phytoliths for application in paleoecology and describing geology in the Hell Creek and Fort Union Formations.

2013 – 2014 Senior Honors Thesis; Dept. of Earth Sciences, Dartmouth College
Preparation, description, and phylogenetic interpretation of a novel species (Family Nodosauridae) from the Wayan Fm of Idaho. I prepared, investigated, and ultimately classified this specimen as a novel species, which I proposed naming *Sauropelta idahoensis*.

2011 – 2013 Undergraduate Research and Field Work; Dept. of Earth Sciences, Dartmouth College
Collected >800 vertebrate microfossils from Badlands National Park. Assisted in the collection of over 2500 microfossils from Badlands National Park (SD) to investigate taphonomic signature of depositional environments and changes in vertebrate communities across the Eocene-Oligocene boundary. Prepared rock samples for chemical analysis and sorted microfossils. Assisted in fieldwork at the Egg Mountain site near Chouteau, MT along with a crew of researchers from Montana State University and Dartmouth College.

PUBLICATIONS AND ABSTRACTS

^denotes student author

Manuscripts

2021 Weaver, Lucas N, Thomas S Tobin, Jordan R Claytor, **Paige K Wilson**, William A Clemens, Gregory P Wilson Mantilla. *[Manuscript submitted for publication to PALAOIS].* 2021: "Revised Stratigraphic Relationships Within the Lower Fort Union Formation (Tullock Member; Garfield County, Montana, U.S.A.) Provide a New Framework for Examining Post K-Pg Mammalian Recovery Dynamics."

Wilson, Paige K, Gregory P Wilson Mantilla, and Caroline AE Strömberg. 2021: "Seafood Salad: A Diverse latest Cretaceous Florule from eastern Montana." *Cretaceous Research.*

2016 **Wilson, Paige K** and Jason R Moore "Assessing the Control of Preservational Environment on Taphonomic and Ecological Patterns in an Oligocene Mammal Fauna from Badlands National Park, South Dakota." 2016: *PlOS One 11(6)*.

2014 **Wilson, PK** [Unpublished manuscript]. 2014: "Preparation, identification, description, and interpretation of a new dinosaur specimen from the Cretaceous Wayan Formation of Idaho, U.S.A." Dept. of Earth Sciences Undergraduate Senior Honors Thesis, *Dartmouth College*.

Manuscripts in Prep

Wilson Deibel, PK, Strömberg, CAE, and Wilson Mantilla, GP. "Plant Community Change Across the Cretaceous-Paleogene Boundary in Northeastern Montana".

^Lavin, S, ^Markham, A, Brightly, W, *Crifò, C, Lowe, A, Novello, A, Stiles, E,* ***Wilson Deibel, P****, Gallaher, TJ, and* Strömberg, CAE. "Enhancing the Utility of Phytoliths for Understanding the Evolution and Paleoecology of the Arecaceae".

Wilson Mantilla, GP, DeMar, D, Grossnickle, D, Fulghum, H, Hovatter, H, Tobin, T, Weaver, L, Wilson Deibel, PK. "Late Cretaceous and earliest Paleocene mammalian fossil localities of the Hell Creek area."

Published Abstracts

2021 ^Taylor, C, **Wilson, P,** Strömberg, CAE, and Wilson Mantilla, GP. "Examining Paleoclimate Across the Cretaceous-Paleogene (K/Pg) Boundary in Northeastern Montana" *GSA Annual Conference in Portland, OR* (Oct 2021).

^Lavin, S, ^Markham, A, Brightly, W, *Crifò, C, Gallaher, TJ, Lowe, A, Novello, A, Stiles, E,* ***Wilson, P****, and* Strömberg, CAE. "Investigating Phylogenetic Patterns of Palm Phytolith Morphology and Applications for Reconstructing the Paleoecology of the Arecaceae" *GSA Annual Conference in Portland, OR* (Oct 2021).

*Weaver, L., Tobin, T., Claytor, JR, **Wilson, P**, Clemens, WA, Wilson Mantilla, GP. "Revised Stratigraphic Relationships Within the Lower Fort Union Formation (Tullock Member; Garfield County, Montana, U.S.A.) Provide a New Framework for Examining Post K-Pg Mammalian Recovery Dynamics." *GSA Annual Conference in Portland, OR* (Oct 2021).

***Wilson, PK**, Strömberg, CAE, and Wilson Mantilla, GP. "Plant Community Turnover at the Cretaceous-Paleogene (K/Pg) Boundary in Northeastern Montana" *Botany 2021* (July 2021).

^Markham, A, ^Lavin, S, ^Armos, Brightly, W, *Crifò, C, Gallaher, TJ, Lowe, A, Novello, A, Stiles, E,* ***Wilson, P****, and* Strömberg, CAE. "The Analysis of Palm Phytolith Morphology as a Paleoecological and Paleobotanical Tool" *Midcontinental Paleobotanical Colloquium Online* (June 2021).

Wilson, PK, ^Phillips, A, Strömberg, CAE, and Wilson Mantilla, GP. "Examining Paleoclimate Across the Cretaceous-Paleogene (K/Pg) Boundary in Northeastern Montana" *Midcontinental Paleobotanical Colloquium Online* (June 2021).

2020 ***Wilson, PK**, Strömberg, CAE, and Wilson Mantilla, GP. "Plant Community Change Across the Cretaceous-Paleogene Boundary in Northeastern Montana" *GSA 2020 Connects Online* (Oct 2020).

Wilson, PK, Strömberg, CAE, and Wilson Mantilla, GP. "Plant Community Change in the latest Cretaceous of northeastern Montana" *Midcontinental Paleobotanical Colloquium Online* (May 2020).

^Lavin, S, ^Armos, B, ^Khem, S, ^Hart, D, Brightly, W, *Crifò, C, Lowe, A, Novello, A, Stiles, E,* ***Wilson, P****, Gallaher, TJ, and* Strömberg, CAE. "Enhancing the Utility of Phytoliths for Understanding the Evolution and Paleoecology of the Arecaceae" *Midcontinental Paleobotanical Colloquium Online* (May 2020).

2019 ***Wilson, PK**, Wilson GP, and Strömberg, CAE. "Seafood Salad: A Diverse Florule from the Late Cretaceous-age Hell Creek Formation of Montana" Oral Presentation *North American Paleontological Conference in Riverside, CA* (Jun 2019).

***Wilson, PK**, Wilson GP, and Strömberg, CAE. "Seafood Salad: A Diverse Florule from the Late Cretaceous-age Hell Creek Formation of Montana" Oral Presentation *ESS Departmental Gala in Seattle, WA* (Apr 2019).

^Armos, B, ^Lavin, S, ^Akbar, S, Brightly, W, *Crifò, C, Gallaher, T, Lowe, A, Novello, A,* ***Wilson, P****,* Strömberg, C. "The utility of palm phytoliths for inferring the evolution and paleoecology of Arecaceae" *Botany 2019 in Tucson, AZ* (July 2019).

2018 ***Wilson, PK.*** "Plant Macrofossils from the Hell Creek of Montana: Evidence of the K-Pg Mass Extinction" Oral Presentation *ESS Departmental Gala in Seattle, WA* (Mar 2018).

2017 **Wilson, PK**, Wilson, GP, and Strömberg, CAE. "Vegetation and Environment Change Across the K-Pg Boundary in the Hell Creek of Montana" Poster session *GSA Annual Conference in Seattle, WA* (Nov 2017).

Wilson, PK. "Environmental Change and Plant Response Across the Cretaceous-Paleogene Boundary in North America: A Study in the Hell Creek Area of NE Montana" Poster session *ESS Departmental Gala in Seattle, WA* (Mar 2017).

2014 **Wilson, PK.** "Preparation, Identification, description, and interpretation of a new dinosaur specimen from the Cretaceous Wayan Formation of Idaho, U.S.A." Poster session *Dartmouth College Wetterhahn Science Symposium* (May 2014).

2012 **Wilson, PK** and Moore, JR. "Quantitative analysis of the taphonomic and ecological patterns recorded by vertebrate assemblages from the Oligocene Poleslide Member of the Brule Formation, Badlands National Park, South Dakota" Poster session *Society of Vert. Paleontology Annual Conference in Raleigh, NC* (Oct 2012).

Wilson, Paige K and Moore, JR. "Broken Bones in the Badlands: Examining Preservational Biasing in Fossil Assemblages form Badlands National Park, SD" Poster session *Dartmouth College Wetterhahn Science Symposium* (May 2012).

*Oral Presentation

INVITED TALKS

Jul 2020	PBS Prehistoric Road Trip Documentary, Featured Researcher in Episode 2
Jan 2020	Utah Museum of Natural History DinoFest "Ferns, Sycamores, and Palm Trees: which plants survived the K-Pg mass extinction?"
Aug 2018	Garfield County Museum Invited Speaker
Jun 2018	Seattle PS Science Fair Invited Speaker
Nov 2017	DIG Field School & Northwest Paleontological Association

HONORS AND AWARDS

2021	George Edward Goodspeed Award (UW ESS)
	Mentor Award, Letters to a Pre-Scientist
2020	AWG Winifred Goldring Award, Honorable Mention
	David A. Johnston Fellowship, Awarded for Research Excellence (UW ESS)
	Robert G. and Nadine E. Bassett Endowed Fund (UW ESS)
2019	Howard A. Coombs Teaching Excellence Award (UW ESS)
	Celebrate UW Women Award
2018	Combined Dr. Jody Bourgeois Fellowship in Sedimentary Geology, Dr. Howard A. Coombs Scholarship Fund, and Marie Ferrell Endowment Fund (UW ESS)
2017	Adam Campbell Award, Earth and Space Sciences UW
2014	Upham Geology Award, Dartmouth College Earth Sciences
2014	Gazzaniga Family Science Award, Dartmouth College
2014	Second Honor Group, Dartmouth College

GRANTS

2019	Paleo Society & The Bearded Lady: Currano Scholarship Research Grant	$1200
	GSA Student Research Grant	$1250
	Evolving Earth Foundation Research Grant	$2922
2017	Quaternary Research Center Research Grant, UW	$4155
	American Philosophical Society- Lewis And Clark Fellowship Research Grant	$3600
	Dr. Jody Bourgeois Endowed Fellowship in Sedimentary Geology (UW ESS)	$2250
	Colorado Scientific Society Research Grant	$900
2013	John Lindsley Fund Research Grant (Dartmouth College)	$3000
2011	John Lindsley Fund Research Grant (Dartmouth College)	$2400

FIELD EXPERIENCE

2017-21 *Hell Creek Area, Montana — 19 weeks cumulatively
Paleobotany prospecting and collections, stratigraphic logging, sediment collection for plant microfossils, vertebrate collection (micro and macro), overseeing large (10+ person) team of volunteers, students, and other researchers

2014 Egg Mountain, Montana—1 week
Assisted in collection of dinosaur nesting site

2014 *Wayan Fm, Idaho—1 week
Stratigraphic logging and sediment collection at previous dinosaur excavation

2012 Dartmouth Geology field camp, various locations in western North America—10 weeks
Comprehensive field methods class including mapping, hydrology, glaciology, and other field techniques

2011 *Palmer Creek Unit, Badlands National Park, South Dakota—1 week

Led the collection of over 700 vertebrate microfossils at two sites

2011 Badlands National Park, South Dakota—7 weeks
Assisted in prospecting and collecting over 3,000 vertebrate micro and macro fossils, assisted in stratigraphic logging

**Denotes field work where I was leading the project*

TEACHING AND CURRICULUM DEVELOPMENT

Teaching Assistant

ESS 210, UW: Physical Geology (2 quarters)
ESS 211, UW: Physical Processes of the Earth (2 quarters)*
ESS 212, UW: Earth Materials (2 quarters)*
ESS 213, UW: Evolution of the Earth (2 quarters)*
ESS 313, UW: Geobiology (2 quarters)
ESS 401, UW: Field Geology with GIS (1 quarter)
BIOL 200, UW: Introductory Biology, Cellular Biology (1 quarter)
EARS 101, Dartmouth College: Introduction to Earth Sciences (1 quarter)

**Denotes contribution of original lab materials or content*

Programming & Curriculum Development

DIG Field School, Burke Museum (2020) -- *Developed and modified new lesson plans for K-12 teachers as part of the DIG Field School program*
Girls In Science, Burke Museum (2019) – *Designed lesson content for a six week after school program for high school girls*

Guest Lecturer

ESS 210, University of Washington: Physical Geology (one sixty minute lecture)
BIOL 475, University of Washington: Paleobiology Field Methods and Research (2018 and 2019)--*Led two days of field methods course in Montana, instructing on paleobotany field techniques*
GY320, Colorado College: Surface Processes and Geomorphology (2020)--*"Cretaceous-Paleogene (K-Pg) Mass Extinction: Plants v. Meteor"* guest lecture

Training

UW CoENV Online Teaching Conference (2020)
UW TA/RA Conference (2016)

MENTORING AND OUTREACH

2021 Mentor, Letters from a Pre-Scientist—*one on one mentorship with a 6th grade student from a low income community*
2019 Instructor, Girls In Science High School Program, Burke Museum UW—*designed and led a six week after school program for HS girls on botany*
2019 Graduate Assistant, DIG Field School, Burke Museum UW—*advertised, reviewed, and made decisions on applications from K-12 teachers; designed new lesson content; managed program logistics (social media, teacher interactions, and planning for summer field program)*
2017 – 2019 Coordinator, Rockin' Out, Earth and Space Sciences UW—*organized in-class visits, campus field trips, and science nights for K-12 students; solicited volunteers and school contacts to set up events, and designed lessons.*
2017 – 2018 Assistant Instructor, Girls In Science High School Program, Burke Museum UW—*assisted in facilitating a six week after school program for HS girls on paleobotany*
2017 – Present Instructor, DIG Field School, Burke Museum UW—*4-day field camp each July for K-12 teachers on geology and paleontology methods, lesson plan development, etc; led teachers in the field to instruct them on geological and paleobotanical methods.*
2016 – 2017 Assistant Instructor, Girls In Science Middle School Program, Burke Museum UW—*assisted in facilitating a weekend program for MS girls on paleobotany*
2016 – Present Volunteer, Rockin' Out, Earth and Space Sciences UW—*visit local K-12 schools to teach lessons on earth science topics*
2016 – Present Volunteer, Burke Museum various public outreach events, UW—*regularly volunteer at events through the Burke Museum speaking with adults and families to share information about fossils, research, and museum collections*

2016 – Present Mentor, Hell Creek Project, UW—*directly mentored eight undergraduate students and five volunteers in cataloging and processing leaf macrofossil specimens, prep work (e.g. scribing and gluing) of fossil specimens, and analytical techniques in paleobiology. I also work co-mentoring the more than 30 undergraduate students in Greg Wilson Mantilla and Caroline Strömberg's labs.*

PROFESSIONAL ORGANIZATIONS AND MEMBERSHIPS

2020 – Present Association for Women Geoscientists
2017 – Present Northwest Paleontological Association
2017 – Present Paleontological Society
2014 – Present Geological Society of America

SERVICE

2021 UW ESS Pod, Unlearning Racism in Geosciences (URGE) Program
Graduate Election Coordinator, UW Earth and Space Sciences Dept.
Midcontinent Paleobotanical Colloquium Organizing Committee
2020 Association for Women Geoscientists PNW Student Chapter, Founder
Midcontinent Paleobotanical Colloquium Organizing Committee
2020 – 2021 College of the Environment Student Academic Grievance Committee
2020 College of the Environment Student Advisory Council
2018 – 2019 ESS Gala (Departmental Conference) Committee, UW Earth and Space Sciences Dept.
2017 – 2019 Rockin' Out Program Coordinator, UW Earth and Space Sciences Dept.
2017 – 2018 First Year Student Feedback Coordinator, UW Earth and Space Sciences Dept.
2016 – 2017 UW Graduate and Professional Student Senate, Earth and Space Sciences Dept. Representative

PROFESSIONAL EXPERIENCE

Jan 2016 – Sep 2016 The Arnold Group, Research Analyst in Seattle, WA
Provided quantitative and qualitative support for a team of consultants on a variety of projects in the tech industry. Responsibilities included client relationship building, data analysis, and presentation of hypothesis-driven findings. Worked on four projects with teams at Microsoft Corporation including product research, new team creation, and corporate reorganization impacting over 15K employees.

Oct 2014 – Dec 2015 Epic Systems Corp, Technical Recruiter in Madison, WI
Managed the application, interview, and hiring process at a healthcare software company which employs nearly 8,000 workers. Personally hired over 200 software developers and technical services analysts.

OTHER SKILLS

Programming and software experience: Proficient in Microsoft Office Suite, R Statistical software, Matlab, Arcmap, ERDAS Imagine, JMP, TNT, Mesquite, Matlab, Past, and photo processing programs (among others)
Field work and wet lab experience: paleontological prospecting, excavation, and prep work; microscopy, benchwork (e.g. phytolith processing); sedimentological logging, collection, and measurement
Set up a new phytolith and pollen processing lab at the Burke Museum (2020), created and maintained various lab websites, ran lab social media (i.e., Twitter), and assisted in creating exhibit and website content for the Burke Museum Paleobotany Division
First Aid and CPR certified (2020)